

MAGNETO-HYDRODYNAMIC FLOW THROUGH A ROTATING RECTANGULAR STRAIGHT AND CURVE DUCT WITH MAGNETIC FIELD

DOCTOR OF PHILOSOPHY

IN APPLIED MATHEMATICS

MOHAMMAD RAFIQU L ISLAM



**Department of Applied Mathematics
Faculty of Science
UNIVERSITY OF DHAKA, DHAKA-1000, BANGLADESH**

NOVEMBER 2023

Magneto-hydrodynamic Flow through a Rotating Rectangular Straight and Curve Duct with Magnetic Field

Thesis Submitted for the Degree of
DOCTOR OF PHILOSOPHY
IN APPLIED MATHEMATICS

by

Mohammad Rafiqul Islam

Supervised by

Professor Dr. Md. Abdus Samad
and
Professor Dr. Md. Mahmud Alam



Department of Applied Mathematics
Faculty of Science
UNIVERSITY OF DHAKA, DHAKA-1000, BANGLADESH

November 2023

Certificate by the Supervisor and Joint Supervisor

We hereby certify that we have assessed the thesis titled “Magneto-hydrodynamic Flow through a Rotating Rectangular Straight and Curve Duct with Magnetic Field” by Mohammad Rafiqul Islam. We declare the followings:

1. This thesis includes new work as compared to previously published publications.
2. No part has been taken directly from another earlier writing unless it is cited properly.
3. The work shown here is the author’s own work.
4. Any outcomes developed by others have not been claimed as the author’s own.

There is no manipulation in data that has been analyzed.

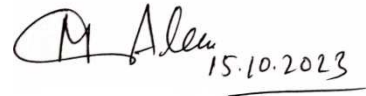
Supervisor



30.10.23

Dr. Md. Abdus Samad
Professor
Department of Applied Mathematics
University of Dhaka
Dhaka-1000, Bangladesh

Joint Supervisor



15.10.2023

Dr. Md. Mahmud Alam
Professor
Mathematics Discipline
Khulna University
Khulna-9208, Bangladesh

Declaration

I hereby declare that this dissertation's materials are presented as my original work, which has been done after registration for the degree of PhD at the Department of Applied Mathematics University of Dhaka, Bangladesh. I also confirm that it has not been previously included in a thesis or dissertation submitted to this university or any other institution for a degree, diploma, or other qualifications.

Signature



Mohammad Rafiqul Islam

Registration number: 43

Session: 2018-2019

Department of Applied Mathematics

University of Dhaka, Bangladesh

Abstract

This research involves a numerical exploration of the characteristics of fully developed, steady, viscous, incompressible flow within a curved duct with square and rectangular cross-sections. The study considers both isothermal and non-isothermal conditions, while also accounting for the influence of magnetic fields, Hall currents, and Ion-slip currents. In this investigation, the dimensions of the cross-section are defined as having a height of $2h$ and a width of $2d$. The analysis covers curved ducts with both square and rectangular cross-sections for both isothermal and non-isothermal flow scenarios. In both cases, the aspect ratio is taken as $l = 1$ or 2 or 3 , whereas the curvature of the duct ranges from 0.01 to 5 . Also, the behaviour of the flow characteristic is investigated for non-isothermal flow through the straight duct in the presence of Hall and Ion-slip currents. A pressure gradient force, known as Dean Forces, is applied in the direction of the curved duct's centreline. This flow is further influenced by a combination of forces, including gravitational force, Lorentz force, centrifugal force, and Coriolis force. The gravitational force exerts its effect on the fluid. Additionally, the Lorentz force results from the interaction of electric and magnetic forces, while centrifugal and Coriolis forces stem from the duct's rotation and curvature. To model this complex system, governing equations are derived from the Navier–Stokes and Energy equations using cylindrical coordinates. These equations are then converted into their non-dimensional forms through the customary non-dimensional analysis. The spectral approach is used as the main instrument to perform the calculations. Additionally, as auxiliary tools, the Newton-Raphson, Collocation, Chebyshev polynomial, and arc-length procedures are employed. The arc-length method has been used to avoid the difficulties near the point of inflection and calculate the results at this point. The flow depends on the

Taylor number $T_r = \frac{2d^2 \sqrt{2\delta} \Omega_0}{\delta v}$ (Rotation parameter), Magnetic parameter $M = \frac{d^2 \sigma \mu_e B_0^2}{\rho v}$,

Grashof Number $G_r = \frac{d^3 \beta g \Delta T}{\nu^2}$ ammeter Hall parameter (m), and Ion-slip parameter (α).

The study examines the impact of T_r , G_r , and D_n on flow characteristics to compare and validate the findings with prior research. The primary objective of this investigation is to elucidate how M , m , and α influence flow characteristics within both rotational square and rectangular curved ducts, as well as in straight square ducts. Both co-rotating and counter-rotating flow patterns are investigated here. Finally, a general discussion and conclusions on the solutions to the problems considered in the research study for different values of the magnetic, Hall, and Ion-slip parameters on the flow properties in some particular cases of Dean Number and different duct curvature are described.

Acknowledgment

I always remember the Almighty Allah, who graced me with the ability to complete this thesis. I am delighted to express my sincere respect and gratitude to Dr. Md Abdus Samad, Professor, Department of Applied Mathematics, University of Dhaka, Bangladesh, for his enthusiastic cooperation and guidance. I am deeply indebted to him for selecting me as his PhD student.

Indeed, I am also grateful to Dr. Md. Mahmud Alam, Professor, Mathematical Discipline, Khulna University, Bangladesh, for his patience, inspiration, enthusiasm, constructive discussion, immense knowledge, adequate direction, and endless enthusiasm in compiling and compiling this thesis. This work could not have been completed without his generous help.

I would like to express my heartfelt gratitude to the examination committee for their thoughtful remarks on this thesis.

I am taking this opportunity to express my deepest gratitude to the Honourable Vice-Chancellor, BSMRSTU, Gopalganj, for granting me three years and six months of study leave to expedite my PhD research. I am also grateful to the University Grants Commission (UGC) Dhaka, Bangladesh, for granting me a PhD research fellowship.

Especially, I feel a huge debt of gratitude to my beloved wife Sonia Nasrin, for her unwavering support and encouragement during my studies. Also, I love my two little sons, S. M. Ahsan-ul-KhaliqinRatin Islam and S. M. Saimum Islam, who have always sacrificed their due rights for my studies.

Finally, I would like to express my gratitude to all of my colleagues, friends, and other well-wishers who have continued encouragement to complete this thesis.

Contents

Certificate by the Supervisor and Joint Supervisor	i
Declaration	ii
Abstract	iii
Acknowledgement	iv
Contents	v-vii
List of Tables and Figures	viii-xv
Dissertation Contents	xvi-xvii
Nomenclature	xviii
Chapter 1	1-24
Literature review	
1.1 Introduction	1
1.2 Bifurcation Phenomena in Curved Duct	3
1.3 Developed Flow in Curved Channels	6
1.4 Developing Flow in Curved Pipes	8
1.5 Fully Developed Flows in Rectangular Curved Ducts	12
1.6 Rotating Duct	14
1.7 Heat Transfer in Curved Duct	15
1.8 Hall Current and Ion-slip	18
1.9 Relevant Parameters Information	18
Chapter 2	25-56
Basic Definitions and Governing Equations	
2.1 Basic Definitions	25
2.1.1 Curvilinear Coordinates	
2.1.2 Gradient, Divergence Curl and Laplacian in Orthogonal Curvilinear Coordinates System	
2.1.3 Hall and Ion-slip Current	
2.2 Basic Governing Equations [Curved Duct]	28
2.2.1 Continuity Equation in Cylindrical Curvilinear Coordinate System	
2.2.2 MHD Momentum Equation with Hall and Ion-slip currents in Cylindrical Curvilinear Coordinate System with Rotation	
2.2.3 Energy equation in cylindrical curvilinear coordinate system	
2.3 Simplifications of the Governing Equations Regarding to the Current Study	40
2.3.1 Transforming Coordinate Variables on the Governing Equations and Mathematical Formulations	
2.3.2 Non-dimensional Analysis	

Chapter 3	57-59
Calculation Techniques	
3.1 Method of Numerical Solutions	57
3.2 Nusselt Number	59
3.3 Flux through the duct and mean axial velocity	59
Chapter 4 60-113	
Magneto-hydrodynamic Isothermal Fluid Flow through a Rotating Curved Duct with Magnetic Field	
4.1 Introduction	60
4.2 Mathematical Formulation	63
4.3 Validation of the numerical simulations	66
4.4 Curved Square Duct for Isothermal Fluid Flow:	67
Hall and Ion-slip Current Effects on Steady Flow through a Rotating Curved Square Duct with Magnetic Field	
4.4.1 Grid Spaces Accuracy	
4.4.2 Results and Discussion	
4.5 Curved Rectangular Duct for Isothermal Fluid Flow:	84
Steady MHD Fluid Flow in a Rotating Curved Rectangular Duct with Hall and Ion-slip Current.	
4.5.1 GridSpaces Accuracy	
4.5.2 Results and Discussion	
4.6 Curved Rectangular Duct for Isothermal Fluid Flow: 98	
Hall and Ion-slip Effects on MHD Fluid Flow in a Rotating Curved Duct with Aspect Ratio 3	
4.6.1 Grid Spaces Accuracy	
4.6.2 Results and Discussion	
Chapter 5 114-155	
Magneto-hydrodynamic Non-Isothermal Fluid Flow through a Rotating Curved Duct with Magnetic Field	
5.1 Introduction	114
5.2 MathematicalFormulation	117
5.3 Validation Test of the Present Numerical Results	120
5.4 Curved Square Duct for Non-Isothermal Fluid Flow:	122
Non-Isothermal Magneto-hydrodynamic Fluid Flow along the Centreline in a Rotating Curved Square Duct with Hall and Ion-slip Current	
5.4.1 Grid Spaces Accuracy	
5.4.2 Results and Discussion	

5.5 Curved Rectangular Duct for Non-Isothermal Fluid Flow:	134
Hall and Ion-slip Current Effects on Non-Isothermal Steady Flow through a Rotating Curved Rectangular Duct with Aspect Ratio 2	
5.5.1 Grid Spaces Accuracy	
5.5.2 Results and Discussion	
5.6 Curved Rectangular Duct for Non-Isothermal Fluid Flow:	147
Non-Isothermal Fluid Flow through a Rotating Curved Duct with Aspect Ratio of 3 in the Presence of Magnetic Field, Hall, and Ion-slip Currents	
5.6.1 Grid Spaces Accuracy	
5.6.2 Results and Discussion	
Chapter 6	156 -177
Straight Duct Flow	
6.1 Basic Governing Equation	156
6.2 Governing Equations for Straight Duct Regarding to the Current Study	160
6.3 Straight Square Duct for Non-Isothermal Fluid Flow:	168
Non-Isothermal Steady Flow through a Rotating Square Straight Duct with Hall and Ion-slip Currents	
6.3.1 Grid Spaces Accuracy	
6.3.2 Results and Discussion	
Chapter 7	178 -184
General Discussion and Conclusions	
7.1 General Discussion	178
7.2 Conclusions	178
7.2.1 Curved Square Duct for Isothermal Flow	
7.2.2 Curved Rectangular Duct with Aspect Ratio of 2 for Isothermal Flow	
7.2.3 Curved Rectangular Duct with Aspect Ratio of 3 for Isothermal Flow	
7.2.4 Curved Square Duct for Non-Isothermal Flow	
7.2.5 Curved Rectangular Duct with Aspect Ratio 2 for Non-Isothermal Flow	
7.2.6 Curved Rectangular Duct with Aspect Ratio 3 for Non-Isothermal Flow	
7.2.7 Curved Square Duct for Non-Isothermal Fluid flow	
References	185-197

List of Tables and Figures

A. List of Tables

Table-1	: Fluxes Q at several pairs of truncation numbers \bar{M} and \bar{N} for fixed $\delta=0.1$, $T_r=10$, $D_n=500$, $M=0$, $m=0$ and $\alpha=0$.	67
Table-2	: Fluxes Q at several pairs of truncation numbers \bar{M} and \bar{N} for fixed $\delta=0.1$, $T_r=20$, $D_n=500$, $M=0$, $m=0$ and $\alpha=0$.	84
Table-3	: Fluxes Q at several pairs of truncation numbers \bar{M} and \bar{N} at fixed values of $\delta=0.1$, $T_r=20$, $D_n=500$, $M=0$, $m=0$ and $\alpha=0$.	98
Table-4	: Fluxes Q and mean Nusselt number Nu_c and Nu_h for distinct pairs of truncation numbers \bar{M} and \bar{N} for fixed $\delta=0.1$, $T_r=20$, $G_r=100$, $D_n=1000$, $P_r=7$, $M=0$, $m=0$ and $\alpha=0$.	122
Table-5	: Fluxes Q and mean Nusselt number Nu_c and Nu_h for distinct pairs of truncation numbers \bar{M} and \bar{N} for fixed $\delta=0.1$, $T_r=20$, $G_r=100$, $D_n=500$, $P_r=7$, $M=0$, $m=0$ and $\alpha=0$.	134
Table-6	: Fluxes Q and mean Nusselt number Nu_c and Nu_h for distinct pairs of truncation numbers \bar{M} and \bar{N} for fixed $\delta=0.1$, $T_r=20$, $G_r=100$, $D_n=1000$, $P_r=7$, $M=0$, $m=0$ and $\alpha=0$.	147
Table-7	: Fluxes Q at distinct pairs of truncation numbers \bar{M} and \bar{N} for fixed $G_r=0$, $T_r=20$, $D_n=500$, $P_r=7$, $M=0$, $m=0$ and $\alpha=0$.	168

B. List of Figures

Figure 2.1	: Cartesian with Curvilinear Coordinate system	25
Figure 2.2	: Cylindrical Coordinate System	26
Figure 2.3	: (a) Fleming's Left Hand Rules (b) Hall effects and Ion-slip	28
Figure 2.4	: Cylindrical curvilinear coordinate system with curved duct	31
Figure 2.5	: Modified Geometrical Configuration of the curved duct	40
Figure 3.1	: (a) Discretization of the square duct cross-section (b) Discretization of the rectangular duct cross-section	57
Figure 4.1	: Coordinate system of Curved duct with isothermal flow (a) Aspect ratio 1 [Square cross-section] (b) Aspect ratio 2 [Rectangular cross-section] (c) Aspect ratio 3 [Rectangular cross-section]	63
Figure 4.2	: Comparisons of the present results with previous published experimental results by the structure of stream lines	66
Figure 4.3	: (a) Solution curve: Flux Q versus Taylor Number T_r for $\delta=0.01$, $D_n=500$, $M=0$, $m=0$ and $\alpha=0$. (b)-(c) Magnifying figure marked by the dashed box on Fig.4.4a	69

	(d) Streamlines ψ (upper) and axial contour flow w (lower) in accordance with the solution curve in Fig.4.3a	71
	(e) Vortex structure of secondary flows versus Taylor number T_r for $\delta = 0.01$, $D_n = 500$, $M=0$, $m=0$ and $\alpha=0$.	71
Figure 4.4 :	(a) Solution curve: Flux Q versus Taylor Number T_r for $\delta=0.1$, $D_n=500$, $M=0$, $m=0$ and $\alpha=0$.	72
	(b) Streamlines ψ (upper) and axial contour flow w (lower) in accordance with the solution curve in Fig.4.4a	72
	(c) Vortex structure of secondary flows versus Taylor number T_r with $\delta = 0.1$, $D_n = 500$, $M=0$, $m=0$ and $\alpha=0$.	73
Figure 4.5 :	(a) Solution curve: Flux Q versus Taylor Number T_r for $\delta=0.5$, $D_n= 500$, $M = 0$, $m = 0$ and $\alpha=0$.	74
	(b) Streamlines ψ (upper) and axial contour flow w (lower) in accordance with the solution curve in Fig.4.5a	74
	(c) Vortex structure of secondary flows versus Taylor number T_r with $\delta = 0.5$, $D_n = 500$, $M=0$, $m=0$ and $\alpha=0$.	75
Figure 4.6 :	(a) Solution curve: Flux Q versus Dean Number D_n for $\delta=0.1$, $T_r=10$, $M=0$, $m=0$ and $\alpha=0$.	75
	(b) Streamlines ψ (upper) and axial contour flow w (lower) in accordance with the solution curve in Fig.4.6a	76
	(c) Vortex structure of secondary flows versus Dean Number D_n with $\delta = 0.1$, $M=0$, $m=0$ and $\alpha=0$.	76
Figure 4.7 :	(a) Solution curve: Flux Q versus Magnetic parameter M for $\delta = 0.1$, $D_n= 500$, $T_r=10$, $m=0$ and $\alpha=0$ with curvatures $\delta = 0.01$, 0.1 and 0.5 .	77
	(b) Streamlines ψ (upper) and axial contour flow w (lower) in accordance with the solution curve in Fig.4.7a.	78
Figure 4.8 :	(a) Solution curve: Flux Q versus Magnetic parameter M for $\delta = 0.1$, $D_n= 1000$, $T_r= 10$, $m = 0$ and $\alpha = 0$.	78
	(b) Streamlines ψ (upper) and axial contour flow w (lower) in accordance with the solution curve in Fig.4.8a	79
Figure 4.9 :	(a) Solution curve: Flux Q versus Hall parameter m for $D_n= 500$, $T_r=10$, $M = 1$ and $\alpha = 0$ with curvatures $\delta = 0.01$, 0.1 and 0.5 .	79
	(b) Streamlines ψ (upper) and axial contour flow w (lower) in accordance with the solution curve in Fig.4.9a	80
Figure 4.10 :	(a) Solution curve: Flux Q versus Hall parameter m for $D_n= 1000$, $T_r=10$, $M = 1$ and $\alpha = 0$	81

	(b)	Streamlines ψ (upper) and axial contour flow w (lower) in accordance with the solution curve in Fig.4.10a	81
Figure 4.11 :	(a)	Solution curve: Flux Q versus Ion-slip parameter α for $D_n= 500, T_r=10, M = 1$ and $m = 5$ with curvatures $\delta = 0.01, 0.1$ and 0.5 .	82
	(b)	Streamlines ψ (upper) and axial contour flow w (lower) in accordance with the solution curve in Fig.4.9a.	82
Figure 4.12 :	(a)	Solution curve: Flux Q versus Ion-slip parameter α for $D_n= 1000, T_r=10, M = 1$ and $m = 5$.	83
	(b)	Streamlines ψ (upper) and axial contour flow w (lower) in accordance with the solution curve in Fig.4.12a.	83
Figure 4.13 :	(a)	Solution curve: Flux Q versus Taylor Number T_r for $D_n= 500, M = 0, m = 0$ and $\alpha=0$ with the curvature $\delta=0.1$.	85
	(b)-(f)	Magnifying figures marked by the dashed box on Fig.4.13a.	86
	(g)	Streamlines ψ (upper) and axial contour flow w (lower) in accordance with the solution curve in Fig.4.13a.	88
	(h)	Vortex number of secondary flows versus Taylor number T_r with curvature $\delta=0.1$ and for fixed values of the parameter $D_n = 500, M = 0, m = 0$ and $\alpha = 0$.	88
Figure 4.14 :	(a)	Solution curve: Flux Q versus Taylor Number T_r for $D_n= 500, M = 0, m = 0$ and $\alpha=0$ with the curvature $\delta=0.5$.	89
	(b)	Magnifying figure marked by the dashed box on Fig.4.14a.	89
	(c)	Streamlines ψ (upper) and axial contour flow w (lower) in accordance with the solution curve in Fig.4.14a.	90
	(d)	Vortex number of secondary flows versus Taylor number T_r with curvature $\delta=0.5$ and fixed values of the parameter $D_n = 500, M = 0, m = 0$ and $\alpha = 0$.	90
Figure 4.15 :	(a)	Solution curve: Flux Q versus Dean Number D_n for $T_r= 20, M = 0, m = 0$ and $\alpha=0$ with the curvature $\delta=0.1$.	91
	(b)	Streamlines ψ (upper) and axial contour flow w (lower) in accordance with the solution curve in Fig.4.15a.	91
Figure 4.16 :	(a)	Solution curve: Flux Q versus magnetic parameter M for $T_r= 20, m = 0$ and $\alpha=0$.	93
	(b)	Streamlines ψ (upper) and axial contour flow w (lower) in accordance with the solution curve in Fig.4.16a.	93
Figure 4.17 :	(a)	Solution curve: Flux Q versus Hall parameter m for $T_r= 20, M = 1$ and $\alpha=0$.	95
	(b)	Streamlines ψ (upper) and axial contour flow w (lower) in accordance with the solution curve in Fig.4.17a.	95

Figure 4.18 :	(a)	Solution curve: Flux Q versus Ion-slip parameter α for $T_r = 20, M = 1$ and $m = 5$.	96
	(b)	Streamlines ψ (upper) and axial contour flow w (lower) in accordance with the solution curve in Fig.4.18a.	97
Figure 4.19 :	(a)	Solution curve: Flux Q versus Taylor Number T_r for $D_n = 500, M = 0, m = 0$ and $\alpha = 0$ with the curvature $\delta = 0.1$.	100
	(b)	Magnifying figures marked by the dashed box from (i) to (v) on Fig. 4.19a.	100
	(c)	Streamlines ψ (upper) and axial contour flow w (lower) in accordance with the solution curve in Fig.4.19a.	101
Figure 4.20 :	(a)	Solution curve: Flux Q versus Dean Number D_n for $T_r = 20, M = 0, m = 0$ and $\alpha = 0$ with the curvature $\delta = 0.1$.	102
	(b)	Magnifying figures marked by the dashed box from (i) to (iv) on Fig.4.20a.	103
	(c)	Streamlines ψ (upper) and axial contour flow w (lower) in accordance with the solution curve in Fig.4.20a.	103
Figure 4.21 :	(a)	Solution curve: Flux Q versus magnetic parameter M .	105
	(b)	Streamlines ψ (upper) and axial contour flow w (lower) in accordance with the solution curve in Fig.4.21 a.	106
Figure 4.22 :	(a)	Solution curve: Flux Q versus Hall parameter m .	108
	(b)	Streamlines ψ (upper) and axial contour flow w (lower) in accordance with the solution curve in Fig.4.22a.	109
Figure 4.23 :	(a)	Solution curve: Flux Q versus Ion-slip parameter α .	111
	(b)	Streamlines ψ (upper) and axial contour flow w (lower) in accordance with the solution curve in Fig.4.23a.	113
Figure 5.1 :		Coordinate system of Curved duct with non-isothermal flow	117
	(a)	Aspect ratio 1 [Square cross-section]	
	(b)	Aspect ratio 2 [Rectangular cross-section]	
	(c)	Aspect ratio 3 [Rectangular cross-section]	
Figure 5.2 :		Comparison of the present numerical results with previous published results by the solution curves of the temperature.	121
Figure 5.3 :	(a)	Solution curve: Grashof number G_r versus (i) flux Q (ii) Mean Nusselt number Nu at the heating and cooling wall for fixed $\delta = 0.1, D_n = 500, T_r = 20, P_r = 7, M = 0, m = 0$ and $\alpha = 0$	124
	(b)	Streamlines ψ (upper) and axial contour flow w (lower) in accordance with the solution curve in Fig.5.3a.	124
Figure 5.4 :	(a)	Solution curve: Taylor number T_r versus (i) flux Q (ii) Mean Nusselt number Nu at the heating and cooling wall for fixed $\delta = 0.1, D_n = 1000, G_r = 100, P_r = 7, M = 0, m = 0$ and $\alpha = 0$	125

	(b)	Streamlines ψ (upper) and axial contour flow w (lower) in accordance with the solution curve in Fig.5.4a.	125
Figure 5.5 :	(a)	Solution curve: Dean Number D_n versus (i) flux Q (ii) Mean Nusselt number Nu at the heating and cooling wall for fixed $\delta=0.1$, $T_r= 20$, $G_r= 100$, $P_r= 7$, $M = 0$, $m = 0$ and $\alpha=0$.	126
	(b)	Magnifying figures marked by the dashed box on Fig.5.5a.	126
	(c)	Streamlines ψ (top), axial Contour flow w (middle) and Temperature profile T (bottom) in accordance with the solution curve in Fig. 5.5a.	127
Figure 5.6 :	(a)	Solution curve: Magnetic parameter M versus (i) flux Q (ii) Mean Nusselt number Nu at the heating and cooling wall for fixed $\delta=0.1$, $G_r= 100$, $T_r= 20$, $P_r= 7$, $m = 0$ and $\alpha=0$ where $D_n = 1000, 3000$ and 5000	128
	(b)	Streamlines ψ (top), axial Contour flow w (middle) and Temperature profile T (bottom) in accordance with the solution curve in Fig. 5.6a.	128
Figure 5.7 :	(a)	Solution curve: Hall parameter m versus (i) flux Q (ii) Mean Nusselt number Nu at the heating and cooling wall for fixed $\delta=0.1$, $G_r= 100$, $T_r= 20$, $P_r= 7$, $M = 1$ and $\alpha=0$ whereas $D_n = 1000, 3000$ and 5000	129
	(b)	Solution curve: Hall parameter m versus (i) flux Q (ii) Mean Nusselt number Nu at the heating and cooling wall for fixed $D_n=1000$, $G_r= 100$, $T_r= 20$, $P_r= 7$, $M = 1$ and $\alpha=0$ where $\delta = 0.01, 0.1$ and 0.5	130
	(c)	Streamlines ψ (top), axial Contour flow w (middle) and Temperature profile T (bottom) in accordance with the solution curve in Fig. 5.7a-b.	130
Figure 5.8 :	(a)	Solution curve: Ion-slip parameter α versus flux Q for the velocity at the Dean Number (i) $D_n=1000$ (ii) $D_n=3000$ (iii) $D_n=5000$ and (iv) Ion-slip parameter α versus Nu at the heating and cooling wall for fixed $\delta=0.1$, $G_r= 100$, $T_r= 20$, $P_r= 7$, $M = 1$ and $m=5$.	131
	(b)	Solution curve: Ion-slip parameter α versus (i) flux Q (ii) Mean Nusselt number Nu at the heating and cooling wall for fixed $D_n=1000$, $G_r= 100$, $T_r= 20$, $P_r= 7$, $M = 1$ and $m=5$ where $\delta = 0.01, 0.1$ and 0.5 .	132
	(c)	Streamlines ψ (top), axial Contour flow w (middle) and Temperature profile T (bottom) in accordance with the solution curve in Fig.5.8a-b.	133
Figure 5.9 :	(a)	Solution Curve: Grashof number G_r versus (i) flux Q (ii) Mean Nusselt number Nu at the heating and cooling wall for fixed $\delta=0.1$, $D_n=500$, $T_r= 20$, $P_r= 7$, $M = 0$ and	135

$m=5$ and $\alpha=20$.

	(b)	Streamlines ψ (top), axial Contour flow w (middle) and Temperature profile T (bottom) in accordance with the solution curve in Fig.5.9a.	136
Figure 5.10 :	(a)	Solution Curve: Taylor number G_r versus (i) flux Q (ii) Mean Nusselt number Nu at the heating and cooling wall for fixed $\delta=0.1$, $D_n=500$, $G_r = 100$, $P_r= 7$, $M = 0$ and $m=0$ and $\alpha= 0$.	137
	(b)	Magnifying figure marked by the dashed box on Fig. 5.10a	137
	(c)	Streamlines ψ (top), axial Contour flow w (middle) and Temperature profile T (bottom) in accordance with the solution curve in Fig. 5.10a.	138
Figure 5.11 :	(a)	Solution Curve: (i)-(iii) Dean Number D_n versus flux Q (iv)-(vi) Dean Number D_n versus Mean Nusselt number Nu at the heating and cooling wall for fixed $\delta=0.1$, $G_r = 100$, $P_r= 7$, $M = 0$ and $m=0$ and $\alpha= 0$.	138
	(b)	Magnifying figure marked by the dashed box on Fig. 5.11.a(iii).	139
	(c)	Streamlines ψ (top), axial Contour flow w (middle) and Temperature profile T (bottom) in accordance with the solution curve in Fig.5.11a.	140
Figure 5.12 :	(a)	Solution Curve: Magnetic parameter M versus (i) flux Q (ii) Mean Nusselt number Nu at the heating and cooling wall for the Case-I : $\delta=0.01$, $D_n= 500$; Case-II : $\delta=0.1$, $D_n= 500$; Case-III : $\delta=0.5$, $D_n= 1000$; with fixed $G_r = 100$, $T_r = 20$, $P_r=7$, $M = 0$ and $m=0$ and $\alpha=0$.	141
	(b)	Streamlines ψ (top), axial Contour flow w (middle) and Temperature profile T (bottom) in accordance with the solution curve in Fig.5.12a.	142
Figure 5.13 :	(a)	Solution Curve: Hall parameter m versus (i) flux Q (ii) Mean Nusselt number Nu at the heating and cooling wall for the Case-I : $\delta=0.01$, $D_n= 500$; Case-II : $\delta=0.1$, $D_n= 500$; Case-III : $\delta=0.5$, $D_n= 1000$; with fixed $G_r= 100$, $T_r=20$, $P_r= 7$, $M = 0$ and $M=4$ and $\alpha= 0$.	143
	(b)	Streamlines ψ (top), axial Contour flow w (middle) and Temperature profile T (bottom) in accordance with the solution curve in Fig.5.13a.	144
Figure 5.14 :	(a)	Solution Curve: Ion-slip parameter α versus (i) flux Q (ii) Mean Nusselt number Nu at the heating and cooling wall for the Case-I : $\delta=0.01$, $D_n= 500$; Case-II : $\delta=0.1$, $D_n= 500$; Case-III : $\delta=0.5$, $D_n= 1000$; with fixed $G_r=100$, $T_r=20$, $P_r=7$, $M = 0$ and $M=4$ and $m= 1$.	145

	(b)	Streamlines ψ (top), axial Contour flow w (middle) and Temperature profile T (bottom) in accordance with the solution curve in Fig.5.14a.	146
Figure 5.15 :	(a)	Solution curve: Grashof Number G_r versus (i) flux Q (ii) Mean Nusselt number Nu at the heating and cooling wall for fixed $\delta=0.1$, $T_r= 20$, $D_n= 300$, $P_r= 7$, $M = 0$, $m = 0$ and $\alpha=0$.	149
	(b)	Streamlines ψ (top), axial Contour flow w (middle) and Temperature profile T (bottom) in accordance with the solution curve in Fig.5.15a.	149
Figure 5.16 :	(a)	Solution curve: Taylor Number T_r versus (i) flux Q (ii) Mean Nusselt number Nu at the heating and cooling wall for fixed $\delta=0.1$, $G_r= 100$, $D_n= 300$, $P_r= 7$, $M = 0$, $m = 0$ and $\alpha=0$.	150
	(b)	Streamlines ψ (top), axial Contour flow w (middle) and Temperature profile T (bottom) in accordance with the solution curve in Fig.5.16a.	150
Figure 5.17 :	(a)	Solution curve: Dean Number D_n versus (i) flux Q (ii) Mean Nusselt number Nu at the heating and cooling wall for fixed $\delta=0.1$, $T_r= 20$, $G_r= 100$, $P_r= 7$, $M = 0$, $m = 0$ and $\alpha=0$.	151
	(b)	Streamlines ψ (top), axial Contour flow w (middle) and Temperature profile T (bottom) in accordance with the solution curve in Fig.5.17a.	151
Figure 5.18 :	(a)	Solution curve: Magnetic parameter M versus (i) flux Q (ii) Mean Nusselt number Nu at the heating and cooling wall for fixed $\delta=0.1$, $D_n= 300$, $T_r= 20$, $G_r= 100$, $P_r= 7$, $m = 0$ and $\alpha=0$.	152
	(b)	Streamlines ψ (top), axial Contour flow w (middle) and Temperature profile T (bottom) in accordance with the solution curve in Fig.5.18a.	153
Figure 5.19 :	(a)	Solution curve: Hall parameter m versus (i) flux Q (ii) Mean Nusselt number Nu at the heating and cooling wall for fixed $\delta=0.1$, $D_n= 300$, $T_r= 20$, $G_r= 100$, $P_r= 7$, $M = 5$ and $\alpha=0$	154
	(b)	Streamlines ψ (top), axial Contour flow w (middle) and Temperature profile T (bottom) in accordance with the solution curve in Fig.5.19a.	154
Figure 5.20 :	(a)	Solution curve: Ion-slip parameter α versus (i) flux Q (ii) Mean Nusselt number Nu at the heating and cooling wall for fixed $\delta=0.1$, $D_n= 300$, $T_r= 20$, $G_r= 100$, $P_r= 7$, $M = 5$ and $m=1$.	155
	(b)	Streamlines ψ (top), axial Contour flow w (middle) and Temperature profile T (bottom) in accordance with the solution curve in Fig.5.20a.	155

Figure 6.1 :	Geometrical model of straight duct	156
Figure 6.2 :	Geometrical model of the present straight square duct	160
Figure 6.3 :	(a) Solution curve:Grashof Number G_r versus (i) flux $Q(ii)$ Mean Nusselt number Nu at the heating and cooling wall for fixed $D_n= 500, T_r= 20, P_r= 7, M = 0, m = 0$ and $\alpha=0$.	169
	(b) Streamlines ψ (top), axial Contour flow w (middle) and Temperature profile T (bottom) in accordance with the solution curvein Fig.6.3a.	170
Figure 6.4 :	(a) Solution curve: Taylor Number T_r versus (i) flux $Q(ii)$ Mean Nusselt number Nu at the heating and cooling wall for fixed $D_n= 10000, G_r= 200, P_r= 7, M = 0, m = 0$ and $\alpha=0$.	171
	(b) Streamlines ψ (top), axial Contour flow w (middle) and Temperature profile T (bottom) in accordance with the solution curvein Fig.6.4a.	171
Figure 6.5 :	(a) Solution curve: Dean Number D_n versus (i) flux $Q(ii)$ Mean Nusselt number Nu at the heating and cooling wall for fixed $T_r= 20, G_r= 200, P_r= 7, M = 0, m = 0$ and $\alpha=0$.	172
	(b) Streamlines ψ (top), axial Contour flow w (middle) and Temperature profile T (bottom) in accordance with the solution curvein Fig.6.5a.	172
Figure 6.6 :	(a) Solution curve: Magnetic parameter M versus (i) flux $Q(ii)$ Mean Nusselt number Nu at the heating and cooling wall for fixed $T_r= 20, G_r= 200, P_r= 7, m = 0$ and $\alpha=0$ where $D_n = 500, 5000 ,10000$.	173
	(b) Streamlines ψ (top), axial Contour flow w (middle) and Temperature profile T (bottom) in accordance with the solution curvein Fig.5.18a.	174
Figure 6.7 :	(a) Solution curve: Hall parameter m versus (i) flux $Q(ii)$ Mean Nusselt number Nu at the heating and cooling wall for fixed $T_r= 20, G_r= 200, P_r= 7, M= 13$ and $\alpha=0$ where $D_n = 500, 5000 ,10000$.	174
	(b) Streamlines ψ (top), axial Contour flow w (middle) and Temperature profile T (bottom) in accordance with the solution curvein Fig.6.7a.	175
Figure 6.8 :	(a) Solution curve: Ion-slip parameter α versus (i) flux $Q(ii)$ Mean Nusselt number Nu at the heating and cooling wall for fixed $T_r= 20, G_r= 200, P_r= 7, M= 13$ and $m=0.1$ where $D_n = 500, 5000 ,10000$.	176
	(b) Streamlines ψ (top), axial Contour flow w (middle) and Temperature profile T (bottom) in accordance with the solution curvein Fig.6.8a.	177

Dissertation Contents

Applying Hall and Ion-slip currents to the magnetic field within duct flow enhances the device's performance and enables more precise flow analysis. This is particularly valuable because the universe is predominantly filled with highly charged particles and enveloped by magnetic fields, offering a broad range of applications in technical and industrial sectors. With this perspective in mind, the aim is to explore dissertation articles with the following titles:

1. Md. Rafiqul Islam, Md. Abdus Samad and Md. Mahmud Alam (2021). "Hall and Ion-slip current effects on steady fluid flow through a rotating curved square duct with magnetic field." *The European Physical Journal Plus*, 136:1204. <https://doi.org/10.1140/epjp/s13360-021-02130-3>. Submitted: 13 August 2021 ; Accepted: 28 October 2021; Published Online: 02 December 2021. Publisher: Springer-Verlag GmbH, Germany.
2. Md. Rafiqul Islam, Md. Abdus Samad and Md. Mahmud Alam(2021). "Steady MHD Fluid Flow in a Rotating Curved Rectangular Duct with Hall and Ion-slip Current." *Ricerche di Matematica*, <https://doi.org/10.1007/s11587-021-00668-z>. Submitted: 11 August 2021 ; Accepted: 21 October 2021; Published Online: 19 November 2021. Publisher: Springer, Italy.
3. Md. Rafiqul Islam, Md. Abdus Samad and Md. Mahmud Alam(2022). "Hall and Ion-slip effects on MHD fluid flow in a rotating curved duct with aspect ratio 3." *AIP Advances*, Vol.12, Issue-1. <https://doi.org/10.1063/5.0063681>. Submitted: 16 July 2021 ; Accepted: 7 November 2021; Published Online: 03 January 2022. Publisher: American Institute of Physics (AIP), USA.
4. Md. Rafiqul Islam, Md. Abdus Samad and Md. Mahmud Alam(2022). "Non-Isothermal magnetohydrodynamic fluid flow along the centerline in a rotating curved square duct with Hall and ion-slip current." *AIP Advances*, Vol.12, Issue-6. <https://doi.org/10.1063/5.0088377>. Submitted: 16 February 2022 ; Accepted: 7 June 2022; Published Online: 29 June 2022. Publisher: American Institute of Physics (AIP), USA.
5. Md. Rafiqul Islam, Md. Abdus Samad and Md. Mahmud Alam (2022). "Hall and Ion-slip Current Effects on Non-Isothermal Steady Flow through a Rotating Curved Rectangular Duct with Aspect Ratio of 2." *Journal of the Egyptian Mathematical Society*, Publisher: Springer, Egypt. Submitted but not yet published.
6. Md. Rafiqul Islam, Md. Abdus Samad and Md. Mahmud Alam (2022). "Non-Isothermal Fluid Flow through a Rotating Curved Duct with Aspect Ratio of 3 in the Presence of Magnetic Field, Hall, and Ion-slip Currents." *European Journal of Engineering and Technology Research*, Vol.7 Issue-3, Belgium. <https://dx.doi.org/10.24018/ejeng.2022.7.3.2829>. Submitted: 28 May 2022; Accepted: 22 June 2022; Published: 27 June 2022. Publisher: European Open Science Publishing, United Kingdom.
7. Md. Rafiqul Islam, Md. Abdus Samad and Md. Mahmud Alam (2022). "Non-Isothermal Steady Flow through a Rotating Square Straight Duct with Hall and Ion-slip Currents." It has not yet been submitted, it is progressing for submission.

The structure of the current dissertation is as follows:

Chapter 1: Available information on square and rectangular curved duct, bifurcation phenomena, rotating curved duct, Heat transfer in curved duct, Hall current and Ion-slip and various parameter effects are summarized and discussed from both analytical and numerical points of view. **Chapter 2:** The usual governing equations and relevant to the problems are discussed. In addition, several basic concepts and relationships are addressed in depth in order to put the governing equations in their standard form for numerical solutions. **Chapter 3:** the methods of solution for resolving the fundamental equations were introduced in Chapter 2. **Chapter 4:** A specific problem of curved duct flow in a rotating isothermal with Hall and Ion-slip current is examined for the aspect ratios of 1, 2, and 3. **Chapter 5:** The same problem for a non-isothermal system of the curved duct has been extended for the aspect ratios of 1, 2, and 3 are considered. **Chapter 6:** The problem of a non-isothermal steady flow through a rotating square straight duct with Hall and Ion-slip currents has been investigated in this section. Finally, general discussions and conclusions on all the problems dealt are given in **Chapter 7**.

Nomenclature

\mathbf{B}	: Magnetic field	l	: Duct cross-sectional aspect ratio
\mathbf{q}	: Fluid velocity	ω_e	: Cyclotron frequency
\mathbf{J}	: Current density	τ_e	: Electron collision time
g	: Acceleration due to the gravity	T	: Fluid temperature
Ω	: Angular velocity	T_0	: Temperature at centre of the duct
B_0	: Constant magnetic induction along y -axis	ΔT	: Temperature difference
x	: Dimensional horizontal axis	Ψ	: Stream function
y	: Dimensional vertical axis	x'	: Non-dimensional horizontal axis
z	: Dimensional axial variable along the main flow	\bar{y}	: Non-dimensional vertical axis
r	: Dimensional radial variable along x -axis	z'	: Non-dimensional axial variable
θ	: Dimensional circumferential angle	u'	: Non-dimensional velocity component along x -direction
u	: Dimensional velocity component along x -direction	v'	: Non-dimensional velocity component along y -direction
v	: Dimensional velocity component along y -direction	w'	: Non-dimensional velocity component along z -direction
w	: Dimensional velocity components along z -direction	p'	: Non-dimensional pressure
p	: Dimensional pressure	D_n	: Dimensionless Dean number
\mathcal{U}	: Kinematic viscosity	G	: Dimensionless mean pressure gradient
h	: Half height of the cross section	G_r	: Grashof number
d	: Half width of the cross section	T_r	: Taylor number
δ	: Curvature of the duct	P_r	: Prandtl number
L	: Radius of the duct curvature	M	: Magnetic parameter
β	: Coefficient of thermal expansion	m	: Hall parameter
k	: Thermal conductivity	α	: Ion-slip parameter
ρ	: Density of the fluid	Nu	: Nusselt number
σ	: Fluid conductivity	Nu_c	: Nusselt number at cooling plate
C_p	: Specific heat at the const. Pressure	Nu_h	: Nusselt number at heating plate
		\bar{M}	: Truncation numbers in x -direction
		\bar{N}	: Truncation numbers in y -direction

Chapter 1

Literature Review

1.1 Introduction

One of the most challenging research domains within the electromagnetic field pertains to understanding the fluid flow mechanisms in ducts within a rotating system. These systems have been used in technical applications such as gas turbine fluid transportation, Heating, Ventilation, and Air Conditioning (HVAC) Systems, turbo-machinery, Automotive Industry, refrigeration, electric generators, heat exchangers, medical ventilators, centrifugal pumps, internal combustion engines, blood Flow Modelling, blade-to-blade passages for modern gas turbines, etc. The dynamic behaviour of fluids within rotating curved ducts has captivated the attention of numerous scientists. Early research on duct fluid flow by Williams et al.(1902), Eustice (1910, 1911, 1925), and Dean(1927, 1928) served as its foundation. As a pioneer author, Dean (1927) was the first to analytically articulate the problem of curved duct fluid flow and demonstrate the existence of a pair of counter-rotating vortices flowing in this duct under fully developed flow. This flow phenomenon is commonly referred to as Dean Flow, and it is also known as Dean Hydrodynamic Instability, with the associated vortices termed Dean Vortices. Over the ensuing decades, researchers delved into the theoretical, mathematical, and empirical exploration of fluid flow within both straight and curved ducts. Here, we provide a brief reference to the scientific contributions of other renowned researchers in this field.

Miyazaki (1973)examined the phenomenon where duct curvature enhances the Coriolis force, causing rotation to align with the direction of fluid flow, referred to as co-rotation. The term 'counter-rotation' denotes a rotational direction opposing the fluid flow. Berger et al. (1983) extensively investigated fully developed flow in curved pipes, encompassing both stable and unstable states, exploring the influence of diverse geometries, wall properties, and fluid characteristics. Nandakumar and Masliyah (1982, 1986) delved into bifurcation within steady laminar flow in curved pipes, alongside heat-transferable vortex flow in coiled and curved tubes. Chandratilleke et al. (2003, 2012, 2013) focused on secondary vortex structures within fluid flow through curved channels, considering laminar flow behaviour and thermal parameters. They also unveiled experimental results on secondary flow for varying aspect ratios. Winters (1987) presented a comprehensive framework that incorporated both symmetric and asymmetric solutions to investigate the laminar bifurcation flow within a curved tube featuring a rectangular cross-section. Ishigaki (1996) conducted a study focusing on the flow characteristics and friction factors in curved circular

ducts, considering both co-rotating and counter-rotating configurations. Wang and Yang (2003, 2004) carried out experimental and numerical investigations of fully developed free and forced convection flow within a rotating curved duct featuring a square cross-section. Yamamoto et al. (1999, 2000, 2006) observed viscous incompressible constant flow within a rotating system, examining square curved ducts and circular cross-sectional helical pipes. They also visualized the Taylor-Dean flow within a curved duct with a square cross-section, and their work included dual solutions derived using the spectral method. Yanase et al. (1989, 2002) scrutinized flow stability in slightly curved circular ducts. Their research also encompassed the study of laminar incompressible fluid flow within a rectangular curved duct, spanning a wide range of aspect ratios, with particular attention to a detailed investigation of the traveling-wave solution. In a more recent study, Lima and Alam (2019) explored the impact of Hall current on flow through a straight pipe in a rotating system, focusing on flow patterns in cases involving large aspect ratios.

Apart from the work of Lima and Alam (2019), no research on fluid flow through curved ducts in the presence of a magnetic field with Hall and Ion-slip currents was found on the websites or any archive. Therefore our interest is that, how to use Hall and Ion-slip current on the mechanical devise. From this angle of view, our goal is to investigate the impact of Hall and Ion-slip currents on steady fluid flow through a square, rectangular straight and curved duct with a magnetic field for the isothermal or non-isothermal state of the duct in a rotating system. From this perspective, the goal is to explore the following titles:

1. Hall and Ion-slip current effects on steady fluid flow through a rotating curved square duct with magnetic field.
2. Steady MHD Fluid Flow in a Rotating Curved Rectangular Duct with Hall and Ion-slip Current.
3. Hall and Ion-slip effects on MHD fluid flow in a rotating curved duct with aspect ratio 3.
4. Non-Isothermal MHD Fluid Flow along the Centre Line in a Rotating Curved Square Duct with Hall and Ion-slip Current.
5. Hall and Ion-slip Current Effects on Non-Isothermal Steady Fluid Flow Passes through a Rotating Curved Rectangular Duct with Aspect Ratio 2
6. Non-Isothermal Fluid Flow through a Rotating Curved Duct with Aspect Ratio of 3 in the Presence of Magnetic Field, Hall, and Ion-slip Currents.
7. Non-Isothermal Steady Flow through a Rotating Square Straight Duct with Hall and Ion-slip Currents

1.2 Bifurcation Phenomena in Curved Duct

After the experiments on water flow in curved pipes by Williams et al. (1902), Eustice (1910, 1911, 1925), as a pioneer author Dean (1927) first formulated the problem mathematically. He has been shown a pair of counter-rotating vortices of a Newtonian fluid flow exists in a curved pipe under the fully developed flow. Dean chose Poiseuille pipe flow as the leading term and used a perturbation technique to solve the problem. He estimated that the radius of curvature of the pipe was much larger than the hydraulic diameter of the cross-section. This assumption is known as the loose cooling approximation. Dean showed that the flow is characterized by a single non-dimensional parameter, now known as the Dean number.

Typically the Dean number is defined as $D_n = R_e \sqrt{d_h / 2R_c}$, where d_h is the hydraulic diameter of the pipe, R_c is the radius of the curvature and R_e is the Reynolds number. A perturbation analysis was used for flow in a curved duct with a square cross-section until the 1950s. Also, Ito (1951) and Cuming (1952) independently used the perturbation analysis and showed the existence of a 2-cell solution using the perturbation analysis. Manton (1971), Hall (1974), Murata et al. (1976), and Todd (1977, 1987) studied the steady laminar motion of the fluid theoretically through a pipe of circular cross-section while centreline of the tube varies locally. Todd's used three kinds of curved pipes for his experiment. Usually, in perturbation analysis, obtain a series of solutions where the solution is only valid for relatively low flow rates. But for higher Dean numbers, a full Numerical simulation is required to solve the governing equations. In the ducts with rectangular cross-sections, 4-cell flows have been predicted by Joseph et al. (1975), Ghia and Sokhey (1977), and De Vriend (1981). For rectangular cross-sections, Joseph et al. (1975), Sugiyama et al. (1983), Hille et al. (1985), and Masliyah (1980) provide experimental confirmation of these 4-cell solutions. For semi-circular ducts with a flat outer wall, Masliyah (1980) provides empirical proof and demonstrates the existence of a dual solution, or the presence of both 2-cell and 4-cell flows at the same Dean number by experimental and numerical evidence.

Collins and Dennis(1975) showed a 2-cell flow in a curved pipe by solving the Navier-Stokes equation. Their results have compared with Adler (1934) experiment, and they found a good agreement. Berger et al.(1983) discussed the boundary layer analysis for a large Dean number in detail. Cheng and Akiyama (1970) and Cheng et al. (1975) used a finite-difference formulation to show the 2-cell solution in a square duct. They also announced the existence of a new 4-vortex solution for the first time. Dennis (1980) applied a new finite difference method on the work of Baylis (1971) to find the steady solution of viscous fluid through a slight curve tube. He showed a second counter-rotating pair of vortices generated, which is smaller than the initial pair and shifted near the centre of the outer wall. Cheng et al. (1976) thought that due to a centrifugal instability, the second pair of vortices formed,

which are smaller than the vortices formed in flow between parallel curved plates Dean (1928). Masliyah (1980) investigated the flow in a curved duct of semi-circular cross-section with a flat outer wall. He showed a range of flow rates exist where 2-cell and 4-cell structure flows consist, and this range is the so-called dual solution region. Both Dennis and Ng (1982), Nandakumar and Masliyah (1982) exhibited the 4-cell flow structure numerically in a curved pipe and dual solution region. Thereafter, Yanase et al. (1988, 1989) studied the stability of the dual solution. They discovered the 2-cell flow to be stable and the 4-cell flow to be unstable to asymmetric disturbances.

It is established that the initial pair of vortices is induced by the pressure gradient force along the top and bottom walls. The additional vortex pair is indeed formed by centrifugal instability. Large vortices introduced by the side walls are called Ekman vortices, and vortices formed by centrifugal instability are called Dean or Taylor vortices, depending on the geometry.

The existence of multiple solutions is not surprising due to the non-linear nature of the Navier Stokes equation. The solution structure of a fully developed or axially irreversible flow is usually present in a bifurcation diagram, showing a characteristic quantity of flow, such as a fractional factor, a function of a control parameter, such as flow rate. Connecting different possible ways, a bifurcation curve or solution curve can consist of several lines (branches). These branches can split and show multiple solutions at the limit point. The concept and mathematical tools of this field have undergone significant development since the original work by Benjamin (1978a).

Yang and Keller (1986); Winters (1987); Daskopoulos and Lenhoff (1989) investigated several studies focusing on the solution structure of curved duct flow and showed that dual solution regions exist both in curved pipes and in curved square ducts. For curved pipe flow, the bifurcation diagram consists of a primary branch of 2-cell flows, starting at flow rate zero and continuing up to high flow rates. A branch of 4-cell solutions begins at a finite flow rate. It appears to be connected to the primary component through a pair of folds, although the upper boundary point is sensitive to grid refining and not accurately determined (Yang and Keller 1986; Daskopoulos and Lenhoff, 1989). Yang and Keller (1986) discovered unstable duct flow on several more branches, including 6-cell and 8-cell flows. Dennis and Riley (1991) studied the 2-cell flow for the limit $D_n \rightarrow \infty$. Their results suggest an asymptomatic solution consisting of an invisible core viscous boundary layer along the pipe wall. Shanthini and Nandakumar (1986) and Winters (1987) investigated the solution structure for the flow in a curved square duct. They showed the primary solution has a 2-cell flow in the branch where $D_n=131$ is confined to the point where the branch folds for a loosely coiled duct. After a second fold at $D_n=113$ the primary branch consists of 4-cell flows. There is a dual solution region between $D_n=131$ and $D_n=113$. A separate

secondary branch of 2-cell and 4-cell flows exists above a Dean number of 191. There is a slight change in the position of the limit points for the curvature ratio above 10, but the limit point of the small curvature ratio moves to an increasingly higher dean number. Winter determined the stability of the solutions and found that 2-cell solutions on both branches are stable. In contrast, the 4-cell flow on the primary branch is unstable concerning the symmetric perturbations. The solutions connecting the two limit points of the primary branch are unstable. Yanase and Nishiyama (1988) studied the bifurcation of a laminar flow at respect ratio equal to 3.02. They found dual solutions, one of which was a 2-cell solution and the other 4-cell solution for the aspect ratio greater than 3.02. Daskopoulos and Lenhoff (1989) extended their study of fully developed flows in a loosely coiled curved square tube up to Dean Numbers about 530. Starting with the perfect flow problem in an infinitely curved channel, they added stickiness to the cell boundary to turn each pair of cells into a curved duct of the rectangular cross-section. Daskopoulos and Lenhoff applied symmetry around the centre plane. They calculated 4 limit points in the secondary 2-cell branch and found three different states, including six vortices. The strength of the two additional rotations in each half of the domain is different. One of these 6-cell states was predicted to be stable for symmetrical disturbances.

Jayanti and Hewitt (1992) investigated the bifurcation structure of laminar flow in a curved tube with a square cross-section. They conducted studies on the effects of numerical accuracy on solutions. This studies have shown that as the Reynolds number of the flows increases, two vortex structures are re-established along a path, involving strongly asymmetric secondary flow patterns. Bara et al.(1992) determined the solutions on the primary branch, including the dual solution region experimentally. He inserted a pin in the radial direction along the line of symmetry at the inlet of the curved section to observe the 4-cell flows in the dual solution region. Though they are unstable concerning asymmetric perturbations, which indicates that growth rates of such asymmetric modes are small and asymmetric disturbances in his apparatus were small. The 4-cell flows can also be observed experimentally. Kao (1992) investigated the bifurcation structure of flow in curved ducts with super circular cross-sections to explain the transition of bifurcation structure with changing cross-sections. A super circular is defined by $\left(\frac{x}{a}\right)^n + \left(\frac{y}{a}\right)^n = 1$ and by baring the exponent n , cross-section range between a circle ($n=2$) and a square ($n\rightarrow\infty$). Kao could not locate the limit point accurately by using the finite difference method because he defined the Dean number in terms of pressure gradient rather than mean velocity by which the result cannot be compared directly. The two limit points of the primary branch move to a higher Dean number as the cross-section changes from a square to a circle. The first limit point, above which no stable 2-cell solution exists, moves to very high flow rates. Kao investigated that the limit point is out of the flow rates range for $n < 2.5$. Kao further

observed that the four solutions are established in the case of asymmetric perturbations by inserting a splitter plane into the stream near the outer wall.

Philip et al.(1996a) conducted a comprehensive investigation, they examined the steady development of incompressible Newtonian fluid flow within a curved duct featuring a square cross-section. This study involved both experimental and numerical approaches, it builds upon the previous research by Bara et al.(1992). The numerical simulations, based on the steady three-dimensional Navier-Stokes equation, provided insights into the emergence of a 6-cell secondary flow pattern. Notably, this 6-cell flow pattern was determined to be unconditionally unstable through numerical stability analysis, setting a critical threshold at a Dean number of 350. Notably, a numerical stability analysis revealed that this 6-cell flow state was inherently unstable. Building upon their foundational research, Philip et al.(1996b) extended their investigations in various directions. In one such extension, they explored the concept of a travelling wave state for incompressible Newtonian currents within the cross-sectional geometry of the curved square duct. In a separate extension, Philip et al.(1996c) delved into the realm of steady spatial oscillations occurring within a square cross-sectional curved duct. These efforts significantly advanced our comprehension of complex fluid flow phenomena within such geometries.

Collins and Dennis (1976a, 1976b) analyzed the flow of a viscous fluid in a region bounded by a right-angled isosceles triangle. The presence of vortices was first observed in the secondary flow at 45° angles of the cross-section. Subsequently made, a detailed study by modifying the grid size of the numerical scheme at all the corner regions. Thus it was possible to observe thirteen vortices at 45° corners and six pairs of vortices at 90° corners. Nandakumar et al.(1993) expressed the available numerical study on curved triangular ducts only. Takami and Sudou (1984), Topakoglu and Ebadain (1985, 1987), and Kotorynski (1986) investigated the flow in a curved pipe of an elliptical cross-section. Topakoglu and Ebadain used elliptical coordinates and followed the unprepared formulation of Topakoglu (1967). The results obtained were systematically plotted against the curvature of the curved pipe's centreline for different Reynolds number.

1.3 Developed Flow in Curved Channels

A few decades ago, many researchers studied on curved channel flows. Kelleher et al. (1980) experimented with the airflow in an 1800 curved channel with a curvature ratio of 47.5 and an aspect ratio of 40. To measure velocities at $\theta=135^\circ$, they used both a hot wire Anemometer and flow visualization with aerosol. The developing flow periodically oscillates with counter-rotating vortices at dean numbers between 78.8 and 112.8 over the entire width of the channels. Dean vortices results are obtained from centrifugal instability; these are similar to the mechanism that creates pairs of Dean Vortices in a square tube. They noted that time-dependent flows combined with stream-based periodic travelling

waves imposed on Dean Vortices for higher flow rates. The results are helpful to explain the phenomenon of travelling waves in a curved channel.

Guo and Finlay (1991) analyzed the two-dimensional Dean vortices stability concerning spanwise perturbations in a curved channel using a temporal formulation. If the number of spanwise waves is greater than the stable region, the two vortex pairs will merge; whereas this number is smaller than the stable region, the vortex pair will split into two vortices. All spanwise numbers of waves are unstable to span wise perturbations for $R_e > 1.5R_{rc}$. The nonlinear flow simulations confirmed their results. Clearly, span wise secondary fluctuations are of fundamental importance in the wave number selection process. Finlay et al. (1988) carried out a numerical investigation of travelling waves in a curved duct flow. They employed a three-dimensional time-dependent pseudospectral technique with spanwise and streamwise periodicity. They identified two varieties of travelling waves: long-wavelength undulating waves and short-wavelength twisting waves. Finlay et al. (1988) hypothesized that Kelleher et al. (1980) saw twisting vortices by contrasting the characteristics of the wavy flow phases. After that, Guo and Finlay (1994) used three-dimensional simulations and spatial stability theory to study the spanwise secondary instability theory of Dean and Gortler vortices. The identical versions of the parabolised Navier-Stokes equations are solved by them using the Legendre spectral method that was also used by Bara et al. (1992). It is easier to compare the results obtained from the spatial formulation with spatiality developing experimental observations. Spanwise was imposed on a few vortices periodically, allowing vortex splitting and aggregation to occur naturally.

Bottaro et al. (1991) studied the developing flow of air in a curved channel numerically and experimentally. The experimental setup has a 270° curved channel with a ratio of 29 and a simple inlet section which ensures a fully developed inlet flow. They used a hot wire Anemometer to measure the secondary velocity in cross-sections and define a perturbation velocity subtracting the secondary of the curved channel Poiseuille flow from the secondary velocity of vortex flow. The shape of Dean vortices can be seen clearly in Contour plots of the perturbation velocity and compared with a three-dimensional time-dependent simulation. However, the vortices develop 40° further downstream in the simulation. For the natural development of the computational domain of aspect ratio of 9, the spin-wise perturbation velocity initially increases linearly. After reaching a maximum state, it settles at a steady value; the vortices seem to have gone a fully developed form.

Matsson and Alfredson (1992) used the same equipment as Bottaro et al. (1991), and they investigated more experimental results on developing unsteady and steady curved channel flow. They analyzed the flow evolution at $D_n = 73,88,116$ and showed that the length of development of Dean vortices decreases with increasing flow rate. Flow velocity spanwise

profiles show minima in the flow region between the vortex pairs, which is consistent with Sugiyama et al. (1988) and Bara et al.(1992).

Bottaro (1993) investigated a full three-dimensional time-dependent elliptic simulation of developing vortices in a curve channel. He used steady Dean Vortices in the early linear stage as inlet flow and showed vortex splitting and merging events within the channel of curvature ratio of 38 and an aspect ratio of 9. When oscillating disturbances are present, dean vortices do not appear in their position, and unsteady interactions can occur between neighbouring vortex pairs. By imposing periodic boundary conditions the disturbances constantly return to the creek of the domain, destroying the convective nature of the flow.

The results of linear stability show that the number of waves selected at the linear growth rates is determined by the rate of increase of the initial instability. Several wavelengths can grow independently. Once the dominant wave number reaches the non-linear phase, it becomes unstable to span-wise secondary instability. Further down, the energy of the other wave numbers is transferred to this span-wise secondary instability. Finally, those wave number with the lowest span-wise secondary instability growth rate will be observed. Three-dimensional simulations show that span-wise secondary instability leads to vortex splitting and merging.

1.4 Developing Flow in Curved Pipes

A lot of work on flow development has been focused on curved pipes. As mentioned in Section 1.2(Bifurcation Phenomena), the dual solution region of the curved pipe is displayed at a very high flow rate so that the 4-cell flow in a curved pipe does not develop spontaneously. Three different approaches have been taken to the numerical investigation of developing flow in a curved pipe. Singh (1974) found a solution to perturbation the development of flow in a simple tube, which is valid only very close to the creek of a loose coiled pipe. The boundary layer method assumes that the flow consists of an inviscid core surrounded by a secondary flow boundary layer. As the flow rate increases, the secondary flow layer becomes thinner near the outer bend and thicker near the inner bend. The boundary layer near the inner bend eventually separates and interacts with the inviscid core.

Barua (1963), Ito (1969, 1970), Fargie and Martin (1971), Yao and Berger (1975, 1988), Smith(1976a, 1976b), Stewartson et al. (1980, 1982), and Yeung (1980) used boundary layer methods and they agreed with the friction factor prediction based on boundary layer models reasonably well with experimental data. Patankar et al. (1974), Humphrey *et al.* (1978, 7985), Soh and Berger(1984), and Snyder and Lovely (1990) performed a fully numerical solution of curved pipe flow; Adler (1934), Austin and Seader (1973), and Agarwall et al. (1978) presented these type of flow experimentally. These studies mainly concerned the boundary layer development and collision near the inner bend. Berger et al.

(1983) and Bara (1992) reviewed the development of curve pipe flow until 1990. Prata and Spalding (1975), Ghia and Sokhey (1977) numerically investigated developing flow in a rectangular curved duct using an ADI finite difference method. They used aspect ratios of 0.5, 1.0, and 2.0 and curvature ratios of 3, 14, and 100. Notably, a transition from 2-cell to 4-cell flow at $D_n=143$ has been observed in a square duct.

Lyne (1970) investigated the study of unsteady flow in curved tubes has generated a lot of interest due to their engineering applications to heat exchangers and chemical reactors as well as their applicability to hydro-dynamical issues (Pedley, 1980) or problems relating to blood flow in human arterial systems. Studies on periodic unstable flow in curved tubes have been conducted both theoretically and experimentally during the past few decades. Humphrey et al. (1977) studied the developing flow in a 90° bend with a curvature ratio of 2.3 at $D_n = 520$ both experimentally and numerically. The fully developed creek flow was strongly influenced by the elliptical effect of the downstream curved duct flow. As a result, a 2-cell secondary flow was already presented in the inlet plane. Secondary vortices in the inlet were up to 15% of the average stream wise velocity and about half the strength of the secondary flow velocity at $\theta=60^\circ$. Only two vortex flows were observed in both experimental and numerical simulations. Experimentally, Taylor et al. (1982) extended the work of Humphrey et al. (1977). They studied both laminar and turbulent flows at Dean Nos. 520 and 26000, respectively. At $D_n = 520$ the highest secondary flow velocities were observed at $\theta = 60^\circ$ with values of the order of $0.6 \bar{v}'_\theta$. They also observed a two vortex flow.

Yee et al. (1980) also investigated the developing flow of 90° bend with a curvature ratio of 2.3 by using a fully elliptic and a parabolic formulation. Heat transfer was included in this study, and they decided that a fully elliptic formulation is necessary to describe the flow accurately in this curved channel. Sugiyama et al. (1983) observed the 4-cell flow pattern in a square duct experimentally. They studied the development of flow in curved rectangular ducts with aspect ratios ranging from 0.5 to 2.5 and a radius of curvature between 5 and 8. Photographs of the visualization of smoke flow in the air were taken at the exit of 180° ducts. They observed a 2-cell state at $D_n=93$, a developing 4-cell state at $D_n=193$, and a fully developed 4-cell state at $D_n=183$ in the square duct. They investigated the smoke visualization pictures that were hard to interpret at higher flow rates, but it was looked like 2-cell states have developed for Dean Numbers 383 and 527. Sugiyama et al. (1983) observed the development of two pairs of Dean Vortices along the other wall of the duct, leading to 6 cell flow states at aspects of 2.0 and 2.5.

Hille et al. (1985) used the laser-Doppler anemometer to study the flow in an 180° bend with a curvature ratio of 6.45. They found a 4-cell flow structure for Dean Numbers between 150 and 300. The second pairs of vortices were symmetrical and smaller than those

observed by Sugiyama et al. (1983). The additional vortices are formed between $\theta = 108^\circ$ and $\theta = 171^\circ$, and the flow still develops at the end of 108° bend. Hille et al. (1985) observed a smooth transition between 2-cell and 4-cell flows without dual solution regions. Ohba et al. (1986), and Tsuda and Ohba (1984) examined the flow development in an 180° -degree curved square duct. They found that at Dean Numbers 217 and 435, where the irregular oscillations with a frequency of around 3 Hz occurred near the span wise centre line, almost midway between the centre and lateral walls, instantaneous velocity doublings and halving were present. Despite the physical impossibility of such instantaneous velocity doublings, Tsuda and Ohba (1984) could not account for the observed events.

Soh (1988) used a fully elliptic formulation of the steady Navier Stokes equations on the work of Hille et al.(1985) and showed the flow development in geometry. They found that the flow for $116.5 < D_n < 130.2$ evolved into one of two solutions that developed the inlet condition. Inlet flow evolved into a 4-cell state with a strong vortex pair for a free vortex pair, much like the 4-cell state calculated by Winters (1987). A much weaker second vortex pair develops with a 4-cell state with a fully developed one-dimensional, fully developed inlet flow. Both 4-cell flows appeared to be fully developed. The weak 4-cell has not been observed by any other researcher and may be a work of an artefact of the thick grid used by Soh (1988).

Sankar et al. (1988) used Patankar's method (Patankar, 1980) to solve a parabolised version of the steady three-dimensional Navier-Stokes equations and investigated the flow development in a curved square duct. They also showed the flow developed into the familiar 2-cell solution for a curvature ratio of 100 and Dean number up to 128. Initially, a 4-cell state was formed for $128 < D_n < 200$, but periodic spatial oscillations between 2-cell and 4-cell states were developed farther downstream. A pair of Dean vortices is periodically formed and destroyed during these spatial oscillations. Sankar et al. (1988) related the development of oscillations with flow asymmetry.

Sugiyama et al. (1988) studied another, more rigorous, flow development in a 270° curved rectangular duct with an aspect ratio of 2.0 and a curvature ratio of 8.0. They used smoke visualization in the air and a component laser-Doppler anemometer to measure three velocity components in this study. Both the flow visualization and the velocity measurement show the development of two pairs of Dean vortices. The onset of this vortex pair is around $\theta = 135^\circ$. Profiles of the streamwise velocity in the spanwise centre plane show two regions of low streamwise velocity, corresponding to the two in flow regions of the vortex pair. These flow zones transport fluids from the outer wall to the centre of the channel with a low flow velocity. As the strength of the two additional vortex pairs increases, they move toward the upper and lower corners along the outer wall. The Dean vortex pairs have folded up into the large Ekman vortices at $\theta=270^\circ$; as a result, it exhibited

a 2-cell flow. Due to the inherent difficulty in interpreting smoke visualization, there seems to be some discrepancy between flow visualization and LDA at $\theta = 225^\circ$ and $\theta = 270^\circ$. Miyake et al. (1988) and Kajishima et al. (1989) solved the elliptic Navier-Stokes equation using a finite difference method for the related study. Though the calculated patterns do not show the four Dean vortices, their simulation of the developing flow in a curved duct with an aspect ratio of 2 shows the development of two pairs of Dean vortices.

Finlay et al. (1993) has numerically investigated the interpretation of flow visualization. They compared simulated numerically smoke or dye patterns with spatially evolving secondary flow patterns calculated in curved channel flow, Görtler flow, and twisted square tube flow. They observed that if the stream wise variation of the secondary flow is small, smoke or dye visualization can represent the boundary flow patterns correctly. However, the secondary flow changes quickly with a stream wise position and it can be miss represented by smoke or dye.

Bara (1992) conducted a comprehensive investigation into developing flow within a curved square duct, specifically focusing on Dean Numbers up to 150. His study centred on a 2700 curved square duct with a curvature ratio of 15.1, utilizing both numerical simulations and experimental techniques. The experimental approach involved the use of a Laser-Doppler anemometer and dye-flow visualization in water. One of the key findings in Bara's research was the transition of flow states as Dean Numbers varied. At a Dean Number of 150, a fully developed 4-cell flow state was observed. However, this flow transitioned to a fully developed 2-cell state at Dean Number 125. Interestingly, an intermediate flow rate (Dean Number 137) caused the flow to develop toward a 4-cell state, which continued to evolve as the flow progressed along the 2700 duct. A notable feature of the 4-cell flow was the relatively low stream-wise velocity in the inflow region, particularly in the centre of the outer wall. Bara's investigations revealed that the length required to reach a fully developed 4-cell state decreased as the flow rate increased, a trend observed both in his numerical simulations and experimental findings.

Yanase (1991) succinctly noted that when examining the Dean number, in cases where a permanent steady solution is absent, the solution exhibits oscillations between the symmetric two-vortex and four-vortex solutions within the context of flow in a curved square duct. However, Yanase et al. (2002) conducted a numerical analysis to delve into the time-dependent behaviour of flow within a curved rectangular duct characterized by high aspect ratios. Their investigation involved calculating the temporal evolution of unstable solutions while considering both symmetry and asymmetry conditions. Their findings indicated that under symmetry conditions, periodic oscillations were achievable, but even in the absence of such symmetry conditions, periodic time evolutions were possible. Bara (1992) also observed for the first time the dual solution region, which was predicted by Winters (1987). A 4-cell flow state was induced for Dean Numbers between 114 and 131 by

inserting a pin along the symmetry line at $\theta=5^0$. The two-cell flow was observed in this region without pins. The pin reduces the development length of the 4-cell flow at a higher flow rate. Although 4-cells are unstable in the case of asymmetrical perturbations, they can be observed when asymmetrically small in the instrument. Sankar et al. (1988) used the developing flow code and calculated the numerical prediction, which agreed with the experimental results. And they have created a fully developed flow code by Shanthini and Nandakumar (1986). The results were consistent with the predictions of Winters (1987). Bara (1992) used the experimental apparatus that did not extend far enough to confirm the spatial oscillations predicted by Sankar et al. (1988). They considered that no unconditionally stable solution exists in a range above $D_n=131$. And Sankara's code did not include time dependence. Bara speculates that time-dependent solutions may develop for higher flow rates.

The developing flow in an 180^0 curved square tube with a curvature ratio of 3.36 was studied by Arnal et al. (1992). They measured the development of stream wise velocity in the line of symmetry for the dean number of 764. The finite difference elliptic calculations were compared well with the measure profiles. The development of two pairs of Dean Vortices at $\theta=135^0$ near the outer wall is shown by this model. Wang & Yang (2004, 2005a) investigated fully developed periodic oscillation in a curved square duct numerically and experimentally. In their experiment, flow visualization was done in the Dean number range of 50 to 500. They demonstrated, mathematically and experimentally, that there are no stable, steady flows and that the temporal oscillation occurs between symmetric and asymmetric 2-cell and 4-cell flows. Additionally, they demonstrated how the flow stability could alter along a solution branch without passing through the limit or bifurcation points. Wang and Yang (2005a) demonstrated through numerical simulation that physically feasible fully developed flows can evolve from a stable, steady symmetric 2-cell flow at lower Dean Numbers to a temporal periodic oscillation, an intermittent temporal oscillation, another fully developed flow, and more. Wang and Yang (2004) and Wang et al. (2005, 2006) carried out a numerical investigation into the stability of flow in a curved duct with a square cross-section and a fully developed bifurcation structure. Only 2-cell flows on the primary symmetric branch and a portion of the isolated symmetric branch were linearly stable, according to their thorough investigation into the solutions' linear stability. Even without reaching any bifurcation or limit points, it was found that the linear stability changed along with several of the solution branches.

1.5 Fully Developed Flows in Rectangular Curved Ducts

The aspect ratio of the duct is defined as the ratio of height and width of its cross-section. The aspect ratio of the square cross-sectional duct is one. Rectangular curved duct is defined by the choice of aspect ratios greater than one and it may be more effective in

explaining the flow characteristics than in square curved ducts. Most numerical work was done for infinite aspect ratio curved channels (no end walls). This hypothesis simplifies the numerical approach by allowing spanwise periodic boundary conditions. Experimental work cannot be done without end wall effects, but the impact of the wall can be minimized by using a channel with a large aspect ratio and observing the flow away from the end walls. Some studies specifically look at the recurrence between the Ekman vortex and the internal vortices on the last wall. The geometry of Dean number is defined as $R_e \frac{2d}{R_i + R_o}$, where d is the width of the duct and R_i and R_o are radius of the inner and outer walls respectively. R_e is defined as $v' \frac{d}{\nu}$, where v' is the average streamwise velocity. The flow between curved plates at a low rate is one-dimensional and strictly streamwise similar to plane channel flow. The streamwise velocity profile moves closer to the parabolic and towards the inner wall, and this flow is referred to as curved channel Poiseuille flow. In critical Dean numbers, the curved channel Poiseuille flow becomes centralized unstable, which leads to streamwise oriented counter-rotating Dean vortices. Dean (1928) was the first to determine the onset of such two-dimensional vortices and calculated the critical Dean number. Reid (1958) extended Dean's work. Brewster et al. (1959) observed Dean vortices experimentally in a channel with an aspect ratio of 35 and a curvature ratio of 12.5. Recently Finley (1989) determined the nonlinear equation of two-dimensional vortices in a curved channel with an infinite aspect ratio using weakly nonlinear perturbation analysis. The vortex flow was expanded as a perturbation of one dimensional curved channel Poiseuille flow. Thangam and Hur (1990) employed a finite volume method in their research. Their study was dedicated to the examination of fully developed flow within a rectangular duct, considering various aspect ratios, including γ values of 1, 2, 4, and 8. They reported 2-cell and 4-cell solutions for aspect ratios of 1, 2, and 4, and 8-cell flow for a duct with an aspect ratio of 8; but did not investigate the range of possible solutions in these geometries and their stability characteristics. The main focus is that the friction factor correlation is defined in terms of the modified dean number D_n/γ , which is valid for $10 \leq D_n \leq 1000$ and $1 \leq \gamma \leq 8$.

Cunff and Bottaro (1993) looked at the nature of the changes from twinning waves to undulating waves in curved channel flow. The one-dimensional streamwise velocity profiles were subjected to linear stability analysis, and the outcomes of the three-dimensional flow conditions were extrapolated. The stability of streamwise and spanwise profiles derived from a complete numerical simulation of steadily increasing Dean vortices was investigated by Cunff and Bottaro. The findings demonstrated that shear instability of the streamwise velocity's spanwise profiles causes twisting waves. Finlay and Nandakumar (1990) analyzed the onset of Dean vortices in curved rectangular channels with an aspect ratio ranging from 20 to 30. They used the finite difference method to show that the vortex pair appears first in the centre of the channel. As the flow rate increases, more vortices are formed towards the

end walls. The largest Ekman vortices near the upper and lower walls appear to have a damp effect on the inner cells resulting in a decrease in vortex amplitude away from the centre of the channel. In contrast, amplitude becomes more uniform with the increase of flow rate. Finley and Nandakumar attempted to derive a model of the vortex amplitude and spacing in the channel by using a Ginzburg-Landau model developed for Taylor-Couette flow. This model correctly describes the vortex amplitude as a function of the flow rate in the centre of the duct. However the model fails to describe the decreasing vortex amplitude near the end walls, mainly due to the effects of Ekman vortices. They point out that the fluid in the Taylor-Couette flow is driven equally over the entire span by the inner cylinder, and the last vortices derive the interior Taylor vortices. The streamwise pressure gradient in the curved channel flow does not effectively drain the fluid near the end wall, resulting in much larger boundary layers. These are just a weak interaction between the Dean vortices and Ekman vortices.

1.6 Rotating Duct

When a curved pipe rotates at a constant angular velocity about its axis of cylindrical symmetry, fluid flows through the ducts under both the Coriolis and a centrifugal force. Such rotating passages are used in cooling systems for conductors of electric generators and for cooling systems for generator motors of pump-storage stations. Ishigaki (1994) studied the fluid flow through a straight duct in a rotating system; in this case, the system is qualitatively similar to a centrifugal process and similar to the secondary flow of a stationary curved system. Barua (1955) and Benton and Baltimore (1956) performed the earliest flow work in a rotating straight pipe for the asymptotic limit of weak and strong rotation. They used perturbation expansion in the Hagen-Poiseuille flow. Mori and Nakayama (1965), Ito and Nanbu (1971), and Wanger and Velkoff (1972) showed an increase in friction factor with rotational speed. They found a good agreement with experiments for low rotational speed and high axial pressure gradient. Duck (1983) numerically studied the flow passes through a straight pipe rotated with circular cross-sections Mansour (1985) and Lei and Hsu (1990) did not reveal multiplicity features, although they recognized a substantial similarity between flows in curved pipes and on rotating tubes. Sharma and Nandakumar (1995) revealed the multiplicity feature in the numerical study on rotating straight pipes. Kheshgi and Scriven (1985), Nandakumar et al. (1991), Speziale (1982), Speziale and Thangam (1983) conducted an analysis of laminar flow within a straight pipe undergoing constant angular rotation around an axis perpendicular to its own. This study explored both square and rectangular cross-sectional geometries. Speziale (1982) presented a numerical investigation of flow within a rotating rectangular duct. Also Speziale and Thangam (1983) showed a transition from a two-cell to a four-cell structure occurs as the Rossby number is changed. Since pipelines have more or

less curved sections, it is interesting to investigate the combined effects of curvature and rotation, which is relevant to flow in a rotating curved duct.

Many experts on duct flow investigated the combined effects of curvature and system rotation on curved ducts. Hocking (1967) established a solution based on the Momentum Integral method. Miyazaki (1971, 1973) defined that when the pressure-driven flow and the sensation of rotation are in the same direction is called co-rotation. In contrast, the rotation is in the opposite direction of the pressure-driven flow is called the counter-rotation. Hoover et al. (1984); Wang and Cheng (1995); Daskopoulos and Lenhoff (1990) performed a reduction in the strength of the secondary flow and even a rotating curved duct. They showed the first and most comprehensive bifurcation study of the combined effects of curvature and rotation, and they have considered circular geometry. Selmi et al. (1994) used the Rossby number as a control parameter to present the bifurcation diagrams. They fixed the Ekman number at 0.01 and considered only a square cross-section in their study.

1.7 Heat Transfer in Curved Duct

In many engineering applications, the heat transfer of the fluid flow through curved ducts is crucial. Therefore, many scientists have attracted considerable attention to the heat transfer in curved duct fluid flow. These kinds of works have been done by the researchers such as Akiyama and Cheng (1974), Dravid et al. (1971), Berg and Bonilla (1950), Janssen and Hoogendroom (1978), Hausen (1943), Kalb and Seader (1972,1974), Kubair and Kuloor (1966), Mori and Nakayama (1965, 1967), Oliver and Asghar (1976), Owhadi et al. (1968), Patankar et al. (1974), Schimdt (1967), Simon et al. (1977), Singh and Bell (1974), Tarbell and Samuels (1973), Zapryanov et al. (1980). This mechanism has found application in various engineering fields, including heat exchangers, chemical reactors, gas turbines, and more. The characteristic of flow in curved ducts is the development of secondary flow, which increases the rate of heat and mass transfer, especially in the case of laminar flow. Due to their practical application in heat exchangers, extensive research has been conducted on conductive heat transfer in coiled pipes and finite elbows. The numerical method has been used to predict heat transfer rates on flow models.

Conductive heat transfer within curved pipes exhibits a distinctive characteristic – the average heat transfer rate surpasses that of a straight pipe at the same flow rate. This enhanced heat transfer is primarily attributed to additional mixing facilitated by the secondary flow. The total Nusselt number, a key parameter in heat transfer analysis, reaches its maximum at the outer bend due to localized stagnation-like flow patterns and also achieves its maximum at the inner bend due to the presence of reverse stagnation-like flow. In a significant study by Yao and Berger (1978), a series solution was derived for fully developed flow, particularly for cases with a small Dean number and the product of Re , Ra where Re is the Rayleigh number. For a horizontally oriented curved pipe, the interplay of

centrifugal and buoyancy forces results in the formation of two skewed vortices. These vortices can be conceptualized as the combination of two horizontal vortices induced by the centrifugal force and two vertical vortices generated by the buoyancy force. This complex flow pattern further contributes to the unique heat transfer characteristics observed in curved pipe systems. The effects of buoyancy on developing heat transfer on laminar flow in a curved square channel were initially studied by Chilukuri and Humphrey in (1981). In particular, Nusselt numbers and secondary flows with streamwise development differed notably in steady numerical projections made with buoyant forces in the primary and opposite directions.

McCormack et al. (1969) have shown that a significant effect of curved ducts might be enhancing heat exchange between two differently heated vertical sidewalls, which stimulates fluid mixing and heat transfer between secondary fluids. Prusa and Yao (1982) used a finite difference method to obtain a solution for a large Dean number, and R_e , R_a . They conducted a comparison between the mass flow rate within a heated curved pipe and that within a straight pipe, subject to the same axial pressure gradient. Their findings revealed that substantial overheating could intensify the secondary flow, increase flow resistance, and ultimately reduce the flow rate. Consequently, it was determined that, under identical axial pressure gradients, a heated curved pipe might be less effective as a heat transfer device when compared to a straight pipe. Additionally, Ganzarolli and Milanez (1995) and Calcagni et al.(2005) undertook both numerical and experimental investigations to explore transient and steady natural convection phenomena in a two-dimensional cavity symmetrically heated from both sides. Meanwhile, Das et al. (2002) delved into the examination of transient and steady natural convection phenomena in enclosures heated from below and symmetrically cooled from the sides. Komiyama (1984) provided computational methods to forecast fully developed Nusselt numbers and secondary flows in steady curved channel flow without buoyancy impacts. Boundary conditions with a steady heat flux were imposed, and channel aspect ratios ranged from 0.8 to 5. Anderson and Lauriat (1986) and November and Nansteel (1987) have independently conducted research on the phenomenon of natural convection within rectangular enclosures. In their studies, these researchers investigated situations where the enclosures were heated from below while being cooled from one side. Regarding transient steady-state natural convection in differential side heated cavities, several experimental and computational research have been published in the literature by Fusegi et al.(1991) and Schladow (1990).

Bejan (1995) demonstrated that natural convection phenomena could be divided into two general categories based on the geometry and orientation of the enclosures: bottom heated enclosures, which lead to the well-studied classical subject of Bernard flow, and side heated enclosures, which have attracted a lot of attention in recent years. Cheng and Akiyama (1970) and Mori et al. (1971) conducted numerical predictions for steady, fully developed

laminar forced convection in channels with uniform heat flux boundary conditions. Their numerical simulations successfully predicted stable, fully developed laminar forced convection in channels with uniform heat flow boundary conditions. Notably, both of these investigations provided clear evidence of secondary flow patterns in both velocity and temperature profiles. Laminar flow in a rectangular channel with concave heating was explored statistically by Chung and Hyun (1992). They demonstrated that hydrodynamics start to affect heat transmission beyond a certain point downstream of the initial curve. Ligrani et al.(1996) experimentally investigated heat transfer in transitional curved channel flow over a range of Dean numbers less than 300 with a channel aspect ratio of 0.979. They showed that secondary vortex formation is more affected by external heat than the inner wall of the passage. Yang and Chang (1994) investigated numerically combined free and forced convection for a flow developed in a heated curved pipe with an arbitrary curvature, mainly for $\kappa' > 0.2$, and demonstrated the existence of a dominant cell flow due to increased Buoyancy force and curvature.

In a rectangular enclosure that was heated from below and cooled from the top, Aydin et al. (1999) addressed the convection of air numerically. They looked into the effects of aspect ratio and Rayleigh number on flow patterns and energy transport. They discovered that the aspect ratio substantially influences the enclosure height, and the Rayleigh number is high. The effect of the Rayleigh number on heat transfer is mainly significant if the enclosure is shallow. Sturgis and Mudawar (1999) studied an experimental investigation to ensure single-phase heat transfer for flow in a rectangular curved channel under concave heat. They showed that the heat transfer in the curved channel increases with increasing velocity, but the fully developed thermal condition cannot be achieved when the heated curved section is left. Chandratilleke (2001) studied flow in a curved rectangular duct with external heat on the exterior wall experimentally. He demonstrated that secondary flow improves convective heat transfer significantly, especially when the Dean vortex emerges on the outside wall. Later, Chandratilleke and Nursubyakto (2003) conducted numerical research aimed at characterizing conductive heat transfer in the context of fully developed laminar flow through curved rectangular ducts with aspect ratios ranging from 1 to 8. The experimental data and numerical findings were found to be in good agreement.

Yanase et al.(2005a, 2005b) conducted numerical studies on both isothermal and non-isothermal flows through a curved rectangular duct. They discussed how secondary flow affected conductive heat transfer for heated vertical sidewalls. Mondal et al. (2006) analyzed non-isothermal flows through a curved square duct with a heated outside wall and a cooled inner wall numerically. The governing equations for curvature up to 0.5 and Dean Number up to 6000 were solved using the spectral method. The transition to a periodic or chaotic state is delayed in this study by increasing curvature. The Nusslet numbers are used to compute the horizontal heat transfer index. They discovered that convection caused by

secondary flow, which is aided by centrifugal force, considerably boosts heat transmission from the heated wall to the fluid.

1.8 Hall Current and Ion-slip

Magnetic fields have an impact on electrical currents. Current encounters resistance when a magnetic field is applied perpendicular to the direction of flow. The Hall Effect is a good indicator of how the Lorentz force operates in this situation. Hall Effect was given its name in 1879 by American physicist Edwin Hall. Hall Effect is the creation of voltage (sometimes referred to as Hall voltage) across a conductor that is perpendicular to both an applied magnetic field and an electric current. This Hall voltage difference in the conductor is referred to as Hall current, and the electrons and protons shifting sensations within the metallic conductor are called Ion-slip. The problem of magneto-hydrodynamic generators, Hall accelerators, and in-flight magneto aerodynamics are all essential engineering applications of Hall current with ion slip. Due to the fact that a large portion of the universe is filled with widely spaced charged particles and permeated by magnetic fields, the continuum assumption becomes applicable, and the MHD fluid flow regime with Hall and Ion-slip current is crucial in geophysics, astrophysics, and many engineering and industrial processes. Lima and Alam (2019) conducted a study exploring the flow characteristics within a straight duct with a significantly large aspect ratio, all within a rotating system. Their research specifically focused on examining the effects of Hall current on the flow dynamics.

1.9 Relevant Parameters Information and Their Significance

(a) Grashof number

Franz Grashof established the Grashof number as a non-dimensional quantity in fluid mechanics and heat convection. The ratio of buoyancy and viscous force that acts on a fluid flow within the boundary layer is defined as this dimensionless parameter. It plays a similar role in natural convection as the Reynolds number does in the forced convection.

According to the Grashof number's definition is denoted and defined by

$$\begin{aligned}
 G_r &= \frac{\text{Inertia forces} \times \text{Buoyancy forces}}{(\text{Viscous forces})^2} \\
 &= \frac{\rho v^2 L^2 \times \rho g L^3 \beta \Delta T}{(\mu L \nu)^2} \\
 \therefore G_r &= \frac{g L^3 \beta \Delta T}{\nu^2} \tag{1.1}
 \end{aligned}$$

Where: ρ is the density of fluid, B is the coefficient of expansion, ΔT is the temperature difference, μ is the dynamic viscosity and ν is the kinematic viscosity.

Significance of Grashof Number:

By calculating the Grashof number for a fluid in a curved duct, it can assess the relative importance of natural convection within that particular geometry. A high Grashof number indicates that natural convection effects are dominant, whereas a low Grashof number suggests that forced convection or other factors may be more significant for heat transfer.

(b) Dean Number

The curvature-induced secondary flow in a curved pipe or duct is described by a dimensionless number called the Dean number, sometimes known as Dean's coefficient. It is employed to explain how centrifugal forces and pressure gradient forces affect fluid flow in curved layouts. In general, higher Dean Numbers lead to a greater pressure drop through the curved duct.

Since our purpose is to seek the emergence of Dean vortices so we begin with the oldest definition of Dean number. The earliest definition of Dean Number κ is defined as

$$\kappa = 2\sqrt{\delta}R_e = \sqrt{\frac{d}{L}} \left(\frac{2d\bar{w}_0}{\nu} \right) \quad (1.2)$$

where, \bar{w}_0 is the mean axial velocity in the pipe and L is the radius of the duct curvature, while, the Dean number's original form was specified by Dean (1928) as

$$K = 2 \left(\frac{d}{L} \right) \left(\frac{dw_0}{\nu} \right)^2 \quad (1.3)$$

where w_0 is only considered as a constant with a velocity dimension. If we take $w_0 = \bar{w}_0$, then κ and K are related by $\kappa = \sqrt{2K}$.

For fully developed flow, in terms of dimensional form of the axial pressure gradient $\frac{1}{L} \frac{\partial p'}{\partial \theta} = -G$ is constant. It can be then defined a non-dimensional constant $C = \frac{Gd^2}{\mu w_0}$ and rewrite (1.3) as

$$K = 2 \left(\frac{d}{R} \right) \left(\frac{d}{\nu} \right)^2 w_0^2 = \frac{2d^3}{\nu^2 R} \left(\frac{Gd^2}{\mu C} \right)^2 \quad (1.4)$$

If we specify w_0 as the maximum velocity w_{\max} in a straight pipe of the same radius and pressure gradient as Dean (1928), it has been taken $C = 4$, and then equation (1.4) becomes

$$K = \frac{2d^3}{\nu^2 L} \left(\frac{Gd^2}{4\mu} \right)^2 = \frac{G^2 d^7}{8\mu^2 \nu^2 L} \quad (1.5)$$

However, if we just set $C = 1$, it becomes

$$K = \frac{2d^3}{\nu^2 L} \left(\frac{Gd^2}{\mu} \right)^2 \quad (1.6)$$

Most investigators have utilized not only all of the above forms of the Dean number since Dean's original work, but they have also used $2d$ instead of d , or vice versa, in curvature of

the duct $\delta = \frac{d}{L}$ and the definition of Reynolds number, or they have used κ^2 or K^2 instead of κ or K . This certainly causes a lot of uncertainty when reading and comprehending the literature. Van Dyke (1978) provides an excellent summary of the relationships between the various versions used in some of the most frequently referenced studies.

For experimental purposes, it's common for Dean numbers based on A , which represents the mean axial velocity, to be the preferred choice among researchers. This is because \bar{w}_0 , being easily observable, offers a more straightforward way to characterize the flow, as opposed to the more challenging measurement of pressure gradients. The choice between using a Dean number based on \bar{w}_0 or any of its variations rooted in G , such as equation (3), doesn't significantly impact the analysis of fully developed flow due to the constant factor, C . Starting with McConalogue and Srivastava (1968) and Nunge and Lin (1973) most theoretical and numerical investigators have used the square root of (5) and designated it by D for this flow.

$$D_n = \sqrt{\frac{2d^3}{v^2 L} \left(\frac{Gd^2}{\mu} \right)} = \frac{Gd^3}{\mu v} \sqrt{\frac{2d}{L}} \quad (1.7)$$

Significance of Dean Number:

The Dean number (D_n), also known as Dean's coefficient, is a dimensionless number that describes the curvature-induced secondary flow in a curved pipe or duct. It is used to describe how fluid flow in curved designs is impacted by centrifugal forces and pressure gradient forces. Generally there is a greater pressure drop through the curved duct with higher Dean Numbers.

(c) Taylor Number (T_r):

The Taylor number (T_r) is a dimensionless number that characterizes the relative importance of inertial forces to viscous forces in a rotating or curved fluid flow. It is particularly significant in the study of fluid dynamics involving curved ducts or pipes with rotation. Geoffrey Ingram Taylor created a dimensionless variable in 1923 that quantifies the relevance of centrifugal forces, also known as inertial forces, caused by fluid rotation around an axis. This number measures the influence of rotation on a convecting system. The scale of the conductive cell, the rate of rotation, and the kinematic viscosity all affect the Taylor number. It is denoted and defined by

$$T_r = \frac{2d^2 \Omega}{\nu} \sqrt{\frac{2}{\delta}} \quad (1.8)$$

where Ω is a characteristic angular velocity, δ is the curvature of the duct and ν is the kinematic viscosity.

Significance of Taylor Number:

The effects of Taylor Number on the curve duct flow means that the rotational affects on the flow. According to the properties of rotation parameter T_r ; positive T_r refers to the rotational direction of the system is similar with the direction of the fluid flow; this is called co-rotation. Whereas for negative T_r , the rotational direction is opposite to the direction of the flow, this is called counter-rotation.

(d) Prandtl Number

The Prandtl number affects how quickly heat moves through a curved duct. When compared to its momentum diffusivity, a low Prandtl number fluid (like air) has a high thermal diffusivity, which means that heat is transmitted more effectively than momentum. A high Prandtl number fluid, on the other hand, has reduced thermal diffusivity and less effective heat transmission because of this. The Prandtl number is a dimensionless number defined as the ratio of momentum diffusivity (kinematic viscosity) and thermal diffusivity and is named after the German scientist Ludwig Prandtl. It is denoted and defined as follows:

$$\begin{aligned} P_r &= \frac{\text{Momentum diffusivity}}{\text{Thermal diffusivity}} \\ &= \frac{\nu}{\alpha} = \frac{\nu}{k / (\rho c_p)} \\ \therefore P_r &= \frac{\rho \nu c_p}{k} \end{aligned} \tag{1.9}$$

where, ν is the momentum diffusivity (or kinematic viscosity),
 α is the thermal diffusivity, k is the thermal conductivity,
 c_p is the specific heat and ρ is the fluid density.

The impact of the fluid's viscosity is observed by the values of $\nu = \frac{\mu}{\rho}$. When the value of ν is small, it results in a narrower viscosity-affected zone, which is referred to as the boundary layer region for small ν . The thermal diffusivity due to heat conduction is represented by the value $\frac{k}{\rho c_p}$. The narrower region impacted by heat conduction was referred to as the thermal boundary layer region for small $\frac{k}{\rho c_p}$. The value of P_r eventually differs from fluid to fluid.

Significance of Prandtl Number:

The following table shows typical P_r ranges for common fluids.

Fluid	P_r
Liquid metals	0.004-0.03
Gases	0.7-1.0
Water	1.7-13.7
Light organic fluid	5-50
Oils	50-100000
Glycerine	2000-100000

Particularly for air at 20°C, $P_r = 0.71$ (approx.), for water at 20°C, $P_r = 7.0$ (approx.), for mercury at 20°C, $P_r = 0.044$ (approx.) but for viscous fluid it may be very large, e.g. for glycerine at 20°C, $P_r = 7250.0$ (approx.).

(e) Magnetic Parameter

The magnetic parameter is a dimensionless variable that describes the effects of a magnetic field on a conducting fluid flow through a curved duct or pipe in fluid dynamics, particularly in magneto-hydrodynamics (MHD). The relative relevance of magnetic forces compared to fluid dynamic forces is quantified. The magnetic parameter is defined as the ratio of electromagnetic force to inertia forces, which provides an approximation of a magnetic field's proportional impact on a flow. It is denoted and defined by

$$M = \frac{\text{Magnetic forces}}{\text{Inertia forces}} = \frac{d\sigma'\mu_e B_0^2}{\rho U_0} \quad (1.10)$$

Where: U_0 is the characteristic values of velocity, ρ is the characteristic values of density of fluid, d is the characteristic values of length, B_0 is the magnetic induction, σ' is the conductivity of the material and μ_e is the coefficient of viscosity.

But in our current research the non-dimensional uniform velocity is defined by $U_0 = \frac{v}{d}$

Therefore equation (10) modified as $M = \frac{d^2 \sigma' \mu_e B_0^2}{\rho v}$ (1.11)

Significance of Magnetic parameter:

In fluid dynamics, particularly in magneto-hydrodynamics (MHD), the magnetic parameter is a dimensionless quantity that explains the effects of a magnetic field on a conducting fluid flow via a curved duct or pipe. The main characteristic of the magnetic parameter is to measure the relative importance of the magnetic force compared to the fluid dynamic force.

(f) Nusselt Number (Nu)

A solid body and a fluid can transfer heat through convection, one of the fundamental mechanisms by which the convective heat transfer coefficient can be measured. The convective to conductive heat transfer ratio at a fluid boundary is defined as the Nusselt number (Nu). The Nusselt number is regulated by both the fluid's physical characteristics and the geometry of the heat transfer system. It is a dimensionless quantity that compares the actual heat transfer from a surface to the heat transfer that would be observed if only conduction could happen. It is frequently employed to gauge how much heat transport is aided by convection.

$$\text{The Nusselt number is defined as } Nu = \frac{hL}{k} \quad (1.12)$$

where, h is the convection heat transfer coefficient, L is the characteristic length, and k is the thermal conductivity of the fluid.

Another way to think of the Nusselt number is as a dimensionless temperature gradient at the surface. $Nu > 0$ denotes enhanced heat transmission from a solid body to a fluid, whereas $Nu < 0$ denotes enhanced heat transfer in the reverse direction.

(g) Hall Parameter (m)

The Hall parameter is a dimensionless number that characterizes the relative importance of the magnetic field to the fluid velocity in a magneto-hydrodynamic (MHD) flow. It is particularly relevant in situations where the magnetic field influences the behaviour of a conducting fluid. The Hall parameter is defined as:

$$\text{Hall Parameter } m = \frac{B \times L}{\rho \times v}$$

Where, B is the magnetic field strength.

L is a characteristic length scale of the flow

ρ is the fluid density.

v is the fluid velocity.

The Hall parameter relates the fluid velocity and the magnetic field strength, indicating how effectively the fluid motion induces a magnetic field. This can be relevant in applications such as plasma confinement, where the Hall effect contributes to magnetic field generation and containment. The Hall parameter is often used to determine the dominance of Hall effects in a magneto-hydrodynamic flow. Hall effects arise due to the interaction between the fluid's motion and the magnetic field. When the Hall parameter is significant, these effects can play a crucial role in the behaviour of the flow.

Significance of Hall Parameter:

The Hall parameter is a dimensionless number that characterizes the relative importance of the magnetic field to the fluid velocity in a magneto-hydrodynamic (MHD) flow. It is particularly relevant in situations where the magnetic field influences the behaviour of a conducting fluid.

(h) Ion-Slip Parameter (α)

The Ion-slip parameter (also known as the Ion-slip velocity) is a dimensionless quantity that characterizes the relative velocity between ions and neutrals in a plasma or ionized gas. It quantifies the degree to which ions, which are charged particles, slip or move independently of the neutrals, which are uncharged particles. The Ion-slip parameter is particularly significant in situations involving charged particle flows, such as in plasma dynamics or ionized gases. It is defined as:

$$\text{Ion-Slip Parameter } \alpha = \frac{v_i - v_n}{v}$$

where, v_i is the ion velocity (mean drift velocity).

v_n is the neutral velocity.

v is the characteristic flow velocity

The Ion-slip parameter affects the momentum transfer between ions and neutrals. When the Ion-slip parameter is significant, ions can have a distinct velocity from the neutrals, leading to differences in momentum exchange and flow behaviour.

In regions with strong Ion-slip effects, electric fields can develop due to the separation of charges. These electric fields, in turn, influence the overall flow behaviour and the distribution of charged particles.

In summary, the Ion-slip parameter is a key factor that influences the behaviour of ionized gases and plasmas. It affects momentum transfer, flow stability, electric fields, and various transport phenomena. Understanding the Ion-slip parameter is crucial for accurately modelling and predicting the behaviour of charged particle flows in a wide range of scientific and engineering contexts.

Significance of Ion-slip parameter:

The Ion-slip parameter (also known as the Ion-slip velocity) is a dimensionless quantity that characterizes the relative velocity between ions and neutrals in a plasma or ionized gas. It quantifies the degree to which ions, which are charged particles, slip or move independently of the neutrals, which are uncharged particles. The Ion-slip parameter is particularly significant in situations involving charged particle flows, such as in plasma dynamics or ionized gases.

Chapter 2

Basic Definitions and Governing Equations

2.1 Basic Definitions

2.1.1 Curvilinear Coordinates

Consider the Cartesian coordinate system (Figure 2.1) in a space and $P(x, y, z)$ be any point on it, which is the function of three independent single valued functions of u_1, u_2, u_3 defined by

$$\left. \begin{aligned} x &= x(u_1, u_2, u_3) \\ y &= y(u_1, u_2, u_3) \\ z &= z(u_1, u_2, u_3) \end{aligned} \right\} \quad (2.1)$$

Also assume that it's corresponding the Jacobean $\frac{\partial(x, y, z)}{\partial(u_1, u_2, u_3)} \neq 0$ so that the transformation (2.1) be invertible.

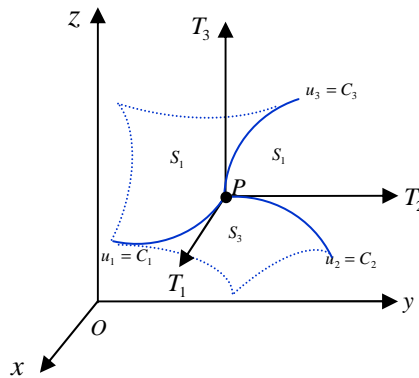


Figure 2.1: Cartesian with Curvilinear Coordinate system

Therefore the variables u_1, u_2, u_3 can be expressed as in terms of x, y, z ; that is

$$\left. \begin{aligned} u_1 &= u_1(x, y, z) \\ u_2 &= u_2(x, y, z) \\ u_3 &= u_3(x, y, z) \end{aligned} \right\} \quad (2.2)$$

Therefore for each point of $P(x, y, z)$, a unique set of new coordinates (u_1, u_2, u_3) has been found. This coordinate is called curvilinear coordinate of P .

If at each point P , the tangents PT_1, PT_2 and PT_3 are mutually perpendicular and parallel to the Cartesian coordinate axes, then (u_1, u_2, u_3) is called orthogonal curvilinear coordinate of P .

The curve $u_1 = C_1$, $u_2 = C_2$ and $u_3 = C_3$ are called the coordinate curves and the surfaces S_1 , S_2 and S_3 are generated by the pair of curves $u_2 = C_2$ & $u_3 = C_3$, $u_3 = C_3$ & $u_2 = C_2$ and $u_1 = C_1$ & $u_2 = C_2$ respectively.

The line element ds in Cartesian coordinates is given by

$$ds = \sqrt{(dx)^2 + (dy)^2 + (dz)^2} \quad (2.3)$$

Now by using (2.1), it is found that

$$\begin{aligned} dx &= \frac{\partial x}{\partial u_1} du_1 + \frac{\partial x}{\partial u_2} du_2 + \frac{\partial x}{\partial u_3} du_3 \\ dy &= \frac{\partial y}{\partial u_1} du_1 + \frac{\partial y}{\partial u_2} du_2 + \frac{\partial y}{\partial u_3} du_3 \\ dz &= \frac{\partial z}{\partial u_1} du_1 + \frac{\partial z}{\partial u_2} du_2 + \frac{\partial z}{\partial u_3} du_3 \end{aligned}$$

Substituting these values in (2.3), and using the orthogonal property of the curvilinear coordinate system, the coefficient of $du_1 du_2$, $du_2 du_3$, $du_3 du_1$ are zero. Therefore, it follows that

$$\begin{aligned} ds &= \sqrt{h_1^2 (du_1)^2 + h_2^2 (du_2)^2 + h_3^2 (du_3)^2} \quad (2.4) \\ \text{where, } \left. \begin{aligned} h_1 &= \left(\frac{\partial x}{\partial u_1} \right)^2 + \left(\frac{\partial y}{\partial u_1} \right)^2 + \left(\frac{\partial z}{\partial u_1} \right)^2 \\ h_2 &= \left(\frac{\partial x}{\partial u_2} \right)^2 + \left(\frac{\partial y}{\partial u_2} \right)^2 + \left(\frac{\partial z}{\partial u_2} \right)^2 \\ h_3 &= \left(\frac{\partial x}{\partial u_3} \right)^2 + \left(\frac{\partial y}{\partial u_3} \right)^2 + \left(\frac{\partial z}{\partial u_3} \right)^2 \end{aligned} \right\} \text{ are known as the scale factor.} \end{aligned}$$

Deduction (i): Rectangular Cartesian coordinate system (x, y, z)

$$\text{Here } (x, y, z) = (u_1, u_2, u_3)$$

$$\text{The line element } ds = \sqrt{(dx)^2 + (dy)^2 + (dz)^2} = \sqrt{h_1^2 (du_1)^2 + h_2^2 (du_2)^2 + h_3^2 (du_3)^2}.$$

$$\text{Or, } h_1 = h_2 = h_3 = 1 \quad \text{and} \quad (u_1, u_2, u_3) = (x, y, z).$$

Deduction (ii): Cylindrical coordinate system $P(r, \theta, z)$

Cylindrical coordinate (r, θ, z) is defined by

$$\begin{aligned} x &= r \cos \theta ; \quad y = r \sin \theta ; \quad z = z \\ r &\geq 0, \quad \theta \in [0, 2\pi] \text{ and } z \in (-\infty, \infty) ; \end{aligned}$$

$$\text{Now } dx = \frac{\partial x}{\partial u_1} du_1 + \frac{\partial x}{\partial u_2} du_2 + \frac{\partial x}{\partial u_3} du_3$$

$$\text{Here } (u_1, u_2, u_3) = (r, \theta, z)$$

$$\therefore dx = \frac{\partial x}{\partial r} dr + \frac{\partial x}{\partial \theta} d\theta + \frac{\partial x}{\partial z} dz$$

$$\text{Or, } dx = \cos \theta dr - r \sin \theta d\theta$$

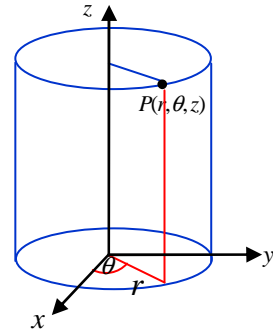


Figure 2.2: Cylindrical Coordinate System

Similarly, $dy = \sin \theta dr + r \cos \theta d\theta$
and $dz = dz$
 $\therefore (ds)^2 = (dx)^2 + (dy)^2 + (dz)^2$
 $= (\cos \theta dr - r \sin \theta d\theta)^2 + (\sin \theta dr + r \cos \theta d\theta)^2 + (dz)^2$
 $= \cos^2 \theta (dr)^2 - 2r \cos \theta \sin \theta dr d\theta + r^2 \sin^2 \theta (d\theta)^2$
 $+ \sin^2 \theta (dr)^2 + 2r \cos \theta \sin \theta dr d\theta + r^2 \cos^2 \theta (d\theta)^2 + (dz)^2$
 $= [\cos^2 \theta + \sin^2 \theta] (dr)^2 + r^2 [\sin^2 \theta + \cos^2 \theta] (d\theta)^2 + (dz)^2$
 $= (dr)^2 + (r d\theta)^2 + (dz)^2$
 $\equiv h_1^2 (du_1)^2 + h_2^2 (du_2)^2 + h_3^2 (du_3)^2$
Or, $h_1 = 1, h_2 = r, h_3 = 1$, and $(u_1, u_2, u_3) = (r, \theta, z)$

2.1.2 Gradient, Divergence Curl and Laplacian in Orthogonal Curvilinear Coordinates System

If ϕ is a scalar function and $\mathbf{A} = \hat{e}_1 A_1 + \hat{e}_2 A_2 + \hat{e}_3 A_3$ a vector function in a curvilinear coordinates u_1, u_2, u_3 it has been found the following results:

1. $\nabla \phi = \text{grad} \phi = \frac{1}{h_1} \frac{\partial \phi}{\partial u_1} \hat{e}_1 + \frac{1}{h_2} \frac{\partial \phi}{\partial u_2} \hat{e}_2 + \frac{1}{h_3} \frac{\partial \phi}{\partial u_3} \hat{e}_3$
2. $\nabla \cdot \mathbf{A} = \text{div} \mathbf{A} = \frac{1}{h_1 h_2 h_3} \left[\frac{\partial}{\partial u_1} (h_2 h_3 A_1) + \frac{\partial}{\partial u_2} (h_3 h_1 A_2) + \frac{\partial}{\partial u_3} (h_1 h_2 A_3) \right]$
3. $\nabla \wedge \mathbf{A} = \text{curl} \mathbf{A} = \frac{1}{h_1 h_2 h_3} \begin{vmatrix} h_1 \hat{e}_1 & h_2 \hat{e}_2 & h_3 \hat{e}_3 \\ \frac{\partial}{\partial u_1} & \frac{\partial}{\partial u_2} & \frac{\partial}{\partial u_3} \\ h_1 A_1 & h_2 A_2 & h_3 A_3 \end{vmatrix}$
4. $\nabla^2 \phi = \text{Laplacian of } \phi = \frac{1}{h_1 h_2 h_3} \left[\frac{\partial}{\partial u_1} \left(\frac{h_2 h_3}{h_1} \frac{\partial \phi}{\partial u_1} \right) + \frac{\partial}{\partial u_2} \left(\frac{h_3 h_1}{h_2} \frac{\partial \phi}{\partial u_2} \right) + \frac{\partial}{\partial u_3} \left(\frac{h_1 h_2}{h_3} \frac{\partial \phi}{\partial u_3} \right) \right]$

These reduces to the usual expression in rectangular coordinates if we replace (u_1, u_2, u_3) by (x, y, z) , in which case \hat{e}_1, \hat{e}_2 and \hat{e}_3 are replace by \hat{i}, \hat{j} and \hat{k} and $h_1 = h_2 = h_3 = 1$.

2.1.3 Hall and Ion-slip current

A magnetic field applied to a conductor that acts perpendicular to the current produces a voltage difference across the electrical conductor, this Hall voltage difference in the conductor is referred to as Hall current. It was discovered in 1879 by Edwin Hall.

Magnetic force $\mathbf{F}_m = q(\mathbf{v} \times \mathbf{B}) \Rightarrow F_m = |\mathbf{F}_m| = qv B \sin \theta$

where θ is the angle between \mathbf{v} and \mathbf{B} . Since $\theta = 90^\circ$ therefore $F_m = qv B$

Again, electrical force $\mathbf{F}_E = q\mathbf{E}$, But $\mathbf{E} = \frac{\mathbf{V}_H}{d}$

$$\therefore \mathbf{F}_E = q \frac{\mathbf{V}_H}{d} \quad \Rightarrow F_E = |\mathbf{F}_E| = \frac{qV_H}{d}$$

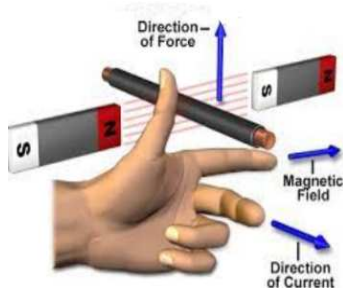


Figure 2.3a: Fleming's Left Hand Rules

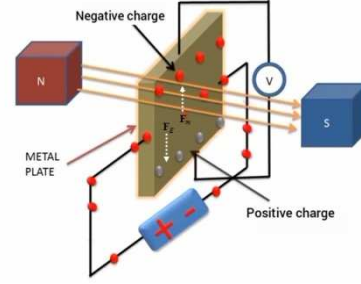


Figure 2.3b: Hall effects and Ion-slip

In equilibrium situation of these forces $\mathbf{F}_m = \mathbf{F}_E \Rightarrow |\mathbf{F}_m| = |\mathbf{F}_E|$

$$\Rightarrow qvB = q \frac{V_H}{d}$$

$$\therefore V_H = vBd$$

This is the Hall voltage; this phenomenon is called the Hall current effect, and Ion-slip refers to the changing sensations of electrons and protons within the metallic conductor.

2.2 Basic Governing Equations [Curved Duct]

The continuity equation for a viscous compressible fluid in vector form is given as follows:

$$\frac{\partial \rho}{\partial t} + \nabla \cdot (\rho \mathbf{q}) = 0$$

For incompressible fluid, this equation can be written as follows

$$\nabla \cdot \mathbf{q} = 0 \quad (2.5)$$

The Navier-Stokes equation for viscous compressible fluid with constant viscosity in vector form as follows

$$\frac{d\mathbf{q}}{dt} = \mathbf{F} - \frac{1}{\rho} \nabla p + \nu \nabla^2 \mathbf{q} + \frac{\nu}{3} \nabla (\nabla \cdot \mathbf{q})$$

$$\text{Or, } \frac{\partial \mathbf{q}}{\partial t} + (\mathbf{q} \cdot \nabla) \mathbf{q} = \mathbf{F} - \frac{1}{\rho} \nabla p + \nu \nabla^2 \mathbf{q} + \frac{\nu}{3} \nabla (\nabla \cdot \mathbf{q}) \quad (2.6)$$

Where, $\mathbf{q} = (u, v, w)$ is the fluid velocity vector, $\mathbf{F} = (F_1, F_2, F_3)$ is the body force, ρ is the fluid density, p is the fluid pressure and ν is the kinematics viscosity.

It is known that from the vector formula: $\nabla \wedge (\nabla \wedge \bar{A}) = \nabla (\nabla \cdot \bar{A}) - (\nabla \cdot \nabla) \bar{A}$

$$\therefore \nabla \wedge (\nabla \wedge \mathbf{q}) = \nabla (\nabla \cdot \mathbf{q}) - \nabla^2 \mathbf{q}$$

$$\text{Or, } \nabla^2 \mathbf{q} = \nabla (\nabla \cdot \mathbf{q}) - \nabla \wedge (\nabla \wedge \mathbf{q})$$

Then equation (2.6) becomes

$$\frac{\partial \mathbf{q}}{\partial t} + (\mathbf{q} \cdot \nabla) \mathbf{q} = \mathbf{F} - \frac{1}{\rho} \nabla p + \nu [\nabla (\nabla \cdot \mathbf{q}) - \nabla \wedge (\nabla \wedge \mathbf{q})] + \frac{\nu}{3} \nabla (\nabla \cdot \mathbf{q})$$

$$\begin{aligned} \text{Or, } \frac{\partial \mathbf{q}}{\partial t} + (\mathbf{q} \cdot \nabla) \mathbf{q} &= \mathbf{F} - \frac{1}{\rho} \nabla p + \nu \nabla (\nabla \cdot \mathbf{q}) - \nu \nabla \wedge (\nabla \wedge \mathbf{q}) + \frac{\nu}{3} \nabla (\nabla \cdot \mathbf{q}) \\ \therefore \frac{\partial \mathbf{q}}{\partial t} + (\mathbf{q} \cdot \nabla) \mathbf{q} &= \mathbf{F} - \frac{1}{\rho} \nabla p + \frac{4}{3} \nu \nabla (\nabla \cdot \mathbf{q}) - \nu \nabla \wedge (\nabla \wedge \mathbf{q}) \end{aligned} \quad (2.7)$$

For incompressible fluid, density ρ is constant. In that case, the equation of continuity becomes $\nabla \cdot \mathbf{q} = 0$. Then equation (2.7) reduces to

$$\frac{\partial \mathbf{q}}{\partial t} + (\mathbf{q} \cdot \nabla) \mathbf{q} = \mathbf{F} - \frac{1}{\rho} \nabla p - \nu \nabla \wedge (\nabla \wedge \mathbf{q}) \quad (2.8)$$

Again from vector formula $\nabla(\vec{A} \cdot \vec{B}) = (\vec{A} \cdot \nabla) \vec{B} + (\vec{B} \cdot \nabla) \vec{A} + \vec{A} \wedge (\nabla \wedge \vec{B}) + \vec{B} \wedge (\nabla \wedge \vec{A})$

$$\therefore \nabla(\mathbf{q} \cdot \mathbf{q}) = (\mathbf{q} \cdot \nabla) \mathbf{q} + (\mathbf{q} \cdot \nabla) \mathbf{q} + \mathbf{q} \wedge (\nabla \wedge \mathbf{q}) + \mathbf{q} \wedge (\nabla \wedge \mathbf{q})$$

$$\text{Or, } \nabla(\mathbf{q} \cdot \mathbf{q}) = 2(\mathbf{q} \cdot \nabla) \mathbf{q} + 2\mathbf{q} \wedge (\nabla \wedge \mathbf{q})$$

$$\text{Or, } \frac{1}{2} \nabla q^2 = (\mathbf{q} \cdot \nabla) \mathbf{q} + \mathbf{q} \times (\nabla \times \mathbf{q})$$

$$\text{Or, } (\mathbf{q} \cdot \nabla) \mathbf{q} = \frac{1}{2} \nabla q^2 - \mathbf{q} \times (\nabla \times \mathbf{q})$$

$$\text{Or, } (\mathbf{q} \cdot \nabla) \mathbf{q} = \frac{1}{2} \nabla q^2 + (\nabla \wedge \mathbf{q}) \wedge \mathbf{q}$$

Then equation (2.8) becomes

$$\frac{\partial \mathbf{q}}{\partial t} + \frac{1}{2} \nabla q^2 - \mathbf{q} \wedge (\nabla \wedge \mathbf{q}) = \mathbf{F} - \frac{1}{\rho} \nabla p - \nu \nabla \wedge (\nabla \wedge \mathbf{q})$$

$$\text{Or, } \frac{\partial \mathbf{q}}{\partial t} - \mathbf{q} \wedge (\nabla \wedge \mathbf{q}) = \mathbf{F} - \frac{1}{\rho} \nabla p - \frac{1}{2} \nabla q^2 - \nu \nabla \wedge (\nabla \wedge \mathbf{q})$$

$$\text{Or, } \frac{\partial \mathbf{q}}{\partial t} + (\nabla \wedge \mathbf{q}) \wedge \mathbf{q} = \mathbf{F} - \nabla \left(\frac{1}{\rho} p - \frac{1}{2} q^2 \right) - \nu \nabla \wedge (\nabla \wedge \mathbf{q})$$

$$\therefore \frac{\partial \mathbf{q}}{\partial t} + \xi \wedge \mathbf{q} = \mathbf{F} - \nabla \left(\frac{1}{\rho} p + \frac{1}{2} q^2 \right) - \nu \nabla \wedge \xi \quad \text{where, } \xi = \nabla \wedge \mathbf{q} \quad (2.9)$$

This is the Lamb's/invariant form of the Navier-Stokes equation (or Momentum equation) for viscous incompressible fluid with constant viscosity.

If the fluid moves through the electromagnetic field in a rotating system, then the Momentum equation (2.9) for a viscous incompressible can be written as follows:

$$\frac{\partial \mathbf{q}}{\partial t} + \xi \wedge \mathbf{q} = \mathbf{F} - \nabla \left(\frac{1}{\rho} p + \frac{1}{2} q^2 \right) - \nu (\nabla \wedge \xi) + \frac{1}{\rho} (\mathbf{J} \wedge \mathbf{B}) - 2(\Omega \wedge \mathbf{q}) \quad (2.10)$$

where, the term $\mathbf{J} \wedge \mathbf{B}$ is the force acting on the fluid per unit volume produced by interaction of the electric and magnetic force field; $\xi \wedge \mathbf{q}$ and $\Omega \wedge \mathbf{q}$ are the forces acting on the fluid per unit volume due to the action of centrifugal and Coriolis force on the system.

The energy equation for viscous incompressible electrically conducting fluid is defined by

$$\frac{dT}{dt} = \frac{k}{\rho C_p} \nabla^2 T$$

$$\text{Or, } \frac{\partial T}{\partial t} + (\mathbf{q} \cdot \nabla) T = \frac{k}{\rho C_p} \nabla^2 T \quad (2.11)$$

Where, k is the thermal conductivity, ρ is the density of the fluid and T is the temperature.

The momentum equation can be expressed in the following form due to the influence of gravitational force on the fluid:

$$\frac{\partial \mathbf{q}}{\partial t} + \xi \wedge \mathbf{q} = \mathbf{F} - \nabla \left(\frac{1}{\rho} p + \frac{1}{2} q^2 \right) - \nu (\nabla \wedge \xi) + \frac{1}{\rho} (\mathbf{J} \wedge \mathbf{B}) - 2(\boldsymbol{\Omega} \wedge \mathbf{q}) + \beta \mathbf{g} T \quad (2.12)$$

where $\mathbf{J} = (J_x, J_y, J_z)$ is the current density, $\mathbf{B} = (B_x, B_y, B_z)$ is the magnetic field vector, $\boldsymbol{\Omega}$ is the angular velocity vector and $\mathbf{g} = (0, 0, g)$ is the gravitational force.

According to the *Ohm's Law* the current density \mathbf{J} is defined by

$$\mathbf{J} = \sigma(\mathbf{E} + \mathbf{q} \wedge \mathbf{B}) \quad (2.13)$$

Due to the action of Hall and ion slip current on the fluid, Ohm's law is generalized as

$$\mathbf{J} = \sigma \mu_e (\mathbf{q} \wedge \mathbf{B}) - \frac{\omega_e \tau_e}{B_0} (\mathbf{J} \wedge \mathbf{B}) + \frac{\omega_e \tau_e \alpha}{B_0^2} (\mathbf{J} \wedge \mathbf{B}) \wedge \mathbf{B}$$

or, $\mathbf{J} = \sigma \mu_e (\mathbf{q} \wedge \mathbf{B}) - \frac{m}{B_0} (\mathbf{J} \wedge \mathbf{B}) + \frac{m \alpha}{B_0^2} (\mathbf{J} \wedge \mathbf{B}) \wedge \mathbf{B} \quad (2.14)$

Here, $m = \omega_e \tau_e$, where ω_e and τ_e are cyclotron frequency and electron collision time.

Also σ, m, α and B_0 are the conductivity of the fluid, the Hall factor and Ion-Slip parameter and the magnetic induction of \mathbf{B} respectively.

2.2.1 Continuity Equation in Cylindrical Curvilinear Coordinate System

Divergence in curvilinear coordinate is given by

$$\nabla \cdot \mathbf{q} = \frac{1}{h_1 h_2 h_3} \left[\frac{\partial}{\partial u_1} (h_2 h_3 q_1) + \frac{\partial}{\partial u_2} (h_3 h_1 q_2) + \frac{\partial}{\partial u_3} (h_1 h_2 q_3) \right]$$

In cylindrical curvilinear coordinate system, it is essential to replace (u_1, u_2, u_3) by (r, θ, z) ; velocity components (q_1, q_2, q_3) by (u, v, w) and scale factor $h_1 = 1, h_2 = r$ & $h_3 = 1$, these yields

$$\begin{aligned} \nabla \cdot \mathbf{q} &= \frac{1}{r} \left[\frac{\partial}{\partial r} (ru) + \frac{\partial v}{\partial \theta} + r \frac{\partial w}{\partial z} \right] \\ &= \frac{1}{r} \left[u + r \frac{\partial u}{\partial r} + \frac{\partial v}{\partial \theta} + r \frac{\partial w}{\partial z} \right] \\ &= \frac{u}{r} + \frac{\partial u}{\partial r} + \frac{1}{r} \frac{\partial v}{\partial \theta} + \frac{\partial w}{\partial z} \end{aligned}$$

Thus the continuity equation for incompressible fluid $\nabla \cdot \mathbf{q} = 0$ becomes

$$\frac{\partial u}{\partial r} + \frac{1}{r} \frac{\partial v}{\partial \theta} + \frac{\partial w}{\partial z} + \frac{u}{r} = 0 \quad (2.15)$$

This is the continuity equation in cylindrical curvilinear coordinate system.

2.2.2 Momentum Equation with Hall and Ion-slip Currents in terms of Cylindrical Coordinate (r, θ, z) through a Rotating Curved Duct.

Consider a two-dimensional, incompressible, MHD viscous fluid flow through the curved duct in a rotating coordinate system. In this system, an angular velocity of Ω causes rotation about the vertical y -axis, with the x and z -axes positioned perpendicular to it. Given the presence of curved duct flow, the governing equations are formulated using cylindrical coordinates (r, θ, z) . Here, r represents the radial variable, θ corresponds to the circumferential angle, and z is utilized as the vertical variable. Let $\mathbf{q}=(q_1, q_2, q_3)$ be the velocity, which directed along the directions of x , y and z respectively. The cylindrical coordinate system with curved duct is shown in Fig. 2.4:

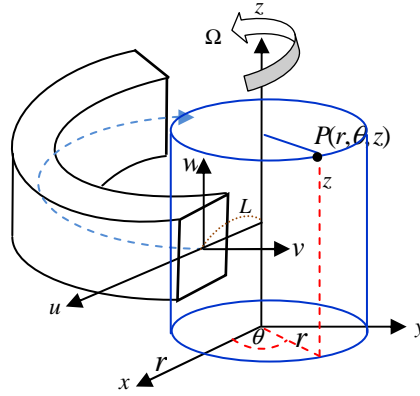


Figure 2.4: Cylindrical coordinate system with curved duct

Suppose the curved duct rotates about its vertical z -axis, then, $\mathbf{\Omega} = (0, 0, \Omega_z)$

But $\nabla \cdot \mathbf{\Omega} = 0$ which gives $\frac{\partial \Omega_z}{\partial z} = 0 \Rightarrow \Omega_z = \text{constant} = \Omega_0$ (say)

Hence $\mathbf{\Omega} = (0, 0, \Omega_0)$

Since the direction of the magnetic force is transverse to the direction of the centreline of the curved duct, therefore $\mathbf{B} = (0, 0, B_z)$

Similarly $\nabla \cdot \mathbf{B} = 0 \Rightarrow \frac{\partial B_z}{\partial z} = 0 \Rightarrow B_z = \text{constant} = B_0$ (say)

Hence $\mathbf{B} = (0, 0, B_0)$

The current density is $\mathbf{J} = (J_x, J_y, J_z)$.

The direction of propagation of the current is considered along x , y -axis and does not have any variation along z -axis.

Thus $\nabla \cdot \mathbf{J} = 0 \Rightarrow \frac{\partial J_z}{\partial z} = 0 \Rightarrow J_z = \text{constant} = 0$ (say) and therefore $\mathbf{J} = (J_x, J_y, 0)$

It gives $\mathbf{g} = \hat{e}_1 \cdot 0 + \hat{e}_2 \cdot 0 + \hat{e}_3 g$, $\mathbf{q} = \mathbf{q}_c = \hat{e}_1 q_1 + \hat{e}_2 q_2 + \hat{e}_3 q_3$ and $\boldsymbol{\xi} = \hat{e}_1 \xi_1 + \hat{e}_2 \xi_2 + \hat{e}_3 \xi_3$

$$\text{Now, } \mathbf{q} \wedge \mathbf{B} = \begin{vmatrix} \hat{e}_1 & \hat{e}_2 & \hat{e}_3 \\ q_1 & q_2 & q_3 \\ 0 & 0 & B_0 \end{vmatrix} = \hat{e}_1 (q_2 B_0) - \hat{e}_2 (q_1 B_0) = q_2 B_0 \hat{e}_1 - q_1 B_0 \hat{e}_2$$

$$\therefore (\mathbf{q} \wedge \mathbf{B}) \wedge \mathbf{B} = \begin{vmatrix} \hat{e}_1 & \hat{e}_2 & \hat{e}_3 \\ q_2 B_0 & -q_1 B_0 & 0 \\ 0 & 0 & B_0 \end{vmatrix} = (-q_1 B_0^2) \hat{e}_1 - (q_2 B_0^2) \hat{e}_2 + 0 = -q_1 B_0^2 \hat{e}_1 - q_2 B_0^2 \hat{e}_2$$

$$\xi \wedge \mathbf{q} = \begin{vmatrix} \hat{e}_1 & \hat{e}_2 & \hat{e}_3 \\ \xi_1 & \xi_2 & \xi_3 \\ q_1 & q_2 & q_3 \end{vmatrix} = \hat{e}_1 (\xi_2 q_3 - \xi_3 q_2) + \hat{e}_2 (\xi_3 q_1 - \xi_1 q_3) + \hat{e}_3 (\xi_1 q_2 - \xi_2 q_1)$$

We know that $\nabla \phi = \frac{\hat{e}_1}{h_1} \frac{\partial \phi}{\partial u_1} + \frac{\hat{e}_2}{h_2} \frac{\partial \phi}{\partial u_2} + \frac{\hat{e}_3}{h_3} \frac{\partial \phi}{\partial u_3}$

$$\therefore \nabla \left(\frac{p}{\rho} + \frac{1}{2} q^2 \right) = \left[\frac{\hat{e}_1}{h_1} \frac{\partial}{\partial u_1} \left\{ \frac{p}{\rho} + \frac{1}{2} (q_1^2 + q_2^2 + q_3^2) \right\} + \frac{\hat{e}_2}{h_2} \frac{\partial}{\partial u_2} \left\{ \frac{p}{\rho} + \frac{1}{2} (q_1^2 + q_2^2 + q_3^2) \right\} + \frac{\hat{e}_3}{h_3} \frac{\partial}{\partial u_3} \left\{ \frac{p}{\rho} + \frac{1}{2} (q_1^2 + q_2^2 + q_3^2) \right\} \right]$$

$$\nabla \wedge \xi = \frac{1}{h_1 h_2 h_3} \begin{vmatrix} h_1 \hat{e}_1 & h_2 \hat{e}_2 & h_3 \hat{e}_3 \\ \frac{\partial}{\partial u_1} & \frac{\partial}{\partial u_2} & \frac{\partial}{\partial u_3} \\ h_1 \xi_1 & h_2 \xi_2 & h_3 \xi_3 \end{vmatrix}$$

$$= \frac{\hat{e}_1}{h_2 h_3} \left(\frac{\partial}{\partial u_2} (h_3 \xi_3) - \frac{\partial}{\partial u_3} (h_2 \xi_2) \right) + \frac{\hat{e}_2}{h_1 h_3} \left(\frac{\partial}{\partial u_3} (h_1 \xi_1) - \frac{\partial}{\partial u_1} (h_3 \xi_3) \right) + \frac{\hat{e}_3}{h_1 h_2} \left(\frac{\partial}{\partial u_1} (h_2 \xi_2) - \frac{\partial}{\partial u_2} (h_1 \xi_1) \right)$$

Body force $\mathbf{F} = \hat{e}_1 F_1 + \hat{e}_2 F_2 + \hat{e}_3 F_3$

$$\Omega \wedge \mathbf{q} = \begin{pmatrix} \hat{e}_1 & \hat{e}_2 & \hat{e}_3 \\ 0 & 0 & \Omega_0 \\ q_1 & q_2 & q_3 \end{pmatrix} = \hat{e}_1 (0 - q_2 \Omega_0) + \hat{e}_2 (q_1 \Omega_0 - 0) + \hat{e}_3 (0 - 0) = -\hat{e}_1 q_2 \Omega_0 + \hat{e}_2 q_1 \Omega_0$$

Generalized Ohm's law is referred to as the following equation because of the influence of Hall and Ion-slip currents on the flow.

$$\mathbf{J} = \sigma \mu_e (\mathbf{q} \wedge \mathbf{B}) - \frac{m}{B_0} (\mathbf{J} \wedge \mathbf{B}) + \frac{m\alpha}{B_0^2} (\mathbf{J} \wedge \mathbf{B}) \wedge \mathbf{B} \quad (2.16)$$

$$\text{Now } \mathbf{J} \wedge \mathbf{B} = \begin{pmatrix} \hat{e}_1 & \hat{e}_2 & \hat{e}_3 \\ J_x & J_y & 0 \\ 0 & 0 & B_0 \end{pmatrix} = \hat{e}_1 (J_y B_0) - \hat{e}_2 (J_x B_0) + \hat{e}_3 \times 0 = \hat{e}_1 J_y B_0 - \hat{e}_2 J_x B_0$$

$$(\mathbf{J} \wedge \mathbf{B}) \wedge \mathbf{B} = \begin{pmatrix} \hat{e}_1 & \hat{e}_2 & \hat{e}_3 \\ J_y B_0 & -J_x B_0 & 0 \\ 0 & 0 & B_0 \end{pmatrix} = \hat{e}_1 (-J_x B_0^2) + \hat{e}_2 (-J_y B_0^2) = -\hat{e}_1 J_x B_0^2 - \hat{e}_2 J_y B_0^2$$

Thus the generalized Ohm's law (2.16) becomes

$$J_x \hat{e}_1 + J_y \hat{e}_2 + J_z \hat{e}_3 = \sigma \mu_e (q_2 B_0 \hat{e}_1 - q_1 B_0 \hat{e}_2) - \frac{m}{B_0} (\hat{e}_1 J_y B_0 - \hat{e}_2 J_x B_0) + \frac{m\alpha}{B_0^2} (-\hat{e}_1 J_x B_0^2 - \hat{e}_2 J_y B_0^2)$$

$$\therefore \left. \begin{aligned} J_x &= \sigma \mu_e q_2 B_0 - m J_y - m \alpha J_x \\ J_y &= -\sigma \mu_e q_1 B_0 + m J_x - m \alpha J_y \\ J_z &= 0 \end{aligned} \right\}$$

$$\text{Or, } \left. \begin{aligned} (1 + m\alpha) J_x + m J_y &= \sigma \mu_e q_2 B_0 \\ (1 + m\alpha) J_y - m J_x &= -\sigma \mu_e q_1 B_0 \\ J_z &= 0 \end{aligned} \right\} \quad (2.17)$$

Multiply 1st equation of (2.17) by m and 2nd equation of (2.17) by $(1+m\alpha)$ then adding, it gives

$$m(1+m\alpha)J_x + m^2J_y + (1+m\alpha)^2J_y - m(1+m\alpha)J_x = \sigma\mu_e q_2 B_0 m - \sigma\mu_e q_1 B_0 (1+m\alpha)$$

$$\text{Or, } [m^2 + (1+m\alpha)^2]J_y = \sigma\mu_e B_0 [q_2 m - q_1 (1+m\alpha)]$$

$$\text{Or, } J_y = \frac{[q_2 m - q_1 (1+m\alpha)]}{[m^2 + (1+m\alpha)^2]} \sigma\mu_e B_0$$

$$\text{Put } A_0 = (1+m\alpha)^2 \text{ and } A_1 = \frac{1}{[m^2 + (1+m\alpha)^2]} = \frac{1}{[m^2 + A_0^2]}$$

$$\text{Then } J_y = A_1 (q_2 m - A_0 q_1) \sigma\mu_e B_0$$

Again multiply 1st equation of (2.17) by $(1+m\alpha)$ and 2nd equation of (2.17) by m then subtracting, it gives

$$(1+m\alpha)^2 J_x + m(1+m\alpha)J_y - [m(1+m\alpha)J_y - m^2 J_x] = \sigma\mu_e q_2 B_0 (1+m\alpha) + m\sigma\mu_e q_1 B_0$$

$$\text{Or, } (1+m\alpha)^2 J_x + m^2 J_x = \sigma\mu_e q_2 B_0 (1+m\alpha) + m\sigma\mu_e q_1 B_0$$

$$\text{Or, } [(1+m\alpha)^2 + m^2]J_x = \sigma\mu_e q_2 B_0 (1+m\alpha) + m\sigma\mu_e q_1 B_0$$

$$\text{Or, } [(1+m\alpha)^2 + m^2]J_x = [q_2 (1+m\alpha) + m q_1] \sigma\mu_e B_0$$

$$\text{Or, } J_x = \frac{[q_2 (1+m\alpha) + m q_1]}{[(1+m\alpha)^2 + m^2]} \sigma\mu_e B_0$$

$$\text{Or, } J_x = \frac{[A_0 q_2 + m q_1]}{[A_0^2 + m^2]} \sigma\mu_e B_0$$

$$\text{Or, } J_x = A_1 (A_0 q_2 + m q_1) \sigma\mu_e B_0$$

$$\text{Hence } J_x = \frac{[m q_1 + q_2 (1+m\alpha)]}{[m^2 + (1+m\alpha)^2]} \sigma\mu_e B_0 \text{ and } J_y = \frac{[q_2 m - q_1 (1+m\alpha)]}{[m^2 + (1+m\alpha)^2]} \sigma\mu_e B_0$$

Finally,

$$\mathbf{J} \wedge \mathbf{B} = \begin{pmatrix} \hat{e}_1 & \hat{e}_2 & \hat{e}_3 \\ J_x & J_y & 0 \\ 0 & 0 & B_0 \end{pmatrix} = \hat{e}_1 \frac{\sigma\mu_e B_0^2}{\rho} \left[\frac{q_2 m - (1+m\alpha)q_1}{m^2 + (1+m\alpha)^2} \right] - \hat{e}_2 \frac{\sigma\mu_e B_0^2}{\rho} \left[\frac{m q_1 + (1+m\alpha)q_2}{(1+m\alpha)^2 + m^2} \right]$$

Putting these obtained values in the momentum equation (2.12)

$$\begin{aligned} & \frac{\partial}{\partial t} (\hat{e}_1 q_1 + \hat{e}_2 q_2 + \hat{e}_3 q_3) + \hat{e}_1 (\xi_2 q_3 - \xi_3 q_2) + \hat{e}_2 (\xi_3 q_1 - \xi_1 q_3) + \hat{e}_3 (\xi_1 q_2 - \xi_2 q_1) \\ & = \hat{e}_1 F_1 + \hat{e}_2 F_2 + \hat{e}_3 F_3 - \frac{\hat{e}_1}{h_1} \frac{\partial}{\partial u_1} \left\{ \frac{p}{\rho} + \frac{1}{2} (q_1^2 + q_2^2 + q_3^2) \right\} - \frac{\hat{e}_2}{h_2} \frac{\partial}{\partial u_2} \left\{ \frac{p}{\rho} + \frac{1}{2} (q_1^2 + q_2^2 + q_3^2) \right\} \\ & \quad - \frac{\hat{e}_3}{h_3} \frac{\partial}{\partial u_3} \left\{ \frac{p}{\rho} + \frac{1}{2} (q_1^2 + q_2^2 + q_3^2) \right\} - \frac{\mathcal{V}\hat{e}_1}{h_2 h_3} \left(\frac{\partial}{\partial u_2} (h_3 \xi_3) - \frac{\partial}{\partial u_3} (h_2 \xi_2) \right) \\ & \quad - \frac{\mathcal{V}\hat{e}_2}{h_1 h_3} \left(\frac{\partial}{\partial u_3} (h_1 \xi_1) - \frac{\partial}{\partial u_1} (h_3 \xi_3) \right) - \frac{\mathcal{V}\hat{e}_3}{h_1 h_2} \left(\frac{\partial}{\partial u_1} (h_2 \xi_2) - \frac{\partial}{\partial u_2} (h_1 \xi_1) \right) \\ & \quad - 2(-\hat{e}_1 q_2 \Omega_0 + \hat{e}_2 q_1 \Omega_0) + \hat{e}_1 \frac{\sigma\mu_e B_0^2}{\rho} \left[\frac{q_2 m - (1+m\alpha)q_1}{m^2 + (1+m\alpha)^2} \right] \end{aligned}$$

$$-\hat{e}_2 \frac{\sigma \mu_e B_0^2}{\rho} \left[\frac{mq_1 + (1+m\alpha)q_2}{(1+m\alpha)^2 + m^2} \right] + \beta(\hat{e}_1 \cdot 0 + \hat{e}_2 \cdot 0 + \hat{e}_3 \cdot g)T$$

By equating the components of the unit vectors \hat{e}_1 , \hat{e}_2 and \hat{e}_3 , it gives

$$\frac{\partial q_1}{\partial t} + (\xi_2 q_3 - \xi_3 q_2) = F_1 - \frac{1}{h_1} \frac{\partial}{\partial u_1} \left\{ \frac{p}{\rho} + \frac{1}{2}(q_1^2 + q_2^2 + q_3^2) \right\} - \frac{v}{h_2 h_3} \left(\frac{\partial}{\partial u_2} (h_3 \xi_3) - \frac{\partial}{\partial u_3} (h_2 \xi_2) \right) + 2q_2 \Omega_0 + \frac{\sigma \mu_e B_0^2}{\rho} \left[\frac{q_2 m - (1+m\alpha)q_1}{m^2 + (1+m\alpha)^2} \right] \quad (2.18a)$$

$$\frac{\partial q_2}{\partial t} + (\xi_3 q_1 - \xi_1 q_3) = F_2 - \frac{1}{h_2} \frac{\partial}{\partial u_2} \left\{ \frac{p}{\rho} + \frac{1}{2}(q_1^2 + q_2^2 + q_3^2) \right\} - \frac{v}{h_1 h_3} \left(\frac{\partial}{\partial u_3} (h_1 \xi_1) - \frac{\partial}{\partial u_1} (h_3 \xi_3) \right) - 2q_1 \Omega_0 - \frac{\sigma \mu_e B_0^2}{\rho} \left[\frac{mq_1 + (1+m\alpha)q_2}{(1+m\alpha)^2 + m^2} \right] \quad (2.18b)$$

$$\frac{\partial q_3}{\partial t} + (\xi_1 q_2 - \xi_2 q_1) = F_3 - \frac{1}{h_3} \frac{\partial}{\partial u_3} \left\{ \frac{p}{\rho} + \frac{1}{2}(q_1^2 + q_2^2 + q_3^2) \right\} - \frac{v}{h_1 h_2} \left(\frac{\partial}{\partial u_1} (h_2 \xi_2) - \frac{\partial}{\partial u_2} (h_1 \xi_1) \right) + \beta g T \quad (2.18c)$$

In cylindrical curvilinear coordinate system, it is essential to replace (u_1, u_2, u_3) by (r, θ, z) ; velocity components (q_1, q_2, q_3) by (u, v, w) and scale factor $h_1 = 1$, $h_2 = r$ & $h_3 = 1$ into the equations (2.18a)-(2.18c). These gives,

$$\frac{\partial u}{\partial t} + (\xi_2 w - \xi_3 v) = F_1 - \frac{\partial}{\partial r} \left\{ \frac{p}{\rho} + \frac{1}{2}(u^2 + v^2 + w^2) \right\} - \frac{v}{r} \left(\frac{\partial \xi_3}{\partial \theta} - \frac{\partial}{\partial z} (r \xi_2) \right) + 2v \Omega_0 + \frac{\sigma \mu_e B_0^2}{\rho} \left[\frac{mv - (1+m\alpha)u}{m^2 + (1+m\alpha)^2} \right] \quad (2.19a)$$

$$\frac{\partial v}{\partial t} + (\xi_3 u - \xi_1 w) = F_2 - \frac{1}{r} \frac{\partial}{\partial \theta} \left\{ \frac{p}{\rho} + \frac{1}{2}(u^2 + v^2 + w^2) \right\} - u \left(\frac{\partial}{\partial z} (\xi_1) - \frac{\partial}{\partial r} (\xi_3) \right) - 2u \Omega_0 - \frac{\sigma \mu_e B_0^2}{\rho} \left[\frac{mu + (1+m\alpha)v}{(1+m\alpha)^2 + m^2} \right] \quad (2.19b)$$

$$\frac{\partial w}{\partial t} + (\xi_1 v - \xi_2 u) = F_3 - \frac{\partial}{\partial z} \left\{ \frac{p}{\rho} + \frac{1}{2}(u^2 + v^2 + w^2) \right\} - \frac{v}{r} \left(\frac{\partial}{\partial r} (r \xi_2) - \frac{\partial}{\partial u_2} (\xi_1) \right) + \beta g T \quad (2.19c)$$

Again we know, $\nabla \wedge \mathbf{q} = \frac{1}{h_1 h_2 h_3} \begin{vmatrix} h_1 \hat{e}_1 & h_2 \hat{e}_2 & h_3 \hat{e}_3 \\ \frac{\partial}{\partial u_1} & \frac{\partial}{\partial u_2} & \frac{\partial}{\partial u_3} \\ h_1 q_1 & h_2 q_2 & h_3 q_3 \end{vmatrix} = \frac{1}{r} \begin{vmatrix} \hat{e}_1 & r \hat{e}_2 & \hat{e}_3 \\ \frac{\partial}{\partial r} & \frac{\partial}{\partial \theta} & \frac{\partial}{\partial z} \\ u & rv & w \end{vmatrix}$

$$\begin{aligned} \text{Or, } \xi &= \nabla \wedge \mathbf{q} = \frac{1}{r} \begin{vmatrix} \hat{e}_1 & r \hat{e}_2 & \hat{e}_3 \\ \frac{\partial}{\partial r} & \frac{\partial}{\partial \theta} & \frac{\partial}{\partial z} \\ u & rv & w \end{vmatrix} \\ &= \frac{\hat{e}_1}{r} \left(\frac{\partial w}{\partial \theta} - \frac{\partial}{\partial z} (rv) \right) + \hat{e}_2 \left(\frac{\partial u}{\partial z} - \frac{\partial w}{\partial r} \right) + \frac{\hat{e}_3}{r} \left(\frac{\partial}{\partial r} (rv) - \frac{\partial u}{\partial \theta} \right) \\ &= \frac{\hat{e}_1}{r} \left(\frac{\partial w}{\partial \theta} - r \frac{\partial v}{\partial z} \right) + \hat{e}_2 \left(\frac{\partial u}{\partial z} - \frac{\partial w}{\partial r} \right) + \frac{\hat{e}_3}{r} \left(v + r \frac{\partial v}{\partial r} - \frac{\partial u}{\partial \theta} \right) \end{aligned}$$

$$\text{Or, } \hat{e}_1 \xi_1 + \hat{e}_2 \xi_2 + \hat{e}_3 \xi_3 = \frac{\hat{e}_1}{r} \left(\frac{\partial w}{\partial \theta} - r \frac{\partial v}{\partial z} \right) + \hat{e}_2 \left(\frac{\partial u}{\partial z} - \frac{\partial w}{\partial r} \right) + \frac{\hat{e}_3}{r} \left(v + r \frac{\partial v}{\partial r} - \frac{\partial u}{\partial \theta} \right)$$

By equating the \hat{e}_1 th, \hat{e}_2 th and \hat{e}_3 th component, it gives

$$\xi_1 = \frac{1}{r} \left[\frac{\partial w}{\partial \theta} - \frac{\partial}{\partial z} (rv) \right] = \frac{1}{r} \left[\frac{\partial w}{\partial \theta} - r \frac{\partial v}{\partial z} \right]$$

$$\xi_2 = \frac{\partial u}{\partial z} - \frac{\partial w}{\partial r}$$

$$\xi_3 = \frac{v}{r} + \frac{\partial v}{\partial r} - \frac{1}{r} \frac{\partial u}{\partial \theta}$$

To use these in various terms of equations (2.18a)-(2.18c) gives

$$\xi_2 w - \xi_3 v = \left(\frac{\partial u}{\partial z} - \frac{\partial w}{\partial r} \right) w - \left(\frac{v}{r} + \frac{\partial v}{\partial r} - \frac{1}{r} \frac{\partial u}{\partial \theta} \right) v \quad (2.20a)$$

$$\xi_3 u - \xi_1 w = \left(\frac{v}{r} + \frac{\partial v}{\partial r} - \frac{1}{r} \frac{\partial u}{\partial \theta} \right) u - \left(\frac{1}{r} \frac{\partial w}{\partial \theta} - \frac{\partial v}{\partial z} \right) w \quad (2.20b)$$

$$\xi_1 v - \xi_2 u = \left(\frac{1}{r} \frac{\partial w}{\partial \theta} - \frac{\partial v}{\partial z} \right) v - \left(\frac{\partial u}{\partial z} - \frac{\partial w}{\partial r} \right) u = \frac{v}{r} \frac{\partial w}{\partial \theta} - v \frac{\partial v}{\partial z} - u \frac{\partial u}{\partial z} + u \frac{\partial w}{\partial r} \quad (2.20c)$$

$$\frac{\partial}{\partial r} \left\{ \frac{p}{\rho} + \frac{1}{2} (u^2 + v^2 + w^2) \right\} = \frac{1}{\rho} \frac{\partial p}{\partial r} + u \frac{\partial u}{\partial r} + v \frac{\partial v}{\partial r} + w \frac{\partial w}{\partial r} \quad (2.21a)$$

$$\frac{1}{r} \frac{\partial}{\partial \theta} \left\{ \frac{p}{\rho} + \frac{1}{2} (u^2 + v^2 + w^2) \right\} = \frac{1}{r \rho} \frac{\partial p}{\partial \theta} + \frac{u}{r} \frac{\partial u}{\partial \theta} + \frac{v}{r} \frac{\partial v}{\partial \theta} + \frac{w}{r} \frac{\partial w}{\partial \theta} \quad (2.21b)$$

$$\frac{\partial}{\partial z} \left\{ \frac{p}{\rho} + \frac{1}{2} (u^2 + v^2 + w^2) \right\} = \frac{1}{\rho} \frac{\partial p}{\partial z} + u \frac{\partial u}{\partial z} + v \frac{\partial v}{\partial z} + w \frac{\partial w}{\partial z} \quad (2.21c)$$

$$\begin{aligned} \frac{v}{r} \left(\frac{\partial \xi_3}{\partial \theta} - \frac{\partial}{\partial z} (r \xi_2) \right) &= \frac{v}{r} \left[\frac{\partial}{\partial \theta} (\xi_3) - \frac{\partial}{\partial z} (r \xi_2) \right] \\ &= \frac{v}{r} \left[\frac{\partial}{\partial \theta} \left(\frac{v}{r} + \frac{\partial v}{\partial r} - \frac{1}{r} \frac{\partial u}{\partial \theta} \right) - r \frac{\partial}{\partial z} \left(\frac{\partial u}{\partial z} - \frac{\partial w}{\partial r} \right) \right] \\ &= \frac{v}{r} \left[\frac{1}{r} \frac{\partial v}{\partial \theta} + \frac{\partial^2 v}{\partial \theta \partial r} - \frac{1}{r} \frac{\partial^2 u}{\partial \theta^2} - r \frac{\partial^2 u}{\partial z^2} + r \frac{\partial^2 w}{\partial z \partial r} \right] \\ &= \frac{v}{r} \left[\left(\frac{1}{r} \frac{\partial v}{\partial \theta} - \frac{1}{r} \frac{\partial^2 u}{\partial \theta^2} - r \frac{\partial^2 u}{\partial z^2} \right) + \left(\frac{\partial^2 v}{\partial \theta \partial r} + r \frac{\partial^2 w}{\partial z \partial r} \right) \right] \end{aligned}$$

Now differentiating continuity equation $\frac{\partial u}{\partial r} + \frac{1}{r} \frac{\partial v}{\partial \theta} + \frac{\partial w}{\partial z} + \frac{u}{r} = 0$ both side w.r.to r

$$i.e. \frac{\partial}{\partial r} \left(\frac{\partial u}{\partial r} + \frac{1}{r} \frac{\partial v}{\partial \theta} + \frac{\partial w}{\partial z} + \frac{u}{r} \right) = 0$$

$$\text{Or, } \frac{\partial^2 u}{\partial r^2} + \frac{1}{r} \frac{\partial^2 v}{\partial r \partial \theta} - \frac{1}{r^2} \frac{\partial v}{\partial \theta} + \frac{\partial^2 w}{\partial r \partial z} + \frac{1}{r} \frac{\partial u}{\partial r} - \frac{u}{r^2} = 0$$

$$\text{Or, } r \frac{\partial^2 u}{\partial r^2} + \frac{\partial^2 v}{\partial r \partial \theta} - \frac{1}{r} \frac{\partial v}{\partial \theta} + r \frac{\partial^2 w}{\partial r \partial z} + \frac{\partial u}{\partial r} - \frac{u}{r} = 0$$

$$\therefore \frac{\partial^2 v}{\partial r \partial \theta} + r \frac{\partial^2 w}{\partial r \partial z} = -\frac{\partial u}{\partial r} + \frac{u}{r} - r \frac{\partial^2 u}{\partial r^2} + \frac{1}{r} \frac{\partial v}{\partial \theta}$$

$$\begin{aligned} \text{Thus } \frac{v}{r} \left(\frac{\partial \xi_3}{\partial \theta} - \frac{\partial}{\partial z} (r \xi_2) \right) &= \frac{v}{r} \left[\left(\frac{1}{r} \frac{\partial v}{\partial \theta} - \frac{1}{r} \frac{\partial^2 u}{\partial \theta^2} - r \frac{\partial^2 u}{\partial z^2} \right) + \left(\frac{\partial^2 v}{\partial \theta \partial r} + r \frac{\partial^2 w}{\partial z \partial r} \right) \right] \\ &= \frac{v}{r} \left[\frac{1}{r} \frac{\partial v}{\partial \theta} - \frac{1}{r} \frac{\partial^2 u}{\partial \theta^2} - r \frac{\partial^2 u}{\partial z^2} - \frac{\partial u}{\partial r} + \frac{u}{r} - r \frac{\partial^2 u}{\partial r^2} + \frac{1}{r} \frac{\partial v}{\partial \theta} \right] \end{aligned}$$

$$\begin{aligned}
&= \frac{v}{r} \left[\frac{2}{r} \frac{\partial v}{\partial \theta} - \frac{1}{r} \frac{\partial^2 u}{\partial^2 \theta} - r \frac{\partial^2 u}{\partial z^2} - \frac{\partial u}{\partial r} + \frac{u}{r} - r \frac{\partial^2 u}{\partial r^2} \right] \\
&= \frac{v}{r} \left[\frac{2}{r} \frac{\partial v}{\partial \theta} + \frac{u}{r} - r \left(\frac{\partial^2 u}{\partial r^2} + \frac{1}{r} \frac{\partial u}{\partial r} + \frac{1}{r^2} \frac{\partial^2 u}{\partial^2 \theta} + \frac{\partial^2 u}{\partial z^2} \right) \right] \\
&= \frac{v}{r} \left[\frac{2}{r} \frac{\partial v}{\partial \theta} + \frac{u}{r} - r \nabla^2 u \right] \\
&= -v \left[\nabla^2 u - \frac{u}{r^2} - \frac{2}{r^2} \frac{\partial v}{\partial \theta} \right] \tag{2.22a}
\end{aligned}$$

$$\begin{aligned}
\text{Again, } v \left(\frac{\partial}{\partial z} (\xi_1) - \frac{\partial}{\partial r} (\xi_3) \right) &= v \left[\frac{\partial}{\partial z} \left(\frac{1}{r} \frac{\partial w}{\partial \theta} - \frac{\partial v}{\partial z} \right) - \frac{\partial}{\partial r} \left(\frac{v}{r} + \frac{\partial v}{\partial r} - \frac{1}{r} \frac{\partial u}{\partial \theta} \right) \right] \\
&= v \left[\frac{1}{r} \frac{\partial^2 w}{\partial z \partial \theta} - \frac{\partial^2 v}{\partial z^2} - \frac{1}{r} \frac{\partial v}{\partial r} + \frac{v}{r^2} - \frac{\partial^2 v}{\partial r^2} + \frac{1}{r} \frac{\partial^2 u}{\partial r \partial \theta} - \frac{1}{r^2} \frac{\partial u}{\partial \theta} \right] \\
&= v \left[\frac{1}{r} \left(\frac{\partial^2 w}{\partial z \partial \theta} + \frac{\partial^2 u}{\partial r \partial \theta} \right) - \frac{\partial^2 v}{\partial z^2} - \frac{1}{r} \frac{\partial v}{\partial r} + \frac{v}{r^2} - \frac{\partial^2 v}{\partial r^2} - \frac{1}{r^2} \frac{\partial u}{\partial \theta} \right]
\end{aligned}$$

Now differentiating continuity equation $\frac{\partial u}{\partial r} + \frac{1}{r} \frac{\partial v}{\partial \theta} + \frac{\partial w}{\partial z} + \frac{u}{r} = 0$ both side w.r.to θ

$$i.e. \frac{\partial}{\partial \theta} \left(\frac{u}{r} + \frac{\partial u}{\partial r} + \frac{1}{r} \frac{\partial v}{\partial \theta} + \frac{\partial w}{\partial z} \right) = 0$$

$$\text{Or, } \frac{1}{r} \frac{\partial u}{\partial \theta} + \frac{\partial^2 u}{\partial \theta \partial r} + \frac{1}{r} \frac{\partial^2 v}{\partial \theta^2} + \frac{\partial^2 w}{\partial \theta \partial z} = 0$$

$$\text{Or, } \frac{\partial^2 u}{\partial \theta \partial r} + \frac{\partial^2 w}{\partial \theta \partial z} = -\frac{1}{r} \frac{\partial u}{\partial \theta} - \frac{1}{r} \frac{\partial^2 v}{\partial \theta^2}$$

$$\begin{aligned}
\text{Thus } v \left(\frac{\partial}{\partial z} (\xi_1) - \frac{\partial}{\partial r} (\xi_3) \right) &= v \left[\frac{1}{r} \left(-\frac{1}{r} \frac{\partial u}{\partial \theta} - \frac{1}{r} \frac{\partial^2 v}{\partial \theta^2} \right) - \frac{\partial^2 v}{\partial z^2} - \frac{1}{r} \frac{\partial v}{\partial r} + \frac{v}{r^2} - \frac{\partial^2 v}{\partial r^2} - \frac{1}{r^2} \frac{\partial u}{\partial \theta} \right] \\
&= v \left[-\frac{1}{r^2} \frac{\partial u}{\partial \theta} - \frac{1}{r^2} \frac{\partial^2 v}{\partial \theta^2} - \frac{\partial^2 v}{\partial z^2} - \frac{1}{r} \frac{\partial v}{\partial r} + \frac{v}{r^2} - \frac{\partial^2 v}{\partial r^2} - \frac{1}{r^2} \frac{\partial u}{\partial \theta} \right] \\
&= v \left[\frac{v}{r^2} - \frac{2}{r^2} \frac{\partial u}{\partial \theta} - \left(\frac{\partial^2 v}{\partial r^2} + \frac{1}{r} \frac{\partial v}{\partial r} + \frac{1}{r^2} \frac{\partial^2 v}{\partial \theta^2} + \frac{\partial^2 v}{\partial z^2} \right) \right] \\
&= v \left[\frac{v}{r^2} - \frac{2}{r^2} \frac{\partial u}{\partial \theta} - \nabla^2 v \right] \tag{2.22b}
\end{aligned}$$

$$\begin{aligned}
\text{Again, } \frac{v}{r} \left(\frac{\partial}{\partial r} (r \xi_2) - \frac{\partial}{\partial u_2} (\xi_1) \right) &= \frac{v}{r} \left[\frac{\partial}{\partial r} \left\{ r \left(\frac{\partial u}{\partial z} - \frac{\partial w}{\partial r} \right) \right\} - \frac{\partial}{\partial \theta} \left(\frac{1}{r} \frac{\partial w}{\partial \theta} - \frac{\partial v}{\partial z} \right) \right] \\
&= \frac{v}{r} \left[\left\{ \left(\frac{\partial u}{\partial z} - \frac{\partial w}{\partial r} \right) + r \left(\frac{\partial^2 u}{\partial r \partial z} - \frac{\partial^2 w}{\partial r^2} \right) \right\} - \left(\frac{1}{r} \frac{\partial^2 w}{\partial \theta^2} - \frac{\partial^2 v}{\partial \theta \partial z} \right) \right] \\
&= \frac{v}{r} \left[\frac{\partial u}{\partial z} - \frac{\partial w}{\partial r} + r \frac{\partial^2 u}{\partial r \partial z} - r \frac{\partial^2 w}{\partial r^2} - \frac{1}{r} \frac{\partial^2 w}{\partial \theta^2} + \frac{\partial^2 v}{\partial \theta \partial z} \right] \\
&= \frac{v}{r} \left[\left(r \frac{\partial^2 u}{\partial r \partial z} + \frac{\partial^2 v}{\partial \theta \partial z} \right) + \left(\frac{\partial u}{\partial z} - \frac{\partial w}{\partial r} - r \frac{\partial^2 w}{\partial r^2} - \frac{1}{r} \frac{\partial^2 w}{\partial \theta^2} \right) \right]
\end{aligned}$$

Now differentiating continuity equation $\frac{\partial u}{\partial r} + \frac{1}{r} \frac{\partial v}{\partial \theta} + \frac{\partial w}{\partial z} + \frac{u}{r} = 0$ both side w.r.to z

$$i.e. \frac{\partial}{\partial z} \left(\frac{u}{r} + \frac{\partial u}{\partial r} + \frac{1}{r} \frac{\partial v}{\partial \theta} + \frac{\partial w}{\partial z} \right) = 0$$

$$\text{Or, } \frac{1}{r} \frac{\partial u}{\partial z} + \frac{\partial^2 u}{\partial z \partial r} + \frac{1}{r} \frac{\partial^2 v}{\partial z \partial \theta} + \frac{\partial^2 w}{\partial z^2} = 0$$

$$\text{Or, } \frac{\partial u}{\partial z} + r \frac{\partial^2 u}{\partial z \partial r} + \frac{\partial^2 v}{\partial z \partial \theta} + r \frac{\partial^2 w}{\partial z^2} = 0$$

$$\therefore r \frac{\partial^2 u}{\partial z \partial r} + \frac{\partial^2 v}{\partial z \partial \theta} = -\frac{\partial u}{\partial z} - r \frac{\partial^2 w}{\partial z^2}$$

$$\begin{aligned} \text{Thus } \frac{v}{r} \left(\frac{\partial}{\partial r} (r \xi_2) - \frac{\partial}{\partial u_2} (\xi_1) \right) &= \frac{v}{r} \left[\left(-\frac{\partial u}{\partial z} - r \frac{\partial^2 w}{\partial z^2} \right) + \left(\frac{\partial u}{\partial z} - \frac{\partial w}{\partial r} - r \frac{\partial^2 w}{\partial r^2} - \frac{1}{r} \frac{\partial^2 w}{\partial \theta^2} \right) \right] \\ &= \frac{v}{r} \left[-r \frac{\partial^2 w}{\partial z^2} - \frac{\partial w}{\partial r} - r \frac{\partial^2 w}{\partial r^2} - \frac{1}{r} \frac{\partial^2 w}{\partial \theta^2} \right] \\ &= -\frac{v}{r} r \left[\frac{\partial^2 w}{\partial z^2} + \frac{1}{r} \frac{\partial w}{\partial r} + \frac{\partial^2 w}{\partial r^2} + \frac{1}{r^2} \frac{\partial^2 w}{\partial \theta^2} \right] \\ &= -v \left[\frac{\partial^2 w}{\partial r^2} + \frac{1}{r} \frac{\partial w}{\partial r} + \frac{1}{r^2} \frac{\partial^2 w}{\partial \theta^2} + \frac{\partial^2 w}{\partial z^2} \right] \\ &= -v \nabla^2 w \end{aligned} \quad (2.22c)$$

$$\text{Where } \nabla^2 = \frac{\partial^2}{\partial r^2} + \frac{1}{r} \frac{\partial}{\partial r} + \frac{1}{r^2} \frac{\partial^2}{\partial \theta^2} + \frac{\partial^2}{\partial z^2}$$

Now using equations (2.20a), (2.21a) and (2.22a) in equation (2.19a), it gives that

(a) u_1 -component of momentum equation:

$$\begin{aligned} \frac{\partial u}{\partial t} + (\xi_2 w - \xi_3 v) &= F_1 - \frac{\partial}{\partial r} \left\{ \frac{p}{\rho} + \frac{1}{2} (u^2 + v^2 + w^2) \right\} - \frac{v}{r} \left(\frac{\partial \xi_3}{\partial \theta} - \frac{\partial}{\partial z} (r \xi_2) \right) + 2v\Omega_0 + \frac{\sigma \mu_e B_0^2}{\rho} \left[\frac{mv - (1 + m\alpha)u}{m^2 + (1 + m\alpha)^2} \right] \\ \therefore \frac{\partial u}{\partial t} + \left(\frac{\partial u}{\partial z} - \frac{\partial w}{\partial r} \right) w - \left(\frac{v}{r} + \frac{\partial v}{\partial r} - \frac{1}{r} \frac{\partial u}{\partial \theta} \right) v &= F_1 - \frac{1}{\rho} \frac{\partial p}{\partial r} - u \frac{\partial u}{\partial r} - v \frac{\partial v}{\partial r} - w \frac{\partial w}{\partial r} - \frac{v}{r} \left(\frac{2}{r} \frac{\partial v}{\partial \theta} + \frac{u}{r} - r \nabla^2 u \right) + 2v\Omega_0 + \frac{\sigma \mu_e B_0^2}{\rho} \left[\frac{mv - (1 + m\alpha)u}{m^2 + (1 + m\alpha)^2} \right] \\ \text{Or, } \frac{\partial u}{\partial t} + w \frac{\partial u}{\partial z} - w \frac{\partial w}{\partial r} - \frac{v^2}{r} - v \frac{\partial v}{\partial r} + \frac{v}{r} \frac{\partial u}{\partial \theta} &= F_1 - \frac{1}{\rho} \frac{\partial p}{\partial r} - u \frac{\partial u}{\partial r} - v \frac{\partial v}{\partial r} - w \frac{\partial w}{\partial r} - v \left(\frac{2}{r^2} \frac{\partial v}{\partial \theta} + \frac{u}{r^2} - \nabla^2 u \right) + 2v\Omega_0 + \frac{\sigma \mu_e B_0^2}{\rho} \left[\frac{mv - (1 + m\alpha)u}{m^2 + (1 + m\alpha)^2} \right] \\ \text{Or, } \frac{\partial u}{\partial t} + w \frac{\partial u}{\partial z} - \frac{v^2}{r} + \frac{v}{r} \frac{\partial u}{\partial \theta} &= F_1 - \frac{1}{\rho} \frac{\partial p}{\partial r} - u \frac{\partial u}{\partial r} + v \left(\nabla^2 u - \frac{u}{r^2} - \frac{2}{r^2} \frac{\partial v}{\partial \theta} \right) + 2v\Omega_0 + \frac{\sigma \mu_e B_0^2}{\rho} \left[\frac{mv - (1 + m\alpha)u}{m^2 + (1 + m\alpha)^2} \right] \\ \text{Or, } \frac{\partial u}{\partial t} + u \frac{\partial u}{\partial r} + \frac{v}{r} \frac{\partial u}{\partial \theta} + w \frac{\partial u}{\partial z} - \frac{v^2}{r} &= F_1 - \frac{1}{\rho} \frac{\partial p}{\partial r} + v \left(\nabla^2 u - \frac{u}{r^2} - \frac{2}{r^2} \frac{\partial v}{\partial \theta} \right) + 2v\Omega_0 + \frac{\sigma \mu_e B_0^2}{\rho} \left[\frac{mv - (1 + m\alpha)u}{m^2 + (1 + m\alpha)^2} \right] \\ \therefore \frac{\partial u}{\partial t} + u \frac{\partial u}{\partial r} + \frac{v}{r} \frac{\partial u}{\partial \theta} + w \frac{\partial u}{\partial z} - \frac{v^2}{r} &= F_1 - \frac{1}{\rho} \frac{\partial p}{\partial r} + \mu \left(\nabla^2 u - \frac{u}{r^2} - \frac{2}{r^2} \frac{\partial v}{\partial \theta} \right) + 2v\Omega_0 + \frac{\sigma \mu_e B_0^2}{\rho} \left[\frac{mv - (1 + m\alpha)u}{m^2 + (1 + m\alpha)^2} \right] \end{aligned} \quad (2.23a)$$

In cylindrical curvilinear coordinate system

$$\mathbf{q} \cdot \nabla = \frac{1}{h_1 h_2 h_3} \left[h_2 h_3 q_1 \frac{\partial}{\partial u_1} + h_3 h_1 q_2 \frac{\partial}{\partial u_2} + h_1 h_2 q_3 \frac{\partial}{\partial u_3} \right]$$

$$\begin{aligned}
&= \frac{1}{r} \left[ru \frac{\partial}{\partial r} + v \frac{\partial}{\partial \theta} + rw \frac{\partial}{\partial z} \right] \\
&= u \frac{\partial}{\partial r} + \frac{v}{r} \frac{\partial}{\partial \theta} + w \frac{\partial}{\partial z} \\
\therefore (\mathbf{q} \cdot \nabla)u &= u \frac{\partial u}{\partial r} + \frac{v}{r} \frac{\partial u}{\partial \theta} + w \frac{\partial u}{\partial z} \\
\therefore \frac{du}{dt} &= \frac{\partial u}{\partial t} + (\mathbf{q} \cdot \nabla)u = \frac{\partial u}{\partial t} + u \frac{\partial u}{\partial r} + \frac{v}{r} \frac{\partial u}{\partial \theta} + w \frac{\partial u}{\partial z}
\end{aligned}$$

Thus we write the equation (2.25a) in the following form:

$$\frac{du}{dt} - \frac{v^2}{r} = F_1 - \frac{1}{\rho} \frac{\partial p}{\partial r} + v \left(\nabla^2 u - \frac{u}{r^2} - \frac{2}{r^2} \frac{\partial v}{\partial \theta} \right) + 2v\Omega_0 + \frac{\sigma \mu_e B_0^2}{\rho} \left[\frac{mv - (1+m\alpha)u}{m^2 + (1+m\alpha)^2} \right]$$

where $\frac{d}{dt} = \frac{\partial}{\partial t} + \mathbf{q} \cdot \nabla$

Again using equations (2.20b), (2.21b) and (2.22b) in equation (2.19b), it gives

(b) u_2 -component of momentum equation:

$$\begin{aligned}
\frac{\partial v}{\partial t} + \left(\frac{v}{r} \frac{\partial v}{\partial r} - \frac{1}{r} \frac{\partial u}{\partial \theta} \right) u - \left(\frac{1}{r} \frac{\partial v}{\partial r} - \frac{\partial v}{\partial z} \right) w &= F_2 - \left[\frac{1}{\rho r} \frac{\partial p}{\partial \theta} + \frac{u}{r} \frac{\partial u}{\partial \theta} + \frac{v}{r} \frac{\partial v}{\partial \theta} + \frac{w}{r} \frac{\partial w}{\partial \theta} \right] - v \left[\frac{v}{r^2} - \frac{2}{r^2} \frac{\partial u}{\partial \theta} - \nabla^2 v \right] - 2u\Omega_0 - \frac{\sigma \mu_e B_0^2}{\rho} \left[\frac{mu + (1+m\alpha)v}{(1+m\alpha)^2 + m^2} \right] \\
\text{Or, } \frac{\partial v}{\partial t} + \frac{uv}{r} + u \frac{\partial v}{\partial r} - \frac{u}{r} \frac{\partial u}{\partial \theta} - \frac{w}{r} \frac{\partial w}{\partial \theta} + w \frac{\partial v}{\partial z} &= F_2 - \frac{1}{\rho r} \frac{\partial p}{\partial \theta} - \frac{u}{r} \frac{\partial u}{\partial \theta} - \frac{v}{r} \frac{\partial v}{\partial \theta} - \frac{w}{r} \frac{\partial w}{\partial \theta} - v \left[\frac{v}{r^2} - \frac{2}{r^2} \frac{\partial u}{\partial \theta} - \nabla^2 v \right] - 2u\Omega_0 - \frac{\sigma \mu_e B_0^2}{\rho} \left[\frac{mu + (1+m\alpha)v}{(1+m\alpha)^2 + m^2} \right] \\
\text{Or, } \frac{\partial v}{\partial t} + \frac{uv}{r} + u \frac{\partial v}{\partial r} + w \frac{\partial v}{\partial z} &= F_2 - \frac{1}{\rho r} \frac{\partial p}{\partial \theta} - \frac{v}{r} \frac{\partial v}{\partial \theta} - v \left[\frac{v}{r^2} - \frac{2}{r^2} \frac{\partial u}{\partial \theta} - \nabla^2 v \right] - 2u\Omega_0 - \frac{\sigma \mu_e B_0^2}{\rho} \left[\frac{mu + (1+m\alpha)v}{(1+m\alpha)^2 + m^2} \right] \\
\text{Or, } \frac{\partial v}{\partial t} + u \frac{\partial v}{\partial r} + \frac{v}{r} \frac{\partial v}{\partial \theta} + w \frac{\partial v}{\partial z} + \frac{uv}{r} &= F_2 - \frac{1}{\rho r} \frac{\partial p}{\partial \theta} - \mu \left[\frac{v}{r^2} - \frac{2}{r^2} \frac{\partial u}{\partial \theta} - \nabla^2 v \right] - 2u\Omega_0 - \frac{\sigma \mu_e B_0^2}{\rho} \left[\frac{mu + (1+m\alpha)v}{(1+m\alpha)^2 + m^2} \right] \\
\text{Or, } \left(\frac{\partial v}{\partial t} + u \frac{\partial v}{\partial r} + \frac{v}{r} \frac{\partial v}{\partial \theta} + w \frac{\partial v}{\partial z} \right) + \frac{uv}{r} &= F_2 - \frac{1}{\rho r} \frac{\partial p}{\partial \theta} - v \left[\frac{v}{r^2} - \frac{2}{r^2} \frac{\partial u}{\partial \theta} - \nabla^2 v \right] - 2u\Omega_0 - \frac{\sigma \mu_e B_0^2}{\rho} \left[\frac{mu + (1+m\alpha)v}{(1+m\alpha)^2 + m^2} \right] \\
\therefore \left(\frac{\partial v}{\partial t} + u \frac{\partial v}{\partial r} + \frac{v}{r} \frac{\partial v}{\partial \theta} + w \frac{\partial v}{\partial z} \right) + \frac{uv}{r} &= F_2 - \frac{1}{\rho r} \frac{\partial p}{\partial \theta} - v \left[\frac{v}{r^2} - \frac{2}{r^2} \frac{\partial u}{\partial \theta} - \nabla^2 v \right] - 2u\Omega_0 - \frac{\sigma \mu_e B_0^2}{\rho} \left[\frac{mu + (1+m\alpha)v}{(1+m\alpha)^2 + m^2} \right] \\
\text{Or, } \frac{dv}{dt} + \frac{uv}{r} &= F_2 - \frac{1}{\rho r} \frac{\partial p}{\partial \theta} + v \left[\nabla^2 v - \frac{v}{r^2} + \frac{2}{r^2} \frac{\partial u}{\partial \theta} \right] - 2u\Omega_0 - \frac{\sigma \mu_e B_0^2}{\rho} \left[\frac{mu + (1+m\alpha)v}{(1+m\alpha)^2 + m^2} \right] \quad (2.23b)
\end{aligned}$$

Again using equations (2.20c), (2.21c) and (2.22c) in equation (2.19c), it gives

(c) u_3 -component of Momentum equation:

$$\begin{aligned}
\frac{\partial w}{\partial t} + \frac{v}{r} \frac{\partial w}{\partial \theta} - v \frac{\partial v}{\partial z} - u \frac{\partial u}{\partial z} + u \frac{\partial w}{\partial r} &= F_3 - \left(\frac{1}{\rho} \frac{\partial p}{\partial z} + u \frac{\partial u}{\partial z} + v \frac{\partial v}{\partial z} + w \frac{\partial w}{\partial z} \right) + v \nabla^2 w + \beta g T \\
\text{Or, } \frac{\partial w}{\partial t} + \frac{v}{r} \frac{\partial w}{\partial \theta} - v \frac{\partial v}{\partial z} - u \frac{\partial u}{\partial z} + u \frac{\partial w}{\partial r} &= F_3 - \frac{1}{\rho} \frac{\partial p}{\partial z} - u \frac{\partial u}{\partial z} - v \frac{\partial v}{\partial z} - w \frac{\partial w}{\partial z} + v \nabla^2 w + \beta g T \\
\text{Or, } \frac{\partial w}{\partial t} + \frac{v}{r} \frac{\partial w}{\partial \theta} + u \frac{\partial w}{\partial r} &= F_3 - \frac{1}{\rho} \frac{\partial p}{\partial z} - w \frac{\partial w}{\partial z} + v \nabla^2 w + \beta g T \\
\text{Or, } \frac{\partial w}{\partial t} + \frac{v}{r} \frac{\partial w}{\partial \theta} + u \frac{\partial w}{\partial r} + w \frac{\partial w}{\partial z} &= F_3 - \frac{1}{\rho} \frac{\partial p}{\partial z} + v \nabla^2 w + \beta g T
\end{aligned}$$

$$\text{Or, } \frac{\partial w}{\partial t} + u \frac{\partial w}{\partial r} + \frac{v}{r} \frac{\partial w}{\partial \theta} + w \frac{\partial w}{\partial z} = F_3 - \frac{1}{\rho} \frac{\partial p}{\partial z} + \nu \nabla^2 w + \beta g T$$

$$\therefore \frac{dw}{dt} = F_3 - \frac{1}{\rho} \frac{\partial p}{\partial z} + \nu \nabla^2 w + \beta g T \quad (2.23c)$$

$$\text{Where, } \frac{d}{dt} = \frac{\partial}{\partial t} + \mathbf{q} \cdot \nabla = \frac{\partial}{\partial t} + u \frac{\partial}{\partial r} + \frac{v}{r} \frac{\partial}{\partial \theta} + w \frac{\partial}{\partial z}$$

Finally it has been found the following three components of Momentum equations in cylindrical coordinate form:

$$\left. \begin{aligned} \frac{du}{dt} - \frac{v^2}{r} &= F_1 - \frac{1}{\rho} \frac{\partial p}{\partial r} + \nu \left(\nabla^2 u - \frac{u}{r^2} - \frac{2}{r^2} \frac{\partial v}{\partial \theta} \right) + 2\nu \Omega_0 + \frac{\sigma \mu_e B_0^2}{\rho} \left[\frac{mv - u(1+m\alpha)}{(1+m\alpha)^2 + m^2} \right] \\ \frac{dv}{dt} + \frac{uv}{r} &= F_2 - \frac{1}{\rho} \frac{1}{r} \frac{\partial p}{\partial \theta} - \nu \left[\frac{v}{r^2} - \frac{2}{r^2} \frac{\partial u}{\partial \theta} - \nabla^2 v \right] - 2u\Omega_0 - \frac{\sigma \mu_e B_0^2}{\rho} \left[\frac{mu + (1+m\alpha)v}{(1+m\alpha)^2 + m^2} \right] \\ \frac{dw}{dt} &= F_3 - \frac{1}{\rho} \frac{\partial p}{\partial z} + \nu \nabla^2 w + \beta g T \end{aligned} \right\}$$

(2.24)

$$\text{Where, } \frac{d}{dt} = \frac{\partial}{\partial t} + u \frac{\partial}{\partial r} + \frac{v}{r} \frac{\partial}{\partial \theta} + w \frac{\partial}{\partial z} \text{ and } \nabla^2 = \frac{\partial^2}{\partial r^2} + \frac{1}{r} \frac{\partial}{\partial r} + \frac{1}{r^2} \frac{\partial^2}{\partial \theta^2} + \frac{\partial^2}{\partial z^2}$$

These equations also can be written as

$$\left. \begin{aligned} \frac{\partial u}{\partial t} + u \frac{\partial u}{\partial r} + \frac{v}{r} \frac{\partial u}{\partial \theta} + w \frac{\partial u}{\partial z} - \frac{v^2}{r} &= F_1 - \frac{1}{\rho} \frac{\partial p}{\partial r} + \nu \left(\frac{\partial^2 u}{\partial r^2} + \frac{1}{r} \frac{\partial u}{\partial r} + \frac{1}{r^2} \frac{\partial^2 u}{\partial \theta^2} + \frac{\partial^2 u}{\partial z^2} - \frac{u}{r^2} - \frac{2}{r^2} \frac{\partial v}{\partial \theta} \right) + 2\nu \Omega_0 + \frac{\sigma \mu_e B_0^2}{\rho} \left[\frac{mv - u(1+m\alpha)}{(1+m\alpha)^2 + m^2} \right] \\ \frac{\partial v}{\partial t} + u \frac{\partial v}{\partial r} + \frac{v}{r} \frac{\partial v}{\partial \theta} + w \frac{\partial v}{\partial z} + \frac{uv}{r} &= F_2 - \frac{1}{\rho} \frac{1}{r} \frac{\partial p}{\partial \theta} + \nu \left(\frac{\partial^2 v}{\partial r^2} + \frac{1}{r} \frac{\partial v}{\partial r} + \frac{1}{r^2} \frac{\partial^2 v}{\partial \theta^2} + \frac{\partial^2 v}{\partial z^2} + \frac{2}{r^2} \frac{\partial u}{\partial \theta} - \frac{v}{r^2} \right) - 2u\Omega_0 - \frac{\sigma \mu_e B_0^2}{\rho} \left[\frac{mu + (1+m\alpha)v}{(1+m\alpha)^2 + m^2} \right] \\ \frac{\partial w}{\partial t} + u \frac{\partial w}{\partial r} + \frac{v}{r} \frac{\partial w}{\partial \theta} + w \frac{\partial w}{\partial z} &= F_3 - \frac{1}{\rho} \frac{\partial p}{\partial z} + \nu \left(\frac{\partial^2 w}{\partial r^2} + \frac{1}{r} \frac{\partial w}{\partial r} + \frac{1}{r^2} \frac{\partial^2 w}{\partial \theta^2} + \frac{\partial^2 w}{\partial z^2} \right) + \beta g T \end{aligned} \right\} \quad (2.25)$$

2.2.3 Energy Equation in Cylindrical Curvilinear Coordinate System

Now energy equation for viscous incompressible electrically conducting fluid is

$$\frac{dT}{dt} = \frac{k}{\rho C_p} \nabla^2 T \quad (2.26)$$

where, k is the thermal conductivity, ρ is the density of the fluid.

Since in cylindrical curvilinear coordinate system

$$\frac{d}{dt} = \frac{\partial}{\partial t} + \mathbf{q} \cdot \nabla = \frac{\partial}{\partial t} + u \frac{\partial}{\partial r} + \frac{v}{r} \frac{\partial}{\partial \theta} + w \frac{\partial}{\partial z}$$

$$\text{and } \nabla^2 = \frac{\partial^2}{\partial r^2} + \frac{1}{r} \frac{\partial}{\partial r} + \frac{1}{r^2} \frac{\partial^2}{\partial \theta^2} + \frac{\partial^2}{\partial z^2}$$

$$\text{Then } \frac{dT}{dt} = \frac{\partial T}{\partial t} + (\mathbf{q} \cdot \nabla) T = \frac{\partial T}{\partial t} + u \frac{\partial T}{\partial r} + \frac{v}{r} \frac{\partial T}{\partial \theta} + w \frac{\partial T}{\partial z}$$

$$\text{and } \nabla^2 T = \frac{\partial^2 T}{\partial r^2} + \frac{1}{r} \frac{\partial T}{\partial r} + \frac{1}{r^2} \frac{\partial^2 T}{\partial \theta^2} + \frac{\partial^2 T}{\partial z^2}$$

Equation (2.26) gives

$$\frac{\partial T}{\partial t} + u \frac{\partial T}{\partial r} + \frac{v}{r} \frac{\partial T}{\partial \theta} + w \frac{\partial T}{\partial z} = \frac{k}{\rho C_p} \left(\frac{\partial^2 T}{\partial r^2} + \frac{1}{r} \frac{\partial T}{\partial r} + \frac{1}{r^2} \frac{\partial^2 T}{\partial \theta^2} + \frac{\partial^2 T}{\partial z^2} \right) \quad (2.27)$$

2.3 Simplifications of Governing Equations for the Curved Duct Regarding to the Current Study

2.3.1 Transforming Coordinate Variables in Governing Equations

Consider a thermally fully developed, incompressible, two-dimensional, MHD viscous fluid flow passes through the curved duct of its height $2h$ and width $2d$. The cross-sectional aspect ratio of this duct is denoted as ' l ' where $l = h/d$. To facilitate a comparison of our findings with previously published results concerning curved duct flow, it is necessary to interchange the coordinate axes, converting them from the rectangular Cartesian coordinate system. In this redefined context, the duct system is rotated about its vertical y -axis with an angular velocity Ω . We introduce a new cylindrical coordinate system (r, θ, y) , where r represents the radial variable, θ signifies the circumferential angle, and y corresponds to the vertical variable. This coordinate system can further be transformed into a non-dimensional rectangular coordinate system (x', z', y') through the following variable transformation.

$$r = L + dx' , \quad y = hy' \quad \text{and} \quad L\theta = dz'$$

The modified geometrical model is shown in Fig.2.5.

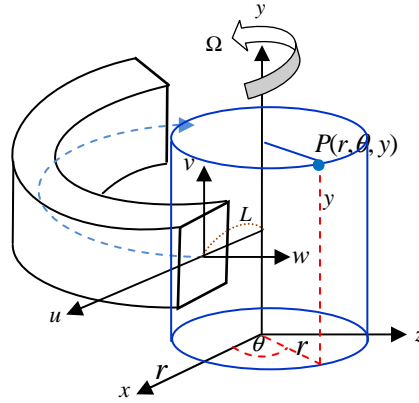


Figure 2.5: Modified Geometrical Configuration of the curved duct

To get the modified governing equations, it is required to interchange the variables y & z and the velocity component v & w each other in the equations (2.15), (2.25) and (2.27). Thus the modified continuity equation for incompressible fluid is

$$\frac{\partial u}{\partial r} + \frac{1}{r} \frac{\partial w}{\partial \theta} + \frac{\partial v}{\partial y} + \frac{u}{r} = 0$$

The modified Momentum equations are

$$\begin{aligned} \frac{\partial u}{\partial t} + u \frac{\partial u}{\partial r} + \frac{w}{r} \frac{\partial u}{\partial \theta} + v \frac{\partial u}{\partial y} - \frac{w^2}{r} &= F_1 - \frac{1}{\rho} \frac{\partial p}{\partial r} + \nu \left(\frac{\partial^2 u}{\partial r^2} + \frac{1}{r} \frac{\partial u}{\partial r} + \frac{1}{r^2} \frac{\partial^2 u}{\partial \theta^2} + \frac{\partial^2 u}{\partial y^2} - \frac{u}{r^2} - \frac{2}{r^2} \frac{\partial w}{\partial \theta} \right) + 2w\Omega_0 + \frac{\sigma \mu_e B_0^2}{\rho} \left[\frac{mw - u(1+m\alpha)}{(1+m\alpha)^2 + m^2} \right] \\ \frac{\partial w}{\partial t} + u \frac{\partial w}{\partial r} + \frac{w}{r} \frac{\partial w}{\partial \theta} + v \frac{\partial w}{\partial y} + \frac{uw}{r} &= F_2 - \frac{1}{\rho} \frac{1}{r} \frac{\partial p}{\partial \theta} + \nu \left(\frac{\partial^2 w}{\partial r^2} + \frac{1}{r} \frac{\partial w}{\partial r} + \frac{1}{r^2} \frac{\partial^2 w}{\partial \theta^2} + \frac{\partial^2 w}{\partial y^2} + \frac{2}{r^2} \frac{\partial u}{\partial \theta} - \frac{w}{r^2} \right) - 2u\Omega_0 - \frac{\sigma \mu_e B_0^2}{\rho} \left[\frac{mu + (1+m\alpha)w}{(1+m\alpha)^2 + m^2} \right] \\ \frac{\partial v}{\partial t} + u \frac{\partial v}{\partial r} + \frac{w}{r} \frac{\partial v}{\partial \theta} + v \frac{\partial v}{\partial y} &= F_3 - \frac{1}{\rho} \frac{\partial p}{\partial y} + \nu \left(\frac{\partial^2 v}{\partial r^2} + \frac{1}{r} \frac{\partial v}{\partial r} + \frac{1}{r^2} \frac{\partial^2 v}{\partial \theta^2} + \frac{\partial^2 v}{\partial y^2} \right) + \beta g T \end{aligned}$$

And the modified Energy equation is

$$\text{Or, } \frac{\partial T}{\partial t} + u \frac{\partial T}{\partial r} + \frac{v}{r} \frac{\partial T}{\partial \theta} + w \frac{\partial T}{\partial z} = \frac{k}{\rho C_p} \left(\frac{\partial^2 T}{\partial r^2} + \frac{1}{r} \frac{\partial T}{\partial r} + \frac{1}{r^2} \frac{\partial^2 T}{\partial \theta^2} + \frac{\partial^2 T}{\partial z^2} \right)$$

Now it is assumed that the body force is absent and all the variables are independent of θ

$$\text{except } p . i.e. (F_1, F_2, F_3) = (0, 0, 0) , \frac{\partial A_1}{\partial t} = 0 \ \& \ \frac{\partial A_2}{\partial \theta} = 0 \ \text{but} \ \frac{\partial p}{\partial \theta} \neq 0$$

where, A_1 = fluid properties and A_2 = fluid variables. Therefore

Continuity equation

$$\frac{\partial u}{\partial r} + \frac{\partial v}{\partial y} + \frac{u}{r} = 0$$

(2.28)

Momentum equations

Radial direction

$$\frac{\partial u}{\partial t} + u \frac{\partial u}{\partial r} + v \frac{\partial u}{\partial y} - \frac{w^2}{r} = -\frac{1}{\rho} \frac{\partial p}{\partial r} + \nu \left(\frac{\partial^2 u}{\partial r^2} + \frac{1}{r} \frac{\partial u}{\partial r} + \frac{\partial^2 u}{\partial y^2} - \frac{u}{r^2} \right) + 2w\Omega_0 + \frac{\sigma \mu_e B_0^2}{\rho} \left[\frac{mw - u(1+m\alpha)}{(1+m\alpha)^2 + m^2} \right]$$

Vertical direction

$$\frac{\partial v}{\partial t} + u \frac{\partial v}{\partial r} + v \frac{\partial v}{\partial y} = -\frac{1}{\rho} \frac{\partial p}{\partial y} + \nu \left(\frac{\partial^2 v}{\partial r^2} + \frac{1}{r} \frac{\partial v}{\partial r} + \frac{\partial^2 v}{\partial y^2} \right) + \beta g T$$

Axial direction

$$\frac{\partial w}{\partial t} + u \frac{\partial w}{\partial r} + v \frac{\partial w}{\partial y} + \frac{uw}{r} = -\frac{1}{\rho} \frac{1}{r} \frac{\partial p}{\partial \theta} + \nu \left(\frac{\partial^2 w}{\partial r^2} + \frac{1}{r} \frac{\partial w}{\partial r} + \frac{\partial^2 w}{\partial y^2} - \frac{w}{r^2} \right) - 2u\Omega_0 - \frac{\sigma \mu_e B_0^2}{\rho} \left[\frac{mu + (1+m\alpha)w}{(1+m\alpha)^2 + m^2} \right]$$

(2.29)

Energy equations

$$\frac{\partial T}{\partial t} + u \frac{\partial T}{\partial r} + v \frac{\partial T}{\partial y} = \frac{k}{\rho C_p} \left(\frac{\partial^2 T}{\partial r^2} + \frac{1}{r} \frac{\partial T}{\partial r} + \frac{\partial^2 T}{\partial y^2} \right) \quad (2.30)$$

2.3.2 Non-dimensional Analysis

To make dimensionless form of the governing equations (2.30)-(2.32), use respective length d and the kinematic viscosity ν , the non-dimensional uniform velocity is defined by

$U_0 = \frac{\nu}{d}$. It has been introduced some dimensionless quantities

$$x' = \frac{x}{d}; \quad \bar{y} = \frac{y}{d}; \quad z' = \frac{z}{d}; \quad u' = \frac{d}{\nu} u; \quad v' = \frac{d}{\nu} v; \quad w' = \frac{d\sqrt{2\delta}}{\nu} w; \quad t' = \frac{\nu}{d^2} t;$$

$$p' = \frac{d^2}{\rho \nu^2} p; \quad \text{and} \quad T' = \frac{T}{\Delta T}$$

where x', \bar{y} and z' are the non-dimensional horizontal, vertical and axial coordinates respectively; u', v', w' are the non-dimensional velocity components in the direction of x', \bar{y} and z' respectively; t' is the non-dimensional time; T' is the non-dimensional temperature; δ is the non-dimensional curvature of curve duct which is defined by $\delta = \frac{d}{L}$

and p' is also the dimensionless pressure.

And it has also been used the transformation equations $r=L+dx'$ and $L\theta=dz'$ [i.e. $r=L+x$ and $L\theta=z$] to transform the above equations in to the rectangular coordinate system. The remaining transformation $y=hy'$ will be use later after simplification of the equations.

Now we calculate necessary terms which are involved in the equations (2.28)-(2.30).

$$\begin{array}{ll}
x = d x'; & y = d \bar{y}; & z = d z' & \partial x = \frac{1}{d} \partial x'; & \partial y = \frac{1}{d} \partial \bar{y}; & \partial z = \frac{1}{d} \partial z' \\
L\theta = z; & t = \frac{d^2}{v} t' & & \partial \theta = \frac{1}{L} \partial z; & \partial t = \frac{d^2}{v} \partial t' & \\
r = L+x = L+dx' = \frac{d}{\delta} + dx' = \frac{d(1+x'\delta)}{\delta} & & & \partial r = d \partial x' & & \\
u = \frac{v}{d} u'; & v = \frac{v}{d} v'; & w = \frac{v}{d\sqrt{2\delta}} w' & \partial u = \frac{v}{d} \partial u'; & \partial v = \frac{v}{d} \partial v'; & \partial w = \frac{v}{d\sqrt{2\delta}} \partial w' \\
p = \frac{\rho v^2}{d^2} p'; & T = \Delta T T' & & \partial p = \frac{\rho v^2}{d^2} \partial p'; & \partial T = \Delta T \partial T' & \\
\frac{\partial u}{\partial t} = \frac{v^2}{d^3} \frac{\partial u'}{\partial t'} & & & \frac{\partial^2 u}{\partial r^2} = \frac{\partial}{\partial r} \left(\frac{v}{d^2} \frac{\partial u'}{\partial x'} \right) = \frac{v}{d^3} \frac{\partial^2 u'}{\partial x'^2} & & \\
\frac{\partial v}{\partial t} = \frac{v^2}{d^3} \frac{\partial v'}{\partial t'} & & & \frac{\partial^2 v}{\partial r^2} = \frac{\partial}{\partial r} \left(\frac{v}{d^2} \frac{\partial v'}{\partial x'} \right) = \frac{v}{d^3} \frac{\partial^2 v'}{\partial x'^2} & & \\
\frac{\partial w}{\partial t} = \frac{v^2}{d^3 \sqrt{2\delta}} \frac{\partial w'}{\partial t'} & & & \frac{\partial^2 w}{\partial r^2} = \frac{\partial}{\partial r} \left(\frac{v}{d^2 \sqrt{2\delta}} \frac{\partial w'}{\partial x'} \right) = \frac{v}{d^3 \sqrt{2\delta}} \frac{\partial^2 w'}{\partial x'^2} & & \\
\frac{\partial u}{\partial r} = \frac{v}{d^2} \frac{\partial u'}{\partial x'} & & & \frac{\partial v}{\partial y} = \frac{v}{d^2} \frac{\partial v'}{\partial \bar{y}} & & \\
\frac{\partial v}{\partial r} = \frac{v}{d^2} \frac{\partial v'}{\partial x'} & & & \frac{\partial p}{\partial r} = \frac{\rho v^2}{d^3} \frac{\partial p'}{\partial x'} & & \\
\frac{\partial w}{\partial r} = \frac{v}{d^2 \sqrt{2\delta}} \frac{\partial w'}{\partial x'} & & & \frac{\partial p}{\partial y} = \frac{\rho v^2}{d^3} \frac{\partial p'}{\partial \bar{y}} & & \\
\frac{\partial w}{\partial y} = \frac{v}{d^2 \sqrt{2\delta}} \frac{\partial w'}{\partial \bar{y}} & & & \frac{\partial p}{\partial \theta} = L \frac{\partial p}{\partial z} & & \\
\frac{\partial T}{\partial t} = \frac{v}{d^2} \Delta T \frac{\partial T'}{\partial t'} & & & \frac{\partial^2 T}{\partial r^2} = \frac{\partial}{\partial r} \left(\frac{\partial T}{\partial r} \right) = \frac{\partial}{\partial r} \left(\frac{\Delta T}{d} \frac{\partial T'}{\partial x'} \right) = \frac{\Delta T}{d^2} \frac{\partial^2 T'}{\partial x'^2} & & \\
\frac{\partial T}{\partial r} = \frac{\Delta T}{d} \frac{\partial T'}{\partial x'} & & & \frac{\partial^2 T}{\partial y^2} = \frac{\partial}{\partial \bar{y}} \left(\frac{\partial T}{\partial \bar{y}} \right) = \frac{\partial}{\partial \bar{y}} \left(\frac{\Delta T}{d} \frac{\partial T'}{\partial \bar{y}} \right) = \frac{\Delta T}{d^2} \frac{\partial^2 T'}{\partial \bar{y}^2} & & \\
\frac{\partial T}{\partial y} = \frac{\Delta T}{d} \frac{\partial T'}{\partial \bar{y}} & & & & &
\end{array}$$

Putting these terms in equations (2.28)-(2.30):

From continuity equation (2.28)

$$\frac{\partial u}{\partial r} + \frac{\partial v}{\partial y} + \frac{u}{r} = 0$$

$$\text{Or, } \frac{v}{d^2} \frac{\partial u'}{\partial x'} + \frac{v}{d^2} \frac{\partial v'}{\partial \bar{y}} + \frac{\delta}{d(1+x'\delta)} \frac{v}{d} u' = 0$$

$$\text{Or, } \frac{v}{d^2} \left(\frac{\partial u'}{\partial x'} + \frac{\partial v'}{\partial \bar{y}} + \frac{\delta}{1+x'\delta} u' \right) = 0$$

$$\therefore \frac{\partial u'}{\partial x'} + \frac{\partial v'}{\partial y} + \frac{\delta}{1+x'\delta} u' = 0$$

From 1st equation of Momentum equation (2.29)

$$\frac{\partial u}{\partial t} + u \frac{\partial u}{\partial r} + v \frac{\partial u}{\partial y} - \frac{w^2}{r} = -\frac{1}{\rho} \frac{\partial p}{\partial r} + v \left(\frac{\partial^2 u}{\partial r^2} + \frac{1}{r} \frac{\partial u}{\partial r} + \frac{\partial^2 u}{\partial y^2} - \frac{u}{r^2} \right) + 2w\Omega_0 + \frac{\sigma\mu_e B_0^2}{\rho} \left[\frac{mw - u(1+m\alpha)}{(1+m\alpha)^2 + m^2} \right]$$

$$\text{Or, } \frac{v^2}{d^3} \frac{\partial u'}{\partial t'} + \frac{v}{d} u' \frac{v}{d^2} \frac{\partial u'}{\partial x'} + \frac{v}{d} v' \frac{v}{d^2} \frac{\partial u'}{\partial y} - \frac{\delta}{d(1+x'\delta)} \frac{v^2}{d^2 2\delta} w'^2 = -\frac{1}{\rho} \frac{\rho v^2}{d^3} \frac{\partial p'}{\partial x'}$$

$$+ v \left(\frac{v}{d^3} \frac{\partial^2 u'}{\partial x'^2} + \frac{\delta}{d(1+x'\delta)} \frac{v}{d^2} \frac{\partial u'}{\partial x'} + \frac{v}{d^3} \frac{\partial^2 u'}{\partial y^2} - \frac{v}{d} u' \frac{\delta^2}{d^2 (1+x'\delta)^2} \right) + \frac{2v}{d\sqrt{2\delta}} w' \Omega_0$$

$$+ \frac{1}{\rho} \frac{\sigma\mu_e B_0^2}{(1+m\alpha)^2 + m^2} \left(\frac{mv}{d\sqrt{2\delta}} w' - \frac{v}{d} u' (1+m\alpha) \right)$$

$$\text{Or, } \frac{v^2}{d^3} \left(\frac{\partial u'}{\partial t'} + u' \frac{\partial u'}{\partial x'} + v' \frac{\partial u'}{\partial y} - \frac{w'^2}{2(1+x'\delta)} \right) = -\frac{v^2}{d^3} \frac{\partial p'}{\partial x'} + \frac{v^2}{d^3} \left(\frac{\partial^2 u'}{\partial x'^2} + \frac{\delta}{1+x'\delta} \frac{\partial u'}{\partial x'} + \frac{\partial^2 u'}{\partial y^2} - \frac{\delta^2}{(1+x'\delta)^2} u' \right)$$

$$+ \frac{2v}{d\sqrt{2\delta}} w' \Omega_0 + \frac{v}{\rho d} \frac{\sigma\mu_e B_0^2}{(1+m\alpha)^2 + m^2} \left(\frac{m}{\sqrt{2\delta}} w' - (1+m\alpha) u' \right)$$

$$\text{Or, } \frac{\partial u'}{\partial t'} + u' \frac{\partial u'}{\partial x'} + v' \frac{\partial u'}{\partial y} - \frac{w'^2}{2(1+\delta x')} = -\frac{\partial p'}{\partial x'} + \left(\frac{\partial^2 u'}{\partial x'^2} + \frac{\delta}{1+\delta x'} \frac{\partial u'}{\partial x'} + \frac{\partial^2 u'}{\partial y^2} - \frac{\delta^2 u'}{(1+\delta x')^2} \right)$$

$$+ \frac{d^3}{v^2} \times \frac{2v}{d\sqrt{2\delta}} w' \Omega_0 + \frac{d^3}{v^2} \times \frac{v}{\rho d} \frac{\sigma\mu_e B_0^2}{(1+m\alpha)^2 + m^2} \left(\frac{m}{\sqrt{2\delta}} w' - (1+m\alpha) u' \right)$$

$$\text{Or, } \frac{\partial u'}{\partial t'} + u' \frac{\partial u'}{\partial x'} + v' \frac{\partial u'}{\partial y} - \frac{w'^2}{2(1+\delta x')} = -\frac{\partial p'}{\partial x'} + \left(\frac{\partial^2 u'}{\partial x'^2} + \frac{\delta}{(1+\delta x')} \frac{\partial u'}{\partial x'} + \frac{\partial^2 u'}{\partial y^2} - \frac{\delta^2 u'}{(1+\delta x')^2} \right)$$

$$+ \frac{1}{2} \times \frac{2d^2 \sqrt{2\delta}}{\delta v} \Omega_0 w' + \frac{d^2 \sigma\mu_e B_0^2}{\rho v} \frac{1}{(1+m\alpha)^2 + m^2} \left(\frac{m}{\sqrt{2\delta}} w' - (1+m\alpha) u' \right)$$

$$\therefore \frac{\partial u'}{\partial t'} + u' \frac{\partial u'}{\partial x'} + v' \frac{\partial u'}{\partial y} - \frac{w'^2}{2(1+\delta x')} = -\frac{\partial p'}{\partial x'} + \left(\frac{\partial^2 u'}{\partial x'^2} + \frac{\delta}{(1+\delta x')} \frac{\partial u'}{\partial x'} + \frac{\partial^2 u'}{\partial y^2} - \frac{\delta^2 u'}{(1+\delta x')^2} \right)$$

$$+ \frac{T_r}{2} w' + \frac{M}{(1+m\alpha)^2 + m^2} \left(\frac{1}{\sqrt{2\delta}} mw' - (1+m\alpha) u' \right)$$

where, $T_r = \frac{2d^2 \sqrt{2\delta}}{\delta v} \Omega_0 = \frac{2d^2 \Omega_0}{v} \sqrt{\frac{2}{\delta}}$ is the Taylor number and $M = \frac{d^2 \sigma\mu_e B_0^2}{\rho v}$ is the

Magnetic parameter.

From 2nd equation of Momentum equation (2.29)

$$\frac{\partial v}{\partial t} + u \frac{\partial v}{\partial r} + v \frac{\partial v}{\partial y} = -\frac{1}{\rho} \frac{\partial p}{\partial y} + v \left(\frac{\partial^2 v}{\partial r^2} + \frac{1}{r} \frac{\partial v}{\partial r} + \frac{\partial^2 v}{\partial y^2} \right) + \beta g T$$

$$\text{Or, } \frac{v^2}{d^3} \frac{\partial v'}{\partial t'} + \frac{v}{d} u' \frac{v}{d^2} \frac{\partial v'}{\partial x'} + \frac{v}{d} v' \frac{v}{d^2} \frac{\partial v'}{\partial y} = -\frac{1}{\rho} \frac{\rho v^2}{d^3} \frac{\partial p'}{\partial y} + v \left(\frac{v}{d^3} \frac{\partial^2 v'}{\partial x'^2} + \frac{\delta}{d(1+x'\delta)} \frac{v}{d^2} \frac{\partial v'}{\partial x'} + \frac{v}{d^3} \frac{\partial^2 v'}{\partial y^2} \right) + \beta g \Delta T T'$$

$$\text{Or, } \frac{v^2}{d^3} \frac{\partial v'}{\partial t'} + \frac{v^2}{d^3} u' \frac{\partial v'}{\partial x'} + \frac{v^2}{d^3} v' \frac{\partial v'}{\partial \bar{y}} = -\frac{v^2}{d^3} \frac{\partial p'}{\partial \bar{y}} + \frac{v^2}{d^3} \left(\frac{\partial^2 v'}{\partial x'^2} + \frac{\delta}{1+x'\delta} \frac{\partial v'}{\partial x'} + \frac{\partial^2 v'}{\partial \bar{y}^2} \right) + \beta g \Delta T T'$$

$$\text{Or, } \frac{\partial v'}{\partial t'} + u' \frac{\partial v'}{\partial x'} + v' \frac{\partial v'}{\partial \bar{y}} = -\frac{\partial p'}{\partial \bar{y}} + \left(\frac{\partial^2 v'}{\partial x'^2} + \frac{\delta}{1+x'\delta} \frac{\partial v'}{\partial x'} + \frac{\partial^2 v'}{\partial \bar{y}^2} \right) + \frac{d^3 \beta g \Delta T}{v^2} T'$$

$$\therefore \frac{\partial v'}{\partial t'} + u' \frac{\partial v'}{\partial x'} + v' \frac{\partial v'}{\partial \bar{y}} = -\frac{\partial p'}{\partial \bar{y}} + \left(\frac{\partial^2 v'}{\partial x'^2} + \frac{\delta}{1+x'\delta} \frac{\partial v'}{\partial x'} + \frac{\partial^2 v'}{\partial \bar{y}^2} \right) + G_r T'$$

where $G_r = \frac{d^3 \beta g \Delta T}{v^2}$ is the Grashof Number.

Again 3rd equation of Momentum equation (2.29)

$$\frac{\partial w}{\partial t} + u \frac{\partial w}{\partial r} + v \frac{\partial w}{\partial y} + \frac{uw}{r} = -\frac{1}{\rho} \frac{1}{r} \frac{\partial p}{\partial \theta} + v \left(\frac{\partial^2 w}{\partial r^2} + \frac{1}{r} \frac{\partial w}{\partial r} + \frac{\partial^2 w}{\partial y^2} - \frac{w}{r^2} \right) - 2u\Omega_0 - \frac{\sigma \mu_e B_0^2}{\rho} \left[\frac{mu + (1+m\alpha)w}{(1+m\alpha)^2 + m^2} \right]$$

$$\begin{aligned} \text{Or, } \frac{v^2}{d^3 \sqrt{2\delta}} \frac{\partial w'}{\partial t'} + \frac{v}{d} u' \frac{v}{d^2 \sqrt{2\delta}} \frac{\partial w'}{\partial x'} + \frac{v}{d} v' \frac{v}{d^2 \sqrt{2\delta}} \frac{\partial w'}{\partial \bar{y}} + \frac{\delta}{d(1+x'\delta)} \frac{v}{d} u' \frac{v}{d \sqrt{2\delta}} w' &= -\frac{1}{\rho} \frac{\delta}{d(1+x'\delta)} L \frac{\partial p}{\partial z} \\ + v \left(\frac{v}{d^3 \sqrt{2\delta}} \frac{\partial^2 w'}{\partial x'^2} + \frac{1}{d(\delta^{-1}+x')} \frac{v}{d^2 \sqrt{2\delta}} \frac{\partial w'}{\partial x'} + \frac{v}{d^3 \sqrt{2\delta}} \frac{\partial^2 w'}{\partial \bar{y}^2} - \frac{1}{d^2(\delta^{-1}+x')^2} \frac{v}{l \sqrt{2\delta}} w' \right) &- 2 \frac{v}{d} u' \Omega_0 \\ - \frac{\sigma \mu_e B_0^2}{\rho [(1+m\alpha)^2 + m^2]} \left(\frac{mv}{d} u' + \frac{v(1+m\alpha)}{d \sqrt{2\delta}} w' \right) & \end{aligned}$$

$$\begin{aligned} \text{Or, } \frac{v^2}{d^3 \sqrt{2\delta}} \left(\frac{\partial w'}{\partial t'} + u' \frac{\partial w'}{\partial x'} + v' \frac{\partial w'}{\partial \bar{y}} + \frac{1}{(\delta^{-1}+x')} u' w' \right) &= -\frac{L}{\rho d} \frac{\delta}{(1+x'\delta)} \frac{\partial p}{\partial z} \\ + \frac{v^2}{d^3 \sqrt{2\delta}} \left(\frac{\partial^2 w'}{\partial x'^2} + \frac{1}{(\delta^{-1}+x')} \frac{\partial w'}{\partial x'} + \frac{\partial^2 w'}{\partial \bar{y}^2} - \frac{1}{(\delta^{-1}+x')^2} w' \right) &- \frac{2v}{d} u' \Omega_0 \\ - \frac{v}{d \rho} \times \frac{\sigma \mu_e B_0^2}{(1+m\alpha)^2 + m^2} \left(mu' + \frac{1+m\alpha}{\sqrt{2\delta}} w' \right) & \end{aligned}$$

$$\begin{aligned} \text{Or, } \frac{\partial w'}{\partial t'} + u' \frac{\partial w'}{\partial x'} + v' \frac{\partial w'}{\partial \bar{y}} + \frac{\delta}{1+x'\delta} u' w' &= -\frac{d^3 \sqrt{2\delta}}{v^2} \times \frac{\delta L}{\rho d} \frac{1}{1+x'\delta} \frac{\partial p}{\partial z} \\ + \left(\frac{\partial^2 w'}{\partial x'^2} + \frac{1}{(\delta^{-1}+x')} \frac{\partial w'}{\partial x'} + \frac{\partial^2 w'}{\partial \bar{y}^2} - \frac{1}{(\delta^{-1}+x')^2} w' \right) &- \frac{d^3 \sqrt{2\delta}}{v^2} \times \frac{2v}{d} u' \Omega_0 \\ - \frac{v}{d \rho} \times \frac{d^3 \sqrt{2\delta}}{v^2} \times \frac{\sigma \mu_e B_0^2}{(1+m\alpha)^2 + m^2} \left(mu' + \frac{1+m\alpha}{\sqrt{2\delta}} w' \right) & \end{aligned}$$

$$\begin{aligned} \text{Or, } \frac{\partial w'}{\partial t'} + u' \frac{\partial w'}{\partial x'} + v' \frac{\partial w'}{\partial \bar{y}} + \frac{\delta}{1+x'\delta} u' w' &= -\frac{d^2 L \delta \sqrt{2\delta}}{\rho v^2} \frac{\partial p}{\partial z} \frac{1}{1+x'\delta} \\ + \left(\frac{\partial^2 w'}{\partial x'^2} + \frac{\delta}{1+x'\delta} \frac{\partial w'}{\partial x'} + \frac{\partial^2 w'}{\partial \bar{y}^2} - \frac{1}{(\delta^{-1}+x')^2} w' \right) &- \frac{2d^2 \sqrt{2\delta}}{v} \Omega_0 u' \\ - \frac{d^2 \sigma \mu_e B_0^2}{\rho v} \times \frac{\sqrt{2\delta}}{(1+m\alpha)^2 + m^2} \left(mu' + \frac{1+m\alpha}{\sqrt{2\delta}} w' \right) & \end{aligned}$$

$$\text{Or, } \frac{\partial w'}{\partial t'} + u' \frac{\partial w'}{\partial x'} + v' \frac{\partial w'}{\partial \bar{y}} + \frac{\delta}{1+x'\delta} u' w' = -\frac{d^2 \delta L \sqrt{2\delta}}{\rho v^2} \frac{\partial p}{\partial z} \frac{1}{1+x'\delta}$$

$$\begin{aligned}
& + \left(\frac{\partial^2 w'}{\partial x'^2} + \frac{\delta}{1+x'\delta} \frac{\partial w'}{\partial x'} + \frac{\partial^2 w'}{\partial \bar{y}^2} - \frac{\delta^2}{(1+x'\delta)^2} w' \right) - \delta \frac{2d^2 \sqrt{2\delta}}{\delta v} \Omega_0 u' \\
& - \frac{d^2 \sigma \mu_e B_0^2}{\rho v} \times \frac{1}{(1+m\alpha)^2 + m^2} \left(m \sqrt{2\delta} u' + (1+m\alpha) w' \right) \\
\therefore \frac{\partial w'}{\partial t'} + u' \frac{\partial w'}{\partial x'} + v' \frac{\partial w'}{\partial \bar{y}} + \frac{\delta}{1+x'\delta} u' w' &= \frac{D_n}{1+x'\delta} \\
& + \frac{\partial^2 w'}{\partial x'^2} + \frac{\delta}{1+x'\delta} \frac{\partial w'}{\partial x'} + \frac{\partial^2 w'}{\partial \bar{y}^2} - \frac{\delta^2}{(1+\delta x')^2} w' - \delta T_{,u'} - M \left(\frac{\sqrt{2\delta} m u' + (1+m\alpha) w'}{(1+m\alpha)^2 + m^2} \right)
\end{aligned}$$

where, $D_n = -\frac{d^2 L \delta \sqrt{2\delta}}{\rho v^2} \frac{\partial p}{\partial z} = \left(-\frac{\partial p}{\partial z} \right) \frac{d^2 L \delta}{\rho v v} \sqrt{2\delta} = P \frac{d^2 d}{\rho v v} \sqrt{2\delta} = \frac{P d^3}{\mu v} \sqrt{\frac{2d}{L}}$ is the Dean

Number, $P = -\frac{\partial p}{\partial z}$ is the pressure gradient and $\delta = \frac{d}{L}$ is the curvature of the duct.

From energy equation (2.30)

$$\begin{aligned}
\frac{\partial T}{\partial t} + u \frac{\partial T}{\partial r} + v \frac{\partial T}{\partial y} &= \frac{k}{\rho C_p} \left[\frac{\partial^2 T}{\partial r^2} + \frac{1}{r} \frac{\partial T}{\partial r} + \frac{\partial^2 T}{\partial y^2} \right] \\
\text{Or, } \frac{v}{d^2} \Delta T \frac{\partial T'}{\partial t'} + \frac{v}{d} u' \frac{\Delta T}{d} \frac{\partial T'}{\partial x'} + \frac{v}{d} v' \frac{\Delta T}{d} \frac{\partial T'}{\partial \bar{y}} &= \frac{k}{\rho C_p} \left(\frac{\Delta T}{d^2} \frac{\partial^2 T'}{\partial x'^2} + \frac{\delta}{d(1+x'\delta)} \frac{\Delta T}{d} \frac{\partial T'}{\partial x'} + \frac{\Delta T}{d^2} \frac{\partial^2 T'}{\partial \bar{y}^2} \right) \\
\text{Or, } \frac{v}{d^2} \Delta T \frac{\partial T'}{\partial t'} + \frac{v}{d^2} \Delta T u' \frac{\partial T'}{\partial x'} + \frac{v}{d^2} \Delta T v' \frac{\partial T'}{\partial \bar{y}} &= \frac{k}{\rho C_p} \frac{1}{d^2} \Delta T \left[\frac{\partial^2 T'}{\partial x'^2} + \frac{\delta}{1+x'\delta} \frac{\partial T'}{\partial x'} + \frac{\partial^2 T'}{\partial \bar{y}^2} \right] \\
\text{Or, } \frac{\partial T'}{\partial t'} + u' \frac{\partial T'}{\partial x'} + v' \frac{\partial T'}{\partial \bar{y}} &= \frac{k}{\rho C_p} \frac{d^2}{v \Delta T} \frac{\Delta T}{d^2} \left[\frac{\partial^2 T'}{\partial x'^2} + \frac{\delta}{1+x'\delta} \frac{\partial T'}{\partial x'} + \frac{\partial^2 T'}{\partial \bar{y}^2} \right] \\
\text{Or, } \frac{\partial T'}{\partial t'} + u' \frac{\partial T'}{\partial x'} + v' \frac{\partial T'}{\partial \bar{y}} &= \frac{k}{v \rho C_p} \left[\frac{\partial^2 T'}{\partial x'^2} + \frac{\delta}{1+x'\delta} \frac{\partial T'}{\partial x'} + \frac{\partial^2 T'}{\partial \bar{y}^2} \right] \\
\therefore \frac{\partial T'}{\partial t'} + u' \frac{\partial T'}{\partial x'} + v' \frac{\partial T'}{\partial \bar{y}} &= \frac{1}{P_r} \left[\frac{\partial^2 T'}{\partial x'^2} + \frac{\delta}{1+x'\delta} \frac{\partial T'}{\partial x'} + \frac{\partial^2 T'}{\partial \bar{y}^2} \right]
\end{aligned}$$

where, $P_r = \frac{v \rho C_p}{k}$ is the Prandtl Number.

Now dropping the primes on the variables, the non-dimensional forms of the above equations are as follows:

Continuity equation

$$\frac{\partial u}{\partial x} + \frac{\partial v}{\partial \bar{y}} + \frac{\delta}{1+x\delta} u = 0 \tag{2.34a}$$

Momentum equation

$$\frac{\partial u}{\partial t} + u \frac{\partial u}{\partial x} + v \frac{\partial u}{\partial y} - \frac{w^2}{2(1+x\delta)} = -\frac{\partial p}{\partial x} + \frac{\partial^2 u}{\partial x^2} + \frac{\delta}{1+x\delta} \frac{\partial u}{\partial x} + \frac{\partial^2 u}{\partial y^2} - \frac{\delta u}{(1+x\delta)^2} + \frac{T_r}{2} w + M \left(\frac{\frac{1}{\sqrt{2\delta}} m w - (1+m\alpha)u}{(1+m\alpha)^2 + m^2} \right) \quad (2.31b)$$

$$\frac{\partial v}{\partial t} + u \frac{\partial v}{\partial x} + v \frac{\partial v}{\partial y} = -\frac{\partial p}{\partial y} + \frac{\partial^2 v}{\partial x^2} + \frac{\delta}{1+x\delta} \frac{\partial v}{\partial x} + \frac{\partial^2 v}{\partial y^2} + G_r T \quad (2.31c)$$

$$\begin{aligned} \frac{\partial w}{\partial t} + u \frac{\partial w}{\partial x} + v \frac{\partial w}{\partial y} + \frac{\delta}{1+x\delta} u w = \frac{1}{1+x\delta} D_n + \frac{\partial^2 w}{\partial x^2} + \frac{\delta}{1+x\delta} \frac{\partial w}{\partial x} + \frac{\partial^2 w}{\partial y^2} - \frac{\delta^2}{(1+x\delta)^2} w \\ - \delta T_r u - M \left(\frac{\sqrt{2\delta} m u + (1+m\alpha)w}{(1+m\alpha)^2 + m^2} \right) \end{aligned} \quad (2.31d)$$

Energy equation

$$\frac{\partial T}{\partial t} + u \frac{\partial T}{\partial x} + v \frac{\partial T}{\partial y} = \frac{1}{P_r} \left(\frac{\partial^2 T}{\partial x^2} + \frac{\delta}{1+x\delta} \frac{\partial T}{\partial x} + \frac{\partial^2 T}{\partial y^2} \right) \quad (2.31e)$$

where, $D_n = \frac{Gd^3}{\mu\nu} \sqrt{\frac{2d}{L}}$ is the Dean Number,

$T_r = \frac{2d^2 \sqrt{2\delta}}{\delta\nu} \Omega_0$ is the Taylor number,

$M = \frac{d^2 \sigma' \mu_e B_0^2}{\rho\nu}$ is the Magnetic parameter

$G_r = \frac{d^3 \beta g \Delta T}{\nu^2}$ is the Grashof number and

$P_r = \frac{\nu \rho C_p}{k}$ is the Prandtl Number.

Now let us consider the sectional stream function

$$u = \frac{1}{1+x\delta} \frac{\partial \psi}{\partial y} \quad \text{and} \quad v = -\frac{1}{1+x\delta} \frac{\partial \psi}{\partial x} \quad (2.32)$$

Clearly these stream functions are satisfies the following continuity equation

$$\frac{\partial u}{\partial x} + \frac{\partial v}{\partial y} + \frac{\delta}{1+x\delta} u = 0$$

To verify

$$\begin{aligned} \text{L.H.S.} &= \frac{\partial}{\partial x} \left(\frac{1}{1+x\delta} \frac{\partial \psi}{\partial y} \right) + \frac{\partial}{\partial y} \left(-\frac{1}{1+x\delta} \frac{\partial \psi}{\partial x} \right) + \frac{\delta}{1+x\delta} \left(\frac{1}{1+x\delta} \frac{\partial \psi}{\partial y} \right) \\ &= \frac{1}{1+x\delta} \frac{\partial^2 \psi}{\partial x \partial y} + \frac{\delta}{(1+x\delta)^2} \frac{\partial \psi}{\partial y} - \frac{1}{1+x\delta} \frac{\partial^2 \psi}{\partial y \partial x} + \frac{\delta}{(1+x\delta)^2} \frac{\partial \psi}{\partial y} \\ &= 0 \\ &= \text{R.H.S.} \end{aligned}$$

$$\begin{aligned} \text{Put } 1+x\delta = z \text{ then} \\ \frac{\partial}{\partial x} \left(\frac{1}{1+x\delta} \right) &= \frac{\partial}{\partial z} \left(\frac{1}{z} \right) \frac{\partial z}{\partial x} \\ &= -\frac{1}{z^2} \frac{\partial}{\partial x} (1+x\delta) \\ &= -\frac{1}{z^2} \frac{\delta}{\partial x} (dx) \\ &= -\frac{\delta}{(1+x\delta)^2} \end{aligned}$$

Hence $u = \frac{1}{1+x\delta} \frac{\partial \psi}{\partial y}$ and $v = -\frac{1}{1+x\delta} \frac{\partial \psi}{\partial x}$ are the appropriate stream function for

governing equations (2.31b)-(2.31e). Now by using these stream functions, these give that From equation (2.31b)

$$\frac{\partial u}{\partial t} + u \frac{\partial u}{\partial x} + v \frac{\partial u}{\partial y} - \frac{w^2}{2(1+x\delta)} = -\frac{\partial p}{\partial x} + \frac{\partial^2 u}{\partial x^2} + \frac{\delta}{1+x\delta} \frac{\partial u}{\partial x} + \frac{\partial^2 u}{\partial y^2} - \frac{\delta^2 u}{(1+x\delta)^2} + \frac{T_r}{2} w + M \left(\frac{\frac{1}{\sqrt{2\delta}} mw - (1+m\alpha)u}{(1+m\alpha)^2 + m^2} \right)$$

$$\begin{aligned} \text{Or, } \frac{\partial}{\partial t} \left(\frac{1}{1+x\delta} \frac{\partial \psi}{\partial y} \right) + \frac{1}{1+x\delta} \frac{\partial \psi}{\partial y} \frac{\partial}{\partial x} \left(\frac{1}{1+x\delta} \frac{\partial \psi}{\partial y} \right) + \left(-\frac{1}{1+x\delta} \frac{\partial \psi}{\partial x} \right) \frac{\partial}{\partial y} \left(\frac{1}{1+x\delta} \frac{\partial \psi}{\partial y} \right) - \frac{w^2}{2(1+x\delta)} \\ = -\frac{\partial p}{\partial x} + \frac{\partial^2}{\partial x^2} \left(\frac{1}{1+x\delta} \frac{\partial \psi}{\partial y} \right) + \frac{\delta}{1+x\delta} \frac{\partial}{\partial x} \left(\frac{1}{1+x\delta} \frac{\partial \psi}{\partial y} \right) + \frac{\partial^2}{\partial y^2} \left(\frac{1}{1+x\delta} \frac{\partial \psi}{\partial y} \right) - \frac{\delta^2}{(1+x\delta)^2} \left(\frac{1}{1+x\delta} \frac{\partial \psi}{\partial y} \right) + \frac{1}{2} T_r w \\ + \frac{M}{(1+m\alpha)^2 + m^2} \left(\frac{1}{\sqrt{2\delta}} mw - (1+m\alpha) \frac{1}{1+x\delta} \frac{\partial \psi}{\partial y} \right) \end{aligned}$$

$$\begin{aligned} \text{Or, } \frac{1}{1+x\delta} \frac{\partial}{\partial t} \left(\frac{\partial \psi}{\partial y} \right) + \frac{1}{1+x\delta} \frac{\partial \psi}{\partial y} \left(\frac{1}{1+x\delta} \frac{\partial^2 \psi}{\partial x \partial y} - \frac{\delta}{(1+x\delta)^2} \frac{\partial \psi}{\partial y} \right) - \frac{1}{(1+x\delta)^2} \frac{\partial \psi}{\partial x} \frac{\partial^2 \psi}{\partial y^2} - \frac{w^2}{2(1+x\delta)} \\ = -\frac{\partial p}{\partial x} + \frac{\partial}{\partial x} \left(\frac{1}{1+x\delta} \frac{\partial^2 \psi}{\partial x \partial y} - \frac{\delta}{(1+x\delta)^2} \frac{\partial \psi}{\partial y} \right) + \frac{\delta}{1+x\delta} \left(\frac{1}{1+x\delta} \frac{\partial^2 \psi}{\partial x \partial y} - \frac{\delta}{(1+x\delta)^2} \frac{\partial \psi}{\partial y} \right) \\ + \frac{1}{1+x\delta} \frac{\partial^3 \psi}{\partial y^3} - \frac{\delta^2}{(1+x\delta)^3} \frac{\partial \psi}{\partial y} + \frac{1}{2} T_r w + \frac{M}{(1+m\alpha)^2 + m^2} \left(\frac{1}{\sqrt{2\delta}} mw - (1+m\alpha) \frac{1}{1+x\delta} \frac{\partial \psi}{\partial y} \right) \end{aligned}$$

$$\begin{aligned} \text{Or, } \frac{1}{1+x\delta} \frac{\partial^2 \psi}{\partial t \partial y} + \frac{1}{(1+x\delta)^2} \frac{\partial \psi}{\partial y} \frac{\partial^2 \psi}{\partial x \partial y} - \frac{\delta}{(1+x\delta)^3} \left(\frac{\partial \psi}{\partial y} \right)^2 - \frac{1}{(1+x\delta)^2} \frac{\partial \psi}{\partial x} \frac{\partial^2 \psi}{\partial y^2} - \frac{w^2}{2(1+x\delta)} \\ = -\frac{\partial p}{\partial x} + \frac{\partial}{\partial x} \left(\frac{1}{1+x\delta} \frac{\partial^2 \psi}{\partial x \partial y} \right) - \frac{\partial}{\partial x} \left(\frac{\delta}{(1+x\delta)^2} \frac{\partial \psi}{\partial y} \right) + \frac{\delta}{(1+x\delta)^2} \frac{\partial^2 \psi}{\partial x \partial y} \\ - \frac{\delta^2}{(1+x\delta)^3} \frac{\partial \psi}{\partial y} + \frac{1}{1+x\delta} \frac{\partial^3 \psi}{\partial y^3} - \frac{\delta^2}{(1+x\delta)^3} \frac{\partial \psi}{\partial y} + \frac{1}{2} T_r w \\ + \frac{M}{(1+m\alpha)^2 + m^2} \left(\frac{1}{\sqrt{2\delta}} mw - (1+m\alpha) \frac{1}{1+x\delta} \frac{\partial \psi}{\partial y} \right) \end{aligned}$$

By putting $1 + \delta x = s$, then

$$\frac{\partial}{\partial x} \left[\frac{\delta}{(1+x\delta)^2} \right] = \delta \frac{\partial}{\partial s} \left(\frac{1}{s^2} \right) \frac{\partial s}{\partial x} = -\frac{2\delta}{s^3} \frac{\partial}{\partial x} (1+x\delta) = -\frac{2\delta}{s^3} \frac{\delta}{\partial x} (dx) = -\frac{2\delta^2}{(1+x\delta)^3}$$

$$\begin{aligned} \text{Or, } \frac{1}{1+x\delta} \frac{\partial^2 \psi}{\partial t \partial y} + \frac{1}{(1+x\delta)^2} \frac{\partial \psi}{\partial y} \frac{\partial^2 \psi}{\partial x \partial y} - \frac{\delta}{(1+x\delta)^3} \left(\frac{\partial \psi}{\partial y} \right)^2 - \frac{1}{(1+x\delta)^2} \frac{\partial \psi}{\partial x} \frac{\partial^2 \psi}{\partial y^2} - \frac{w^2}{2(1+x\delta)} \\ = -\frac{\partial p}{\partial x} + \frac{\partial}{\partial x} \left(\frac{1}{1+x\delta} \frac{\partial^2 \psi}{\partial x \partial y} \right) - \frac{\partial}{\partial x} \left(\frac{\delta}{(1+x\delta)^2} \frac{\partial \psi}{\partial y} \right) + \frac{\delta}{(1+x\delta)^2} \frac{\partial^2 \psi}{\partial x \partial y} \\ - \frac{\delta^2}{(1+x\delta)^3} \frac{\partial \psi}{\partial y} + \frac{1}{1+x\delta} \frac{\partial^3 \psi}{\partial y^3} - \frac{\delta^2}{(1+x\delta)^3} \frac{\partial \psi}{\partial y} + \frac{1}{2} T_r w \\ + \frac{M}{(1+m\alpha)^2 + m^2} \left(\frac{1}{\sqrt{2\delta}} mw - (1+m\alpha) \frac{1}{1+x\delta} \frac{\partial \psi}{\partial y} \right) \end{aligned}$$

$$\begin{aligned}
\text{Or, } & \frac{1}{1+x\delta} \frac{\partial^2 \psi}{\partial t \partial \bar{y}} + \frac{1}{(1+x\delta)^2} \frac{\partial \psi}{\partial \bar{y}} \frac{\partial^2 \psi}{\partial x \partial \bar{y}} - \frac{\delta}{(1+x\delta)^3} \left(\frac{\partial \psi}{\partial \bar{y}} \right)^2 - \frac{1}{(1+x\delta)^2} \frac{\partial \psi}{\partial x} \frac{\partial^2 \psi}{\partial \bar{y}^2} - \frac{w^2}{2(1+x\delta)} \\
& = -\frac{\partial p}{\partial x} + \left[\frac{1}{1+x\delta} \frac{\partial^3 \psi}{\partial x^2 \partial \bar{y}} - \frac{\delta}{(1+x\delta)^2} \frac{\partial^2 \psi}{\partial x \partial \bar{y}} \right] - \left[\frac{\delta}{(1+x\delta)^2} \frac{\partial^2 \psi}{\partial x \partial \bar{y}} - \frac{2\delta^2}{(1+x\delta)^3} \frac{\partial \psi}{\partial \bar{y}} \right] \\
& \quad + \frac{\delta}{(1+x\delta)^2} \frac{\partial^2 \psi}{\partial x \partial \bar{y}} - \frac{2\delta^2}{(1+x\delta)^3} \frac{\partial \psi}{\partial \bar{y}} + \frac{1}{1+x\delta} \frac{\partial^3 \psi}{\partial \bar{y}^3} + \frac{1}{2} T_{r,w} \\
& \quad + \frac{M}{(1+m\alpha)^2 + m^2} \left[\frac{1}{\sqrt{2\delta}} mw - (1+m\alpha) \frac{1}{1+x\delta} \frac{\partial \psi}{\partial \bar{y}} \right] \\
\text{Or, } & \frac{1}{1+x\delta} \frac{\partial^2 \psi}{\partial t \partial \bar{y}} + \frac{1}{(1+x\delta)^2} \frac{\partial \psi}{\partial \bar{y}} \frac{\partial^2 \psi}{\partial x \partial \bar{y}} - \frac{\delta}{(1+x\delta)^3} \left(\frac{\partial \psi}{\partial \bar{y}} \right)^2 - \frac{1}{(1+x\delta)^2} \frac{\partial \psi}{\partial x} \frac{\partial^2 \psi}{\partial \bar{y}^2} - \frac{w^2}{2(1+x\delta)} \\
& = -\frac{\partial p}{\partial x} + \frac{1}{1+x\delta} \frac{\partial^3 \psi}{\partial x^2 \partial \bar{y}} - \frac{\delta}{(1+x\delta)^2} \frac{\partial^2 \psi}{\partial x \partial \bar{y}} - \frac{\delta}{(1+x\delta)^2} \frac{\partial^2 \psi}{\partial x \partial \bar{y}} + \frac{2\delta^2}{(1+x\delta)^3} \frac{\partial \psi}{\partial \bar{y}} \\
& \quad + \frac{\delta}{(1+x\delta)^2} \frac{\partial^2 \psi}{\partial x \partial \bar{y}} - \frac{2\delta^2}{(1+x\delta)^3} \frac{\partial \psi}{\partial \bar{y}} + \frac{1}{1+x\delta} \frac{\partial^3 \psi}{\partial \bar{y}^3} + \frac{1}{2} T_{r,w} \\
& \quad + \frac{M}{(1+m\alpha)^2 + m^2} \left[\frac{1}{\sqrt{2\delta}} mw - (1+m\alpha) \frac{1}{1+x\delta} \frac{\partial \psi}{\partial \bar{y}} \right] \\
\therefore & \frac{1}{1+x\delta} \frac{\partial^2 \psi}{\partial t \partial \bar{y}} + \frac{1}{(1+x\delta)^2} \frac{\partial \psi}{\partial \bar{y}} \frac{\partial^2 \psi}{\partial x \partial \bar{y}} - \frac{\delta}{(1+x\delta)^3} \left(\frac{\partial \psi}{\partial \bar{y}} \right)^2 - \frac{1}{(1+x\delta)^2} \frac{\partial \psi}{\partial x} \frac{\partial^2 \psi}{\partial \bar{y}^2} - \frac{w^2}{2(1+x\delta)} \\
& = -\frac{\partial p}{\partial x} + \frac{1}{1+x\delta} \frac{\partial^3 \psi}{\partial x^2 \partial \bar{y}} - \frac{\delta}{(1+x\delta)^2} \frac{\partial^2 \psi}{\partial x \partial \bar{y}} + \frac{1}{1+x\delta} \frac{\partial^3 \psi}{\partial \bar{y}^3} + \frac{1}{2} T_{r,w} + \frac{M}{(1+m\alpha)^2 + m^2} \left(\frac{m}{\sqrt{2\delta}} w - \frac{1+m\alpha}{1+x\delta} \frac{\partial \psi}{\partial \bar{y}} \right)
\end{aligned}$$

From equation (2.31c)

$$\begin{aligned}
& \frac{\partial v}{\partial t} + u \frac{\partial v}{\partial x} + v \frac{\partial v}{\partial \bar{y}} = -\frac{\partial p}{\partial y} + \frac{\partial^2 v}{\partial x^2} + \frac{\delta}{1+x\delta} \frac{\partial v}{\partial x} + \frac{\partial^2 v}{\partial \bar{y}^2} + G_{,T} \\
\text{Or, } & \frac{\partial}{\partial t} \left(-\frac{1}{1+x\delta} \frac{\partial \psi}{\partial x} \right) + \frac{1}{1+x\delta} \frac{\partial \psi}{\partial \bar{y}} \frac{\partial}{\partial x} \left(-\frac{1}{1+x\delta} \frac{\partial \psi}{\partial x} \right) + \left(-\frac{1}{1+x\delta} \frac{\partial \psi}{\partial x} \right) \frac{\partial}{\partial \bar{y}} \left(-\frac{1}{1+x\delta} \frac{\partial \psi}{\partial x} \right) \\
& = -\frac{\partial p}{\partial \bar{y}} + \frac{\partial^2}{\partial x^2} \left(-\frac{1}{1+x\delta} \frac{\partial \psi}{\partial x} \right) + \frac{\delta}{1+x\delta} \frac{\partial}{\partial x} \left(-\frac{1}{1+x\delta} \frac{\partial \psi}{\partial x} \right) + \frac{\partial^2}{\partial \bar{y}^2} \left(-\frac{1}{1+x\delta} \frac{\partial \psi}{\partial x} \right) + G_{,T} \\
\text{Or, } & -\frac{1}{1+x\delta} \frac{\partial}{\partial t} \left(\frac{\partial \psi}{\partial x} \right) - \frac{1}{1+x\delta} \frac{\partial \psi}{\partial \bar{y}} \frac{\partial}{\partial x} \left(\frac{1}{1+x\delta} \frac{\partial \psi}{\partial x} \right) + \frac{1}{1+x\delta} \frac{\partial \psi}{\partial x} \frac{\partial}{\partial \bar{y}} \left(\frac{1}{1+x\delta} \frac{\partial \psi}{\partial x} \right) \\
& = -\frac{\partial p}{\partial \bar{y}} - \frac{\partial^2}{\partial x^2} \left(\frac{1}{1+x\delta} \frac{\partial \psi}{\partial x} \right) - \frac{\delta}{1+x\delta} \frac{\partial}{\partial x} \left(\frac{1}{1+x\delta} \frac{\partial \psi}{\partial x} \right) - \frac{\partial^2}{\partial \bar{y}^2} \left(\frac{1}{1+x\delta} \frac{\partial \psi}{\partial x} \right) + G_{,T} \\
\text{Or, } & -\frac{1}{1+x\delta} \frac{\partial^2 \psi}{\partial t \partial x} - \frac{1}{1+x\delta} \frac{\partial \psi}{\partial \bar{y}} \left(\frac{1}{1+x\delta} \frac{\partial^2 \psi}{\partial x^2} - \frac{\delta}{(1+x\delta)^2} \frac{\partial \psi}{\partial x} \right) + \frac{1}{(1+x\delta)^2} \frac{\partial \psi}{\partial x} \frac{\partial^2 \psi}{\partial \bar{y} \partial x} \\
& = -\frac{\partial p}{\partial \bar{y}} - \frac{\partial}{\partial x} \left(\frac{1}{1+x\delta} \frac{\partial^2 \psi}{\partial x^2} - \frac{\delta}{(1+x\delta)^2} \frac{\partial \psi}{\partial x} \right) - \frac{\delta}{1+x\delta} \left(\frac{1}{1+x\delta} \frac{\partial^2 \psi}{\partial x^2} - \frac{\delta}{(1+x\delta)^2} \frac{\partial \psi}{\partial x} \right) \\
& \quad - \frac{1}{1+x\delta} \left(\frac{\partial^3 \psi}{\partial \bar{y}^2 \partial x} \right) + G_{,T}
\end{aligned}$$

$$\begin{aligned} \text{Or, } & -\frac{1}{1+x\delta} \frac{\partial^2 \psi}{\partial t \partial x} - \frac{1}{(1+x\delta)^2} \frac{\partial \psi}{\partial \bar{y}} \frac{\partial^2 \psi}{\partial x^2} + \frac{\delta}{(1+x\delta)^3} \frac{\partial \psi}{\partial x} \frac{\partial \psi}{\partial \bar{y}} + \frac{1}{(1+x\delta)^2} \frac{\partial \psi}{\partial x} \frac{\partial^2 \psi}{\partial \bar{y} \partial x} \\ & = -\frac{\partial p}{\partial \bar{y}} - \left[\left\{ \frac{1}{1+x\delta} \frac{\partial^3 \psi}{\partial x^3} - \frac{\delta}{(1+x\delta)^2} \frac{\partial^2 \psi}{\partial x^2} \right\} - \left\{ \frac{\delta}{(1+x\delta)^2} \frac{\partial^2 \psi}{\partial x^2} - \frac{2\delta^2}{(1+x\delta)^3} \frac{\partial \psi}{\partial x} \right\} \right] \\ & \quad - \left(\frac{\delta}{(1+x\delta)^2} \frac{\partial^2 \psi}{\partial x^2} - \frac{\delta^2}{(1+x\delta)^3} \frac{\partial \psi}{\partial x} \right) - \frac{1}{1+x\delta} \frac{\partial^3 \psi}{\partial \bar{y}^2 \partial x} + G_r T \end{aligned}$$

$$\begin{aligned} \text{Or, } & -\frac{1}{1+x\delta} \frac{\partial^2 \psi}{\partial t \partial x} - \frac{1}{(1+x\delta)^2} \frac{\partial \psi}{\partial \bar{y}} \frac{\partial^2 \psi}{\partial x^2} + \frac{\delta}{(1+x\delta)^3} \frac{\partial \psi}{\partial x} \frac{\partial \psi}{\partial \bar{y}} + \frac{1}{(1+x\delta)^2} \frac{\partial \psi}{\partial x} \frac{\partial^2 \psi}{\partial \bar{y} \partial x} \\ & = -\frac{\partial p}{\partial \bar{y}} - \frac{1}{1+x\delta} \frac{\partial^3 v}{\partial x^3} + \frac{\delta}{(1+x\delta)^2} \frac{\partial^2 v}{\partial x^2} + \frac{\delta}{(1+x\delta)^2} \frac{\partial^2 \psi}{\partial x^2} - \frac{2\delta^2}{(1+x\delta)^3} \frac{\partial \psi}{\partial x} \\ & \quad - \frac{\delta}{(1+x\delta)^2} \frac{\partial^2 \psi}{\partial x^2} + \frac{\delta^2}{(1+x\delta)^3} \frac{\partial \psi}{\partial x} - \frac{1}{1+x\delta} \frac{\partial^3 \psi}{\partial \bar{y}^2 \partial x} + G_r T \end{aligned}$$

$$\begin{aligned} \therefore & -\frac{1}{1+x\delta} \frac{\partial^2 \psi}{\partial t \partial x} - \frac{1}{(1+x\delta)^2} \frac{\partial \psi}{\partial \bar{y}} \frac{\partial^2 \psi}{\partial x^2} + \frac{\delta}{(1+x\delta)^3} \frac{\partial \psi}{\partial x} \frac{\partial \psi}{\partial \bar{y}} + \frac{1}{(1+x\delta)^2} \frac{\partial \psi}{\partial x} \frac{\partial^2 \psi}{\partial \bar{y} \partial x} \\ & = -\frac{\partial p}{\partial \bar{y}} - \frac{1}{1+x\delta} \frac{\partial^3 \psi}{\partial x^3} + \frac{\delta}{(1+x\delta)^2} \frac{\partial^2 \psi}{\partial x^2} - \frac{\delta^2}{(1+x\delta)^3} \frac{\partial \psi}{\partial x} - \frac{1}{1+x\delta} \frac{\partial^3 \psi}{\partial \bar{y}^2 \partial x} + G_r T \end{aligned}$$

From equation (2.31d)

$$\begin{aligned} \frac{\partial w}{\partial t} + u \frac{\partial w}{\partial x} + v \frac{\partial w}{\partial \bar{y}} + \frac{\delta}{1+x\delta} u w = \frac{1}{1+x\delta} D_n + \frac{\partial^2 w}{\partial x^2} + \frac{\delta}{1+x\delta} \frac{\partial w}{\partial x} + \frac{\partial^2 w}{\partial \bar{y}^2} - \frac{\delta^2}{(1+x\delta)^2} w \\ - \delta T_r u - M \left(\frac{\sqrt{2\delta} m u + (1+m\alpha) w}{(1+m\alpha)^2 + m^2} \right) \end{aligned}$$

$$\begin{aligned} \text{Or, } \frac{\partial w}{\partial t} + \frac{1}{1+x\delta} \frac{\partial \psi}{\partial \bar{y}} \frac{\partial w}{\partial x} - \frac{1}{1+x\delta} \frac{\partial \psi}{\partial x} \frac{\partial w}{\partial \bar{y}} + \frac{\delta w}{1+x\delta} \frac{1}{1+x\delta} \frac{\partial \psi}{\partial \bar{y}} = \frac{D_n}{1+x\delta} + \frac{\partial^2 w}{\partial x^2} + \frac{\delta}{1+x\delta} \frac{\partial w}{\partial x} \\ + \frac{\partial^2 w}{\partial \bar{y}^2} - \frac{\delta^2 w}{(1+x\delta)^2} - \delta T_r \left(\frac{1}{1+x\delta} \frac{\partial \psi}{\partial \bar{y}} \right) - \frac{M}{(1+m\alpha)^2 + m^2} \left[\frac{\sqrt{2\delta} m}{1+x\delta} \frac{\partial \psi}{\partial \bar{y}} + (1+m\alpha) w \right] \end{aligned}$$

$$\begin{aligned} \text{Or, } (1+x\delta) \frac{\partial w}{\partial t} + \frac{\partial \psi}{\partial \bar{y}} \frac{\partial w}{\partial x} - \frac{\partial \psi}{\partial x} \frac{\partial w}{\partial \bar{y}} + \frac{\delta w}{1+x\delta} \frac{\partial \psi}{\partial \bar{y}} = D_n + (1+x\delta) \frac{\partial^2 w}{\partial x^2} + \delta \frac{\partial w}{\partial x} + (1+x\delta) \frac{\partial^2 w}{\partial \bar{y}^2} \\ - \frac{\delta^2 w}{1+x\delta} - \delta T_r \frac{\partial \psi}{\partial \bar{y}} - \frac{(1+x\delta) M}{(1+m\alpha)^2 + m^2} \left(\frac{\sqrt{2\delta} m}{1+x\delta} \frac{\partial \psi}{\partial \bar{y}} + (1+m\alpha) w \right) \end{aligned}$$

$$\begin{aligned} \text{Or, } (1+x\delta) \frac{\partial w}{\partial t} = - \left(\frac{\partial \psi}{\partial \bar{y}} \frac{\partial w}{\partial x} - \frac{\partial \psi}{\partial x} \frac{\partial w}{\partial \bar{y}} \right) - \frac{\delta w}{1+x\delta} \frac{\partial \psi}{\partial \bar{y}} + D_n + (1+x\delta) \left(\frac{\partial^2 w}{\partial x^2} + \frac{\partial^2 w}{\partial \bar{y}^2} \right) + \delta \frac{\partial w}{\partial x} \\ - \frac{\delta^2}{1+x\delta} w - \delta T_r \frac{\partial \psi}{\partial \bar{y}} - \frac{M}{(1+m\alpha)^2 + m^2} \left(\sqrt{2\delta} m \frac{\partial \psi}{\partial \bar{y}} + (1+x\delta)(1+m\alpha) w \right) \end{aligned}$$

$$\text{Or, } (1+x\delta) \frac{\partial w}{\partial t} = - \left(\frac{\partial \psi}{\partial \bar{y}} \frac{\partial w}{\partial x} - \frac{\partial \psi}{\partial x} \frac{\partial w}{\partial \bar{y}} \right) + \delta \frac{\partial w}{\partial x} + D_n + (1+x\delta) \left(\frac{\partial^2 w}{\partial x^2} + \frac{\partial^2 w}{\partial \bar{y}^2} \right) - \frac{\delta^2}{1+x\delta} w$$

$$\begin{aligned}
& -\frac{\delta w}{1+x\delta} \frac{\partial \psi}{\partial \bar{y}} - \delta T_r \frac{\partial \psi}{\partial \bar{y}} - \frac{M}{(1+m\alpha)^2 + m^2} \left(\sqrt{2\delta} m \frac{\partial \psi}{\partial \bar{y}} + (1+x\delta)(1+m\alpha)w \right) \\
\therefore (1+x\delta) \frac{\partial w}{\partial t} = & -\left(\frac{\partial \psi}{\partial \bar{y}} \frac{\partial w}{\partial x} - \frac{\partial \psi}{\partial x} \frac{\partial w}{\partial \bar{y}} \right) + \delta \frac{\partial w}{\partial x} + D_n + (1+x\delta) \left[\left(\frac{\partial^2}{\partial x^2} + \frac{\partial^2}{\partial \bar{y}^2} \right) w - \frac{\delta^2}{(1+x\delta)^2} w \right] \\
& -\frac{\delta w}{1+x\delta} \frac{\partial \psi}{\partial \bar{y}} - \delta T_r \frac{\partial \psi}{\partial \bar{y}} - \frac{M}{(1+m\alpha)^2 + m^2} \left(\sqrt{2\delta} m \frac{\partial \psi}{\partial \bar{y}} + (1+x\delta)(1+m\alpha)w \right)
\end{aligned}$$

From equation (2.31e)

$$\begin{aligned}
\frac{\partial T}{\partial t} + u \frac{\partial T}{\partial x} + v \frac{\partial T}{\partial \bar{y}} &= \frac{1}{P_r} \left(\frac{\partial^2 T}{\partial x^2} + \frac{\delta}{1+x\delta} \frac{\partial T}{\partial x} + \frac{\partial^2 T}{\partial \bar{y}^2} \right) \\
\text{Or, } \frac{\partial T}{\partial t} + \frac{1}{1+x\delta} \frac{\partial \psi}{\partial \bar{y}} \frac{\partial T}{\partial x} - \frac{1}{1+x\delta} \frac{\partial \psi}{\partial x} \frac{\partial T}{\partial \bar{y}} &= \frac{1}{P_r} \left(\frac{\partial^2 T}{\partial x^2} + \frac{\delta}{1+x\delta} \frac{\partial T}{\partial x} + \frac{\partial^2 T}{\partial \bar{y}^2} \right) \\
\text{Or, } \frac{\partial T}{\partial t} + \frac{1}{1+x\delta} \left(\frac{\partial \psi}{\partial \bar{y}} \frac{\partial T}{\partial x} - \frac{\partial \psi}{\partial x} \frac{\partial T}{\partial \bar{y}} \right) &= \frac{1}{P_r} \left(\frac{\partial^2 T}{\partial x^2} + \frac{\delta}{1+x\delta} \frac{\partial T}{\partial x} + \frac{\partial^2 T}{\partial \bar{y}^2} \right) \\
\text{Or, } \frac{\partial T}{\partial t} + \frac{1}{1+x\delta} \left(\frac{\partial \psi}{\partial \bar{y}} \frac{\partial T}{\partial x} - \frac{\partial \psi}{\partial x} \frac{\partial T}{\partial \bar{y}} \right) &= \frac{1}{P_r} \left(\frac{\partial^2 T}{\partial x^2} + \frac{\delta}{1+x\delta} \frac{\partial T}{\partial x} + \frac{\partial^2 T}{\partial \bar{y}^2} \right) \\
\text{Or, } (1+x\delta) \frac{\partial T}{\partial t} + \left(\frac{\partial \psi}{\partial \bar{y}} \frac{\partial T}{\partial x} - \frac{\partial \psi}{\partial x} \frac{\partial T}{\partial \bar{y}} \right) &= \frac{(1+x\delta)}{P_r} \left(\frac{\partial^2 T}{\partial x^2} + \frac{\delta}{1+x\delta} \frac{\partial T}{\partial x} + \frac{\partial^2 T}{\partial \bar{y}^2} \right) \\
\therefore (1+x\delta) \frac{\partial T}{\partial t} + \left(\frac{\partial \psi}{\partial \bar{y}} \frac{\partial T}{\partial x} - \frac{\partial \psi}{\partial x} \frac{\partial T}{\partial \bar{y}} \right) &= \frac{(1+x\delta)}{P_r} \left[\left(\frac{\partial^2}{\partial x^2} + \frac{\partial^2}{\partial \bar{y}^2} \right) T + \frac{\delta}{1+x\delta} \frac{\partial T}{\partial x} \right]
\end{aligned}$$

Momentum equation

Tangential u -component

$$\begin{aligned}
& \frac{1}{1+x\delta} \frac{\partial^2 \psi}{\partial \bar{y}^2} + \frac{1}{(1+x\delta)^2} \frac{\partial \psi}{\partial \bar{y}} \frac{\partial^2 \psi}{\partial x \partial \bar{y}} - \frac{\delta}{(1+x\delta)^3} \left(\frac{\partial \psi}{\partial \bar{y}} \right)^2 - \frac{1}{(1+x\delta)^2} \frac{\partial \psi}{\partial x} \frac{\partial^2 \psi}{\partial \bar{y}^2} - \frac{w^2}{2(1+x\delta)} \\
& = -\frac{\partial p}{\partial x} + \frac{1}{1+x\delta} \frac{\partial^3 \psi}{\partial x^2 \partial \bar{y}} - \frac{\delta}{(1+x\delta)^2} \frac{\partial^2 \psi}{\partial x \partial \bar{y}} + \frac{1}{1+x\delta} \frac{\partial^3 \psi}{\partial \bar{y}^3} + \frac{1}{2} T_r w + \frac{M}{(1+m\alpha)^2 + m^2} \left(\frac{m}{\sqrt{2\delta}} w - \frac{1+m\alpha}{1+x\delta} \frac{\partial \psi}{\partial \bar{y}} \right) \quad (2.32a)
\end{aligned}$$

Vertical v -component

$$\begin{aligned}
& -\frac{1}{1+x\delta} \frac{\partial^2 \psi}{\partial \bar{y}^2} - \frac{1}{(1+x\delta)^2} \frac{\partial \psi}{\partial \bar{y}} \frac{\partial^2 \psi}{\partial x^2} + \frac{\delta}{(1+x\delta)^3} \frac{\partial \psi}{\partial x} \frac{\partial \psi}{\partial \bar{y}} + \frac{1}{(1+x\delta)^2} \frac{\partial \psi}{\partial x} \frac{\partial^2 \psi}{\partial \bar{y} \partial x} \\
& = -\frac{\partial p}{\partial \bar{y}} - \frac{1}{1+x\delta} \frac{\partial^3 \psi}{\partial x^3} + \frac{\delta}{(1+x\delta)^2} \frac{\partial^2 \psi}{\partial x^2} - \frac{\delta^2}{(1+x\delta)^3} \frac{\partial \psi}{\partial x} - \frac{1}{1+x\delta} \frac{\partial^3 \Psi}{\partial \bar{y}^2 \partial x} \psi + G_r T \quad (2.32b)
\end{aligned}$$

Axial w -component

$$\begin{aligned}
(1+x\delta) \frac{\partial w}{\partial t} = & -\left(\frac{\partial \psi}{\partial \bar{y}} \frac{\partial w}{\partial x} - \frac{\partial \psi}{\partial x} \frac{\partial w}{\partial \bar{y}} \right) + \delta \frac{\partial w}{\partial x} + D_n + (1+x\delta) \left[\left(\frac{\partial^2}{\partial x^2} + \frac{\partial^2}{\partial \bar{y}^2} \right) w - \frac{\delta^2}{(1+x\delta)^2} w \right] \\
& -\frac{\delta w}{1+x\delta} \frac{\partial \psi}{\partial \bar{y}} - \delta T_r \frac{\partial \psi}{\partial \bar{y}} - \frac{M}{(1+m\alpha)^2 + m^2} \left(\sqrt{2\delta} m \frac{\partial \psi}{\partial \bar{y}} + (1+x\delta)(1+m\alpha)w \right)
\end{aligned} \quad (2.32c)$$

Energy equation

$$(1+x\delta) \frac{\partial T}{\partial t} + \left(\frac{\partial \psi}{\partial \bar{y}} \frac{\partial T}{\partial x} - \frac{\partial \psi}{\partial x} \frac{\partial T}{\partial \bar{y}} \right) = \frac{(1+x\delta)}{P_r} \left[\left(\frac{\partial^2}{\partial x^2} + \frac{\partial^2}{\partial \bar{y}^2} \right) T + \frac{\delta}{1+x\delta} \frac{\partial T}{\partial x} \right] \quad (2.32d)$$

To find the unique equation for streamlines of the secondary velocity, it is required to combine the tangential and vertical component of momentum equations. To do this differentiate the equation (2.32a) with respect to \bar{y} and equation (2.32b) with respect to x , and then subtract them.

By differentiating equation (2.31a), with respect to y gives

$$\begin{aligned} \frac{\partial}{\partial \bar{y}} \left[\frac{1}{1+x\delta} \frac{\partial^2 \psi}{\partial t \partial \bar{y}} + \frac{1}{(1+x\delta)^2} \frac{\partial \psi}{\partial \bar{y}} \frac{\partial^2 \psi}{\partial x \partial \bar{y}} - \frac{\delta}{(1+x\delta)^3} \left(\frac{\partial \psi}{\partial \bar{y}} \right)^2 - \frac{1}{(1+x\delta)^2} \frac{\partial \psi}{\partial x} \frac{\partial^2 \psi}{\partial \bar{y}^2} - \frac{w^2}{2(1+x\delta)} \right] \\ = \frac{\partial}{\partial \bar{y}} \left[-\frac{\partial p}{\partial x} + \frac{1}{1+x\delta} \frac{\partial^3 \psi}{\partial x^2 \partial \bar{y}} - \frac{\delta}{(1+x\delta)^2} \frac{\partial^2 \psi}{\partial x \partial \bar{y}} + \frac{1}{1+x\delta} \frac{\partial^3 \psi}{\partial \bar{y}^3} + \frac{1}{2} T_r w + \frac{M}{(1+m\alpha)^2 + m^2} \left(\frac{m}{\sqrt{2\delta}} w - \frac{1+m\alpha}{1+x\delta} \frac{\partial \psi}{\partial \bar{y}} \right) \right] \end{aligned}$$

$$\begin{aligned} \text{Or, } \frac{1}{1+x\delta} \frac{\partial^3 \psi}{\partial t \partial \bar{y}^2} + \frac{1}{(1+x\delta)^2} \left(\frac{\partial^2 \psi}{\partial \bar{y}^2} \frac{\partial^2 \psi}{\partial x \partial \bar{y}} + \frac{\partial \psi}{\partial \bar{y}} \frac{\partial^3 \psi}{\partial x \partial \bar{y}^2} \right) \\ - \frac{\delta}{(1+x\delta)^3} 2 \frac{\partial \psi}{\partial \bar{y}} \frac{\partial^2 \psi}{\partial \bar{y}^2} - \frac{1}{(1+x\delta)^2} \left(\frac{\partial \psi}{\partial x} \frac{\partial^3 \psi}{\partial \bar{y}^3} + \frac{\partial^2 \psi}{\partial \bar{y} \partial x} \frac{\partial^2 \psi}{\partial \bar{y}^2} \right) - \frac{1}{2(1+x\delta)} 2w \frac{\partial w}{\partial \bar{y}} \\ = -\frac{\partial}{\partial \bar{y}} \left(\frac{\partial p}{\partial x} \right) + \frac{1}{1+x\delta} \frac{\partial^4 \psi}{\partial x^2 \partial \bar{y}^2} - \frac{\delta}{(1+x\delta)^2} \frac{\partial^3 \psi}{\partial x \partial \bar{y}^2} + \frac{1}{1+x\delta} \frac{\partial^4 \psi}{\partial \bar{y}^4} + \frac{T_r}{2} \frac{\partial w}{\partial \bar{y}} \\ + \frac{M}{(1+m\alpha)^2 + m^2} \left(\frac{m}{\sqrt{2\delta}} \frac{\partial w}{\partial \bar{y}} - \frac{1+m\alpha}{1+x\delta} \frac{\partial^2 \psi}{\partial \bar{y}^2} \right) \end{aligned}$$

$$\begin{aligned} \text{Or, } \frac{1}{1+x\delta} \frac{\partial^3 \psi}{\partial t \partial \bar{y}^2} + \frac{1}{(1+x\delta)^2} \left(\frac{\partial^2 \psi}{\partial \bar{y}^2} \frac{\partial^2 \psi}{\partial x \partial \bar{y}} + \frac{\partial \psi}{\partial \bar{y}} \frac{\partial^3 \psi}{\partial x \partial \bar{y}^2} \right) - \frac{\delta}{(1+x\delta)^3} 2 \frac{\partial \psi}{\partial \bar{y}} \frac{\partial^2 \psi}{\partial \bar{y}^2} \\ - \frac{1}{(1+x\delta)^2} \left(\frac{\partial \psi}{\partial x} \frac{\partial^3 \psi}{\partial \bar{y}^3} + \frac{\partial^2 \psi}{\partial \bar{y} \partial x} \frac{\partial^2 \psi}{\partial \bar{y}^2} \right) - \frac{1}{(1+x\delta)} w \frac{\partial w}{\partial \bar{y}} \\ = -\frac{\partial}{\partial \bar{y}} \left(\frac{\partial p}{\partial x} \right) + \frac{1}{1+x\delta} \frac{\partial^4 \psi}{\partial x^2 \partial \bar{y}^2} - \frac{\delta}{(1+x\delta)^2} \frac{\partial^3 \psi}{\partial x \partial \bar{y}^2} + \frac{1}{1+x\delta} \frac{\partial^4 \psi}{\partial \bar{y}^4} + \frac{T_r}{2} \frac{\partial w}{\partial \bar{y}} \\ + \frac{M}{(1+m\alpha)^2 + m^2} \left(\frac{m}{\sqrt{2\delta}} \frac{\partial w}{\partial \bar{y}} - \frac{1+m\alpha}{1+x\delta} \frac{\partial^2 \psi}{\partial \bar{y}^2} \right) \end{aligned}$$

$$\begin{aligned} \therefore \frac{1}{1+x\delta} \frac{\partial^3 \psi}{\partial t \partial \bar{y}^2} + \frac{1}{(1+x\delta)^2} \frac{\partial^2 \psi}{\partial \bar{y}^2} \frac{\partial^2 \psi}{\partial x \partial \bar{y}} + \frac{1}{(1+x\delta)^2} \frac{\partial \psi}{\partial \bar{y}} \frac{\partial^3 \psi}{\partial x \partial \bar{y}^2} \\ - \frac{2\delta}{(1+x\delta)^3} \frac{\partial \psi}{\partial \bar{y}} \frac{\partial^2 \psi}{\partial \bar{y}^2} - \frac{1}{(1+x\delta)^2} \frac{\partial \psi}{\partial x} \frac{\partial^3 \psi}{\partial \bar{y}^3} - \frac{1}{(1+x\delta)^2} \frac{\partial^2 \psi}{\partial \bar{y} \partial x} \frac{\partial^2 \psi}{\partial \bar{y}^2} - \frac{1}{(1+x\delta)} w \frac{\partial w}{\partial \bar{y}} \\ = -\frac{\partial^2 p}{\partial \bar{y} \partial x} + \frac{1}{1+x\delta} \frac{\partial^4 \psi}{\partial x^2 \partial \bar{y}^2} - \frac{\delta}{(1+x\delta)^2} \frac{\partial^3 \psi}{\partial x \partial \bar{y}^2} + \frac{1}{1+x\delta} \frac{\partial^4 \psi}{\partial \bar{y}^4} + \frac{T_r}{2} \frac{\partial w}{\partial \bar{y}} \\ + \frac{M}{(1+m\alpha)^2 + m^2} \left(\frac{m}{\sqrt{2\delta}} \frac{\partial w}{\partial \bar{y}} - \frac{1+m\alpha}{1+x\delta} \frac{\partial^2 \psi}{\partial \bar{y}^2} \right) \quad (2.33a) \end{aligned}$$

Again by differentiating equation (2.32b), with respect to x gives

$$\begin{aligned}
& \left[\frac{1}{(1+x\delta)^2} \frac{\partial \psi}{\partial \bar{y}} \frac{\partial^3 \psi}{\partial x^3} + \frac{1}{(1+x\delta)^2} \frac{\partial^2 \psi}{\partial x \partial \bar{y}} \frac{\partial^2 \psi}{\partial x^2} - \frac{1}{(1+x\delta)^2} \frac{\partial \psi}{\partial x} \frac{\partial^3 \psi}{\partial \bar{y} \partial x^2} - \frac{1}{(1+x\delta)^2} \frac{\partial^2 \psi}{\partial x^2} \frac{\partial^2 \psi}{\partial \bar{y} \partial x} \right. \\
& + \frac{1}{(1+x\delta)^2} \frac{\partial^2 \psi}{\partial \bar{y}^2} \frac{\partial^2 \psi}{\partial x \partial \bar{y}} + \frac{1}{(1+x\delta)^2} \frac{\partial \psi}{\partial \bar{y}} \frac{\partial^3 \psi}{\partial x \partial \bar{y}^2} - \frac{1}{(1+x\delta)^2} \frac{\partial \psi}{\partial x} \frac{\partial^3 \psi}{\partial \bar{y}^3} - \frac{1}{(1+x\delta)^2} \frac{\partial^2 \psi}{\partial \bar{y} \partial x} \frac{\partial^2 \psi}{\partial \bar{y}^2} \\
& \left. - \frac{1}{1+x\delta} \frac{\partial^4 \psi}{\partial x^4} - \frac{1}{1+x\delta} \frac{\partial^4 \psi}{\partial \bar{y}^2 \partial x^2} - \frac{1}{1+x\delta} \frac{\partial^4 \psi}{\partial x^2 \partial \bar{y}^2} - \frac{1}{1+x\delta} \frac{\partial^4 \psi}{\partial \bar{y}^4} \right] \\
& + \left[-\frac{2\delta}{(1+x\delta)^3} \frac{\partial \psi}{\partial \bar{y}} \frac{\partial^2 \psi}{\partial x^2} - \frac{\delta}{(1+x\delta)^3} \frac{\partial \psi}{\partial x} \frac{\partial^2 \psi}{\partial x \partial \bar{y}} - \frac{\delta}{(1+x\delta)^3} \frac{\partial^2 \psi}{\partial x^2} \frac{\partial \psi}{\partial \bar{y}} - \frac{2\delta}{(1+x\delta)^3} \frac{\partial \psi}{\partial \bar{y}} \frac{\partial^2 \psi}{\partial \bar{y}^2} \right. \\
& \left. + \frac{2\delta}{(1+x\delta)^3} \frac{\partial \psi}{\partial x} \frac{\partial^2 \psi}{\partial \bar{y} \partial x} + \frac{2\delta}{(1+x\delta)^2} \frac{\partial^3 \psi}{\partial x^3} + \frac{\delta}{(1+x\delta)^2} \frac{\partial^3 \psi}{\partial \bar{y}^2 \partial x} + \frac{\delta}{(1+x\delta)^2} \frac{\partial^3 \psi}{\partial x \partial \bar{y}^2} \right] \\
& + \left[\frac{3\delta^2}{(1+x\delta)^4} \frac{\partial \psi}{\partial x} \frac{\partial \psi}{\partial \bar{y}} - \frac{3\delta^2}{(1+x\delta)^3} \frac{\partial^2 \psi}{\partial x^2} + \frac{M}{(1+m\alpha)^2 + m^2} \frac{1+m\alpha}{1+x\delta} \frac{\partial^2 \psi}{\partial \bar{y}^2} \right] \\
& + \left[-\frac{1}{(1+x\delta)} w \frac{\partial w}{\partial \bar{y}} + \frac{3\delta^3}{(1+x\delta)^4} \frac{\partial \psi}{\partial x} - \frac{T_r}{2} \frac{\partial w}{\partial \bar{y}} - \frac{M}{(1+m\alpha)^2 + m^2} \frac{m}{\sqrt{2\delta}} \frac{\partial w}{\partial \bar{y}} \right] + G_r \frac{\partial T}{\partial x}
\end{aligned}$$

Or, $\frac{\partial}{\partial t} \left(\frac{\partial^2 \psi}{\partial x^2} + \frac{\partial^2 \psi}{\partial \bar{y}^2} \right) - \frac{\delta}{1+x\delta} \frac{\partial^2 \psi}{\partial t \partial x}$

$$\begin{aligned}
& = \left[-\frac{1}{(1+x\delta)} \frac{\partial \psi}{\partial \bar{y}} \frac{\partial^3 \psi}{\partial x \partial \bar{y}^2} + \frac{1}{(1+x\delta)} \frac{\partial \psi}{\partial x} \frac{\partial^3 \psi}{\partial \bar{y}^3} - \frac{1}{(1+x\delta)} \frac{\partial \psi}{\partial \bar{y}} \frac{\partial^3 \psi}{\partial x^3} + \frac{1}{(1+x\delta)} \frac{\partial \psi}{\partial x} \frac{\partial^3 \psi}{\partial \bar{y} \partial x^2} + \frac{\partial^4 \psi}{\partial \bar{y}^2 \partial x^2} + \frac{\partial^4 \psi}{\partial \bar{y}^4} + \frac{\partial^4 \psi}{\partial x^4} + \frac{\partial^4 \psi}{\partial \bar{y}^2 \partial x^2} \right] \\
& + \left[\frac{3\delta}{(1+x\delta)^2} \frac{\partial \psi}{\partial \bar{y}} \frac{\partial^2 \psi}{\partial x^2} - \frac{\delta}{(1+x\delta)^2} \frac{\partial \psi}{\partial x} \frac{\partial^2 \psi}{\partial \bar{y} \partial x} + \frac{2\delta}{(1+x\delta)^2} \frac{\partial \psi}{\partial \bar{y}} \frac{\partial^2 \psi}{\partial \bar{y}^2} - \frac{2\delta}{(1+x\delta)} \frac{\partial^3 \psi}{\partial x^3} - \frac{2\delta}{(1+x\delta)} \frac{\partial^3 \psi}{\partial x \partial \bar{y}^2} \right] \\
& + \left[-\frac{3\delta^2}{(1+x\delta)^3} \frac{\partial \psi}{\partial x} \frac{\partial \psi}{\partial \bar{y}} + \frac{3\delta^2}{(1+x\delta)^2} \frac{\partial^2 \psi}{\partial x^2} - \frac{M(1+m\alpha)}{(1+m\alpha)^2 + m^2} \frac{\partial^2 \psi}{\partial \bar{y}^2} \right] \\
& + \left[w \frac{\partial w}{\partial \bar{y}} + (1+\delta x) \frac{T_r}{2} \frac{\partial w}{\partial \bar{y}} - \frac{3\delta^3}{(1+x\delta)^3} \frac{\partial \psi}{\partial x} + \frac{M}{(1+m\alpha)^2 + m^2} \frac{m}{\sqrt{2\delta}} (1+x\delta) \frac{\partial w}{\partial \bar{y}} \right] - G_r (1+x\delta) \frac{\partial T}{\partial x}
\end{aligned}$$

Hence the central line (axial) direction of Momentum equation

$$\begin{aligned}
(1+x\delta) \frac{\partial w}{\partial t} & = - \left(\frac{\partial \psi}{\partial \bar{y}} \frac{\partial w}{\partial x} - \frac{\partial \psi}{\partial x} \frac{\partial w}{\partial \bar{y}} \right) + \delta \frac{\partial w}{\partial x} + D_n + (1+x\delta) \left[\left(\frac{\partial^2}{\partial x^2} + \frac{\partial^2}{\partial \bar{y}^2} \right) w - \frac{\delta^2}{(1+x\delta)^2} w \right] \\
& - \frac{\delta w}{1+x\delta} \frac{\partial \psi}{\partial \bar{y}} - \delta T_r \frac{\partial \psi}{\partial \bar{y}} - \frac{M}{(1+m\alpha)^2 + m^2} \left(\sqrt{2\delta} m \frac{\partial \psi}{\partial \bar{y}} + (1+x\delta)(1+m\alpha)w \right) \quad (2.34a)
\end{aligned}$$

Stream line for the secondary velocity of Momentum equation

$$\begin{aligned}
& \frac{\partial}{\partial t} \left(\frac{\partial^2 \psi}{\partial x^2} + \frac{\partial^2 \psi}{\partial \bar{y}^2} \right) - \frac{\delta}{1+x\delta} \frac{\partial^2 \psi}{\partial t \partial x} \\
& = \left[-\frac{1}{(1+x\delta)} \frac{\partial \psi}{\partial \bar{y}} \frac{\partial^3 \psi}{\partial x \partial \bar{y}^2} + \frac{1}{(1+x\delta)} \frac{\partial \psi}{\partial x} \frac{\partial^3 \psi}{\partial \bar{y}^3} - \frac{1}{(1+x\delta)} \frac{\partial \psi}{\partial \bar{y}} \frac{\partial^3 \psi}{\partial x^3} + \frac{1}{(1+x\delta)} \frac{\partial \psi}{\partial x} \frac{\partial^3 \psi}{\partial \bar{y} \partial x^2} + \frac{\partial^4 \psi}{\partial \bar{y}^2 \partial x^2} + \frac{\partial^4 \psi}{\partial \bar{y}^4} + \frac{\partial^4 \psi}{\partial x^4} + \frac{\partial^4 \psi}{\partial \bar{y}^2 \partial x^2} \right] \\
& + \left[\frac{3\delta}{(1+x\delta)^2} \frac{\partial \psi}{\partial \bar{y}} \frac{\partial^2 \psi}{\partial x^2} - \frac{\delta}{(1+x\delta)^2} \frac{\partial \psi}{\partial x} \frac{\partial^2 \psi}{\partial \bar{y} \partial x} + \frac{2\delta}{(1+x\delta)^2} \frac{\partial \psi}{\partial \bar{y}} \frac{\partial^2 \psi}{\partial \bar{y}^2} - \frac{2\delta}{(1+x\delta)} \frac{\partial^3 \psi}{\partial x^3} - \frac{2\delta}{(1+x\delta)} \frac{\partial^3 \psi}{\partial x \partial \bar{y}^2} \right] \\
& + \left[-\frac{3\delta^2}{(1+x\delta)^3} \frac{\partial \psi}{\partial x} \frac{\partial \psi}{\partial \bar{y}} + \frac{3\delta^2}{(1+x\delta)^2} \frac{\partial^2 \psi}{\partial x^2} - \frac{M(1+m\alpha)}{(1+m\alpha)^2 + m^2} \frac{\partial^2 \psi}{\partial \bar{y}^2} \right]
\end{aligned}$$

$$+ \left[w \frac{\partial w}{\partial \bar{y}} + (1+\delta x) \frac{T_r}{2} \frac{\partial w}{\partial \bar{y}} - \frac{3\delta^3}{(1+x\delta)^3} \frac{\partial \psi}{\partial x} + \frac{M}{(1+m\alpha)^2 + m^2} \frac{m}{\sqrt{2\delta}} (1+x\delta) \frac{\partial w}{\partial \bar{y}} \right] - G_r (1+x\delta) \frac{\partial T}{\partial x} \quad (2.34b)$$

And the Energy equation

$$(1+x\delta) \frac{\partial T}{\partial t} + \left(\frac{\partial \psi}{\partial \bar{y}} \frac{\partial T}{\partial x} - \frac{\partial \psi}{\partial x} \frac{\partial T}{\partial \bar{y}} \right) = \frac{(1+x\delta)}{P_r} \left[\left(\frac{\partial^2}{\partial x^2} + \frac{\partial^2}{\partial \bar{y}^2} \right) T + \frac{\delta}{1+x\delta} \frac{\partial T}{\partial x} \right] \quad (2.34c)$$

It is now looking forward to putting the remaining transformation $y = hy'$.

Since the non-dimensional transformation $\bar{y} = \frac{y}{d} \Rightarrow y = d \bar{y}$

Therefore $d\bar{y} = hy' \Rightarrow \bar{y} = \frac{h}{d} y' \therefore \bar{y} = ly'$,

where, $l = h/d$ is the aspect ratio of this duct. Hence, by using $\bar{y} = ly'$ in to the equations (2.34a)-(2.34c), and thereafter remove prime on this variable for the sake simplicity, it yield

The central line (axial) direction of Momentum equation

$$(1+x\delta) \frac{\partial w}{\partial t} = -\frac{1}{l} \left(\frac{\partial \psi}{\partial y} \frac{\partial w}{\partial x} - \frac{\partial \psi}{\partial x} \frac{\partial w}{\partial y} \right) + \delta \frac{\partial w}{\partial x} + D_n + (1+x\delta) \left[\left(\frac{\partial^2}{\partial x^2} + \frac{1}{l^2} \frac{\partial^2}{\partial y^2} \right) w - \frac{\delta^2}{(1+x\delta)^2} w \right] \\ - \frac{\delta w}{1+x\delta} \frac{1}{l} \frac{\partial \psi}{\partial y} - \frac{\delta}{l} T_r \frac{\partial \psi}{\partial y} - \frac{M}{(1+m\alpha)^2 + m^2} \left(\sqrt{2\delta} m \frac{1}{l} \frac{\partial \psi}{\partial y} + (1+x\delta)(1+m\alpha)w \right) \quad (2.35a)$$

Combined radial and tangential direction of Momentum equation

$$\frac{\partial}{\partial t} \left(\frac{\partial^2 \psi}{\partial x^2} + \frac{1}{l^2} \frac{\partial^2 \psi}{\partial y^2} \right) - \frac{\delta}{1+x\delta} \frac{\partial^2 \psi}{\partial t \partial x} \\ = \left[-\frac{1}{(1+x\delta)l^3} \frac{1}{\partial y} \frac{\partial \psi}{\partial x} \frac{\partial^3 \psi}{\partial x \partial y^2} + \frac{1}{(1+x\delta)l^3} \frac{1}{\partial x} \frac{\partial \psi}{\partial y} \frac{\partial^3 \psi}{\partial y^3} - \frac{1}{(1+x\delta)l} \frac{1}{\partial y} \frac{\partial \psi}{\partial x} \frac{\partial^3 \psi}{\partial x^3} + \frac{1}{(1+x\delta)l} \frac{1}{\partial x} \frac{\partial \psi}{\partial y} \frac{\partial^3 \psi}{\partial y \partial x^2} + \frac{2}{l^2} \frac{\partial^4 \psi}{\partial y^2 \partial x^2} + \frac{1}{l^4} \frac{\partial^4 \psi}{\partial y^4} + \frac{\partial^4 \psi}{\partial x^4} \right] \\ + \left[\frac{3\delta}{(1+x\delta)^2} \frac{1}{l} \frac{\partial \psi}{\partial y} \frac{\partial^2 \psi}{\partial x^2} - \frac{\delta}{(1+x\delta)^2} \frac{1}{l} \frac{\partial \psi}{\partial x} \frac{\partial^2 \psi}{\partial y \partial x} + \frac{2\delta}{(1+x\delta)^2} \frac{1}{l^3} \frac{\partial \psi}{\partial y} \frac{\partial^2 \psi}{\partial y^2} - \frac{2\delta}{(1+x\delta)} \frac{\partial^3 \psi}{\partial x^3} - \frac{2\delta}{(1+x\delta)} \frac{1}{l^2} \frac{\partial^3 \psi}{\partial x \partial y^2} \right] \\ + \left[-\frac{3\delta^2}{(1+x\delta)^3} \frac{1}{l} \frac{\partial \psi}{\partial x} \frac{\partial \psi}{\partial y} + \frac{3\delta^2}{(1+x\delta)^2} \frac{\partial^2 \psi}{\partial x^2} - \frac{M(1+m\alpha)}{(1+m\alpha)^2 + m^2} \frac{1}{l^2} \frac{\partial^2 \psi}{\partial y^2} \right] \\ + \left[\frac{1}{l} w \frac{\partial w}{\partial y} + \frac{(1+\delta x)}{2l} T_r \frac{\partial w}{\partial y} - \frac{3\delta^3}{(1+x\delta)^3} \frac{\partial \psi}{\partial x} + \frac{M}{(1+m\alpha)^2 + m^2} \frac{m}{\sqrt{2\delta}} \frac{(1+x\delta)}{l} \frac{\partial w}{\partial y} \right] - G_r (1+x\delta) \frac{\partial T}{\partial x} \quad (2.35b)$$

And the Energy equation

$$(1+x\delta) \frac{\partial T}{\partial t} + \frac{1}{l} \left(\frac{\partial \psi}{\partial y} \frac{\partial T}{\partial x} - \frac{\partial \psi}{\partial x} \frac{\partial T}{\partial y} \right) = \frac{(1+x\delta)}{P_r} \left[\left(\frac{\partial^2}{\partial x^2} + \frac{1}{l^2} \frac{\partial^2}{\partial y^2} \right) T + \frac{\delta}{1+x\delta} \frac{\partial T}{\partial x} \right] \quad (2.35c)$$

For steady flow, the fluid properties are independent of time, therefore these equations can be written as follows:

Central line (axial) flow of Momentum equation

$$-\frac{1}{l} \left(\frac{\partial \psi}{\partial y} \frac{\partial w}{\partial x} - \frac{\partial \psi}{\partial x} \frac{\partial w}{\partial y} \right) + \delta \frac{\partial w}{\partial x} + D_n + (1+x\delta) \left[\left(\frac{\partial^2}{\partial x^2} + \frac{1}{l^2} \frac{\partial^2}{\partial y^2} \right) w - \frac{\delta^2}{(1+x\delta)^2} w \right]$$

$$-\frac{\delta}{1+x\delta} \frac{1}{l} w \frac{\partial \psi}{\partial y} - \frac{\delta}{l} T_r \frac{\partial \psi}{\partial y} - \frac{M}{(1+m\alpha)^2 + m^2} \left(\frac{\sqrt{2\delta}}{l} \frac{m}{\partial y} \frac{\partial \psi}{\partial y} + (1+x\delta)(1+m\alpha)w \right) = 0 \quad (2.36a)$$

Stream line for the secondary velocity of Momentum equation

$$\begin{aligned} & -\frac{1}{l^2} \frac{\partial \psi}{\partial y} \frac{\partial^3 \psi}{\partial x \partial y^2} + \frac{1}{l^2} \frac{\partial \psi}{\partial x} \frac{\partial^3 \psi}{\partial y^3} - \frac{\partial \psi}{\partial y} \frac{\partial^3 \psi}{\partial x^3} + \frac{\partial \psi}{\partial x} \frac{\partial^3 \psi}{\partial y \partial x^2} + l(1+x\delta) \left(\frac{\partial^4 \psi}{\partial x^4} + \frac{2}{l^2} \frac{\partial^4 \psi}{\partial y^2 \partial x^2} + \frac{1}{l^4} \frac{\partial^4 \psi}{\partial y^4} \right) \\ & + \frac{3\delta}{1+x\delta} \frac{\partial \psi}{\partial y} \frac{\partial^2 \psi}{\partial x^2} - \frac{\delta}{1+x\delta} \frac{\partial \psi}{\partial x} \frac{\partial^2 \psi}{\partial y \partial x} + \frac{2\delta}{1+x\delta} \frac{1}{l^2} \frac{\partial \psi}{\partial y} \frac{\partial^2 \psi}{\partial y^2} - 2l\delta \frac{\partial^3 \psi}{\partial x^3} - \frac{2\delta}{l} \frac{\partial^3 \psi}{\partial x \partial y^2} \\ & - \frac{3\delta^2}{(1+x\delta)^2} \frac{\partial \psi}{\partial x} \frac{\partial \psi}{\partial y} + \frac{3l\delta^2}{1+x\delta} \frac{\partial^2 \psi}{\partial x^2} - \frac{M(1+m\alpha)}{(1+m\alpha)^2 + m^2} \frac{(1+x\delta)}{l} \frac{\partial^2 \psi}{\partial y^2} + (1+x\delta)w \frac{\partial w}{\partial y} \\ & + \frac{(1+x\delta)^2}{2} T_r \frac{\partial w}{\partial y} - \frac{3l\delta^3}{(1+x\delta)^2} \frac{\partial \psi}{\partial x} + \frac{M}{(1+m\alpha)^2 + m^2} \frac{m}{\sqrt{2\delta}} (1+x\delta)^2 \frac{\partial w}{\partial y} - G_r l(1+x\delta) \frac{\partial T}{\partial x} = 0 \end{aligned} \quad (2.36b)$$

And the Energy equation

$$\frac{\partial \psi}{\partial y} \frac{\partial T}{\partial x} - \frac{\partial \psi}{\partial x} \frac{\partial T}{\partial y} = \frac{l(1+x\delta)}{P_r} \left[\left(\frac{\partial^2}{\partial x^2} + \frac{1}{l^2} \frac{\partial^2}{\partial y^2} \right) T + \frac{\delta}{1+x\delta} \frac{\partial T}{\partial x} \right] \quad (2.36c)$$

Chapter 3

Calculation Techniques

3.1 Numerical Methods of Solution

To solve coupled-partial differential equations 2.36(a)-(c), Gottlieb and Orszag (1977) was adopted Spectral method to solve these kinds of equations numerically. The main goal of this method is to make use of the expansion of polynomial functions. That is the axial velocity component $w(x, y)$, stream function for the secondary flow $\psi(x, y)$ and the temperature $T(x, y)$ are expanded in a series in terms of functions consisting in the Chebyshev polynomials, which are defined as follows:

$$\left. \begin{aligned} w(x, y) &= \sum_{m=0}^{\bar{M}} \sum_{n=0}^{\bar{N}} w_{mn} \Phi_m(x) \Phi_n(y) \\ \psi(x, y) &= \sum_{m=0}^{\bar{M}} \sum_{n=0}^{\bar{N}} \psi_{mn} \Psi_m(x) \Psi_n(y) \\ T(x, y) &= \sum_{m=0}^{\bar{M}} \sum_{n=0}^{\bar{N}} T_{mn} \Phi_m(x) \Phi_n(y) + x \end{aligned} \right\} \quad (3.1)$$

Expansion functions $\Phi_n(x)$ and $\Psi_n(x)$ are defined as follows:

$$\left. \begin{aligned} \Phi_n(x) &= (1-x^2) C_n(x) \\ \Psi_n(x) &= (1-x^2)^2 C_n(x) \end{aligned} \right\} \quad (3.2)$$

where, $C_n(x) = \cos(n \cos^{-1} x)$ is the Chebyshev polynomial of order n , which is defined within the ranges from -1 to +1. Since the duct cross-section are defined within the ranges -1 to +1 for both x - and y -directions, therefore these solution domains are approximated by Chebyshev polynomial. Here, \bar{M} and \bar{N} are the numbers of truncation in x - and y -directions respectively.

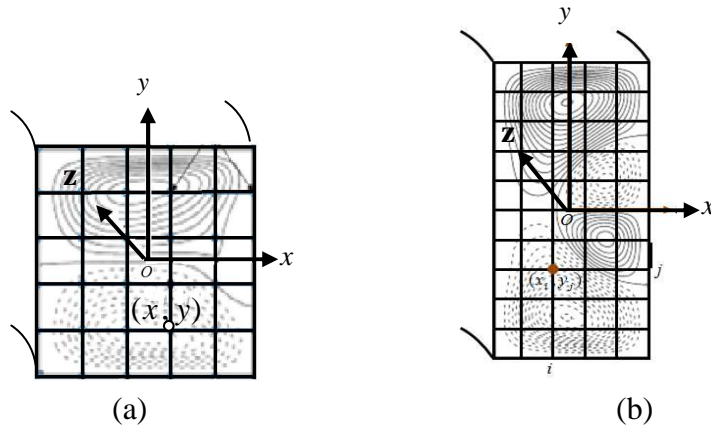


Figure 3.1: Discretization of the (a) square duct cross-section (b) rectangular duct cross-section

The collocation method is applied to discretize the duct cross-sectional solution domain. The collocation points are as follows:

$$\left. \begin{aligned} x_i &= \cos\left\{\pi\left(1 - \frac{i}{\bar{M} + 2}\right)\right\}, \quad i = 1, \dots, \bar{M} + 1 \\ y_i &= \cos\left\{\pi\left(1 - \frac{i}{\bar{N} + 2}\right)\right\}, \quad i = 1, \dots, \bar{N} + 1 \end{aligned}\right\} \quad (3.3)$$

Clearly its domain is bounded by $-1 < x < 1$ and $-1 < y < 1$.

To obtain the steady solution $w(x, y)$, $\psi(x, y)$ and $T(x, y)$, the expansion series (3.1) is then substituted in to the simplified governing equations (2.36a-c). Thereafter equating the expansion coefficients w_{mn} , ψ_{mn} and T_{mn} from these equations, the nonlinear algebraic equations in terms of w_{mn} , ψ_{mn} and T_{mn} are obtained as follows:

$$\left. \begin{aligned} f_{ij}(w_{00}, \dots, w_{\bar{M}\bar{N}}, \psi_{00}, \dots, \psi_{\bar{M}\bar{N}}, T_{00}, \dots, T_{\bar{M}\bar{N}}) &= 0 \\ g_{ij}(w_{00}, \dots, w_{\bar{M}\bar{N}}, \psi_{00}, \dots, \psi_{\bar{M}\bar{N}}, T_{00}, \dots, T_{\bar{M}\bar{N}}) &= 0 \\ h_{ij}(w_{00}, \dots, w_{\bar{M}\bar{N}}, \psi_{00}, \dots, \psi_{\bar{M}\bar{N}}, T_{00}, \dots, T_{\bar{M}\bar{N}}) &= 0 \end{aligned}\right\} \quad (3.3)$$

where $1 \leq i \leq \bar{M} + 1$ and $1 \leq j \leq \bar{N} + 1$. The above obtained equations (3.3) may expressed as

$$\left. \begin{aligned} \Gamma_{11}w + \Gamma_{12}w + \Gamma_{13}w &= \Delta_1(w_{mn}, \psi_{mn}, T_{mn}) \\ \Gamma_{21}w + \Gamma_{22}w + \Gamma_{23}w &= \Delta_2(w_{mn}, \psi_{mn}, T_{mn}) \\ \Gamma_{31}w + \Gamma_{32}w + \Gamma_{33}w &= \Delta_3(w_{mn}, \psi_{mn}, T_{mn}) \end{aligned}\right\} \quad (3.4)$$

where Γ_{ij} are form a square matrix with dimension $(\bar{M} + 1) \times (\bar{N} + 1)$ and Δ_i 's are nonlinear operators. The required steady solutions have been determined by solving equations of (3.4) with the help of the following Newton-Raphson iteration method provided that all of the coefficients are time-independent.

$$\left. \begin{aligned} w^{(\tau+1)} &= \Delta_1(w_{mn}^{(\tau)}, \psi_{mn}^{(\tau)}, T_{mn}^{(\tau)}) \\ \psi^{(\tau+1)} &= \Delta_2(w_{mn}^{(\tau)}, \psi_{mn}^{(\tau)}, T_{mn}^{(\tau)}) \\ T^{(\tau+1)} &= \Delta_3(w_{mn}^{(\tau)}, \psi_{mn}^{(\tau)}, T_{mn}^{(\tau)}) \end{aligned}\right\} \quad (3.5)$$

where τ denotes the number of iterations. To avoid the difficulties near the point of inflection for steady solution the arc-length method (Keller-1987) has been used, which can also help detect the bifurcation points. The arc-length s plays a vital role in this method.

$$\text{The equation of arc-length is } \sum_{m=0}^{\bar{M}} \sum_{n=0}^{\bar{N}} \left[\left(\frac{dw_{mn}}{ds} \right)^2 + \left(\frac{d\psi_{mn}}{ds} \right)^2 + \left(\frac{dT_{mn}}{ds} \right)^2 \right] = 1 \quad (3.6)$$

This equation is solved simultaneously with the equations of (3.4) by using the Newton-Raphson iteration method. An initial approximation of the equations is regarded as $s + \Delta s$ from point s as follows:

$$\left. \begin{aligned} w_{mn}(s + \Delta s) &= w_{mn}(s) + \frac{dw_{mn}}{ds} \Delta s \\ \psi_{mn}(s + \Delta s) &= \psi_{mn}(s) + \frac{d\psi_{mn}}{ds} \Delta s \\ T_{mn}(s + \Delta s) &= T_{mn}(s) + \frac{dT_{mn}}{ds} \Delta s \end{aligned}\right\} \quad (3.7)$$

Taking error tolerance $\varepsilon_\tau < 10^{-8}$ guarantees the convergence of the steady solution, where subscript τ indicates the iteration number and the error tolerance ε_τ is defined as

$$\varepsilon_\tau = \sum_{m=0}^{\bar{M}} \sum_{n=0}^{\bar{N}} \left[\left(w_{mn}^{\tau+1} - w_{mn}^\tau \right)^2 + \left(\psi_{mn}^{\tau+1} - \psi_{mn}^\tau \right)^2 + \left(T_{mn}^{\tau+1} - T_{mn}^\tau \right)^2 \right] \quad (3.8)$$

3.2 Nusselt Number (Nu)

To see the temperature distribution of the fluid flow, it is required to determine the Nusselt Number. The Nusselt number is significant in heat transfer analysis and engineering design because it helps determine the rate of heat transfer from a surface to a fluid. The Nusselt number describes the efficiency of convective heat transport. It expresses how much convective heat transfer improves overall heat transmission as compared to conduction alone.

For the steady case, the Nusselt number Nu has been determined by

$$Nu = -\frac{d}{\Delta T} \left\langle \frac{\partial T}{\partial x} \Big|_{x=0} \right\rangle \quad (3.9)$$

Here, $\langle \rangle$ refers to the average value of the heat transfer from the duct surface to the fluid; d indicates the distance between facing walls and ΔT difference of the temperature. To see the temperature distribution of the duct flow it is also required to calculate the heat transfer at cooled and heated walls. For steady solution,

$$\text{Nusselt number at the cooling wall is denoted by } Nu_c = -\frac{1}{2} \int_{-1}^1 \left\langle \frac{\partial T}{\partial x} \Big|_{x=-1} \right\rangle dy \quad (3.10)$$

$$\text{And at the heating wall is denoted by } Nu_h = -\frac{1}{2} \int_{-1}^1 \left\langle \frac{\partial T}{\partial x} \Big|_{x=1} \right\rangle dy \quad (3.11)$$

3.3 Flux and Mean Axial velocity through the Duct

FORTTRAN (Developer Studio) code has been used in the equations (2.36a)-(2.36c) to calculate numerical simulation using the spectrum method as a key instrument and the Chebyshev polynomial, Newton-Raphson, Collocation, and Arc-length methods are used as auxiliary tools. The curvature of the duct δ ranges from 0.01 to 0.5 and the aspect ratio of the duct is taken 1, 2, and 3 for both isothermal and non-isothermal fluid flow as well as for the straight duct flow, where $\delta=0$.

The dimensional flux Q through the duct is defined by

$$Q = \int_{-h}^h \int_{-d}^d w dx dy, \quad (3.10)$$

But the non-dimensional flux is defined by

$$Q = \int_{-1}^1 \int_{-1}^1 w dx dy \quad (3.11)$$

The mean axial velocity is defined by

$$\bar{w} = \frac{Q}{4hd} \quad (3.12)$$

Chapter 4

Magneto-hydrodynamic Isothermal Fluid Flow through a Rotating Curved Duct with Magnetic Field

This study conducts a numerical investigation to analyze the influence of Hall and Ion-slip currents on a fully developed, two-dimensional, steady, incompressible flow within a rotating curved duct, featuring both square and rectangular cross-sections while being subjected to a magnetic field. The governing equations are derived from the Navier-Stokes equations, expressed in cylindrical coordinates (r, θ, y) to account for the curved nature of the duct. A pressure gradient force, known as the Dean Number, is applied as an external force along the centreline of the curved duct. The Lorentz force is generated by the interaction of electric and magnetic fields, and this Lorentz force is further modified by the presence of Hall and Ion-slip currents. As a result, the flow is influenced by the combined forces of the pressure gradient and Lorentz forces. Additionally, the flow is accelerated due to the combined effects of Coriolis and Centrifugal forces, which are a consequence of the system's rotation and the duct's curvature. In a fully developed flow, most variables are independent of the circumferential angle except for pressure. The study considers a range of curvatures from 0.01 to 0.5. Numerical calculations are primarily carried out using the spectral method. Complementary techniques, including the Newton-Raphson, Chebyshev polynomial, Collocation, and arc-length procedures, are also employed. The arc-length method is particularly useful for calculating results near points of inflection in the solution curve. The primary objective of this paper is to demonstrate how the magnetic, Hall, and ion-slip parameters impact the flow characteristics within a rotational curved duct. The study investigates the flow characteristics for various values of these parameters in conjunction with specific Dean Numbers and varying duct curvatures. It includes the presentation and brief explanation of the revealed streamlines of the secondary flow and contour lines of axial flow.

4.1 Introduction

The study of fully developed fluid flow within curved ducts holds significant importance in engineering applications. A particularly challenging area in the field of electromagnetic involves understanding fluid flow in rotating systems. Consequently, scientists have dedicated their efforts to the analysis of curved duct flow within rotating systems. These rotating systems find extensive use in engineering applications, including turbo-machinery, air conditioning systems, refrigeration units, electric generators, ventilators, centrifugal pumps, heat exchangers, internal combustion engines, gas turbine fluid transport, and blade-

to-blade passages in modern gas turbines, among others. Pioneering this research, the esteemed mathematician Dean (1927, 1928) provided mathematical evidence for the existence of a pair of counter-rotating vortices within a curved pipe, known as Dean's vortices, in fully developed curved duct flow. Investigating the flow condition within the duct, often referred to as Dean's hydro-dynamical instability, became a central focus. Over the following decades, numerous researchers delved into the analysis of fluid flow through both straight and curved ducts using analytical, numerical, and experimental methods, keeping Dean's vortices and their associated flow characteristics in mind. As a valuable reference, the following section briefly describes the research contributions of some scholars in the field of duct flow.

Berger et al. (1983) conducted a comprehensive examination of fully developed curved duct flow within tubes and pipes, encompassing both stable and unstable flow conditions. They scrutinized a range of factors, including various geometries, fluid properties, wall properties, and Dean Numbers, to assess their influence on the behaviour of curved duct flow. Furthermore, Nandakumar and Masliyah (1982, 1986) delved into the study of bifurcation in steady laminar flow within curved pipes and the heat-transferable vortex flow within coiled and curved tubes. Winters (1987) conducted two-dimensional bifurcation research on the flow within a square curved duct, revealing a complex structure characterized by multiple asymmetric and symmetric solutions for the square cross-section duct. Ishigaki (1996) performed a numerical analysis of flow structure and friction factors within both counter-rotating and co-rotating circular pipes with slight curvature. Wang and Yang (2003, 2004) in their studies, utilized a combination of numerical simulations and experimental data to investigate fully developed forced and free convection flow within a rotating square curve. Yamamoto et al. (1999, 2000) examined the characteristics of steady viscous incompressible flow within a rotating system, considering both square curved ducts and circular cross-sectional helical pipes. Yanase et al. (2005a) investigated heat transfer within a curved rectangular duct, utilizing numerical calculations to analyze the unsteady non-isothermal flow characteristics associated with convection flow. In a system featuring both rotation and curvature, Zhang and collaborators (2001) delved into the combined effects of centrifugal and Coriolis forces on isothermal flows within curved rectangular ducts. Selmi et al. (1994, 1999) investigated the impact of Coriolis and centrifugal forces on the bifurcation structure of pressure-driven two-dimensional flows within a rotating curved duct with a square cross-section. They employed numerical computations, utilizing the spectral method to determine dual solutions. Yanase et al. (1989, 2002) explored flow stability within a slightly curved circular duct. Furthermore, they conducted a study on laminar incompressible fluid flow within a rectangular curved duct, exploring a wide aspect ratio range from 1 to 12. Yamamoto et al. (2006) employed a visualization technique to investigate the characteristics of secondary flow within a curved tube featuring a square cross-section. Humphrey et al. (1977) examined laminar water flow within a square duct with a cross-section of 40×40 mm, revealing significant curvature effects. Within a curved

duct with a square cross-section, Wang and Liu (2007) delved into the fully developed bifurcation structure of forced convection flows. They also considered initial conditions, the influence of instability and stability, and a curvature ratio of $5E-06$. Wang and Liu (2007) revisited the study of the fully developed bifurcation structure of forced convection within a tightly wound square cross-section duct, characterized by a curvature ratio of 0.5 in regions with high Dean numbers. Yanase et al. (2008) utilized spectral methods to investigate the intricacies of travelling-wave solutions and compared them to numerical 2D analyses and experimental studies of flow within a curved pipe featuring a square cross-section. Norouzi et al. (2009) focused on the complex interplay of primary and secondary normal pressure variations in forced convective heat transfer in viscoelastic fluid flow within curved ducts. Their study also explored how elastic properties impact the average Nusselt number and secondary flow intensity. Liu and Wang (2009) discussed the bifurcation and stability of fully developed forced convection within curved rectangular ducts. They also delved into the physical mechanisms responsible for creating various flow structures.

Fellouah et al. (2010) conducted a comprehensive study, involving both experimental and computational research, to determine the influence of rheological fluid behaviour on power law Dean Instability and Bingham fluid flow within a rectangular cross-section of a curved duct. Chandratilleke et al. (2012) utilized numerical investigations to explore the behaviour of laminar flow and associated thermal parameters in fluid flow through curved channels, with a specific focus on the secondary vortex structure. Wu et al. (2013) delved into the study of streamline secondary flow in a curved duct featuring a square cross-section, employing spectral methods for their research. Kun et al. (2014) utilized ultrasonic Doppler velocimetry and microphones to investigate both laminar and turbulent flow of pseudo-plastic fluids within a square duct characterized by significant curvature. Razavi et al. (2015) conducted a study to examine the effects of second law analysis, Dean number, and dimensionless heat flux at the wall on the entropy generation resulting from forced convection laminar flow in a rotating curved duct featuring a square cross-section. Li et al. (2016) conducted both experimental and numerical investigations on fully developed three-dimensional flow within a curved rectangular duct, considering various curvature profiles, including spiral, double circular, and linear curvatures. Their study also explored the influence of Reynolds number, aspect ratio, and different curvatures on Dean instability, with a specific focus on precisely identifying the centre of secondary base vortices. Lima and Alam (2019) delved into the impact of Hall current on flow through a straight pipe within a rotating system, in the presence of a magnetic field. Their research in a straightforward duct with a high aspect ratio revealed features of secondary flow streamlines and an axial flow contour map.

There is currently no available research on fluid flow in a curved duct in the presence of a magnetic field with Hall and ion-slip currents in online sources or archives. This is a significant research gap, considering that much of the universe consists of highly charged particles and is enveloped by a magnetic field. MHD (magneto-hydrodynamics) fluid flow,

which encompasses Hall and Ion-slip currents, holds crucial relevance in numerous engineering and industrial processes. This underscores the importance of exploring and applying Hall and ion-slip current principles within this particular research domain. Therefore, the aim is to numerically examine the

1. *Hall and Ion-slip Current Effects on Steady Fluid Flow through a Rotating Curved Square Duct with Magnetic Field.*
2. *2. Steady MHD Fluid Flow in a Rotating Curved Rectangular Duct with Hall and Ion-slip Current*
3. *Hall and Ion-slip Effects on MHD Fluid Flow in a Rotating Curved Duct with Aspect Ratio 3*

4.2 Mathematical Formulation

It has been considered a scenario involving incompressible viscous two-dimensional fluid flow that is fully developed and passes through a curved duct. This duct is subjected to rotation with an angular velocity, Ω , around its vertical y -axis. The z -axis is aligned along the centreline direction of the duct, and the x -axis is perpendicular to both the y and z -axes. Within this configuration, let C represent the centre of the duct's cross-section, and L denotes the radius of curvature. The duct's cross-section has a height of $2h$ and a width of $2d$. In this context, an external force in the form of a pressure gradient, denoted as $G = -\frac{\partial p}{\partial z}$, has been applied along the centreline direction of the duct. Furthermore, the application of electric and magnetic fields generates a Lorentz force. This Lorentz force undergoes modification due to the presence of Hall and Ion-slip currents, resulting in a combination of forces that influence the flow. Additionally, the flow is accelerated due to the collective effect of Coriolis forces and Centrifugal forces, both of which arise as consequences of the system's rotation and the curvature of the duct. The coordinate system with the relevant notation is shown in Fig. 4.1:

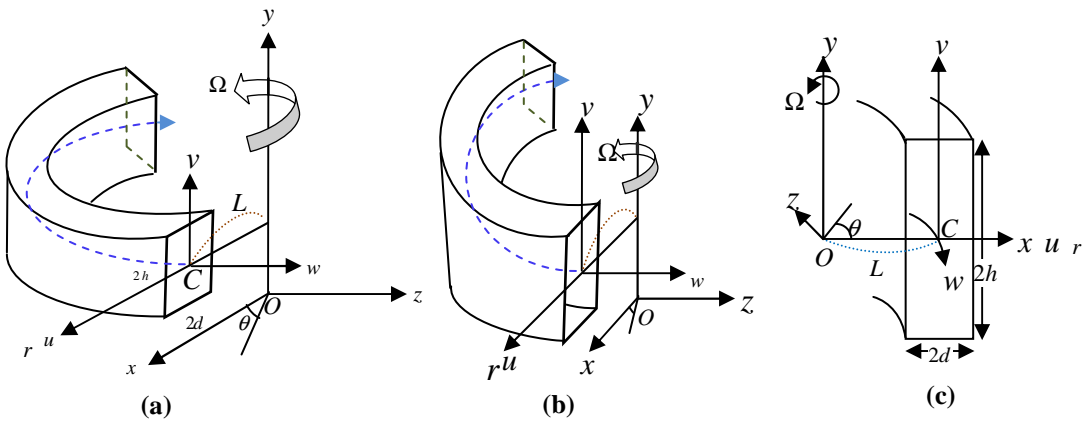


Figure 4.1: Coordinate system of Curved duct with
 (a) Aspect ratio 1 [square cross-section]
 (b) Aspect ratio 2 and (c) Aspect ratio 3 [rectangular cross-section]

Electrically conducting fluids are indeed affected by Hall and Ion-slip currents. As a result of these currents, Ohm's law is generalized as follows:

$$\mathbf{J} = \sigma\mu_e (\mathbf{q} \wedge \mathbf{B}) - \frac{m}{B_0} (\mathbf{J} \wedge \mathbf{B}) + \frac{m\alpha}{B_0^2} (\mathbf{J} \wedge \mathbf{B}) \wedge \mathbf{B}$$

where, $\omega_e \tau_e = m$; τ_e , ω_e are electron collision time and cyclotron frequency.

In the absence of body forces and considering the assumptions mentioned above, the governing equations are derived from the Navier-Stokes equation, expressed in terms of cylindrical coordinates (r, θ, y) . These equations are as follows:

Continuity Equation:

$$u \frac{\partial u}{\partial r} + v \frac{\partial v}{\partial y} + \frac{u}{r} = 0 \quad (4.2.1)$$

Momentum Equations:

$$u \frac{\partial u}{\partial r} + v \frac{\partial u}{\partial y} - \frac{w^2}{r} = -\frac{1}{\rho} \frac{\partial p}{\partial r} + \nu \left(\frac{\partial^2 u}{\partial r^2} + \frac{1}{r} \frac{\partial u}{\partial r} + \frac{\partial^2 u}{\partial y^2} - \frac{u}{r^2} \right) + 2w\Omega_0 + \frac{\sigma\mu_e B_0^2}{\rho} \left[\frac{mw - u(1+m\alpha)}{(1+m\alpha)^2 + m^2} \right] \quad (4.2.2)$$

$$u \frac{\partial v}{\partial r} + v \frac{\partial v}{\partial y} = -\frac{1}{\rho} \frac{\partial p}{\partial y} + \nu \left(\frac{\partial^2 v}{\partial r^2} + \frac{1}{r} \frac{\partial v}{\partial r} + \frac{\partial^2 v}{\partial y^2} \right) \quad (4.2.3)$$

$$u \frac{\partial w}{\partial r} + v \frac{\partial w}{\partial y} + \frac{uw}{r} = -\frac{1}{\rho} \frac{1}{r} \frac{\partial p}{\partial \theta} + \nu \left(\frac{\partial^2 w}{\partial r^2} + \frac{1}{r} \frac{\partial w}{\partial r} + \frac{\partial^2 w}{\partial y^2} - \frac{w}{r^2} \right) - 2u\Omega_0 - \frac{\sigma\mu_e B_0^2}{\rho} \left[\frac{mu + (1+m\alpha)w}{(1+m\alpha)^2 + m^2} \right] \quad (4.2.4)$$

where, $r = L + x$ is the radial variable, θ is the circumferential angle and y is the vertical variable; And the symbols u , v and w are the velocity components in the directions of x , y , and z -axes respectively, also ρ and ν refer to the density and kinematic viscosity. The coordinate (r, θ, y) has been changed to the dimensionless rectangular coordinate (x', z', y') under the following transform of variables

$$r = L + x'd, \quad y = hy', \quad \text{and} \quad L\theta = z'd$$

The characteristic length d and the kinematic viscosity ν are used to make dimensionless form of the velocity U_0 , which is defined by $\frac{\nu}{d}$. The other dimensionless variables are introduced by using the following transformation:

$$x' = \frac{x}{d}; \quad \bar{y} = \frac{y}{d}; \quad z' = \frac{z}{d}; \quad u' = \frac{d}{\nu} u; \quad v' = \frac{d}{\nu} v; \quad w' = \frac{d\sqrt{2\delta}}{\nu} w \quad \text{and} \quad p' = \frac{d^2}{\rho\nu^2} p$$

Thus the transform equations $r = L + x'd$ and $L\theta = z'd$ (i.e. $r = L + x$ and $L\theta = z$) are used into the above equations to transform its rectangular coordinate form, where x' , \bar{y} and z' are the non-dimensional radial, vertical and axial coordinates respectively and δ is the dimensionless curvature of curve duct which is defined by $\delta = \frac{d}{L}$. Here u' , v' , w' are the dimensionless velocity components in the direction of x' , \bar{y} and z' , also p' is the dimensionless pressure. Using the above dimensionless quantities into the equations (4.2.1)-

(4.2.4) and removing the prime over the variables, the following equations are obtained as follows:

Continuity Equation:

$$\frac{\partial u}{\partial x} + \frac{\partial v}{\partial \bar{y}} + \frac{\delta}{1+x\delta} u = 0 \quad (4.2.5)$$

Momentum Equations:

$$u \frac{\partial u}{\partial x} + v \frac{\partial u}{\partial \bar{y}} - \frac{w^2}{2(1+x\delta)} = -\frac{\partial p}{\partial x} + \left(\frac{\partial^2 u}{\partial x^2} + \frac{\delta}{1+x\delta} \frac{\partial u}{\partial x} + \frac{\partial^2 u}{\partial \bar{y}^2} - \frac{\delta^2 u}{(1+x\delta)^2} \right) + \frac{T_r}{2} w + M \left(\frac{\frac{1}{\sqrt{2\delta}} m w - (1+m\alpha)u}{(1+m\alpha)^2 + m^2} \right) \quad (4.2.6)$$

$$u \frac{\partial v}{\partial x} + v \frac{\partial v}{\partial \bar{y}} = -\frac{\partial p}{\partial \bar{y}} + \left(\frac{\partial^2 v}{\partial x^2} + \frac{\delta}{1+x\delta} \frac{\partial v}{\partial x} + \frac{\partial^2 v}{\partial \bar{y}^2} \right) \quad (4.2.7)$$

$$u \frac{\partial w}{\partial x} + v \frac{\partial w}{\partial \bar{y}} + \frac{\delta}{1+x\delta} u w = \frac{D_n}{1+x\delta} \frac{\partial^2 w}{\partial x^2} + \frac{\delta}{1+x\delta} \frac{\partial w}{\partial x} + \frac{\partial^2 w}{\partial \bar{y}^2} - \frac{\delta^2}{(1+x\delta)^2} w - \delta T_r u - M \left(\frac{\sqrt{2\delta} m u + (1+m\alpha)w}{(1+m\alpha)^2 + m^2} \right) \quad (4.2.8)$$

where, $D_n = \frac{G d^3}{\mu \nu} \sqrt{\frac{2d}{L}}$ refers to the Dean number $T_r = \frac{2d^2 \sqrt{2\delta}}{\delta \nu}$ Ω_0 refers to the Taylor number ; $M = \frac{d^2 \sigma \mu_e B_0^2}{\rho \nu}$ refers to the Magnetic parameter, m refers to the Hall parameter and

α refers to the Ion-slip parameter. Again, introducing the sectional stream function ψ , which is related to the velocity components u and v by the relations:

$$u = \frac{1}{1+x\delta} \frac{\partial \psi}{\partial \bar{y}} \quad \text{and} \quad v = -\frac{1}{1+x\delta} \frac{\partial \psi}{\partial x}$$

The continuity equation (4.2.5) is satisfied by this sectional stream function, therefore, it can be used in the other governing equations. Another one transformation $y = hy'$ has been used, which gives a unique variable y' such that $\bar{y} = ly'$, where $l = h/d$ is the aspect ratio of the duct. Thereafter remove prime over the variables for the sake simplicity, it yields

Central line (axial) flow of Momentum equation

$$\begin{aligned} & -\frac{1}{l} \left(\frac{\partial \psi}{\partial y} \frac{\partial w}{\partial x} - \frac{\partial \psi}{\partial x} \frac{\partial w}{\partial y} \right) + \delta \frac{\partial w}{\partial x} + D_n + (1+x\delta) \left[\left(\frac{\partial^2}{\partial x^2} + \frac{1}{l^2} \frac{\partial^2}{\partial y^2} \right) w - \frac{\delta^2}{(1+x\delta)^2} w \right] \\ & - \frac{\delta}{1+x\delta} \frac{1}{l} w \frac{\partial \psi}{\partial y} - \frac{\delta}{l} T_r \frac{\partial \psi}{\partial y} - \frac{M}{(1+m\alpha)^2 + m^2} \left(\frac{\sqrt{2\delta}}{l} m \frac{\partial \psi}{\partial y} + (1+x\delta)(1+m\alpha)w \right) = 0 \end{aligned} \quad (4.2.9)$$

Stream line for the secondary velocity of Momentum equation

$$\begin{aligned} & -\frac{1}{l^2} \frac{\partial \psi}{\partial y} \frac{\partial^3 \psi}{\partial x \partial y^2} + \frac{1}{l^2} \frac{\partial \psi}{\partial x} \frac{\partial^3 \psi}{\partial y^3} - \frac{\partial \psi}{\partial y} \frac{\partial^3 \psi}{\partial x^3} + \frac{\partial \psi}{\partial x} \frac{\partial^3 \psi}{\partial y \partial x^2} + l(1+x\delta) \left(\frac{\partial^4 \psi}{\partial x^4} + \frac{2}{l^2} \frac{\partial^4 \psi}{\partial y^2 \partial x^2} + \frac{1}{l^4} \frac{\partial^4 \psi}{\partial y^4} \right) \\ & + \frac{3\delta}{1+x\delta} \frac{\partial \psi}{\partial y} \frac{\partial^2 \psi}{\partial x^2} - \frac{\delta}{1+x\delta} \frac{\partial \psi}{\partial x} \frac{\partial^2 \psi}{\partial y \partial x} + \frac{2\delta}{1+x\delta} \frac{1}{l^2} \frac{\partial \psi}{\partial y} \frac{\partial^2 \psi}{\partial y^2} - 2l\delta \frac{\partial^3 \psi}{\partial x^3} - \frac{2\delta}{l} \frac{\partial^3 \psi}{\partial x \partial y^2} \\ & - \frac{3\delta^2}{(1+x\delta)^2} \frac{\partial \psi}{\partial x} \frac{\partial \psi}{\partial y} + \frac{3l\delta^2}{1+x\delta} \frac{\partial^2 \psi}{\partial x^2} - \frac{M(1+m\alpha)}{(1+m\alpha)^2 + m^2} \frac{(1+x\delta)}{l} \frac{\partial^2 \psi}{\partial y^2} + (1+x\delta)w \frac{\partial w}{\partial y} \end{aligned}$$

$$+ \frac{(1+\delta x)^2}{2} T_r \frac{\partial w}{\partial y} - \frac{3l\delta^3}{(1+x\delta)^2} \frac{\partial \psi}{\partial x} + \frac{M}{(1+m\alpha)^2 + m^2} \frac{m}{\sqrt{2\delta}} (1+x\delta)^2 \frac{\partial w}{\partial y} = 0 \quad (4.2.10)$$

Boundary conditions for w and ψ are used as

$$w(\pm 1, y) = w(x, \pm 1) = \psi(\pm 1, y) = \psi(x, \pm 1) = \frac{\partial \psi}{\partial x}(\pm 1, y) = \frac{\partial \psi}{\partial y}(x, \pm 1) = 0 \quad (4.2.11)$$

4.3 Validation Test of the Present Numerical Results

First, it is required to verify the present numerical results. These results are verified by comparing it with the previously published experimental result. Comparisons have been shown by using the visualization method:

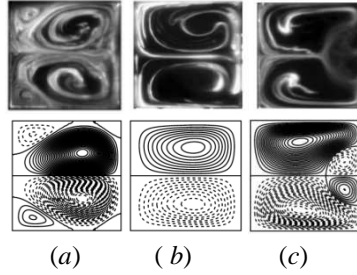


Figure 4.2(i): Experimental result (top) at the fixed values of
 (a) Negative rotation, $D_n = 32$ (b) $T_r = 150, D_n = 114$ (c) $T_r = 150, D_n = 176$
 Our present numerical result (bottom) at the fixed values of
 (a) Negative rotation $T_r = -120, D_n = 500, \delta = 0.03$ (b) $T_r = 150, D_n = 76, \delta = 0.03$
 (c) $T_r = 150, D_n = 415, \delta = 0.03$

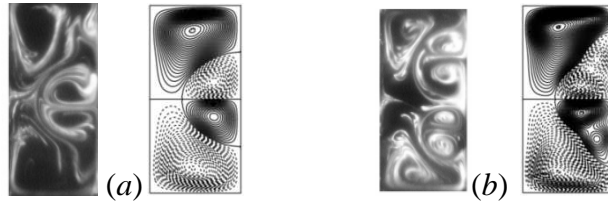


Figure 4.2(ii): Experimental results (left) of (a) at $K = 262$ and (b) at $K = 321$
 Our present numerical results (right) of (a) at $D_n = 240$ and (b) at $D_n = 500$

- A.** The experimental results have been presented by Yamamoto et al. (2006) as the first investigators for both positive and negative rotation, where Taylor number $T_r=150$ and curvature $\delta=0.03$. They have transferred water from an overflow tank through the curved, square duct. The comparisons between the present numerical results (bottom) and experimental results (top) are shown in Fig.4.2i (a)-(c).
- B.** Chandratilleke (2001) have established the experimental results for different aspect ratios of 2. The comparison of experimental data [left of (a) and (b)] versus present numerical results [right of (a) and (b)] is shown in Fig.4.2(ii) in order to validate the numerical results presented.

To validate our numerical results, it is shown that essentially identical flow patterns appear at other points of parameterization while in our current experiment the magnetic, Hall, and ion-slip parameters are taken as zero. It is noted that there is a strong correlation between

our numerical findings and the outcomes of the experiment, both qualitatively and quantitatively. It can therefore draw the conclusion that there is a good correlation between our numerical results and the experimental data.

4.4 Curved Square Duct for Isothermal Fluid Flow:

Hall and Ion-slip Current Effects on Steady Flow through a Rotating Curved Square Duct with Magnetic Field

This study deals with the numerical prediction of two-dimensional fully developed steady viscous incompressible flow through a curved duct with a square cross-section in the presence of magnetic fields, Hall, and ion-slip currents. Due to the square cross-section of the duct, the aspect ratio of the duct is taken as $l=h/d=1$. The spectral method is the main instrument used to perform the calculations numerically. On the other hand, auxiliary tools such as the Chebyshev polynomial, Newton-Raphson, collocation, and arc-length approaches are employed. A pressure gradient force (Dean Number) is applied to the centreline direction of duct. The experiment has been done for both positive and negative rotations within the ranges of Taylor number $-5000 \leq T_r \leq 5000$ at Dean Number $D_n = 500$. Also the Dean Number effects have been investigated over wide ranges $0 \leq D_n \leq 6000$, while Taylor number is fixed at $T_r=10$. The behaviour of the exposed secondary flow streamlines and axial flow contour lines for various values of the magnetic, Hall, and Ion-slip parameters on the flow characteristics for two particular cases of Dean number, Case-I: $D_n = 500$ and Case-II: $D_n = 1000$ with the different choice of duct curvature ranges from 0.01 to 0.5, is briefly explained. Only one parameter of D_n , T_r , M , m and α are varied with others are fixed at a significant value of the parameters.

4.4.1 Grid Spaces Accuracy

Before executing the FORTRAN program; it is required to discuss about grid space accuracy. Due to the square cross-section of the duct, it is preferable to use similar values for \bar{M} and \bar{N} to obtain reasonable accuracy. To find the best grid space accuracy, the flux Q has been calculated for several pairs of truncation numbers (\bar{M}, \bar{N}) such as (16, 16), (18, 18), (20, 20) and (22, 22). These are displayed in Table-1.

\bar{M}	\bar{N}	Q
16	16	197.0759190059835
18	18	197.0754422863984
20	20	197.0755267907014
22	22	197.0755606640706

Table-1: Fluxes Q at several pairs of truncation numbers \bar{M} and \bar{N} for fixed $\delta=0.1$, $T_r = 10$, $D_n = 500$, $M = 0$, $m = 0$ and $\alpha = 0$.

From this table, it can be determined that the numerical outcomes are accurate enough at $\bar{M} = 20$ and $\bar{N} = 20$.

4.4.2 Results and Discussion

Fully developed steady flow of incompressible viscous fluid through the square cross-sectioned curve duct that rotates with an angular velocity Ω around its vertical y -axis. The Dean Number (pressure gradient force), when present in a magnetic field with Hall and Ion-slip current along the central line of the duct, affects the main flow. Aspect ratio $l = 1$ should always be taken due to square curved duct analysis. The increments $\Delta w = 4$ and $\Delta \psi = 0.3$ are used to visualise well and clear to display the flow structures. The shape of the flow pattern becomes almost symmetric because the Coriolis force balances with the centrifugal force as the rotation increase. It is required to discuss about the square box in each figure of the flow pattern. The square box is the duct cross-section at a certain point on the solution curve. The outside of the curved duct is indicated by the right side of the box in the illustration. The dotted lines are in the clockwise or negative directed flow for the velocity distribution, whereas the solid lines are in the anti-clockwise or positive directed flow.

First, it has been investigated the effects of Taylor number (T_r) for the three cases; Case-I: $\delta=0.1$, $D_n=500$ Case-II: $\delta=0.01$, $D_n=500$ Case-III: $\delta=0.5$, $D_n=500$ and the Dean Number (D_n) for the curvature $\delta=0.1$ on the velocity distribution. These are shown in figures from Fig.4.3 to Fig.4.6. As the new findings of this study, the effects of the magnetic parameter (M), Hall parameter (m), and Ion-slip parameter (α) on the velocity have been shown in figures from Fig.4.7 to Fig.4.12, and its corresponding flow behaviour are investigated for the two cases of Dean Numbers such as **Case-I:** $D_n = 500$ and **Case-II:** $D_n = 1000$ with different choice of the curvature δ .

A. Effects of Taylor Number (T_r)

Case-I: $\delta=0.01$, $D_n=500$

The rotational effects on the curve duct flow for the fixed values of $M = 0$, $m = 0$, $\alpha = 0$ with Dean Number at $D_n=500$ and the duct curvature $\delta=0.01$ are shown in Figs.4.3a-e. The flux Q against Taylor number T_r solution curve is shown in Fig. 4.4a. It is bounded within the range of Taylor number $-4865.8 \leq T_r \leq 4770.4$. Several bifurcation curves; almost 19 branches of solution curves have been discovered within this range. Figures 4.3b and 4.3c are the enlarging areas indicated by the rectangular boxes (i) and (ii) in Figure 4.3a are plotted.

Figure 4.3d shows the corresponding vortex structures of the flow pattern. The streamlines ψ of the secondary flow (top) and contours of the axial flow w (bottom) at several distinct points $T_r = -4500, -2500, -350, -172.21, 100, 1500, 2500, \text{ and } 4500$ on the solution curve of Fig. 4.3a.

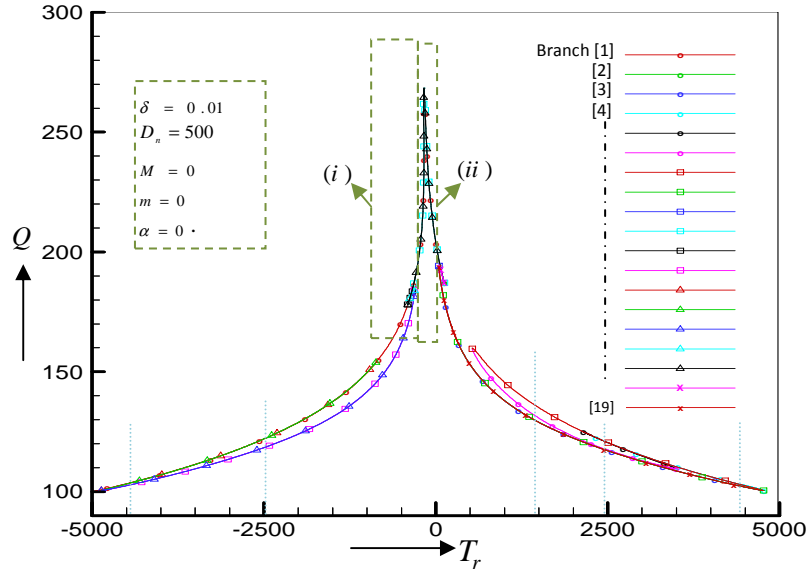


Figure 4.3a: Solution curve: Flux Q versus Taylor Number T_r with the fixed values of $\delta=0.01$, $D_n=500$, $M=0$, $m=0$ and $\alpha=0$.

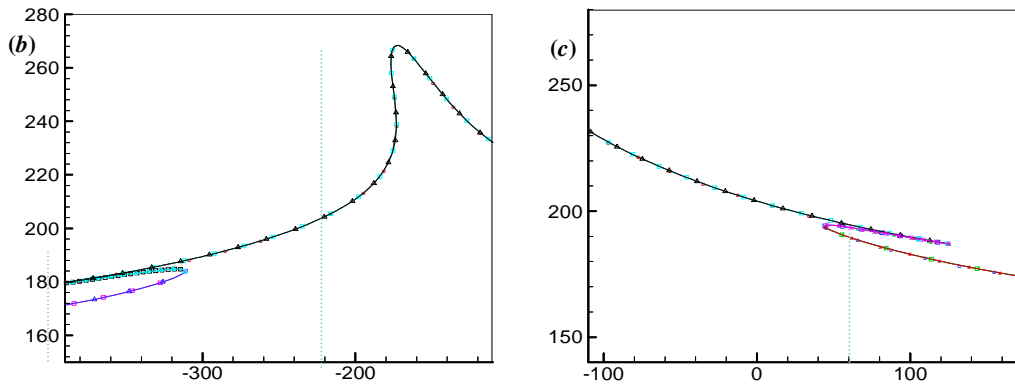
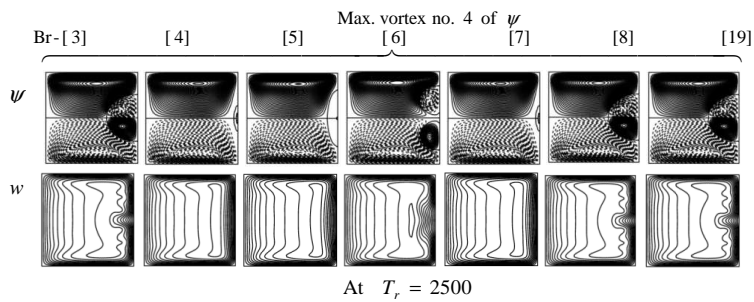
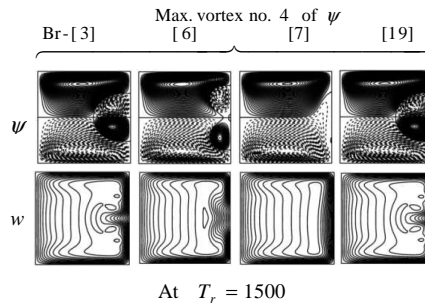
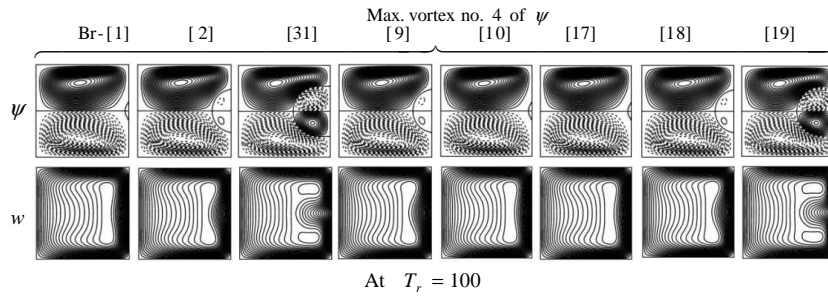
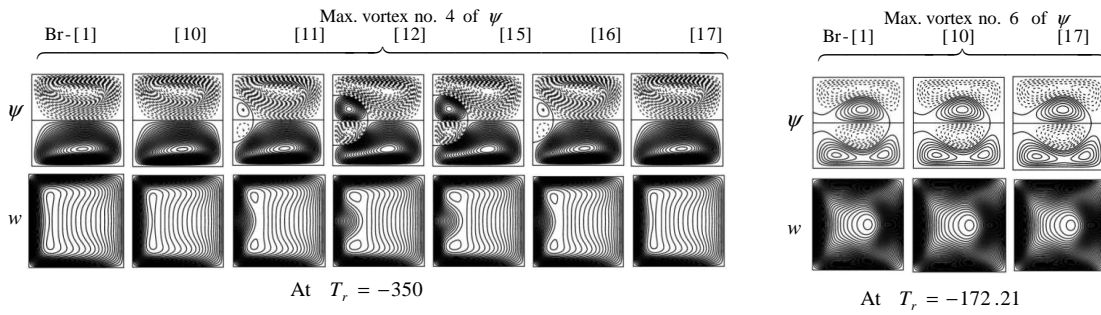
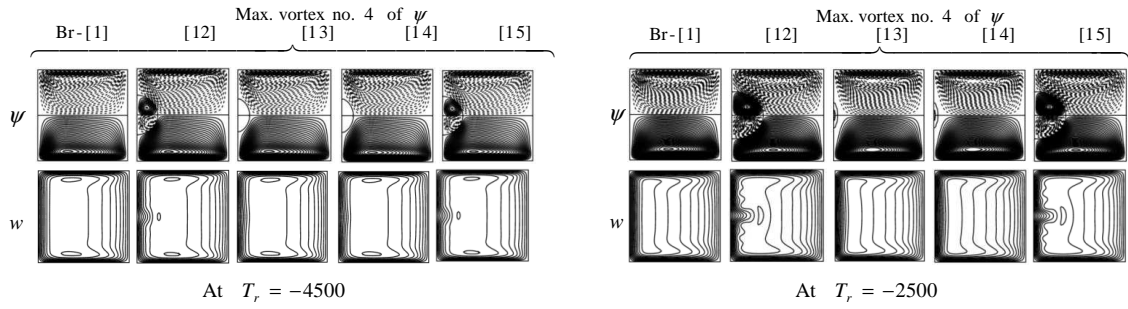


Figure 4.3b-c: Magnifying figures marked by the dashed box in Fig.4.3a

Five branches of the solution curve are shown crossed at $T_r = -4500$. Branches 12 and 15 exhibited similar behaviour, but close to the duct's interior wall, two strong counter-rotating symmetric vortices with two weaker vortices in addition to the streamline are generated. The behaviour of branches 13 and 14 is also the same, but it branch 1 exhibits the structure of two cells of symmetric vortices, and the contour plot of the axial flow w is displaced close to the duct's inner wall. On the opposite side at $T_r = 4500$, it is discovered that branches 3, 8, and 19 shares the same pattern, also the same pattern are shown in the branches 4 and 7, but in this case additional two weak vortices form close to the outer wall of duct. Whereas, the axial flow's contour is switched to the outside wall of the curved duct. Two, four, or six vortices have been discovered at the other remaining points for streamline. But for the axial flow, the highest amount of flow is also moved near the duct's boundary wall for large values of $|T_r|$.



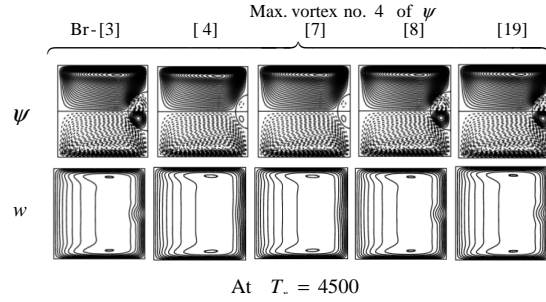


Figure 4.3d: Streamlines ψ (upper) and axial contour flow w (lower) in accordance with the solution curve in Fig.4.3a

The secondary flow's Taylor number versus vortices number plane is depicted in Fig.4.4e by a bar diagram that corresponds to the solution curve in Fig.4.4a. The many bifurcation curves, where two-, four-, and six-vortex flow patterns are discovered using this diagram.

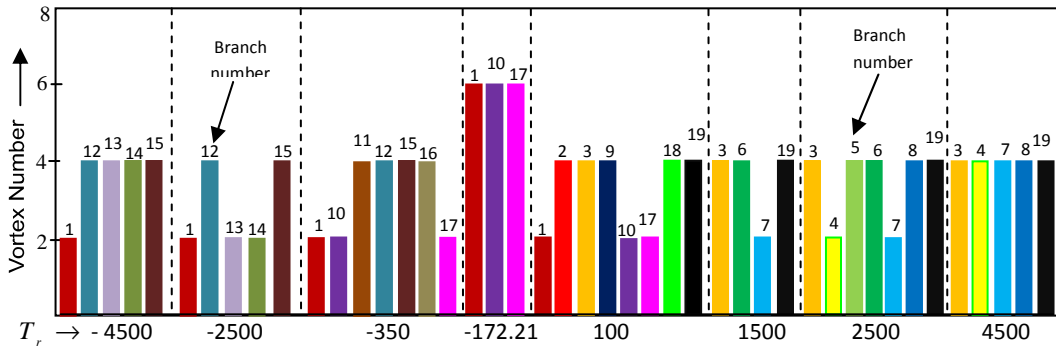


Figure 4.3e: Taylor number T_r versus vortex number of secondary flows with $\delta = 0.01$, $D_n = 500$, $M = 0$, $m = 0$ and $\alpha = 0$.

Case-II: $\delta=0.1, D_n=500$

The rotational effects on the curve duct flow for the fixed values of $M = 0$, $m = 0$, $\alpha = 0$ over a wide range of Taylor number $-5000 \leq T_r \leq 5000$ with the duct curvature $\delta = 0.1$ are shown in Figs.4.3a-c. Figure 4.4a depicts the solution curve for the flux Q versus Taylor number T_r . This solution curve is divided into three sections such as (i) section (a) to (b), (ii) section (b) to (c), (iii) section (c) to (d). In the curve segment (b)-(c), the flows represent more intricate features, it contains a bifurcation solution curves in a narrow range of Taylor numbers. In all the sections, the flux gradually decreases with the increase of Taylor numbers in both positive and negative directions.

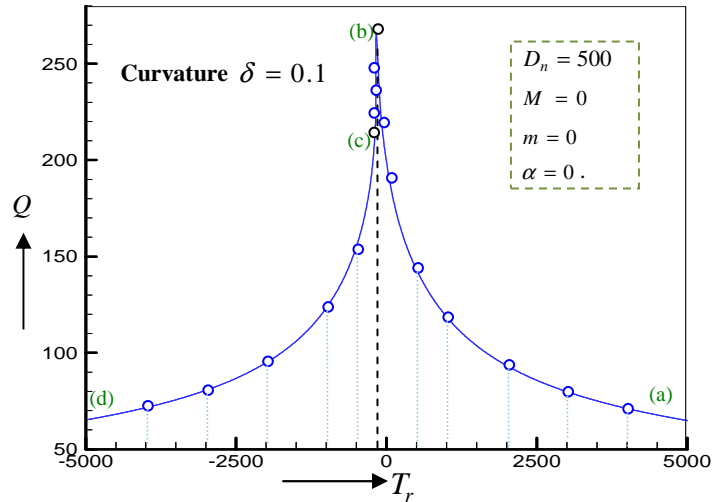


Figure 4.4a: Solution curve: Flux Q versus Taylor Number T_r with the fixed values of $\delta=0.1$, $D_n=500$, $M=0$, $m=0$ and $\alpha=0$.

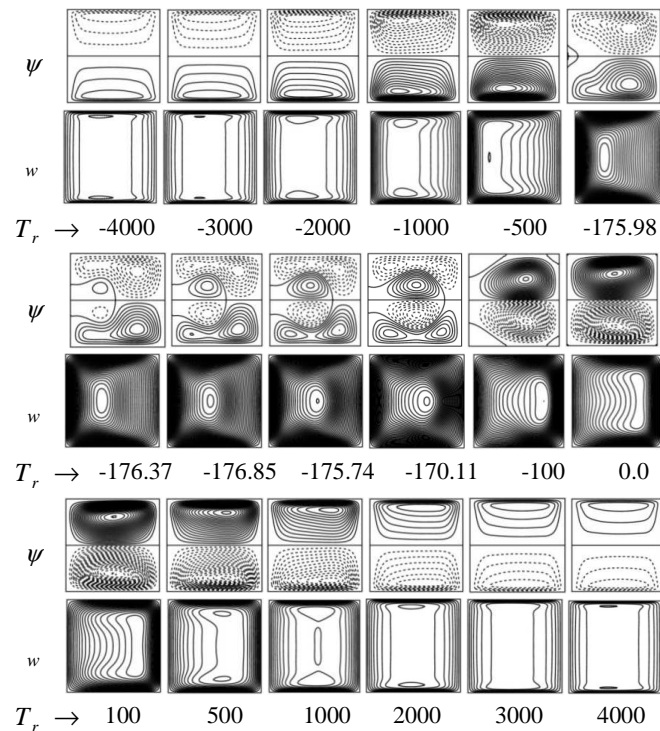


Figure 4.4b: Streamlines ψ (upper) and axial contour flow w (lower) in accordance with the solution curve in Fig.4.4a

Figure 4.4b displayed the streamlines ψ of the secondary flow (top) and contours of the axial flow w (bottom) at several distinct points on the solution curve of Fig. 4.4a. The secondary flows are discovered to be symmetrical two, four, or six vortex flow patterns. At $T_r = 0$ (i.e. no rotation on the duct), it has been discovered that the flow pattern inside the duct has a two-vortex structure. The two strong vortices flow formed in the middle of the duct are visible in the velocity structures at Taylor number $T_r = -100$, together with four weak vortices close to the four corners. This point is called the critical point for the Taylor

number. The two-cell vortex flow structure of the secondary flow has been observed in the curve segment (a)-(b), where the maximum quantity of flow is shifted toward the vertical boundary and its trends weaken over time with rising values of T_r . Another curve segment (b)-(c); especially at $T_r = -175.98, -176.37, -176.85$ and -175.74 , there are six vortex structures has been found. Almost the peak value of the flux $Q = 268.39$ has been found at $T_r = -171.99$. Whereas, the curve section (c)-(d) displays the vortex structure of the secondary flow flowing in the opposite direction from the main flow. The maximum amount of flow for the radial velocity has been pushed close to the upper and lower boundary as the increase of T_r . The strength of flow pattern gradually becomes weak with the increase of T_r in both positive and negative direction. In contrast, the axial flow's contour has been relocated to the duct's centre, and its trends are likewise becoming steadily weaker as T_r values rise. Similarly, in curve section (b)-(d) on this figure, the velocity's contour has been pushed to the duct's centre, and its trend are also dropped gradually as T_r values rise in negative direction.

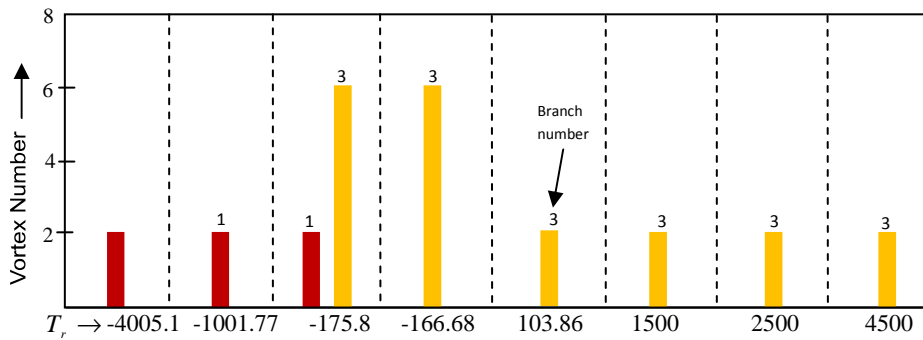


Figure 4.4c : Taylor number T_r versus vortex number of secondary flows with $\delta = 0.1$, $D_n = 500$, $M = 0$, $m = 0$ and $\alpha = 0$

To better understand the radial flow vortex structure: Fig. 4.4c illustrated the bar diagram for the Taylor number vs vortex number plane. The number of branches is indicated at the top of each bar in the diagram. This graphic shows that as the Taylor number rises, the vortices become progressively weaker.

The rotational effects on the curve duct flow for the fixed values of $M = 0$, $m = 0$, $\alpha = 0$ over a wide range of Taylor number $-5000 \leq T_r \leq 5000$ with the duct curvature $\delta = 0.1$ are shown in Figs.4.3a-c.

Case-III: $\delta=0.5, D_n=500$

The rotational effects on the curve duct flow for the fixed values of $M = 0$, $m = 0$, $\alpha = 0$ with Dean Number at $D_n=500$ and the duct curvature $\delta=0.5$ are shown in Figs.4.5a-c. The flux Q against Taylor number T_r solution curve is shown in Fig. 4.5a. As can be observed from the illustration, a single branch solution curve appears here, and as values of

T_r increase in both positive and negative directions, the trend of the flow pattern quickly adopts a weak form.

The streamlines of the secondary flow ψ (top) and contour plots of the axial flow w (bottom) are shown in Fig.4.5b at various Taylor number locations. In the tiny range, symmetric four vortices have been discovered, and out of this range, two vortices structures are found for the secondary velocity. In contrast, at rising values of T_r , the max amount of axial flow is pushed toward the duct's inner wall. By using a bar diagram that corresponds to the solution curve, Fig. 4.5c shows the Taylor number vs vortices number plane for the streamlines among the range $-3000 \leq T_r \leq 3000$.

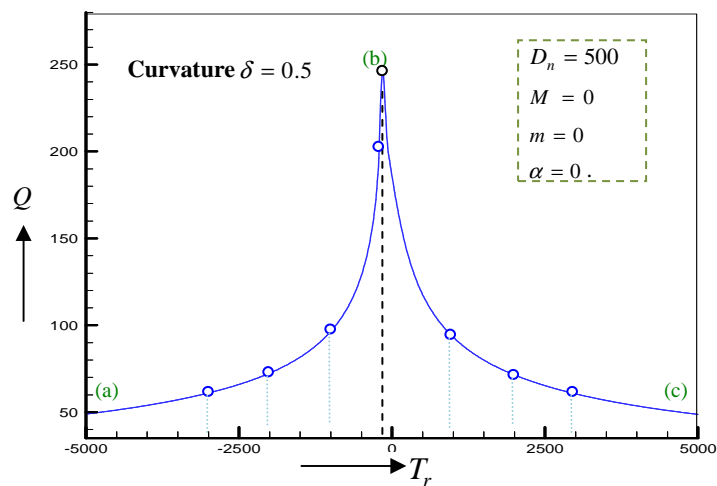


Figure 4.5a: Solution curve: Flux Q versus Taylor Number T_r with the fixed values of $\delta=0.5$, $D_n=500$, $M=0$, $m=0$ and $\alpha=0$.

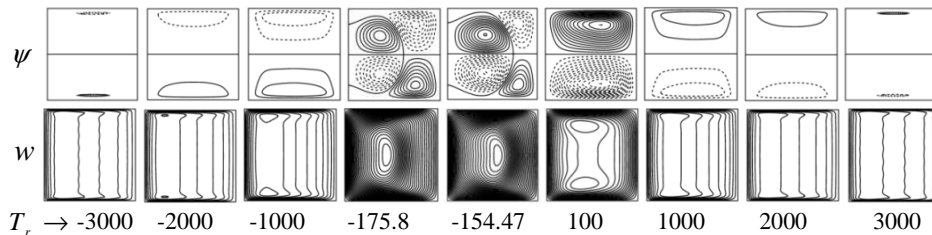


Figure 4.5b: Streamlines ψ (upper) and axial contour flow w (lower) in accordance with the solution curve in Fig.4.5a

Now, the solution curves are examined in terms of the flux Q against Taylor number T_r with respect to the curvature of ducts $\delta = 0.1$, $\delta = 0.01$ and $\delta = 0.5$, which are plotted in Figs. 4.3a, 4.4a, and 4.5a, respectively.

Bar diagrams Fig.4.3c, Fig.4.4e and Fig.4.5c make it abundantly clear that the vortex tendency declines with increasing curvature δ . It is observed that the sharp peak value of flux 268.38 has been found at $T_r = -172.21$, 266.82 at $T_r = -170.11$, and 245.45 at $T_r = -154.47$ when curvature of the duct $\delta = 0.01$, $\delta = 0.1$ and $\delta = 0.5$ respectively. As

opposed to many bifurcation curves for $\delta = 0.01$, weak bifurcation curves for $\delta = 0.1$ and no bifurcation for $\delta = 0.5$ have been discovered. It means that when curvature values increase, the pick value of the flux and the number of branches gradually decrease.

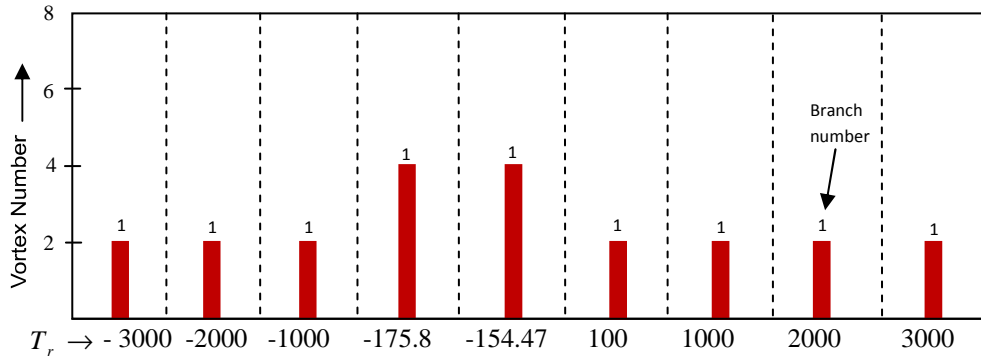


Figure 4.5c: Taylor number T_r versus vortex number of secondary flows with $\delta = 0.5$, $D_n = 500$, $M = 0$, $m = 0$ and $\alpha = 0$.

B. Effects of Dean Number (D_n):

The Dean number effects on the curve duct flow for the fixed values of $T_r = 10$, $M = 0$, $m = 0$, $\alpha = 0$ are shown in Figs.4.6a-c. The solution curve of the flux Q against Dean Number D_n with the duct curvature $\delta=0.1$ is shown in Fig. 4.6a. Fig. 4.6a (ii) displays the enlarged figure of the portion marked by rectangle symbol on solution curve in Fig. 4.6a(i). It provided three steady state solution branches, the first of which is indicated by the colour red from (a) to (b), the second by the colour green from (b) to (c), and the third by the colour blue from (c) to (d). A pair of counter-rotating vortices have been exist for the secondary flow in all branches of the steady-state solution curve, and also the fluxes increase with the increase of D_n . Figure 4.6b exhibits the axial flow's contours and secondary flow's structures at various locations of Dean Numbers to the solution curve in Fig.4.6a. From these graphs, it can be seen that symmetric two-, four-, or six-vortices have been discovered for the streamline. With an increase in Dean Number, vortices grow in

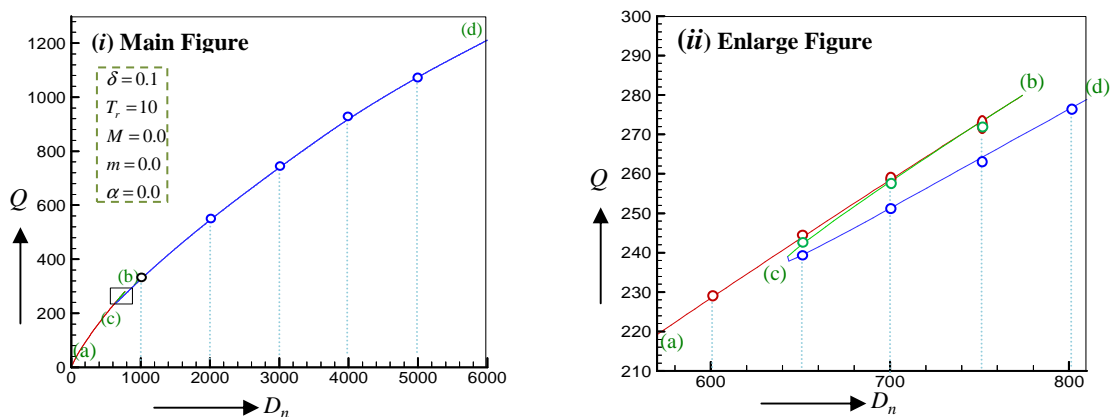


Figure 4.6a: Solution curve: Flux Q versus Taylor Number T_r with the fixed values of $\delta=0.1$, $T_r=10$, $M=0$, $m=0$ and $\alpha=0$.

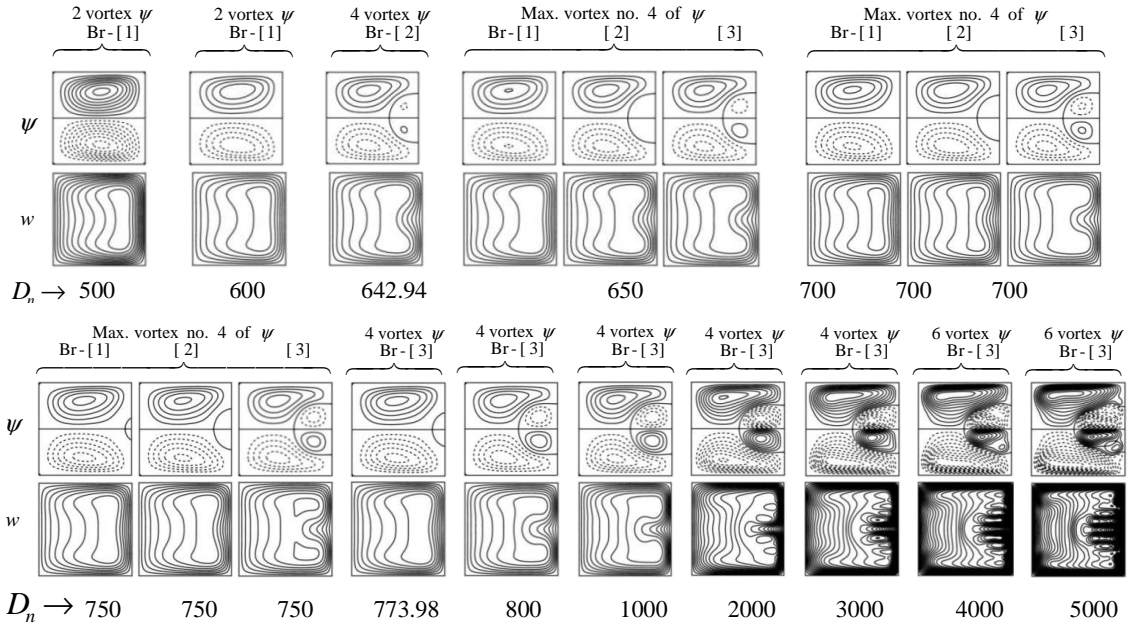


Fig.4.6b: Streamlines ψ (upper) and axial contour flow w (lower) in accordance with the solution curve in Fig.4.6a

number. When $D_n > 700$ (approximately) in the first branch, additional vortices have begun to form. In contrast to this, for the axial flow for large Dean Numbers, several contours w have been observed and the number of contours grew gradually as D_n increased.

For all values of D_n , a most portion of the axial fluid has flowed close to the duct's outer wall. In the curve section from point (a) to point (b), the vortices increase; they then diminish from point (b) to point (c), Again it grows once more from point (c) to point (d) with the increase of D_n . At every location within $642.94 < D_n < 773.98$, three separate vortex structures of secondary flow have been discovered. Two strong vortices flow symmetrically in the first branch, and two strong vortices flow symmetrically in the second branch with two weak vortices near the outer wall. Additionally, the third branch features two vortices that are stronger than the two on the second branch. In contrast, it is discovered that the contour structure for axial flow has initially been simple in the first and second branches before gradually becoming complex. As D_n rises, the contours increase in the first branch, decrease in the second branch, and then increase once more in the third branch.

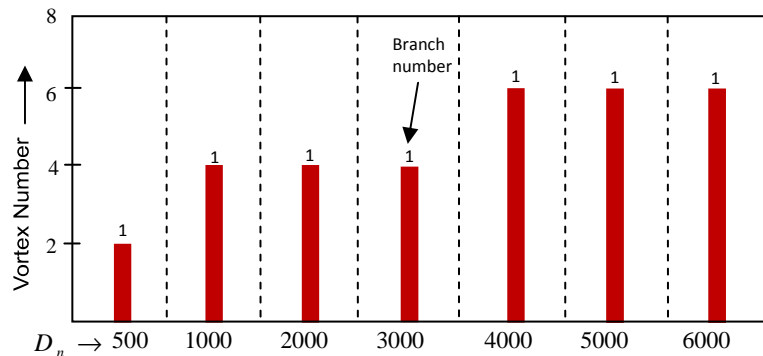


Figure 4.6c: Dean Number D_n versus vortex number of secondary flows with $\delta = 0.1$, $M = 0.0$, $m = 0.0$ and $\alpha = 0.0$

The Dean number vs vortex number plane for secondary flow is depicted in Fig.4.6c by a bar diagram with a curvature of $\delta = 0.1$ in the range of $0 \leq D_n \leq 6000$. It is clear from the bar diagram that as the Dean number rises, the vortex propensity also gradually rises.

The main objective is to look at how magnetic (M), Hall parameters (m) and ion-slip parameters (α) affect the flow characteristics in the curve duct with rotation. The investigation is performed under the various values of M , m and α for the two cases of Dean Numbers; **Case-I:** $D_n = 500$ and **Case-II:** $D_n = 1000$, while the Taylor number is fixed at $T_r = 10$. In Case-I, the flow pattern has been examined for three different values of curvature, $\delta = 0.01, 0.1$ and 0.5 . But in Case-II, the research has only been done for $\delta = 0.1$ due to the conditions are the same as in Case-I.

C. Effects of Magnetic Parameter (M)

Case-I: $D_n = 500$

The effects of Magnetic parameter on the curve duct flow for the fixed values of $D_n = 500$, $T_r = 10$, $m = 0$, $\alpha = 0$ with duct curvatures at $\delta = 0.01, 0.1$ and 0.5 are shown in Figs.4.7a-b. The solution curve of the flux Q against Magnetic Parameter M for the different choices of the duct curvature $\delta=0.01, 0.1$, and 0.5 is illustrated in Fig. 4.7a. A single branch of the steady-state solution is found in each case of the curvature values. These solution curves are all the decreasing functions. As a result, it may indicate that the flux reduces as the magnetic parameter increases. Providing the magnetic parameter with a large value can bring the velocity closer to zero.

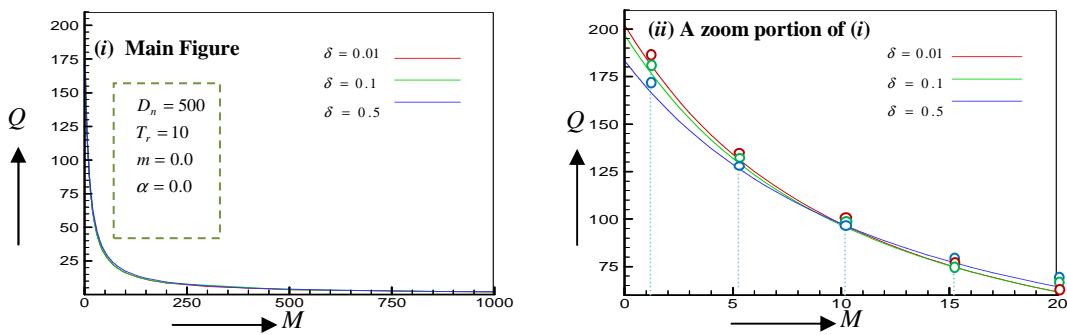


Figure 4.7a: Solution curve: Flux Q versus Magnetic parameter M with the fixed values of $\delta=0.1, D_n = 500, T_r = 10, m=0$ and $\alpha=0$. for curvatures $\delta = 0.01, 0.1$ and 0.5

Fig. 4.7b depicts vortex structure of the stream function ψ and the contour of the axial flow w at various locations along M corresponding to the solution curve in Fig. 4.7a. At each value of M , symmetric two vortex structures have been discovered for the secondary flow, whereas this trend gradually weakens as M increases. The secondary flow is slightly

impacted by the increasing values of δ . In contrast, for an axial flow, the highest fluid flow occurs close to the outside wall at low values of M and it shifts to the duct's centre at low curvatures with higher values of M . The flows are shifted to the duct's interior wall side due to the larger values of the curvature. With raising the values of M , its strength is also steadily losing strength.

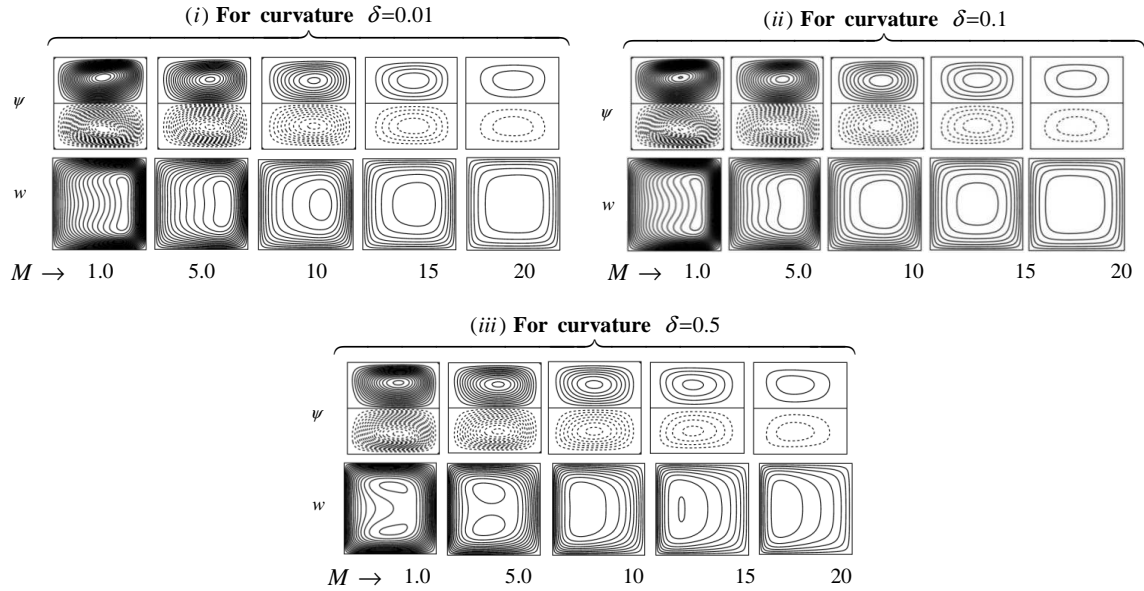


Figure 4.7b: Stream lines ψ (upper) and axial contour flow w (lower) corresponding to the solution curve in Fig.4.7a

Case-II: $D_n = 1000$

Fig.4.8a demonstrates the solution curve of flux Q vs M for the fixed values of $D_n = 1000$, $T_r = 10$, $m = 0$, $\alpha = 0$ at the duct's curvatures $\delta = 0.1$. A small range of magnetic parameter $2.103 < M < 3.736$ exist, where three branches of solution curve have been found. The green colour in the curve section (b) - (c) indicates that the solution curve was discovered in the reverse direction from $M = 3.73644919$ till $M = 2.1030904$, after that it reversed once more. This solution curves in all branches are clearly a decreasing functions. As a result, it may indicate that the flux decreases as the magnetic parameter increases.

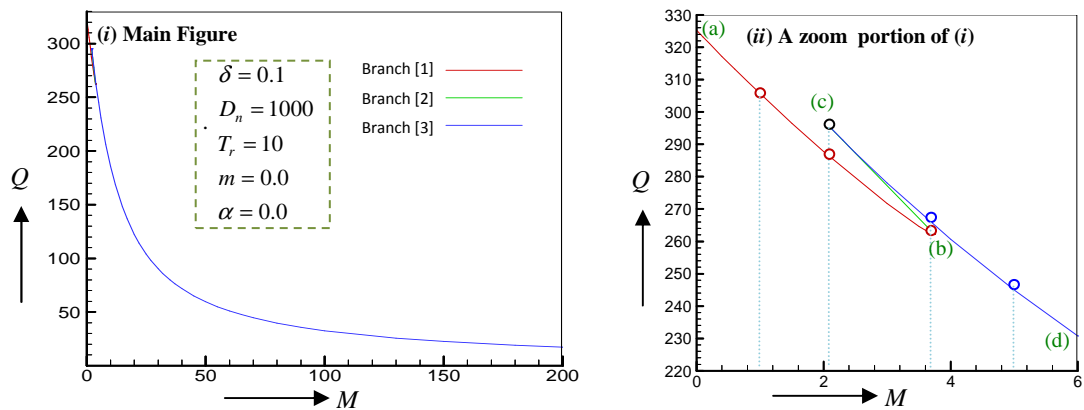


Fig.4.8a: Solution curve of the flux Q versus Magnetic parameter M at the fixed values of $\delta = 0.1$, $T_r = 10$, $D_n = 1000$, $m = 0$ and $\alpha = 0$.

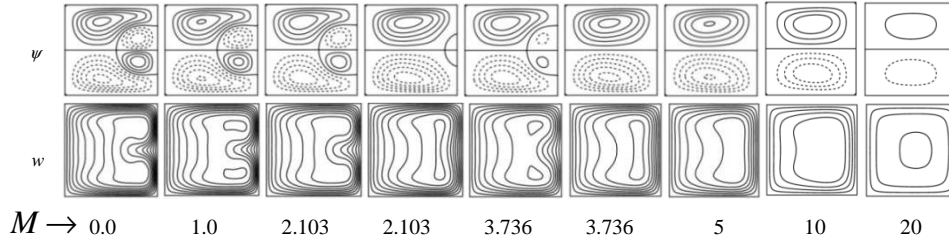


Figure 4.8b: Stream lines ψ of the secondary flow (upper) and contour of the axial flow w (lower) corresponding to the solution curve Fig.4.8a

Fig.4.8b exhibits the vortex structure of the stream lines ψ and contour plot of the axial w flow at some distinct points of M corresponding to the solution curve in Fig. 4.8a. There is one pair of counter-rotating vortices with additional two vortices developed for the secondary flow of streamlines in the curve section (a)-(b), whereas, more than one contour has been identified for the axial flow. The greatest axial flow is relocated close to the duct's outer wall. Additional vortices are eliminated from point $M = 2.1030904$ for the secondary flow, and it then displays a symmetric two-cell structure for rising values of M , whilst the axial flow gradually loses strength, takes on a simple contour, and shifts its centre toward the centre of the duct.

D. Effects of Hall Parameter (m)

Case-I: $D_n = 500$

Figs.4.9a-b exhibits the effects of Hall parameter on the curve duct flow for the fixed values of $D_n = 500$, $T_r = 10$, $M = 1.0$, $m = 0$, $\alpha = 0$ with duct curvatures at $\delta = 0.01, 0.1$, and 0.5 . For all values of the curvature, a single branch of steady solutions has been discovered and also all the curves are increasing function. The flux Q increases rapidly with the increase of Hall parameter in a certain range $0 \leq m \leq 5$ approximately, and then it has a minor increasing effect. It has steady state solution after a certain values of m in all the cases of the curvature.

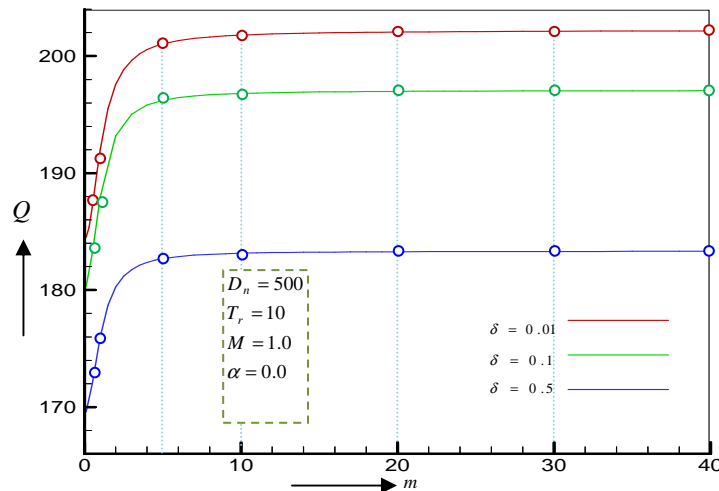


Figure 4.9a: Solution curve of the flux Q versus Hall parameter m at the fixed values of $T_r = 10$, $D_n = 500$, $M = 1.0$ and $\alpha = 0$ for curvatures $\delta = 0.01, 0.1$ and 0.5

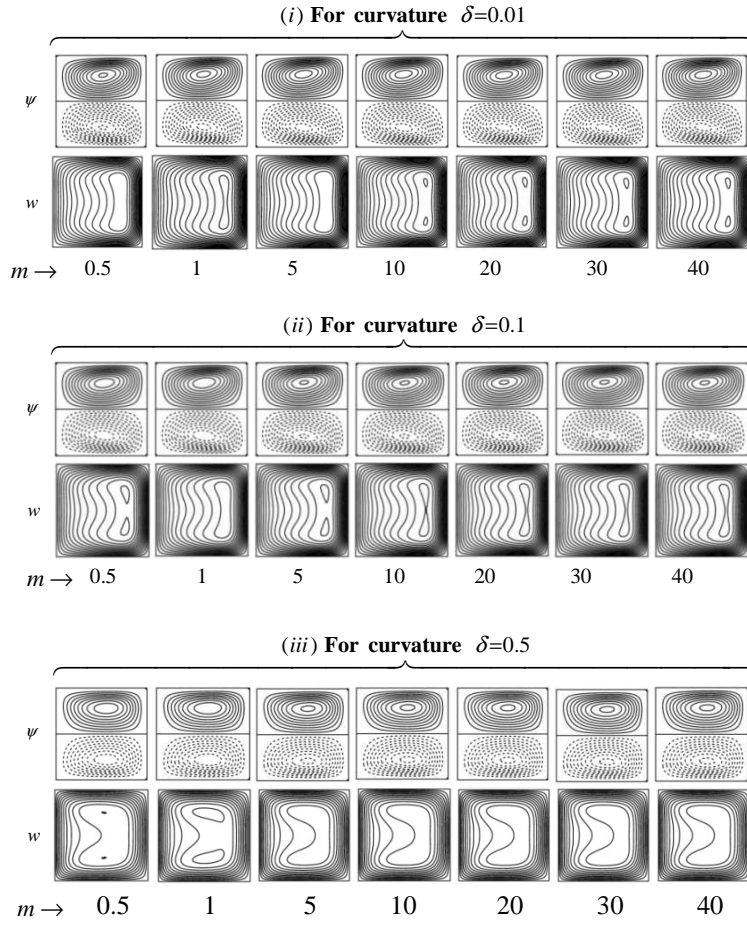


Figure 4.9b: Stream lines ψ of the secondary flow (upper) and contour of the axial flow w (lower) corresponding to the solution curve Fig.4.9a

Fig.4.9b shows the vortex structure of the stream lines ψ and contour plot of the axial flow w at some distinct points of m corresponding to the solution curve in Fig. 4.9a. The figure demonstrates how symmetric two-cell vortices are generated for the secondary flow's streamline. For each value of m , the majority of the axial flow is located close to the duct's outer wall. The alteration of the Hall parameter m led to slight changes in the layout of the axial and secondary flow. Furthermore, it is noted that the highest amounts of flux Q has been found 202.15, 197.04, and 183.31 at the curvatures $\delta=0.01$, 0.1, and 0.5 respectively. The steady-state solution is discovered at $m > 40$ (approx.).

Case-II: $D_n = 1000$

Fig.4.10a demonstrates the solution curve of flux Q vs Hall parameter m for the fixed values of $D_n = 1000$, $T_r = 10$, $M = 1.0$, $\alpha = 0$ at the duct's curvatures $\delta = 0.1$. In this case, only one branch of steady-state solutions has been identified. Clearly this solution curve is an increasing functions, therefore the flux Q rises with the rise in the Hall parameter m , however, it rises quickly inside $0 \leq m < 5$ and then rises gradually with the rise in m . A stable solution has been discovered after a specific value of m .

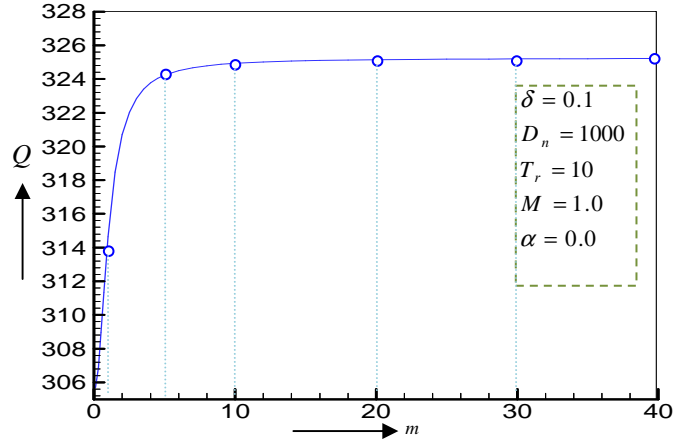


Figure 4.10a: Solution curve: Flux Q versus Hall parameter m with the fixed values of $T_r = 10$, $D_n = 1000$, $M = 1.0$ and $\alpha = 0$.

Fig.4.10b depicts the vortex structure of the stream lines ψ and contour plot of the axial flow w at some distinct points of m corresponding to the solution curve in Fig. 4.10a. While axial flow was found to have numerous contours, in contrast, streamlines ψ were found to have symmetrical two vortices with an additional two vortex structures close to the outside wall. For each value of m , the majority of the axial flow is located close to the duct's outer wall. Variations in the Hall parameter m cause a little change in the axial and secondary flow layouts. Steady state solution is found when $m > 40$ approximately.

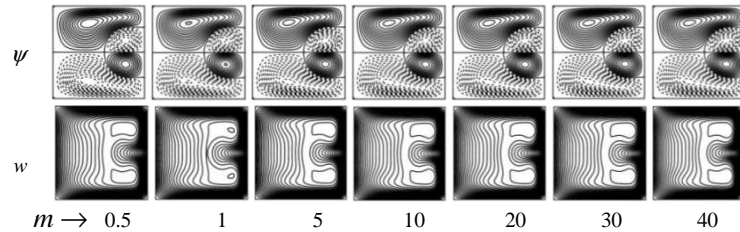


Figure 4.10b: Stream lines ψ of the secondary flow (upper) and contour of the axial flow w (lower) corresponding to the solution curve Fig.4.10a

E. Effects of Ion-slip Parameter (α)

Case-I: $D_n = 500$

Figures.4.11a-b exhibits the effects of Hall parameter on the curve duct flow for the fixed values of $D_n = 500$, $T_r = 10$, $M = 1.0$, $m = 5.0$ with duct curvatures at $\delta=0.01$, 0.1, and 0.5. A single branch of steady solutions has also been discovered for all values of the curvature. The flux Q initially rapidly decreases within the range $0 \leq \alpha < 0.8$, then quickly increases within $0.8 \leq \alpha < 10$, and finally has just a tiny growing influence as grows of α . Furthermore, it is also noted that the max amounts of flux Q has been found 202.15, 197.04, and 183.31 at the curvatures $\delta=0.01$, 0.1, and 0.5 respectively and approximate steady-state situation has been found when $\alpha > 40$.

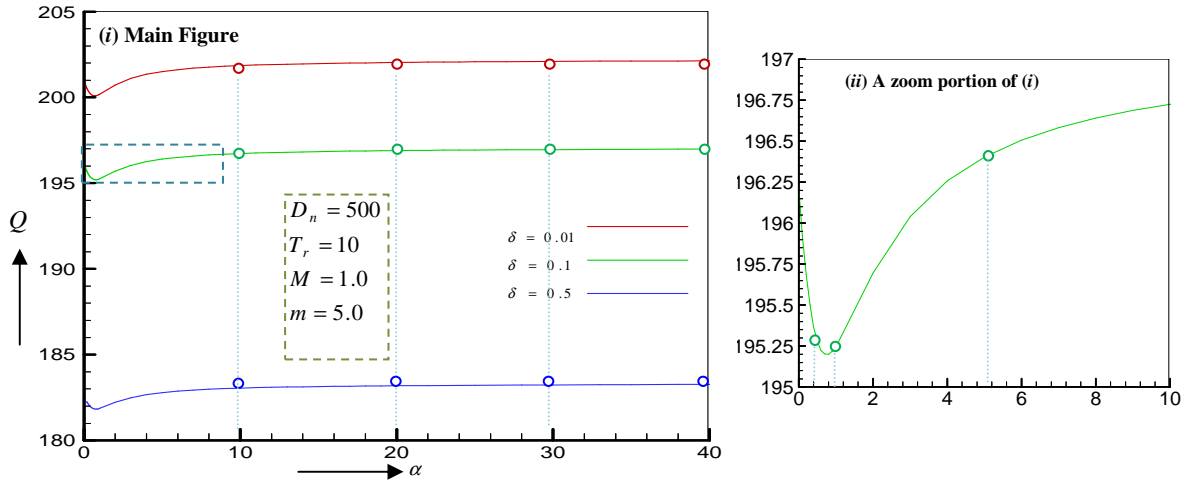


Figure 4.11a: Solution curve of the flux Q versus Ion-slip parameter α at the fixed values of $T_r = 10$, $D_n = 500$, $M = 1.0$ and $m = 5$ for curvatures $\delta = 0.01, 0.1$ and 0.5

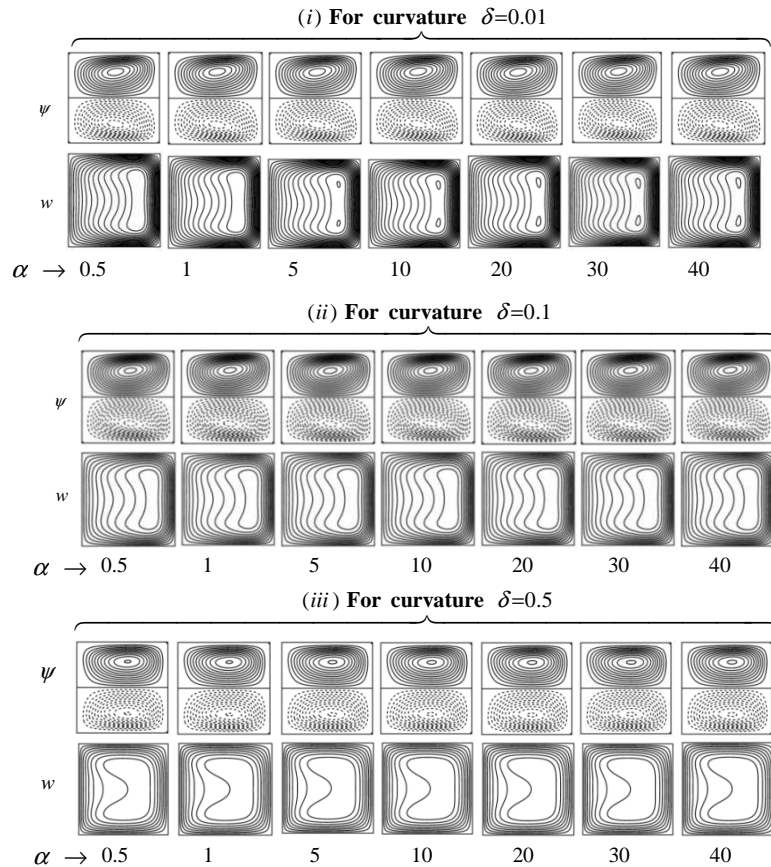


Figure 4.11b: Stream lines ψ of the secondary flow (upper) and contour plot of the axial flow w (lower) corresponding to the solution curve Fig.4.9a

Figure.4.11b displays the vortex structure of the stream lines ψ and contour plot of the axial flow w at some distinct points of α corresponding to the solution curve in Fig. 4.11a. For each value of α with small curvature δ , two-cell symmetric vortices have been created for the streamline, whereas, the majority of the axial flows pass close to the duct's outer wall. The axial flows are moved to the square duct's centre, whereas, the contours lose their

strength and complexity for large values of α . As the value of the ion-slip parameter α changes, the structure of the axial and secondary flows is observed to remain unchanged.

Case-II: $D_n = 1000$

Figure.4.12a demonstrates the solution curve of flux Q vs Ion-slip parameter α for the fixed values of $D_n = 1000$, $T_r = 10$, $M = 1.0$, $m = 5.0$ at the duct's curvatures $\delta = 0.1$.

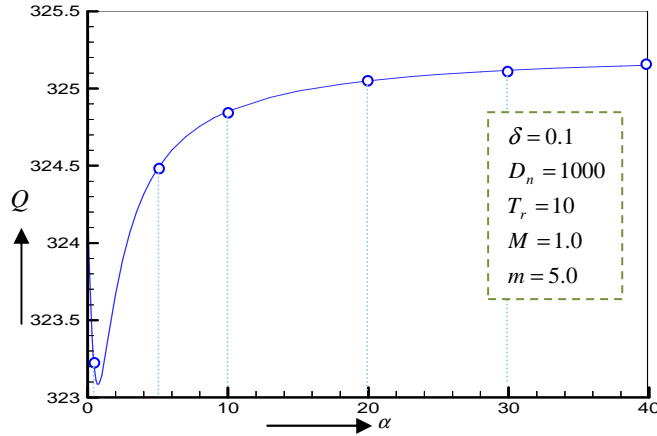


Fig.4.12a: Solution curve of the flux Q versus Ion-slip parameter α with the fixed values of $T_r = 10$, $D_n = 1000$, $M = 1.0$ and $m = 5.0$.

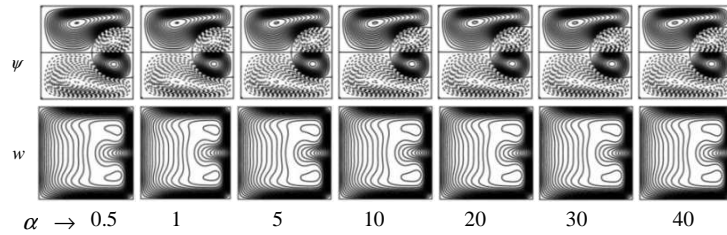


Figure 4.12b: Stream lines ψ of the secondary flow (upper) and contour of the axial flow w (lower) corresponding to the solution curve Fig.4.12a

And the vortex structure of the secondary flow ψ and contour of axial flow w at various points of α are illustrated in Fig.4.12b corresponding to the solution curve in Fig. 4.12a. A single branch of steady solutions has also been discovered. The flux Q initially rapidly decreases within the range $0 \leq \alpha < 0.8$, then quickly increases within $0.8 \leq \alpha < 5$, and finally has just a tiny growing influence as grows of α . There are symmetric two-cell vortex structures with four strong vortices found to streamline of the secondary flow; on the other hand, the majority of axial flows w pass close to the duct's outer wall for any value of α . An increase in the Ion-slip parameter α has very little impact on the axial and secondary flow structures. From this observation, it can be seen that the flow structure does not change for any increasing values of α after a particular value of α .

4.5 Curved Rectangular Duct for Isothermal Fluid Flow (Aspect Ratio 2): *Steady MHD Fluid Flow in a Rotating Curved Rectangular Duct with Hall and Ion-slip Current*

Numerical analysis is used to explore the steady two-dimensional viscous incompressible fluid flow through a rotating curved rectangular duct with a curvature ranging from 0.1 to 0.5 in the presence of a magnetic field with Hall and Ion-slip current. Due to the rectangular cross-section of the duct, the aspect ratio is taken as $l = h/d = 2$. The spectral method is the main instrument used to perform the calculations numerically. On the other hand, auxiliary tools such as the Chebyshev polynomial, Newton-Raphson, collocation, and arc-length approaches are employed. A pressure gradient force (Dean Number) is applied to the centreline direction of duct. A pressure gradient force (Dean Number) is applied to the centreline direction of duct. On such flow, the impact of the parameters magnetic, Hall, Ion-slip, rotation, and Dean Number are explored. This investigation's goal is to demonstrate how the magnetic, Hall, and ion-slip parameters affect the flow characteristics in the rectangular duct with a rotational curve. The behaviour of the exposed secondary flow streamlines and axial flow contour lines for various values of the magnetic, Hall, and Ion-slip parameters on the flow characteristics for three particular cases such as Case-I: $\delta = 0.1, D_n = 500$, Case-II: $\delta = 0.5, D_n = 500$ and Case-III: $\delta = 0.1, D_n = 800$, while the rotational parameters keep fixed at $T_r = 20$. Only one parameter of D_n, T_r, M, m and α are varied with others are fixed at a significant value of the parameters.

4.5.1 Grid Spaces Accuracy

It is required to discuss about grid space accuracy before executing the FORTRAN program. The equations are numerically solved for various pairs of truncation numbers in order to obtain the requisite grid space precision. Due to the rectangular cross-section of the duct with aspect ratio of 2, it is preferable to use the values for \bar{N} is twice of \bar{M} to obtain reasonable accuracy. To find the best grid space accuracy, the flux Q has been calculated for several pairs of truncation numbers (\bar{M}, \bar{N}) such as (08, 16), (09, 18), (10, 20) and (11, 22). These are displayed in Table-2.

\bar{M}	\bar{N}	Q
08	16	77.05173978747959
09	18	77.05197466821699
10	20	77.05241720673571
11	22	77.05232885353998
12	24	77.05227321211437

Table-2: Fluxes Q at several pairs of truncation numbers \bar{M} and \bar{N} at fixed values of $\delta=0.1, T_r = 20, D_n = 500, M = 0, m = 0$ and $\alpha=0$

From this table, it can be determined that the numerical outcomes are accurate enough at $\bar{M} = 10$ and $\bar{N} = 20$.

4.5.2 Results and Discussion

To study the characteristics of the flow, a fully developed steady flow of incompressible viscous fluid is considered. This flow occurs through a rectangular cross-section curved duct that rotates with an angular velocity Ω around its vertical y -axis. The curvature of the duct is set to two different values, 0.1 and 0.5, for the purpose of investigation. The rectangular cross-section of the duct has an aspect ratio of 2. For visualizing the flow structure, incremental values of $\Delta w = 4$ and $\Delta \psi = 0.3$ are employed. The initial investigation focuses on the impact of the Taylor number (T_r) and Dean Number (D_n) on the velocity distribution, and these findings are presented in figures from Fig. 4.13 to Fig. 4.15. In this study, new insights are revealed regarding the effects of the magnetic parameter (M), Hall parameter (m), and Ion-slip parameter (α) on the velocity, which are illustrated in figures from Fig. 4.16 to Fig. 4.18. The flow characteristics are elucidated through solution curves, and their corresponding vortex structures are depicted for three distinct cases:

Case-I : $\delta = 0.1, D_n = 500$

Case-II : $\delta = 0.5, D_n = 500$

Case-III : $\delta = 0.1, D_n = 800$

It's important to note that the rotational parameters remain fixed at $T_r = 20$, while only one of the parameters, D_n (Dean Number), T_r (Taylor Number), M (Magnetic Parameter), m (Hall Parameter), or α (Ion-slip Parameter), is varied. The other parameters are held constant at significant values during the investigation.

A. Effects of Taylor Number (T_r) on the Velocity

In Figure 4.13a, the solution curve illustrates the relationship between the flux Q and the Taylor Number T_r . This curve is presented for the case where the duct curvature δ is set at 0.1. The values of other parameters are kept fixed, with $D_n = 500, M=0, m=0,$ and $\alpha=0$. Over an extensive selection of Taylor numbers – $6000 \leq T_r \leq 6000$, the rotational effects on

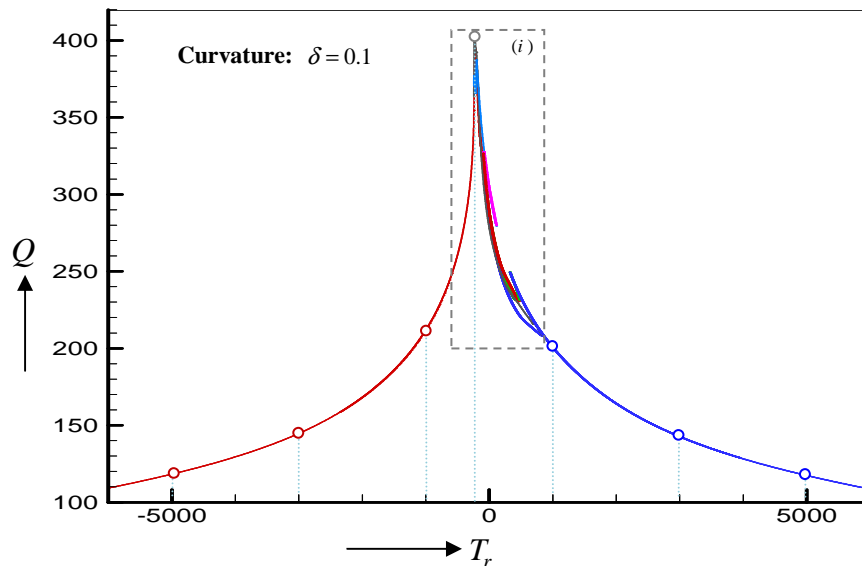


Figure 4.13a: Solution curve: Flux Q versus Taylor Number T_r for $D_n = 500, M = 0, m = 0$ and $\alpha=0$ with the curvature $\delta=0.1$.

the curve duct flow are explained. Within a certain range indicated by the dashed rectangular box in Fig. 4.13a, nine bifurcation curves have been discovered; their magnified representations are displayed in Fig. 4.13b. To identify these branches, different colours have been used on the solution curve. Additionally, Figures 4.13c-f have shown enlarged portions of the areas designated in Fig. 13.b marked by dashes boxes (ii), (iii), (iv), and (v).

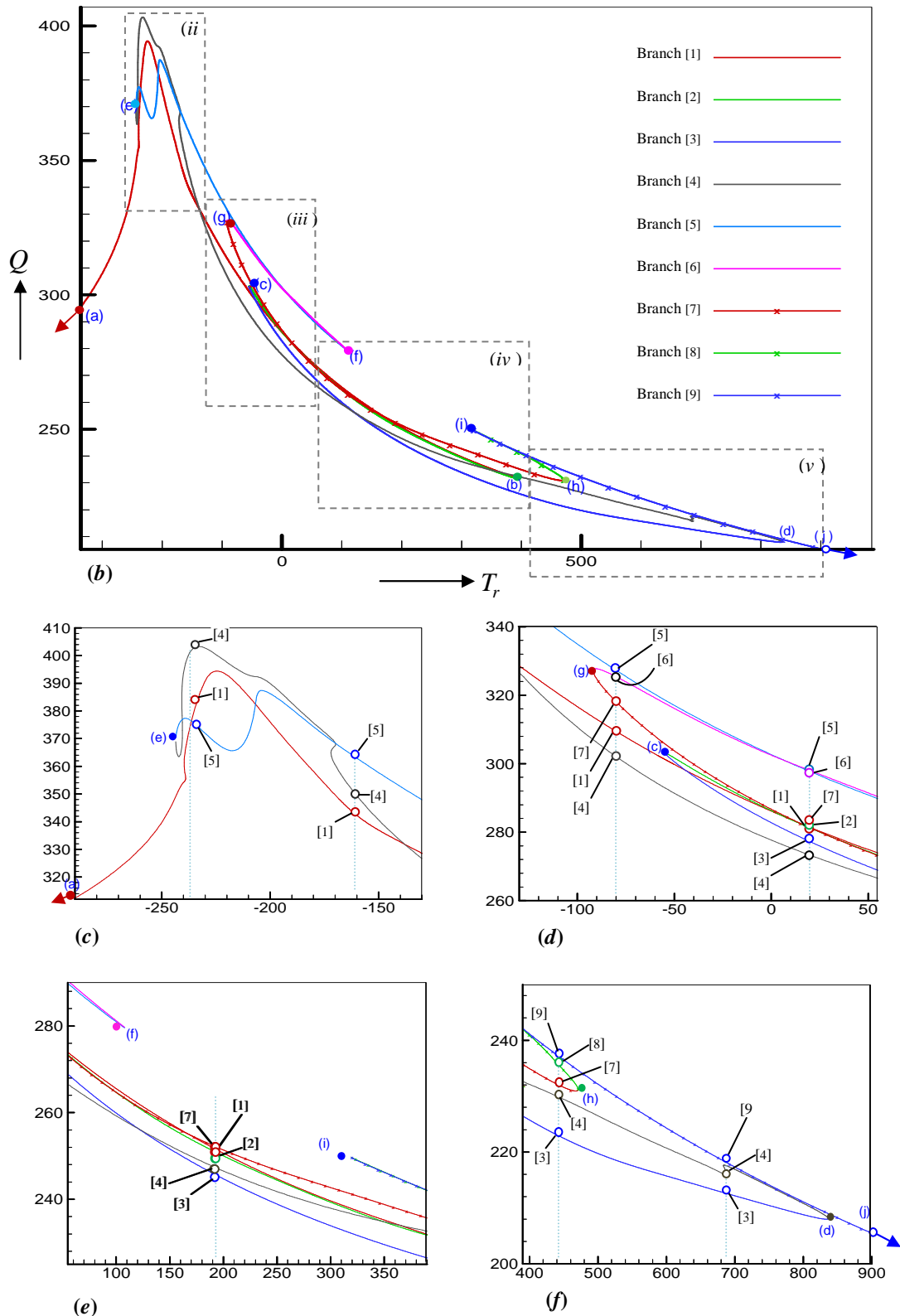
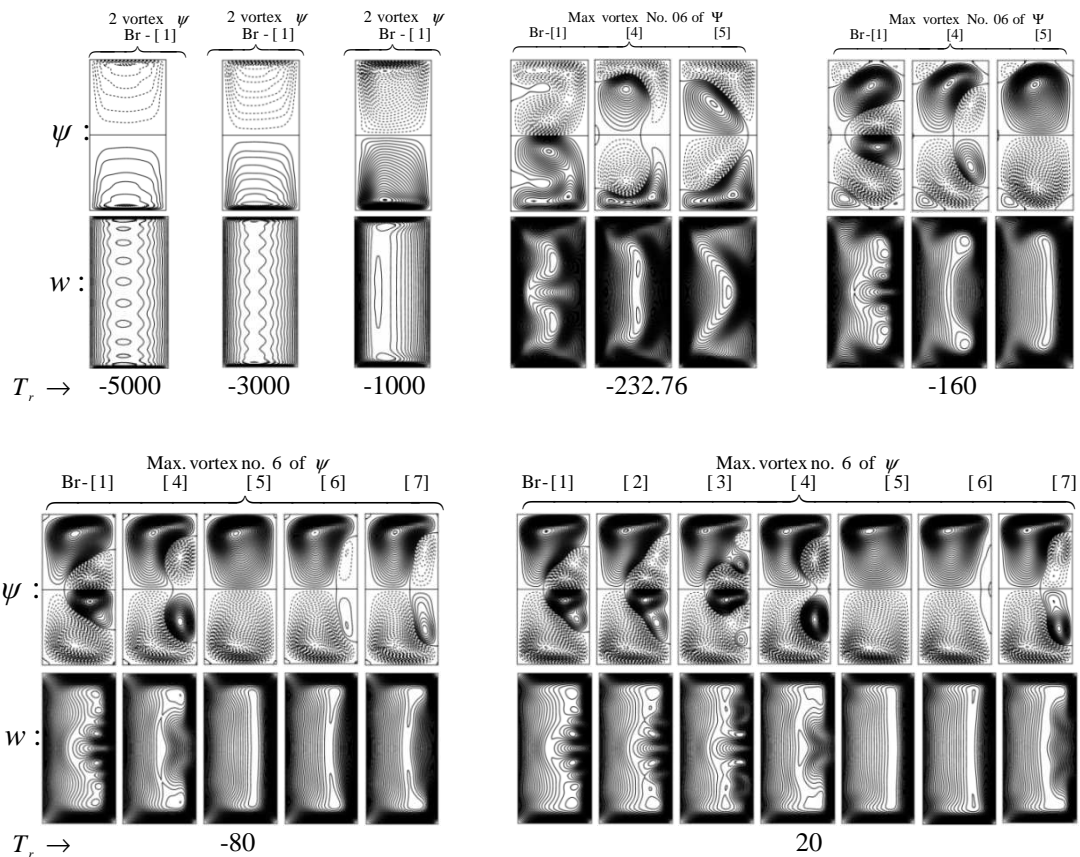


Figure 4.13b-f: Magnifying figures marked by the dashed box on Fig.4.13a.

Figure 4.13g depicted two key elements: the streamlines ψ illustrating the secondary flow in the upper part, and the contours of axial flow denoted as w in the lower part. These visualizations were observed at distinct points corresponding to the solution curve detailed in Figure 4.13a. As the absolute value of $|T_r|$ increases, it has been observed a significant shift in a majority of the streamlines toward the upper and lower boundaries, while the central point of the axial flow contour migrates toward the duct's midsection. Simultaneously, the axial flow redistributes, shifting towards both the inner and outer walls of the duct. With higher $|T_r|$ values, there is a gradual deterioration in the axial flow contour and the secondary flow vortex. At $T_r = -232.76$, we identify the maximum value of flux Q , nearly reaching 403.29363. The bifurcation section reveals the secondary flow streamlines ψ and axial flow contours w at select points: $T_r = -232.76, -160, -80, 20, 200, 440,$ and 685 . Among these points, $T_r = -232.76, -160,$ and 685 exhibits three branches of the solution curve, while $T_r = -80, 200,$ and 440 display five branches. At $T_r = 20$, we observe seven branches, whereas the other points have only a single branch. At these specific locations, the secondary flow manifests itself through symmetric solutions, including two, four, six, and eight vortices. As the values of $|T_r|$ increase, the strength of the vortices diminishes. Additional vortices emerge near the outer boundary of the duct, with one, two, or more contours present in the axial flow. It's worth noting that the axial velocity of the flow within the curved duct significantly influences the strength of the secondary vortices.



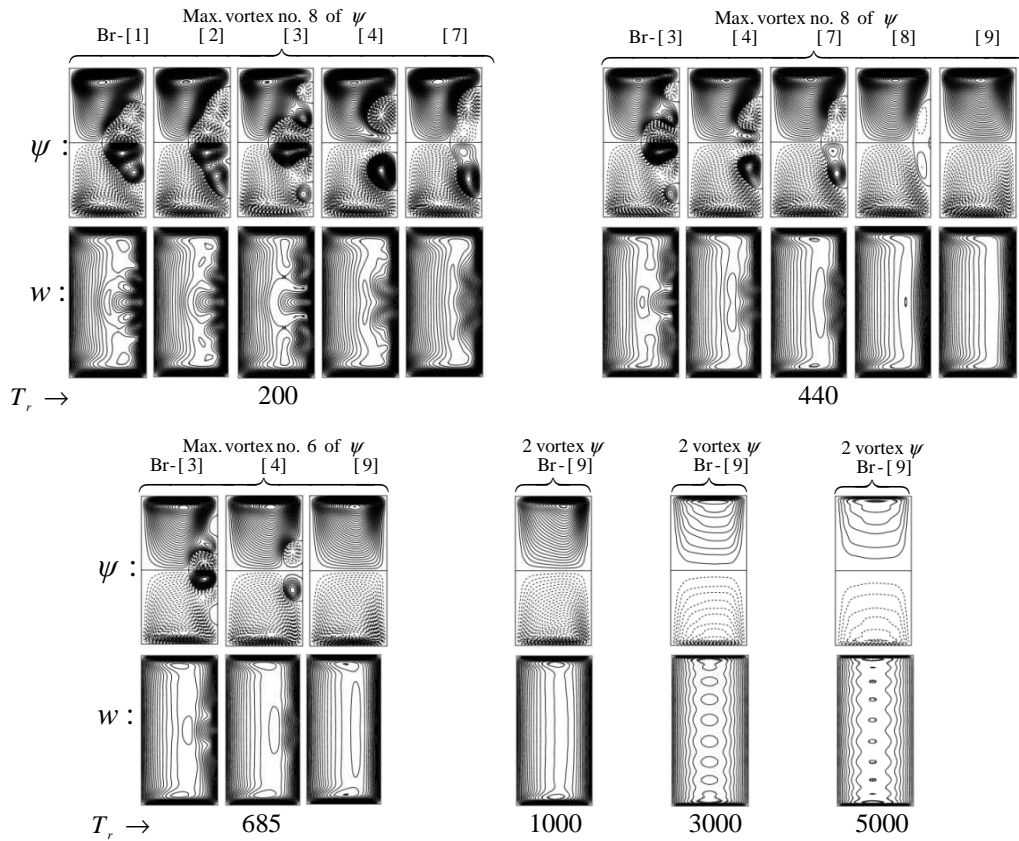


Figure 4.13g: Streamlines ψ (upper) and axial contour flow w (lower) in accordance with the solution curve in Fig.4.13a.

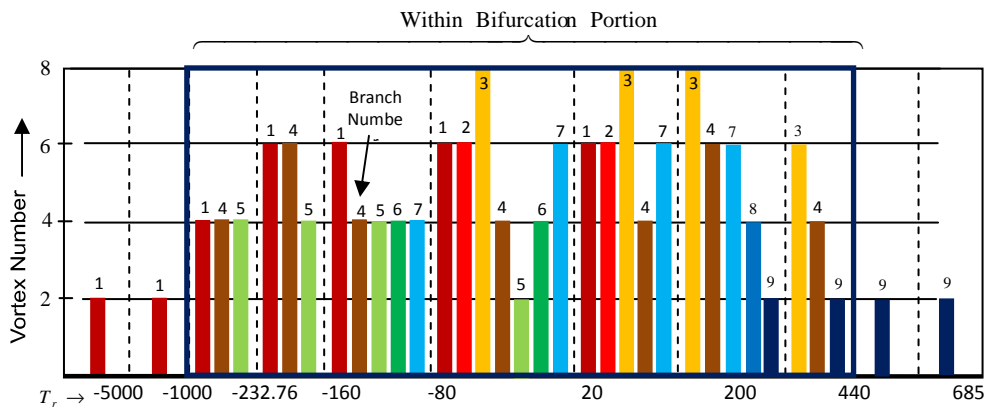


Figure 4.13h: Taylor number T_r versus vortex number of secondary flows with curvature $\delta = 0.1$ and for fixed values of the parameter $D_n = 500$, $M=0$, $m=0$, and $\alpha=0$

To further better understand, a bar chart plotting the Taylor number against the vortex count for the secondary flow within the range of -6000 to 6000 is presented in Figure 4.13h. The numerical values positioned at the top of each bar are indicative of the corresponding curve branch numbers. An examination of the bar graph in Figure 4.13h, as well as Figures 4.13a-f, reveals the following: The first branch encompasses flow structures characterized by two, four, and six vortices. This branch exists within the Taylor number range of -6000 to 391.57. The second branch is exclusively comprised of flow configurations featuring six

vortices. This occurs within the Taylor number range of 397.57 to 54.97. The third branch consists of flow configurations with six and eight vortices, encapsulated within the Taylor number range of 54.97 to 836.26. The fourth branch showcases a flow structure with four and six vortices, occupying the Taylor number range of 836.26 to -243.52. In the fifth branch, flow structures exhibit two and four vortices, occurring in the Taylor number range of -243.52 to 107.97. The sixth branch is characterized by flow structures featuring six vortices, within the Taylor number range of 107.97 to -91.85. The seventh branch features flow structures with four and six vortices, falling within the Taylor number range of -91.85 to 470.86. The eighth branch comprises flow structures with four vortices, found within the Taylor number range of 470.86 to 319.35. The ninth and final branch is exclusively composed of flow structures with two vortices, residing in the Taylor number range of 319.35 to 6000.

Figure 4.14a presents the solution curve illustrating the relationship between the flux Q and the Taylor Number T_r , with the duct curvature set at $\delta = 0.5$. This curve is generated under specific fixed conditions: $D_n = 500$, $M=0$, $m=0$, and $\alpha=0$. Figures 4.14a to 4.14d are presented solely for the purpose of comparing flow structures to those observed with a duct curvature of $\delta = 0.1$. Given the succinct nature of this comparison, a detailed discussion is not necessary.

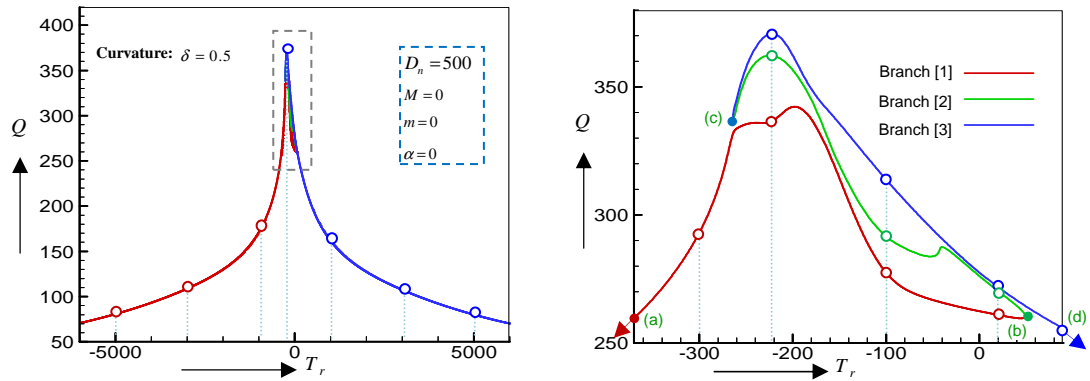
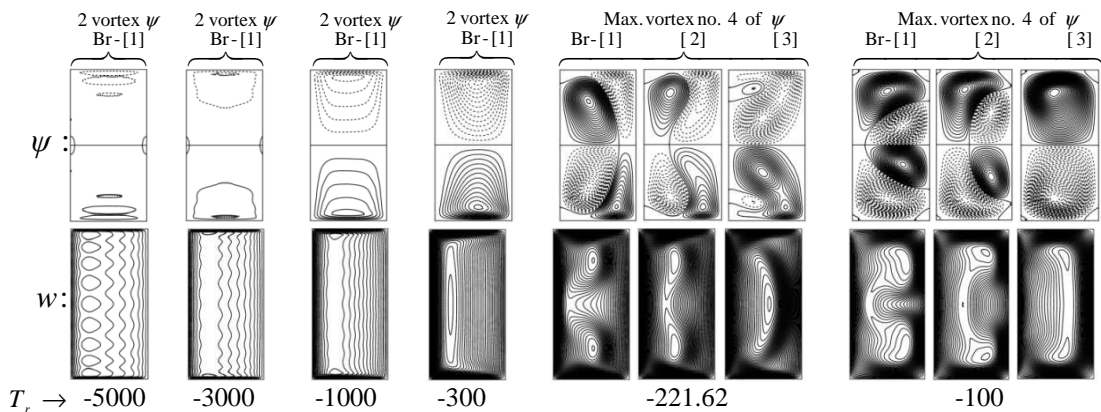


Figure 4.14: (a) Solution curve: Flux Q versus Taylor Number T_r for $D_n = 500$, $M = 0$, $m = 0$ and $\alpha=0$ with the curvature $\delta=0.5$. (b) Magnifying figure marked by the dashed box on Fig.4.14a.



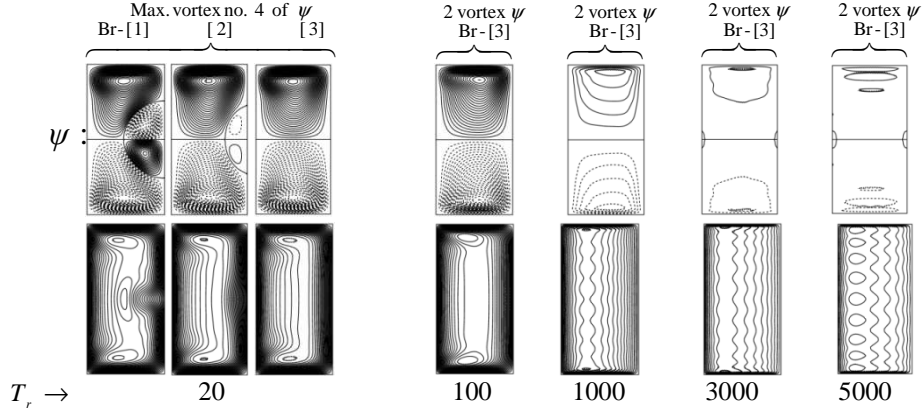


Figure 4.14c: Streamlines ψ (upper) and axial contour flow w (lower) in accordance with the solution curve in Fig.4.14a.

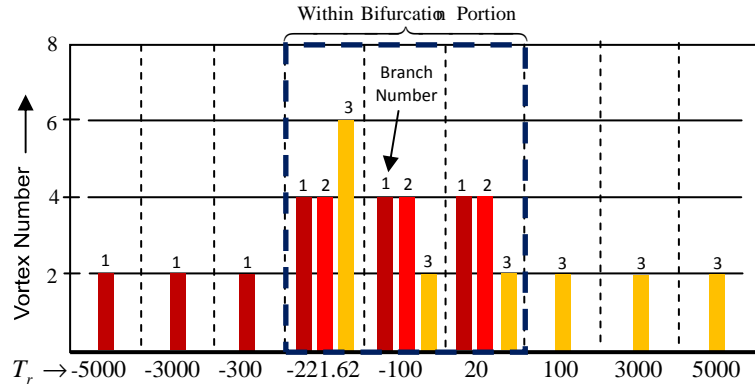


Figure 4.14d: Taylor number T_r versus vortex number of secondary flows with curvature $\delta=0.5$ and fixed values of the parameter $D_n=500$, $M=0$, $m=0$ and $\alpha=0$

In brief, the solution curve with $\delta = 0.5$ is characterized by a simpler flow structure when contrasted with the solution curve for $\delta = 0.1$. Notably, only three separation curves are identified in this case. The secondary flow exhibits fewer and more straightforward outlines and contains fewer vortices compared to the $\delta = 0.1$ scenario. It's evident that the flow's quality degrades rapidly as the absolute value of $|T_r|$ increases. This succinct description highlights the key differences between the two scenarios.

B. Effects of Dean Number (D_n) on the Velocity

In Figure 4.15a, it can observe a solution curve that relates the flux Q to the Dean Number D_n . This particular curve is relevant to the case where the duct curvature is set at $\delta = 0.1$. Meanwhile, other parameters, such as the Taylor Number (T_r), which is fixed at 20, as well as the magnetic parameter (M), Hall parameter (m), and ion-slip parameter (α), all maintained at 0, remain consistent during this analysis. The solution curve is depicted in various colours, highlighting seven distinct bifurcation curves that have been identified within this particular region. The bifurcation section of the analysis displays secondary flow streamlines represented as ψ and axial flow contours denoted as w which shows in Fig.4.15b. This visualization is presented at specific points, corresponding to various values of the Dean Number (D_n), including 100, 240, 400, 500, 700, 1000 and 1100.

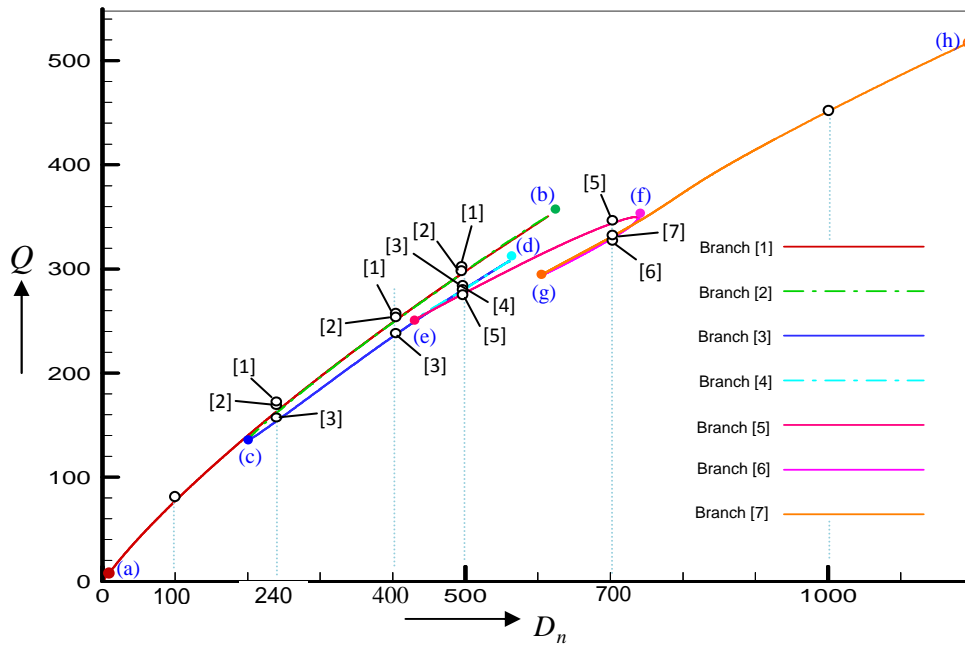


Figure 4.15a: Solution curve: Flux Q versus Dean Number D_n for $T_r = 20$, $M = 0$, $m = 0$ and $\alpha = 0$ with the curvature $\delta = 0.1$.

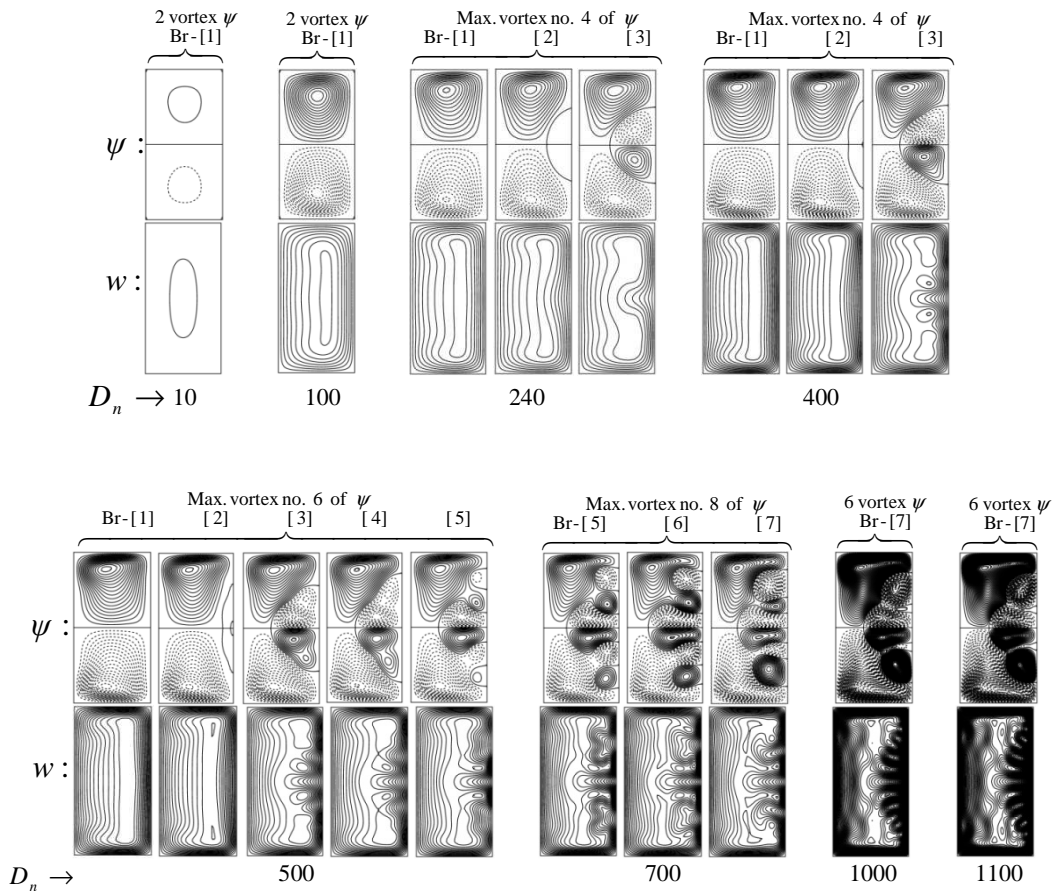


Figure 4.15b: Streamlines ψ (upper) and axial contour flow w (lower) in accordance with the solution curve in Fig. 4.15a.

There exists a critical range between Dean Numbers 201.5 and 738.26 where multiple branches converge at a single point. In this region, a notable trend emerges: as the branch transitions, the contours of axial flow and the secondary flow vortices steadily increase in complexity. This trend suggests that with an increase in the Dean Number, the fluid flow undergoes a continuous enhancement. The maximum number of vortices also gradually rises in response to the rising Dean Number, up to a certain critical value of D_n . Beyond this point, the number of vortices starts to decrease, but it still maintains a robust and significant structure. Additionally, it's observed that for high Dean Numbers, multiple contours are found in the axial flow.

Significantly, all of the additional secondary flow vortices and axial flow contours are generated in the proximity of the duct's outer wall. Consequently, as the Dean Number continues to rise, the flux becomes progressively stronger, further underscoring the dynamic relationship between the Dean Number and the characteristics of the flow.

The principal objective of this study is to analyze how the flow characteristics are influenced by three key parameters: magnetic (M), Hall (m), and ion-slip (α), within the context of a rotational curved rectangular duct. This investigation explores a range of values for M , m , and α across three distinct cases, which are as follows:

Case-I : $\delta = 0.1, D_n = 500$

Case-II : $\delta = 0.5, D_n = 500$

Case-III : $\delta = 0.1, D_n = 800$

while the Taylor number is fixed at $T_r=20$. These cases allow us to examine and compare the effects of these parameters on the flow characteristics in different scenarios within the rotational curved rectangular duct.

C. Effects of Magnetic Parameter (M) on the Velocity

Figure 4.16a displays the solution curve depicting the relationship between the flux Q and the Magnetic Parameter (M) for the above-mentioned three distinct cases. These cases are examined under fixed conditions, with $T_r = 20, D_n = 500, m=0$, and $\alpha=0$. The corresponding secondary flow structures, denoted as ψ , and contour plots of the axial flow, represented as w , are provided at specific points along the magnetic parameter in Figure 4.16b. This comprehensive analysis allows for a detailed exploration of the impact of the Magnetic Parameter (M) on the flux Q and associated flow structures in the context of these three cases.

Across all three cases, the solution curves exhibit a consistent decreasing trend. This leads to the conclusion that as the magnetic parameter M increases, the flux Q experiences a rapid

decrease. For Cases-I and II, a common observation is the presence of symmetric two-vortex streamline structures. However, it's noteworthy that the contours of the axial flow in

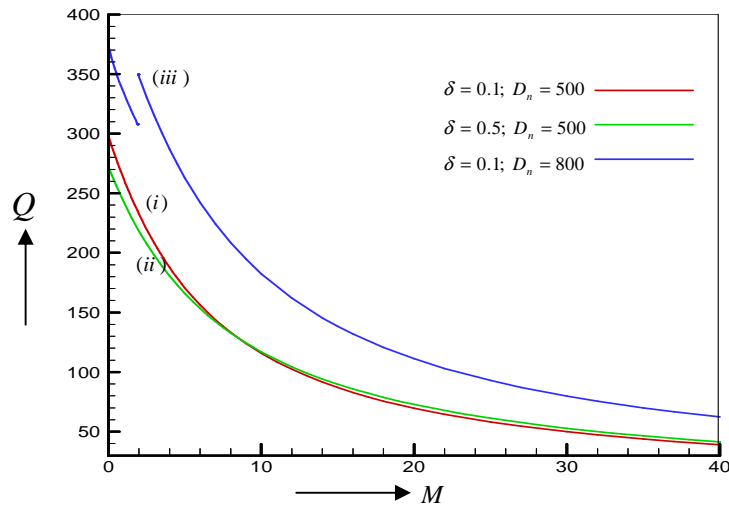


Figure 4.16a: Solution curve: Flux Q versus magnetic parameter M for $T_r = 20$, $m = 0$ and $\alpha = 0$.

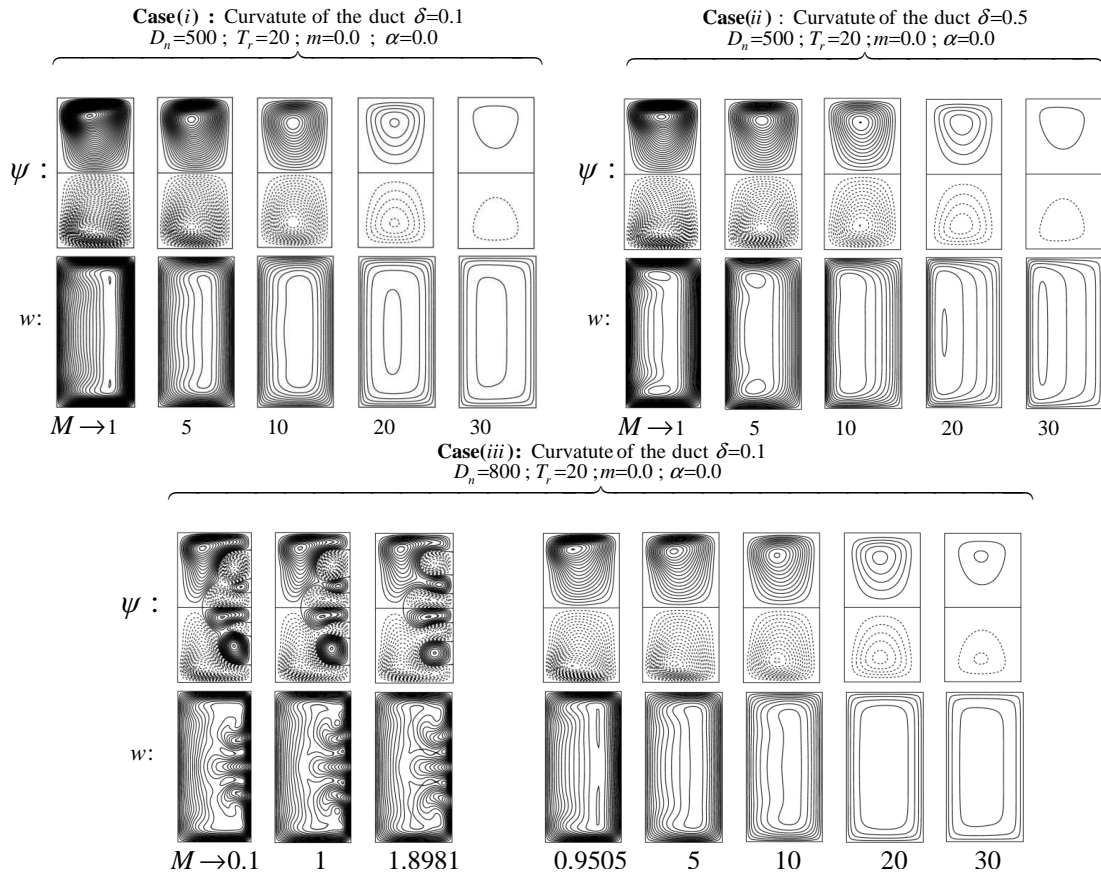


Figure 4.16b (i)- (iii) : Streamlines ψ (upper) and axial contour flow w (lower) in accordance with the solution curve in Fig.4.16a.

Case-II are more extensive than those in Case-I. In contrast, the vortices in the secondary flow of Case-II are weaker compared to Case-I. Additionally, as the duct's curvature

increases, a noticeable shift of the majority of the axial flow is observed, moving it closer to the inner wall. This highlights the impact of duct curvature on the flow distribution within the system.

In Case-III, specifically at $\delta = 0.1$, $D_n = 800$, a distinctive behaviour is observed. Within a limited range of $0 \leq M \leq 1.898169638$, multiple axial flow contours and symmetric six-vortex structures are identified. However, beyond this range, the solution curve experiences a discontinuity. For $M \geq 0.9505067255$, simple axial flow contours are present, accompanied by a pair of counter-rotating vortex structures in the secondary flow. Generally speaking, it can be asserted that the strength of both flow structures undergoes a discernible deterioration as M increases. Notably, for high values of the magnetic parameter, a steady-state solution has been identified. This distinct behaviour in Case-III highlights the sensitivity of the flow characteristics to variations in the magnetic parameter.

D. Effects of Hall Parameter (m) on the Velocity

Figure 4.17a presents the solution curve depicting the relationship between the flux Q and the Hall parameter (m) for the three previously mentioned cases. These cases are consistently evaluated under fixed conditions, with $T_r = 20$, $D_n = 500$, $M=1$, and $\alpha=0$. Corresponding secondary flow structures, represented as ψ , and contour plots of axial flow, denoted as w , are featured in Figure 4.17b. Across all three cases, a common trend is observed: the solution curves exhibit an increasing function. This suggests that the flux Q experiences rapid growth as the Hall parameter m is increased. Beyond a certain value of m , a steady solution is identified. Cases-I and II, symmetric two-vortex solutions for the secondary flow are detected. Interestingly, it is noted that changes in the curvature δ do not significantly impact either the secondary flow structures or the shape of the axial flow in Cases-I and II. However, it's worth noting that as the curvature δ increases, the axial flow displays a greater number of contours. This underscores the influence of curvature on the axial flow configuration while highlighting the robust impact of the Hall parameter on the flux Q .

In Case-III, specifically at $\delta = 0.1$, $D_n = 800$, a distinctive behavior is observed. Over a range of the Hall parameter m , symmetric six-vortex solutions for the secondary flow are identified, along with numerous contours in the axial flow. Interestingly, as m increases within this range, there is only a minor alteration in the secondary flow and axial flow structures. It's also worth noting that the steady-state flux values for Cases-I, II, and III have been determined as 297.67, 271.78, and 373.12, respectively. This information underscores the differences in flux levels across these cases and demonstrates the impact of varying parameters on the steady-state characteristics of the system.

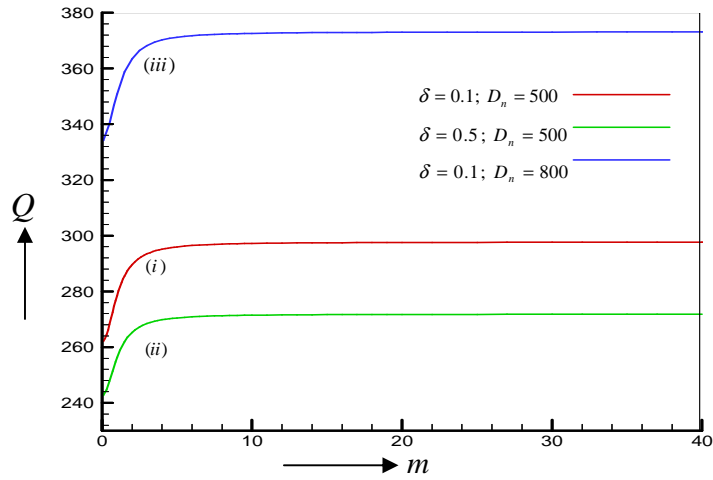


Figure 4.17a: Solution curve: Flux Q versus Hall parameter m for $T_r = 20$, $M = 1$ and $\alpha = 0$.

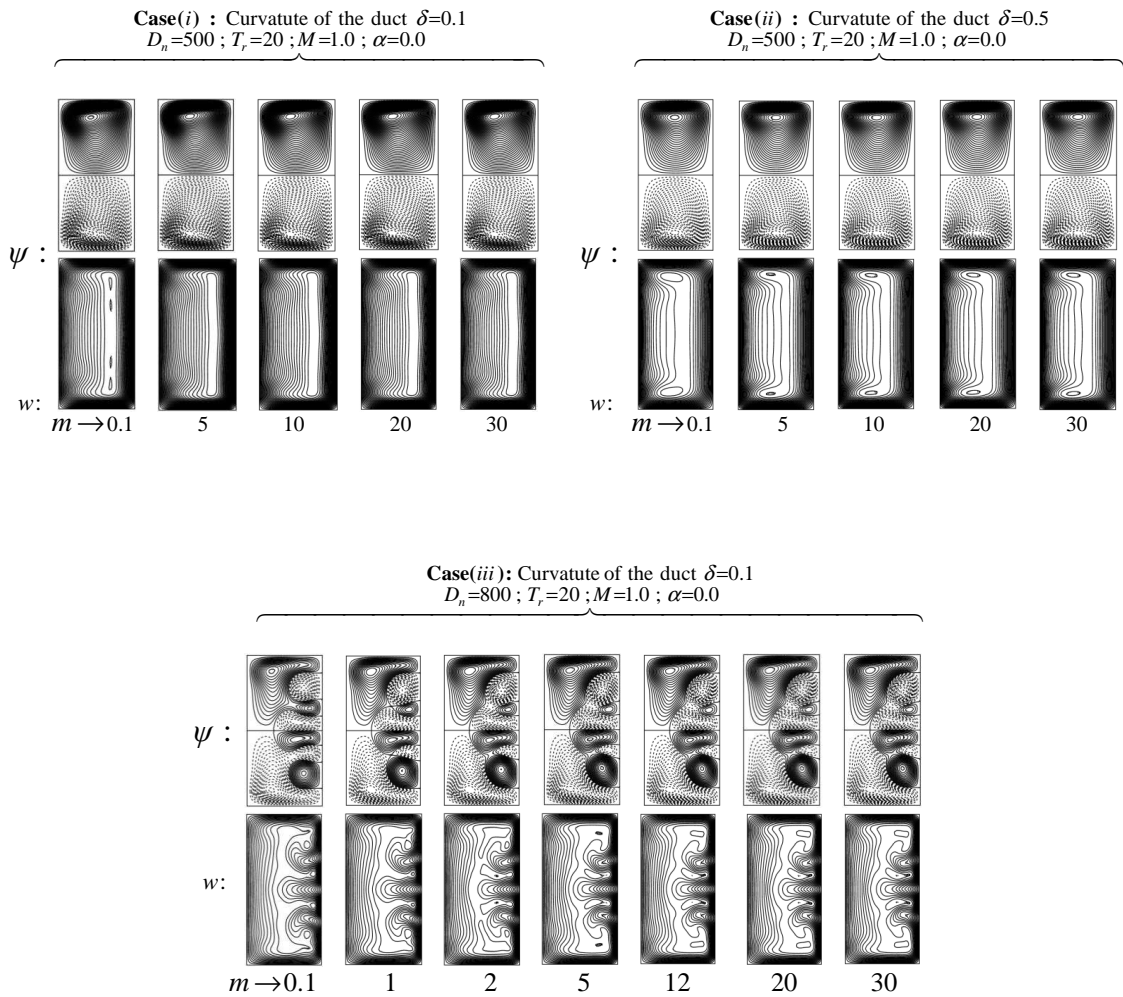


Figure 4.17b (i)- (iii) : Streamlines ψ (upper) and axial contour flow w (lower) in accordance with the solution curve in Fig.4.17a

E. Effects of Ion-slip Parameter (α) on the Velocity

Figure 4.18a decorates the solution curve depicting the relationship between the flux Q and the Ion-slip parameter (α) for the three previously mentioned cases. These cases are consistently evaluated under fixed conditions, with $T_r = 20$, $D_n = 500$, $M=1$, and $m=5$. Corresponding secondary flow structures, represented as ψ , and contour plots of axial flow, denoted as w , are featured in Figure 4.18b.

The behaviour of the flux Q in response to variations in the ion-slip parameter α is interesting. Initially, the flux Q experiences a decrease within a narrow range of α values, but after this initial drop, it begins to increase rapidly with further increments in α . Beyond a specific threshold value of α , a steady solution for the flux is identified. In cases-I and II, symmetric two-vortex solutions for the secondary flow are observed. Interestingly, changes in the curvature, δ , have a minor impact on both the shape of the axial flow and the characteristics of the secondary flow vortices. This behaviour suggests that the curvature, in these cases, does not lead to significant alterations in the flow structures.

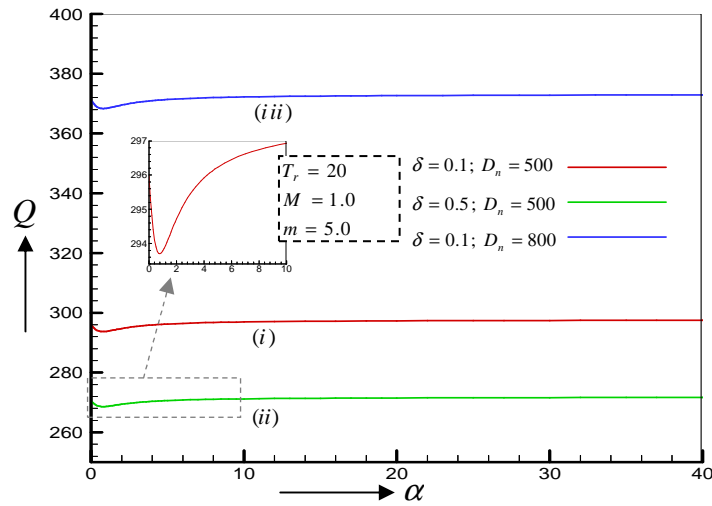
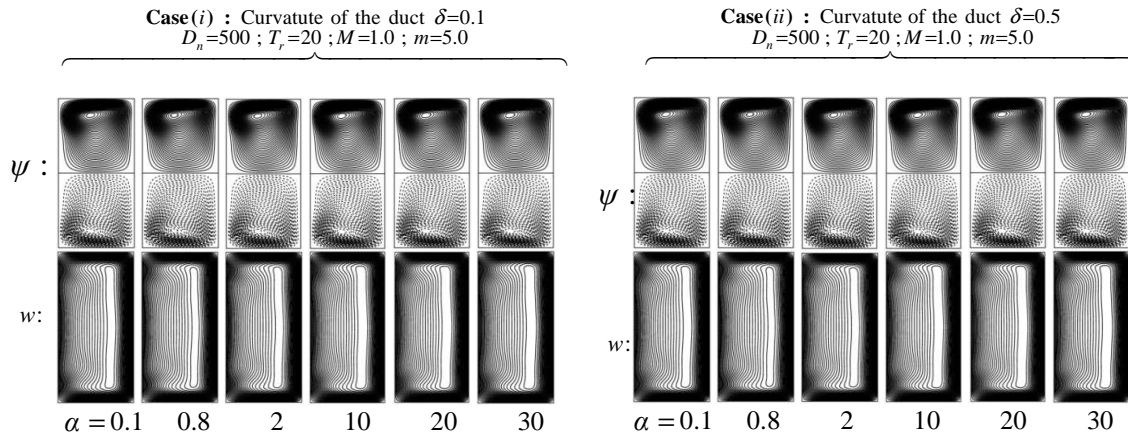


Figure 4.18a: Solution curve: Flux Q versus Ion-slip parameter α for $T_r = 20$, $M = 1$ and $m=5$.



Case (iii) : Curvature of the duct $\delta=0.1$
 $D_n=800 ; T_r=20 ; M=1.0 ; m=5.0$

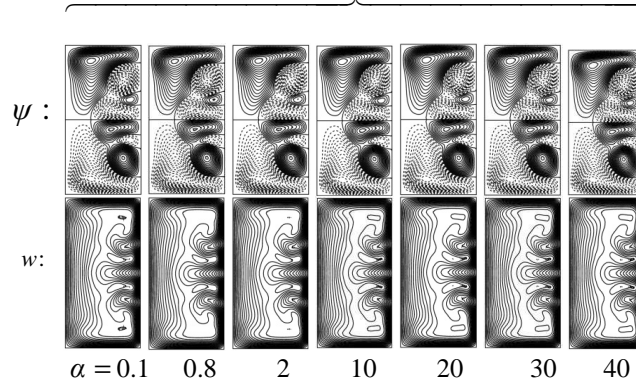


Figure 4.18b (i)- (iii) : Streamlines ψ (upper) and axial contour flow w (lower) in accordance with the solution curve in Fig.4.18a

In case-III, specifically at $\delta = 0.1$, $D_n = 800$, distinct behaviour is observed. Symmetric eight-vortex solutions are discovered for the streamlines, and multiple contours of the axial flow are present over a broad range of the ion-slip parameter α . Surprisingly, with an increase in the ion-slip parameter α , the secondary flow and axial flow exhibit negligible change. Furthermore, it's noted that the flux gradually becomes less powerful as the curvature (δ) decreases. This suggests that a more curved duct configuration has a stronger influence on the flux in this case. Additionally, the figure demonstrates that flux values tend to rise with increasing Dean Number (D_n). This finding highlights the impact of the Dean Number on the overall flow characteristics, particularly in the context of flux variations.

4.6 Curved Rectangular Duct for Isothermal Fluid Flow (Aspect Ratio 3):

Hall and Ion-slip Effects on MHD Fluid Flow in a Rotating Curved Duct with Aspect Ratio 3

In this research, a fully developed, laminar, steady, viscous, incompressible magneto-hydrodynamic fluid flow through a rotating, curved duct with a relatively high aspect ratio is investigated numerically. Due to the rectangular cross-section of the duct with a large aspect ratio, aspect ratio $l=3$ is considered in this study. The values of the duct's curvature $\delta=0.01, 0.1$ and 0.5 are used to compute the result. A pressure gradient force (namely, Dean Forces) affects the flow's velocity in the axial direction of the curved duct. Due to the rotation of the system and curvature of the duct, the combined effect of the Coriolis and centrifugal forces also accelerates the flow. As the primary tool for numerical calculations, the spectral method approach has been utilized. The arc-length, Collocation, Newton-Raphson methods, and Chebyshev polynomials are also used as auxiliary tools. The effects of the Dean number, rotation, magnetic, Hall, and ion-slip parameters are examined on that flow. The principal goal is to examine the impact of the magnetic parameter (M), Hall parameter (m), and ion-slip parameter (α) on the flow characteristics in the rotationally curved rectangular duct with a large aspect ratio in this study. For the five cases such as Case I: $\delta=0.01, D_n=500$, Case II: $\delta=0.1, D_n=500$, Case III: $\delta=0.5, D_n=500$, Case IV: $\delta=0.1, D_n=800$, and Case V: $\delta=0.5, D_n=800$, the investigation is performed with different values of M, m and α whereas the Taylor number is fixed at $T_r=20$.

4.6.1 Grid Spaces Accuracy

It is necessary to discuss grid space accuracy prior to running the FORTRAN application. To achieve good accuracy, it is assumed that the value of \bar{N} is three times that of \bar{M} . The flux Q has been calculated for several pairs of truncation numbers (\bar{M}, \bar{N}) such as (06, 18), (08, 24), (10, 30) and (12, 36). These are shown in Table-3.

\bar{M}	\bar{N}	Q
06	18	91.49935102513669
08	24	91.50519829891833
10	30	91.50511704308377
12	36	91.50507322128173

Table-3: Fluxes Q at several pairs of truncation numbers \bar{M} and \bar{N} at fixed values of $\delta=0.1, D_n=500, T_r=20, M=0, m=0$ and $\alpha=0$

From this table, it can be decided that the obtained numerical results can be accurate enough by the choice of pair $(\bar{M}, \bar{N})=(10, 30)$

4.6.2 Results and Discussion

This study investigates a fully developed steady laminar flow of incompressible viscous fluid through a rectangular cross-section curved duct with an aspect ratio of 3. The duct rotates with an angular velocity Ω around its vertical y-axis, and different curvature values ($\delta = 0.01, 0.1, \text{ and } 0.5$) are considered to analyze the results. The large rectangular cross-section of the duct maintains an aspect ratio of 3. To visualize the flow structure, distance of two path-lines increments $\Delta w = 4$ and $\Delta\psi = 0.3$ are employed. The study begins by exploring the effects of the Taylor number (T_r) and Dean Number (D_n) on the velocity distribution, as presented in figures from Fig. 4.19 to Fig. 4.20. Following these findings, the study delves into the effects of the magnetic parameter (M), Hall parameter (m), and ion-slip parameter (α) on the velocity, which are displayed in figures from Fig. 4.21 to Fig. 4.23. To provide insight into the behaviour of the flow characteristics, solution curves and their corresponding vortex structures are presented for five distinct cases:

Case-I : $\delta = 0.01, D_n = 500$

Case-II : $\delta = 0.1, D_n = 500$

Case-III: $\delta = 0.5, D_n = 500$

Case-IV: $\delta = 0.1, D_n = 800$

Case-V : $\delta = 0.5, D_n = 800$

Each figure includes a square box representing the duct cross-section at a specific point on the solution curve. The right side of each duct box corresponds to the outer wall of the curved duct. Solid lines indicate the anti-clockwise direction of the flow, representing the positive directed flow, while dotted lines depict the clockwise or negative directed flow for the velocity distribution. These visualizations and analyses provide valuable insights into the flow characteristics within the considered parameters and conditions.

A. Effects of the Taylor Number (T_r) on the Fluid Flow

Figure 4.19a presents the solution curve of the flux Q as a function of the Taylor Number T_r . The analysis is conducted under fixed conditions with $\delta = 0.1, D_n = 500, M=0, m=0$ and $\alpha=0$, spanning a broad range of Taylor numbers, $-5000 \leq T_r \leq 5000$. Multiple bifurcation curves are observed within this Taylor number range, distinguished by the use of different coloured lines.

Figure 4.19b provides a magnified view of the region from (i) to (v) in Figure 4.19a. This closer inspection includes several selected points along the solution curve, allowing for the observation of trends in the secondary flow streamlines ψ and the contour plot of the axial flow w . Notably, for larger values of $|T_r|$, it's evident that the contours of the axial flow and the vortices in the secondary flow gradually weaken. At $T_r = -271.93$, the peak value of the flux Q is approximately 439.43986259. This observation suggests that the axial velocity within the curved duct has a significant influence on the strength of the secondary velocity vortices. These visualizations and measurements provide valuable insights into the behaviour of the system under varying conditions of the Taylor Number.

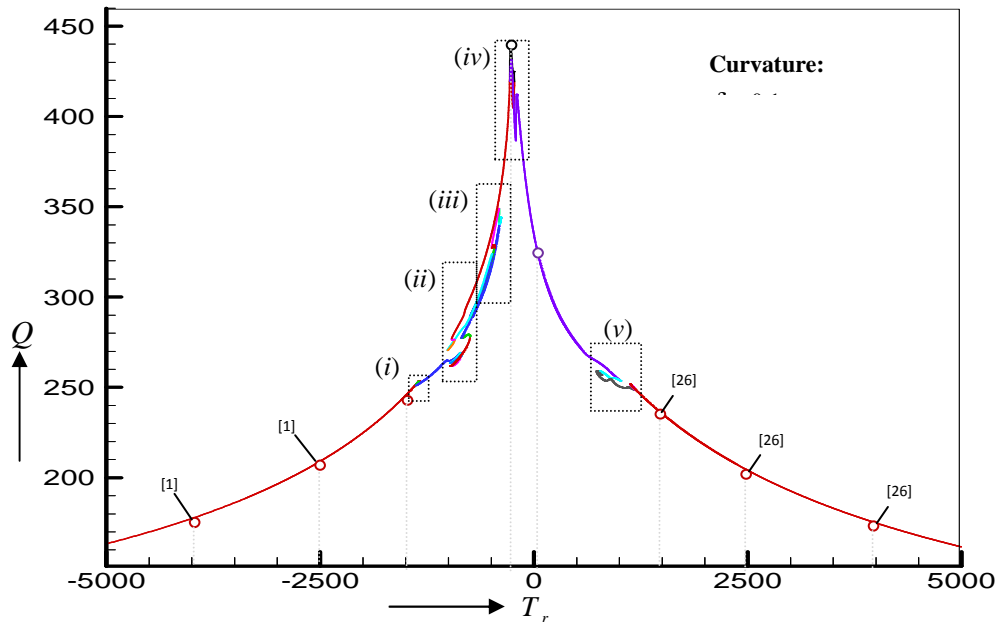


Figure 4.19a : Solution curve: Flux Q versus Taylor Number T_r , for $D_n = 500, M = 0, m = 0$ and $\alpha=0$ with the curvature $\delta=0.1$.

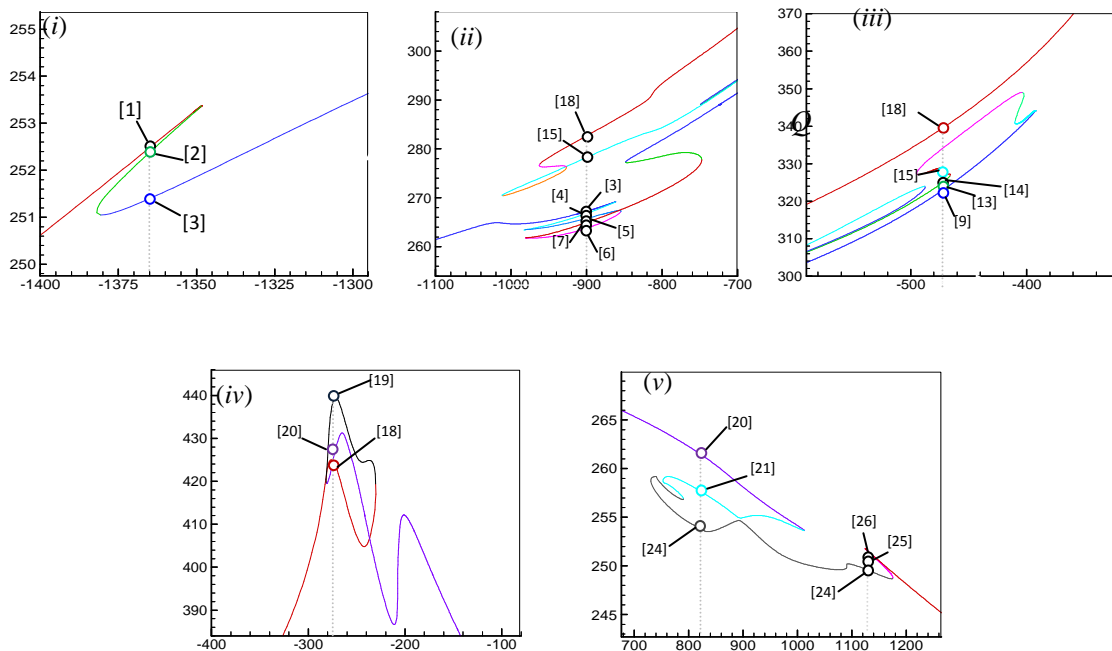


Figure 4.19b: Magnifying figures marked by the dashed box from (i) to (v) on Fig. 4.19a.

At various specific points along the solution curve, which includes $T_r = -4000, -2500, -1500, -1365, -900, -500, -271.93, 20, 840, 1160, 1500, 2500,$ and 4000 , the secondary flow's solution structure and the contour plot of the axial flow are observed. The solution curve exhibits interesting behaviour, intersecting approximately three branches at the locations $T_r = -1365, -271.93, 840,$ and 1160 , and five branches at $T_r = 500$. At $T_r = -900$, it intersects seven branches, while at other locations, only a single branch is observed. Regarding the secondary flow, it's observed that the steady flow comprises symmetric two-, four-, six-,

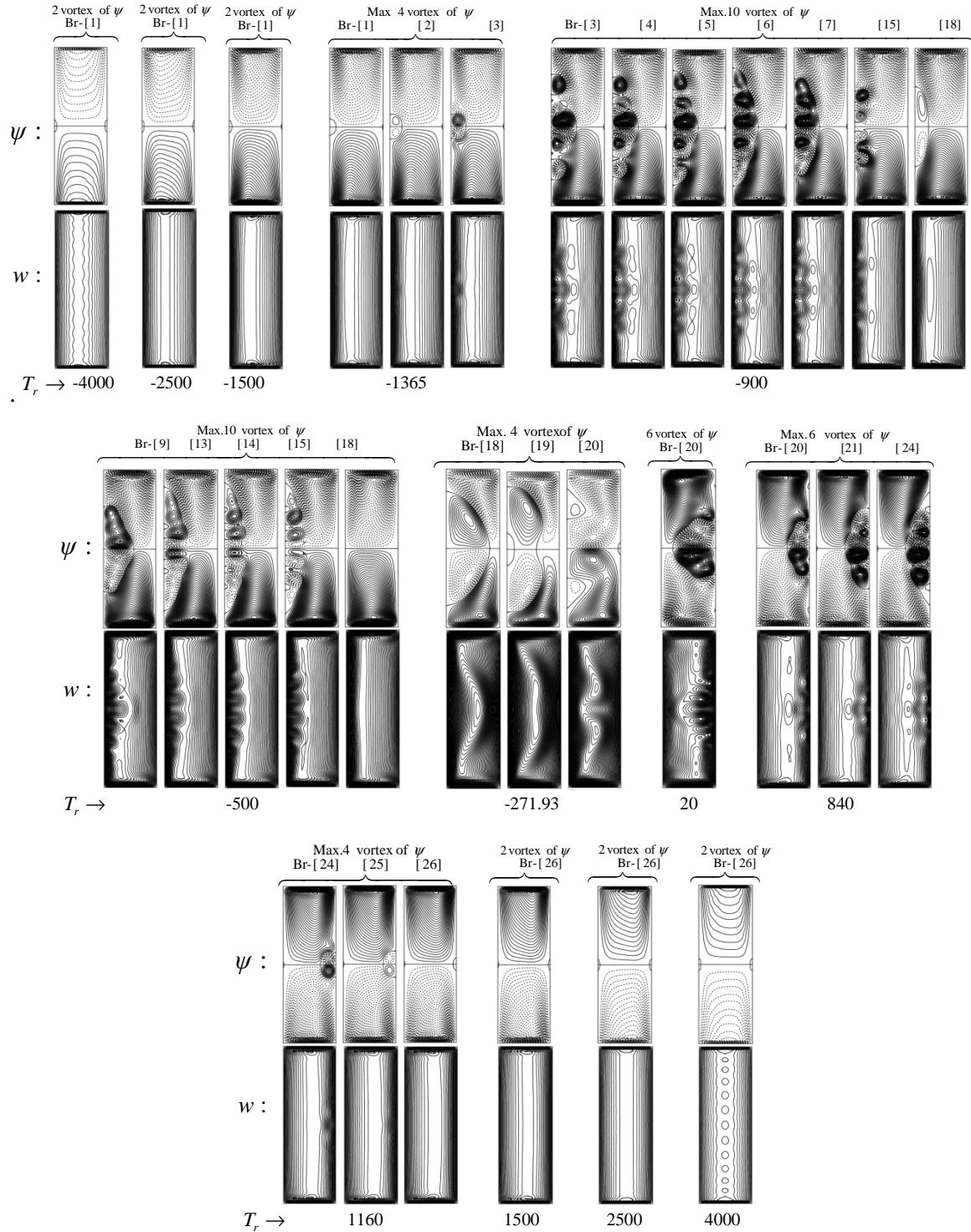


Figure 4.19c: Streamlines ψ (upper) and axial contour flow w (lower) in accordance with the solution curve in Fig.4.19a

eight-, and ten-vortex solutions. Simultaneously, the centreline flow exhibits numerous contours. Additional vortices and multiple contours are generated near the inner side of the duct for negative T_r values and the outer side of the duct for positive T_r values. As $|T_r|$ increases, both the vortices and the shape of the flow structures gradually lose their strength. This information provides a detailed insight into the complex flow characteristics and the impact of the Taylor Number on these behaviours.

B. Effects of the Dean Number (D_n) on the Fluid Flow

Figure 4.20a illustrates the solution curve, depicting the relationship between the Dean Number D_n and the dimensionless flux Q . This analysis is carried out with a duct curvature of $\delta = 0.1$ and under fixed conditions of $T_r = 20$, $M = 0$, $m = 0$ and $\alpha = 0$. The study covers a wide range of Dean Numbers, specifically $0 < D_n \leq 1500$, to explore the influence of the Dean Number on the flow characteristics. Multiple bifurcation curves are observed within various ranges of Dean Numbers, highlighted by dotted rectangular boxes in Figure 4.20a. These regions are further examined in magnified views presented in Figure 4.20b. A notable observation is that all branches of the solution curves exhibit an increasing trend. Consequently, as the Dean Number increases, the dimensionless flux Q also experiences growth. This behaviour underscores the impact of the Dean Number on the flow and highlights how changes in D_n affect the overall flow characteristics.

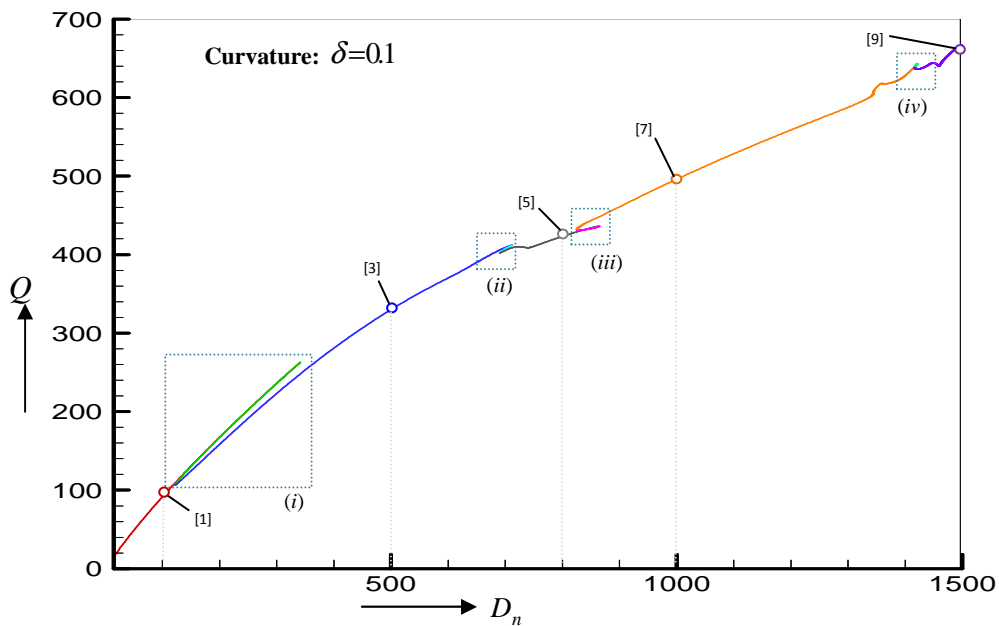
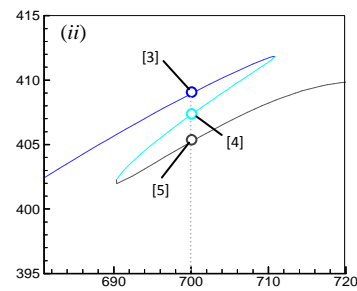
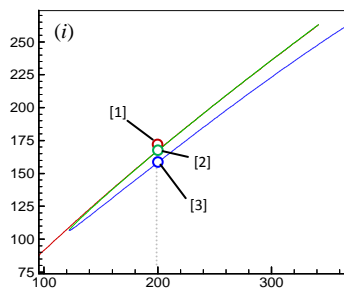


Figure 4.20a: Solution curve: Flux Q versus Dean Number D_n for $T_r = 20$, $M = 0$, $m = 0$ and $\alpha = 0$ with the curvature $\delta = 0.1$.



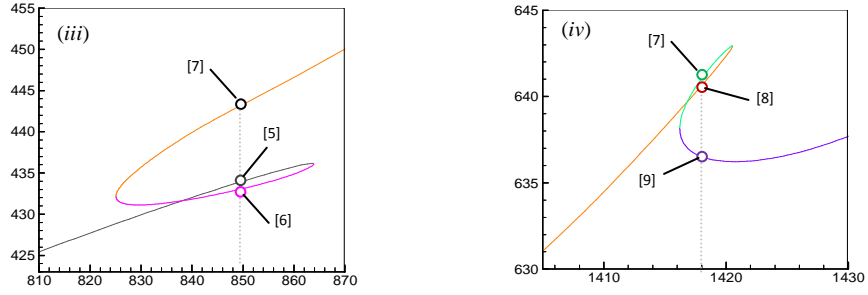


Figure 4.20b: Magnifying figures marked by the dashed box from (i) to (iv) on Fig.4.20a

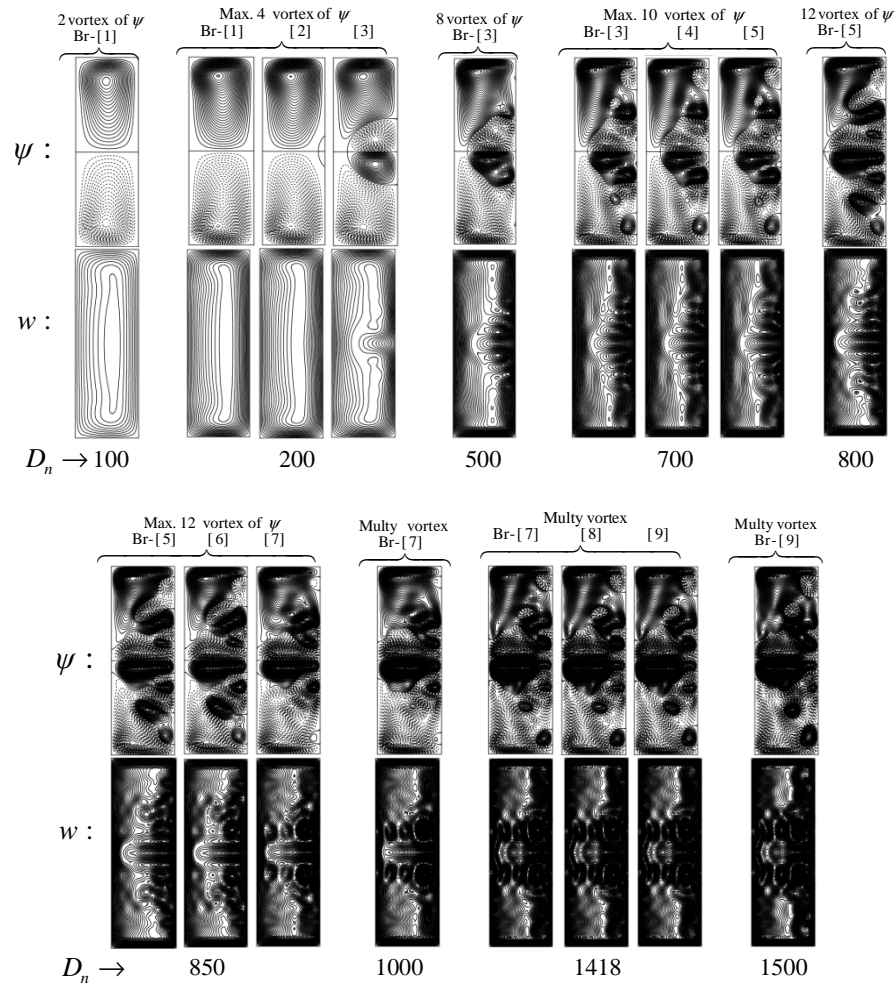


Figure 4.20c: Streamlines ψ (upper) and axial contour flow w (lower) in accordance with the solution curve in Fig.4.20a

In Figure 4.20c, the streamlines ψ of the secondary flow (top) and contours of the axial flow w (bottom) are presented at various randomly selected points, such as $D_n = 100, 200, 500, 700, 800, 850, 1000, 1418$ and 1500 . These points correspond to the solution curve depicted in Figure 4.20a. Among these points, it's noteworthy that the Dean Numbers at 200, 700, 850, and 1418 contain more than one branch of the solution curve. Figure 4.20c reveals that the secondary flow structure consists of symmetric two-, four-, and multiple-vortex streamlines, and multiple contour plots are present in the axial flow. When the Dean Number D_n exceeds 200 and falls on the third branch of the solution curve, additional

vortices in the secondary flow and contours in the axial flow begin to form. Moreover, as the Dean Number increases, more vortices and contours are generated. This is indicative of the positive correlation between the Dean Number and the strength of both flow components, highlighting how the Dean Number influences the flow characteristics.

The primary aim of this study is to explore how the flow characteristics are influenced by variations in the magnetic parameter (M), Hall parameter (m), and ion-slip parameter (α) within a rotational system featuring a curved duct with an aspect ratio of 3. The investigation considers different values of M , m , and α , while keeping the Taylor number fixed at $T_r = 20$. This analysis is carried out across five distinct cases: Case-I : $\delta = 0.01$, $D_n = 500$, Case-II : $\delta = 0.1$, $D_n = 500$, Case-III: $\delta = 0.5$, $D_n = 500$, Case-IV: $\delta = 0.1$, $D_n = 800$ and Case-V: $\delta = 0.5$, $D_n = 800$. To observe the physical behaviour of the flow patterns, only one parameter at a time among M , m , and α is varied, while the other parameters are held at fixed and significant values. This approach allows for a detailed examination of the influence of each parameter on the flow characteristics within the specified cases.

C. Effects of Magnetic parameter (M) on the Fluid Flow

Figure 4.21a presents solution curves showing the relationship between the magnetic parameter (M) and the dimensionless flux (Q). The purpose of this analysis is to investigate the effects of the magnetic parameter on the flow for five distinct cases. Among these cases: The first three cases involve fixed values of $T_r = 20$, $m=0$ and $\alpha=0$; the last two cases are conducted with $T_r = 20$, $m=0$ and $\alpha=1$. The corresponding structures of both flow components are displayed in Figure 4.21b. This visual representation and analysis provide insights into how changes in the magnetic parameter influence the flow characteristics in these specific cases.

Case-I: $\delta = 0.01$, $D_n = 500$

In Figure 4.21a (Case-I), the solution curve depicts the relationship between the magnetic parameter (M) and the dimensionless flux (Q) within the range of $0 \leq M \leq 7.85$. Notably, the solution curve, in this case, is a decreasing function. This indicates that the flux gradually decreases as the magnetic parameter's values rise. In terms of the flow structures, multiple contours are observed for the axial flow. On the other hand, the secondary flow's structure in Case-I consists of symmetric four- and six-vortex streamlines, as depicted in Figure 4.21b (Case-I). As the magnetic parameter is increased, the flow's strength steadily diminishes. This behaviour is a characteristic impact of the magnetic parameter on the flow characteristics.

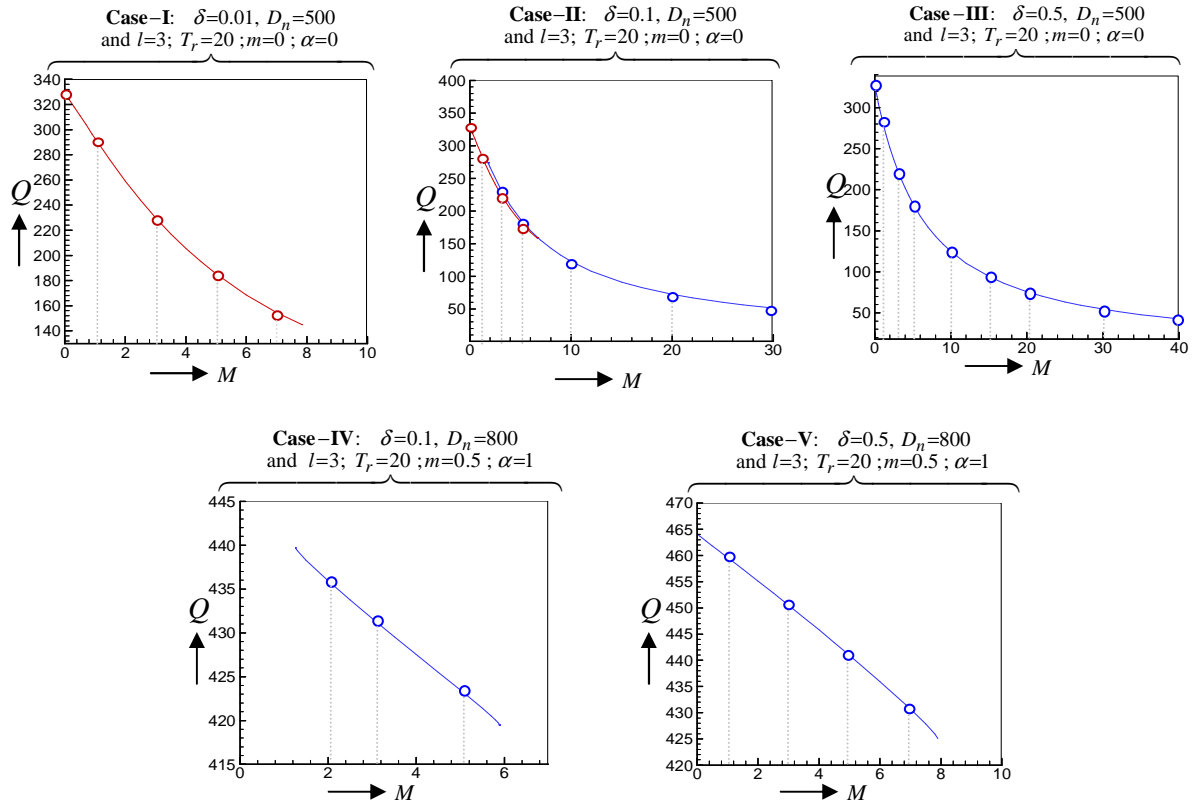


Figure 4.21a: Solution curve: Flux Q versus magnetic parameter M .

Case-II: $\delta = 0.1, D_n = 500$

In Figure 4.21a (Case-II), the solution curve displays the relationship between the magnetic parameter (M) and the dimensionless flux (Q) within the entire range of the magnetic parameter ($M \geq 0$), but it exhibits two distinct branches. Both branches of the solution curves are decreasing functions, indicating that the flux gradually decreases as the magnetic parameter values increase. Notably, after reaching a certain value of M , a steady-state solution is observed. In terms of flow structures, the secondary flow comprises symmetric two-, four-, and six-vortices, while the axial flow exhibits multiple contours, as depicted in Figure 4.21b (Case-II). With an increase in the magnetic parameter, the strength of both flow components declines gradually and quickly. This behaviour illustrates the impact of the magnetic parameter on the flow characteristics in this specific case.

Case-III: $\delta = 0.5, D_n = 500$

In Figure 4.21a (Case-III), the solution curve presents the relationship between the magnetic parameter (M) and the dimensionless flux (Q), covering the entire range ($M \geq 0$) of the magnetic parameter. However, it exhibits a single branch of the solution curve. Similar to the previous cases, this solution curve is a decreasing function, indicating that the flux gradually decreases as the magnetic parameter values increase. After reaching a specific value of M , a steady-state solution is observed. In terms of flow structures, the axial flow in Case-III exhibits simple contours, while the secondary flow structure consists of symmetric

two-vortex streamlines, as depicted in Figure 4.21*b* (Case-III). With increasing magnetic parameters, the strength of both flow components gradually declines and eventually tends to disappear. The flow structure in this case is observed to be weaker than the structures in Case-I and Case-II. This behaviour demonstrates the impact of the magnetic parameter on the flow characteristics in this specific case.

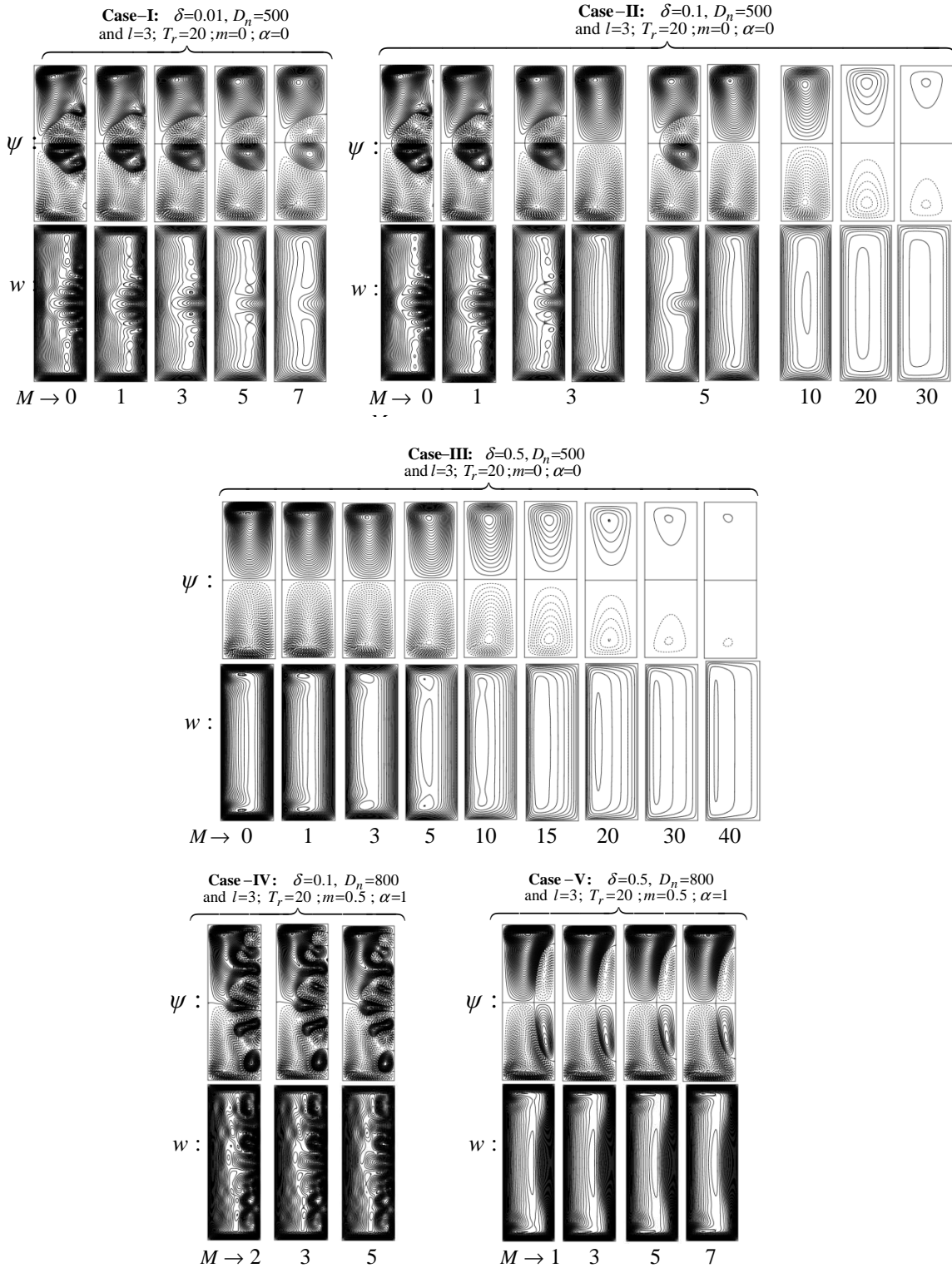


Figure 4.21*b*: Streamlines ψ (upper) and axial contour flow w (lower) in accordance with the solution curve in Fig.4.21*a*

Case-IV: $\delta = 0.1, D_n = 800$

In Figure 4.21a (Case-IV), the solution curve represents the relationship between the magnetic parameter (M) and the dimensionless flux (Q), covering the range $1.26155 \leq M \leq 5.88738402$. As the magnetic parameter increases within this range, the flux steadily decreases. The flow structures in this case are distinctive. The secondary flow's solution structure is characterized by asymmetric ten-vortex streamlines, as opposed to the symmetric vortices observed in the previous cases. Additionally, the axial flow exhibits numerous contours, as shown in Figure 4.21b (Case-IV). With the increase in the magnetic parameter, the strength of both flow components steadily declines. The behaviour observed in this case underscores the substantial influence of the magnetic parameter on the flow characteristics, with the emergence of complex flow structures.

Case-V: $\delta = 0.5, D_n = 800$

In Figure 4.21a (Case-V), the solution curve depicts the relationship between the magnetic parameter (M) and the dimensionless flux (Q) within the range $0 \leq M \leq 7.92$. Consistent with the previous cases, the flux steadily decreases as the magnetic parameter increases. Regarding the flow structures, the axial flow is characterized by simple contours. In contrast, the secondary flow's solution structure consists of symmetric four-vortex streamlines, as shown in Figure 4.21b (Case-V). As the magnetic parameter increases, both flow strengths eventually experience modest declines. This behaviour illustrates the influence of the magnetic parameter on the flow characteristics in this specific case, and it is noteworthy that the flow structures, in this case, are comparatively simpler than those in some of the previous cases.

D. Effects of Hall parameter (m) on the Fluid Flow

Figure 4.22a presents solution curves depicting the relationship between the Hall parameter (m) and the dimensionless flux (Q). This analysis aims to explore the effects of the Hall parameter on the flow for five distinct cases: The first three cases involve fixed values of $T_r = 20$, $M = 5$ and $\alpha = 0$; The last two cases are conducted with $T_r = 20$, $M = 5$ and $\alpha = 1$. The corresponding structures of both flow components are displayed in Figure 4.22b. This visual representation and analysis provide insights into how variations in the Hall parameter influence the flow characteristics in the specified cases.

Case-I: $\delta = 0.01, D_n = 500$

In Figure 4.22a (Case-I), the solution curve illustrates the relationship between the Hall parameter (m) and the dimensionless flux (Q) within the entire range of the Hall parameter ($m \geq 0$). In this case, it exhibits a single branch of the solution curve. Notably, the solution curve is an increasing function, meaning that the flux increases rapidly within the range $0 \leq m \leq 5$, after which it increases more gradually. A steady solution is observed after a specific value of m . The flow structures in this case are characterized by symmetric four-, six-, and

eight-vortex streamlines in the secondary flow. Additionally, multiple contours are observed for the axial flow, as shown in Figure 4.22b (Case-I). As the Hall parameter increases within the interval $0 \leq m \leq 5$, the strength of both flow components experiences minor increases. The flux reaches an approximate constant value of 328.5, reflecting the effect of the Hall parameter on the flow characteristics in this specific case.

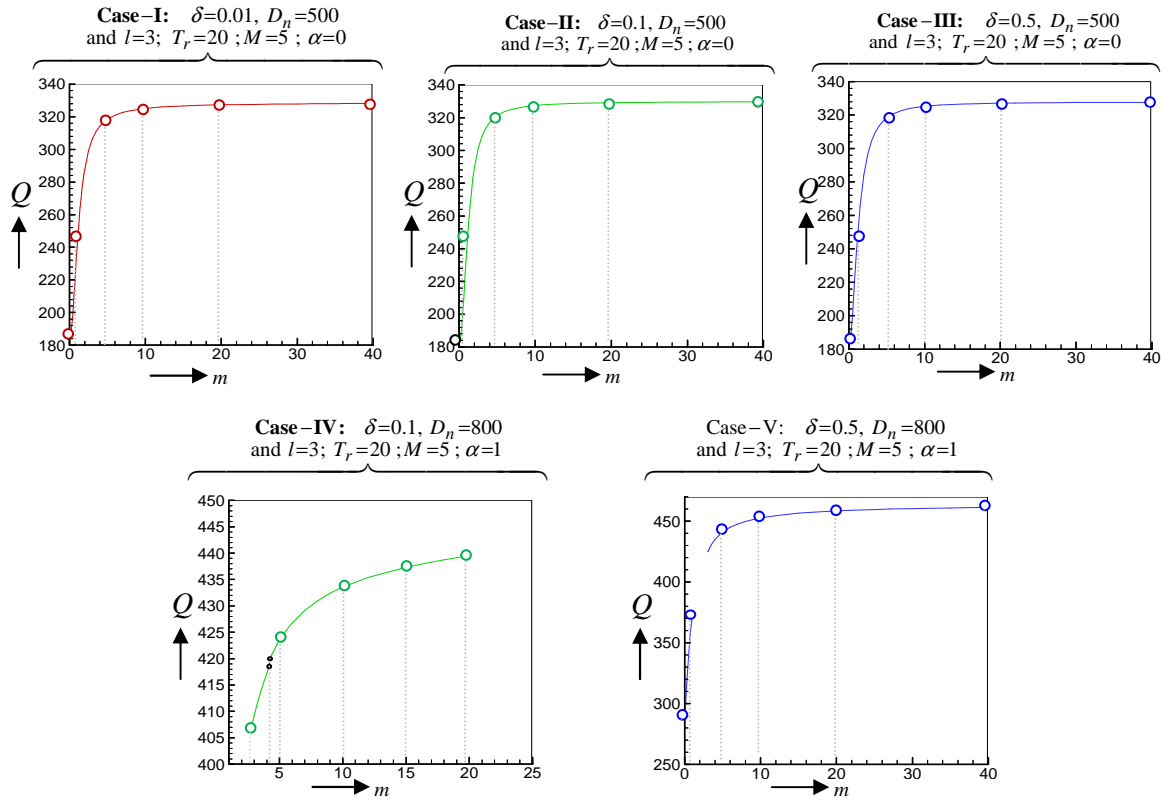


Figure 4.22a: Solution curve: Flux Q versus Hall parameter m .

Case-II: $\delta = 0.1, D_n = 500$

In Figure 4.22a (Case-II), the solution curve presents the relationship between the Hall parameter (m) and the dimensionless flux (Q), covering the entire range of the Hall parameter ($m \geq 0$). The flow's structures and behaviours in this case closely resemble those in Case-I. Notably, the flux in Case-II also reaches a uniform value, which is approximately 329.8, as the steady solution. This behaviour indicates that the Hall parameter has a similar effect on the flow characteristics as observed in Case-I.

Case-III: $\delta = 0.5, D_n = 500$

In Figure 4.22a (Case-III), the solution curve illustrates the relationship between the Hall parameter (m) and the dimensionless flux (Q), covering the entire range of the Hall parameter ($m \geq 0$). This solution curve exhibits behaviour that is similar to that observed in Cases I and II. However, it's worth noting that the flow structure in this case appears to be weaker compared to the structures identified in Cases I and II. Throughout the entire range of Hall parameters, only symmetric two-vortex streamlines of the secondary flow and

simple contours of the axial flow are observed, as depicted in Figure 4.22*b* (Case-III). As the Hall parameter increases, the strength of both flow components experiences slight variations. The flux exhibits an approximate constant value of 327.7, reflecting the effect of the Hall parameter on the flow characteristics in this specific case.

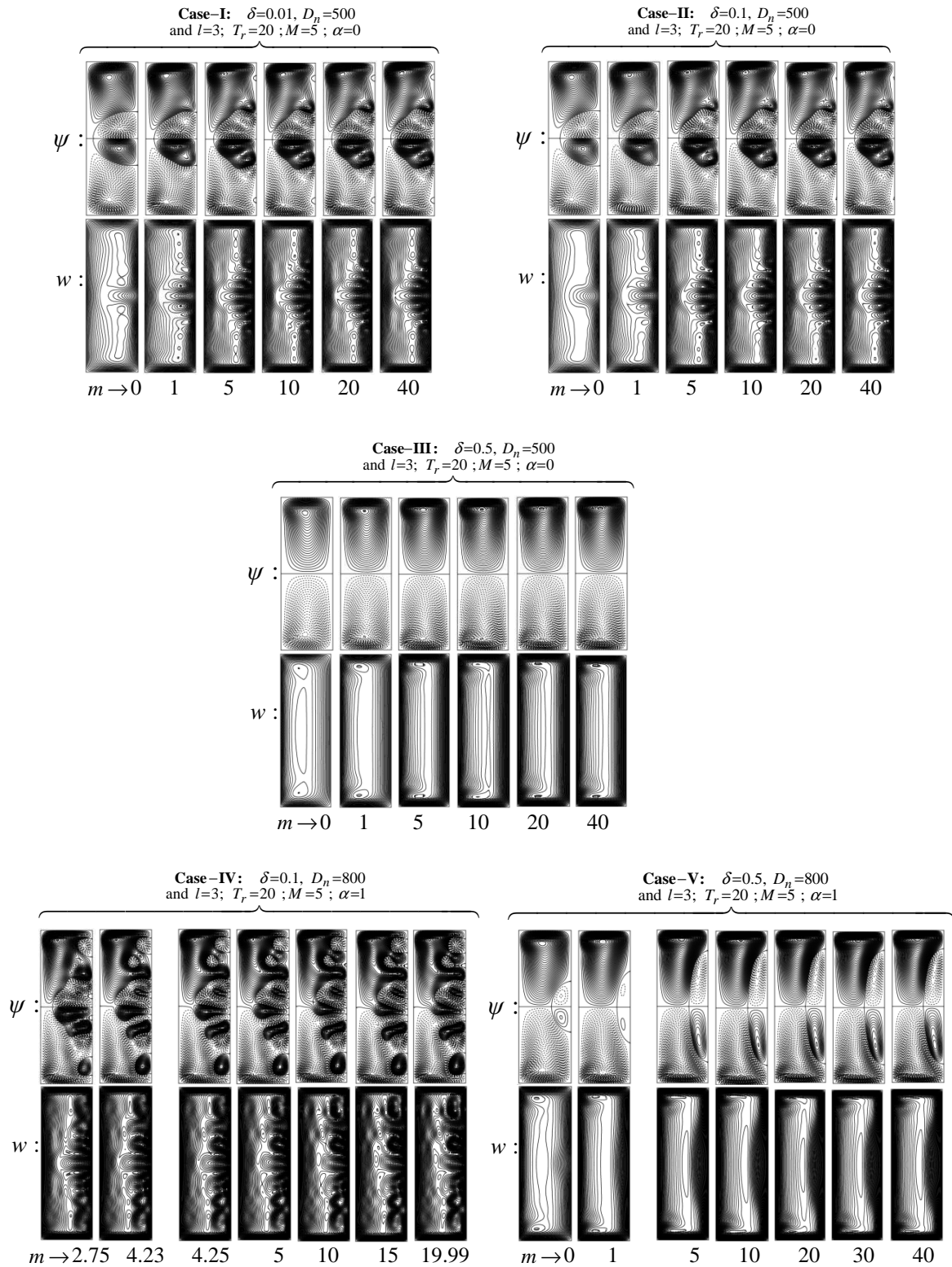


Figure 4.22*b*: Streamlines ψ (upper) and axial contour flow w (lower) in accordance with the solution curve in Fig.4.22*a*

Case-IV: $\delta = 0.1, D_n = 800$

In Figure 4.22a (Case-IV), the solution curve presents the relationship between the Hall parameter (m) and the dimensionless flux (Q). Interestingly, this case includes two distinct ranges of the Hall parameter; the ranges are $2.75 \leq m \leq 4.23$ and $4.25 \leq m \leq 19.99$. Both solution curves within these ranges are increasing functions, signifying that the flux increases as the Hall parameter (m) rises. The flow structures in this case are characterized by symmetric four-, six-, and eight-vortex streamlines in the secondary flow, while multiple contours are observed for the axial flow, as shown in Figure 4.22b (Case-IV). As the Hall parameter increases within these ranges, both flow intensities experience slight variations. The approximate steady value of the flux in this case is 439.6, indicating the influence of the Hall parameter on the flow characteristics.

Case-V: $\delta = 0.5, D_n = 800$

In Figure 4.22a (Case-V), the solution curve illustrates the relationship between the Hall parameter (m) and the dimensionless flux (Q) within two different ranges: These ranges are $0 \leq m \leq 1$ and $m \geq 3.08$. Within both of these ranges, the solution curves are increasing functions, indicating that the flux increases as the Hall parameter (m) rises. It's noteworthy that, in the second range of the Hall parameter, a steady solution is observed after a specific value of m . The flow structures, in this case, show that the axial flow exhibits simple contours in both ranges, while the secondary flow has symmetric four-vortex streamlines as its solution structure, as depicted in Figure 4.22b (Case-V). As the Hall parameter increases within the range $0 \leq m \leq 1$, the strength of both flow components steadily weakens, while it remains relatively stable in the other regions. The flux reaches an approximate constant value of 461.25, indicating the impact of the Hall parameter on the flow characteristics in this specific case.

E. Effects of Ion-slip parameter (α) on the Fluid Flow

Figure 4.23a displays the solution curves representing the relationship between the Ion-slip parameter (α) and the dimensionless flux (Q) for five distinct cases. In each case, the values of $T_r = 20$, $M = 5$, and $m = 5$ are held constant. The corresponding flow structures for both secondary flow and axial flow are presented in Figure 4.23b for each of these cases, helping to illustrate the effects of the Ion-slip parameter on the flow characteristics.

Case-I: $\delta = 0.01, D_n = 500$

In Figure 4.23a (Case-I), the solution curve depicts the relationship between the Ion-slip parameter (α) and the dimensionless flux (Q). This case covers the entire range of the Ion-slip parameter ($\alpha \geq 0$) and features a single branch of the solution curve. Notably, the behaviour of the flux with respect to α is quite interesting in this case. The flux initially experiences a rapid decrease within the range $0 \leq \alpha \leq 0.7$. Subsequently, it begins to grow

rapidly within the range of $0.7 \leq \alpha \leq 4$. After this, the flux exhibits a slower increase. A steady solution is observed after a specific value of α . The flow structures in this case indicate that the axial flow is characterized by multiple contours, while the solution structure of the secondary flow consists of symmetric eight-vortex streamlines, as shown in Figure 4.23b (Case-I). The flux in the steady-state solution is approximately 328.4, reflecting the influence of the Ion-slip parameter on the flow characteristics in this specific case.

Case-II: $\delta = 0.1, D_n = 500$

In Figure 4.23a (Case-II), the solution curve illustrates the relationship between the Ion-slip parameter (α) and the dimensionless flux (Q) across the entire range of the Ion-slip parameter ($\alpha \geq 0$). The behaviour of the flux with respect to α in this case is consistent with Case-I of E. The flow structures and characteristics in Case-II resemble those observed in Case-I of E. The steady-state value of the flux in this case is approximately 329.5, indicating the steadiness of the flux in the presence of the Ion-slip parameter α .

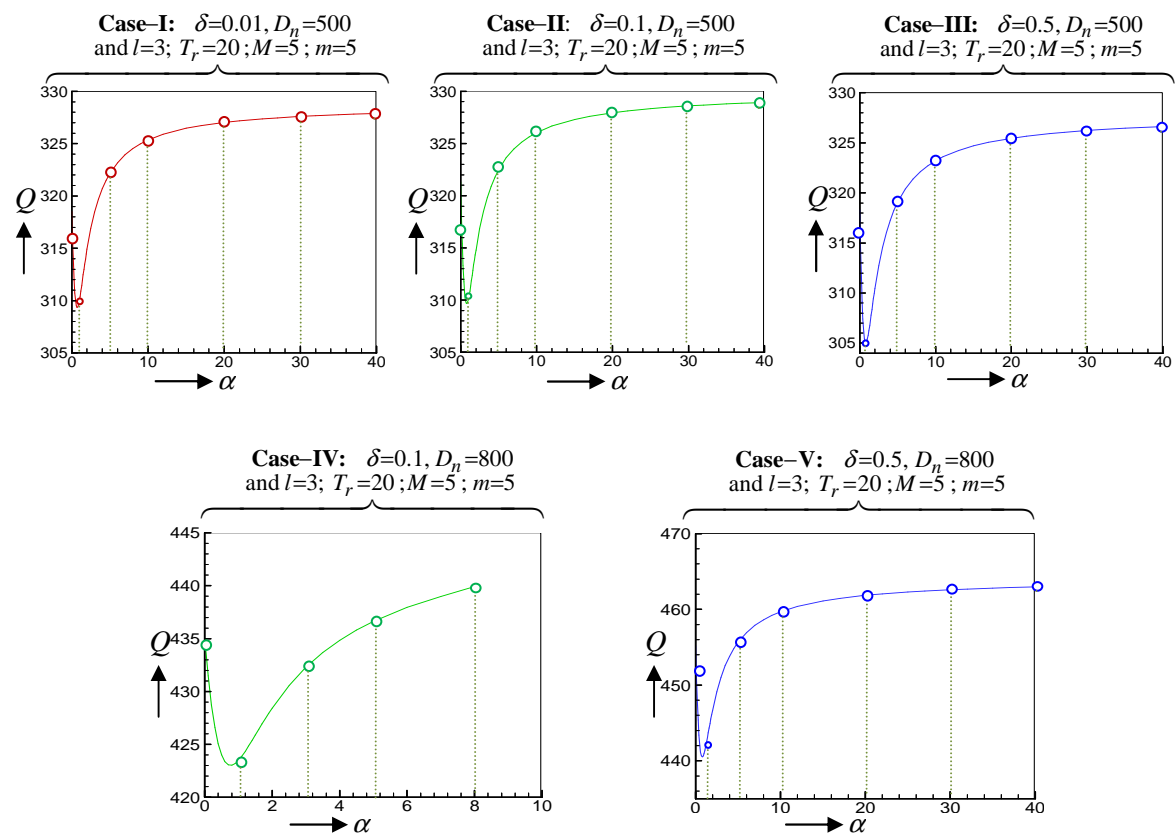


Figure 4.23a: Solution curve: Flux Q versus Ion-slip parameter α .

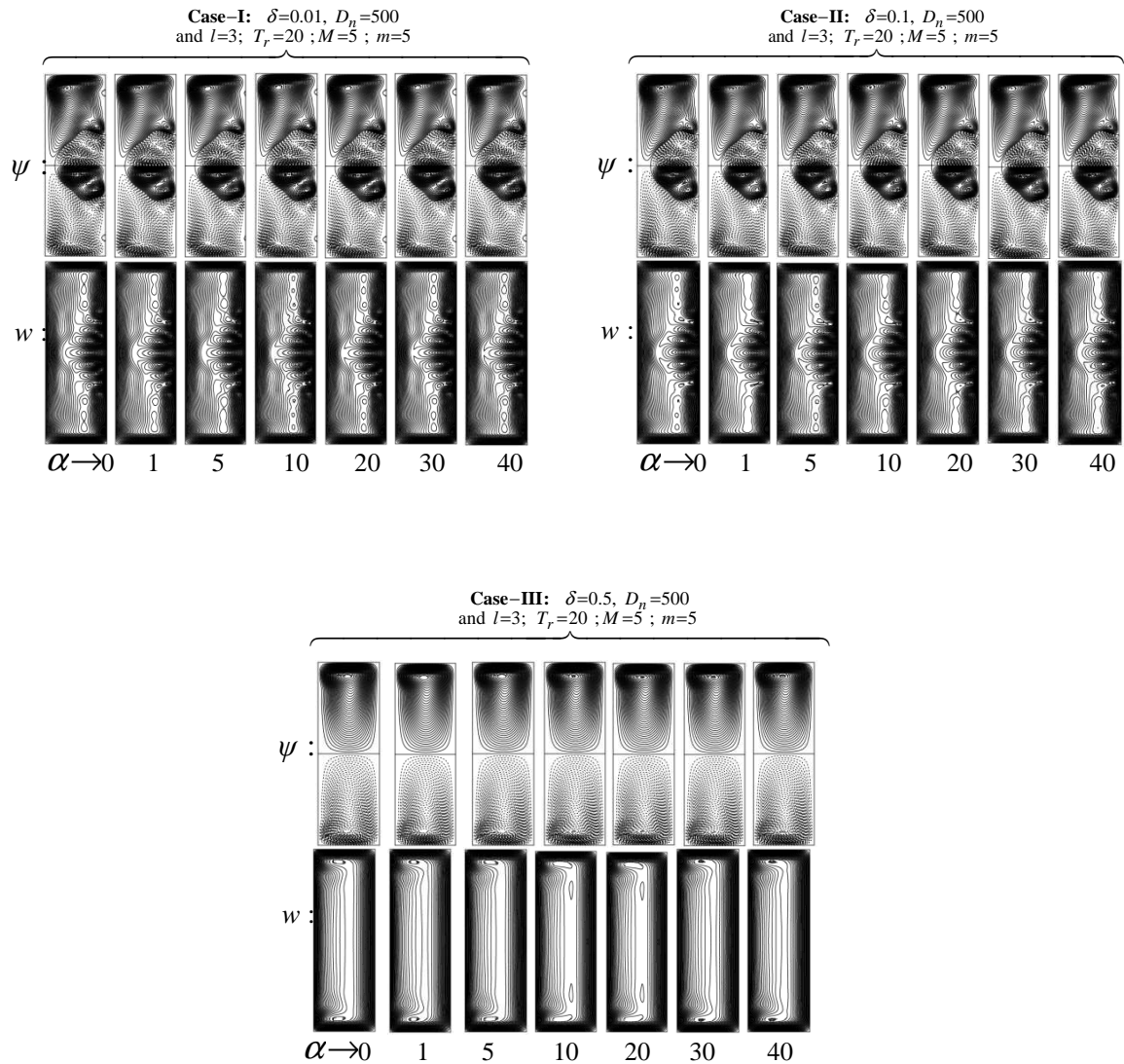
Case-III: $\delta = 0.5, D_n = 500$

In Figure 4.23a (Case-III), the solution curve presents the relationship between the Ion-slip parameter (α) and the dimensionless flux (Q), covering the entire range of the Ion-slip parameter ($\alpha \geq 0$). The behaviour of the solution curve in this case is similar to what was

observed in Cases I and II of E. Notably, within all ranges of the Ion-slip parameter, Case-III shows that only symmetric two-vortex streamlines are observed in the secondary flow, and the axial flow exhibits simple contours, as shown in Figure 4.23b (Case-III). The increase in the Ion-slip parameter has minimal impact on the strength of both flows, and the flux remains at an approximate steady value of 327.33, indicating the stability of the flux in response to variations in the Ion-slip parameter α in this specific case.

Case-IV: $\delta = 0.1, D_n = 800$

In Figure 4.23a (Case-IV), the solution curve illustrates the relationship between the Ion-slip parameter (α) and the dimensionless flux (Q), and it is confined to the range $0 \leq \alpha \leq 8.03$ of the Ion-slip parameter. This case features a single branch of the solution curve. Within the range of α from 0 to 8, the flux experiences a rapid decrease, followed by a



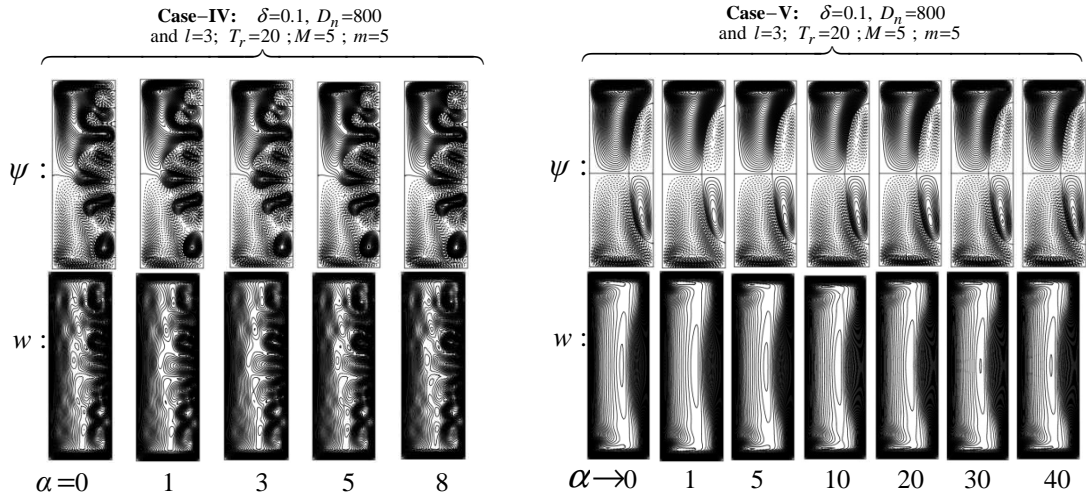


Figure 4.23b: Streamlines ψ (upper) and axial contour flow w (lower) in accordance with the solution curve in Fig.4.23a

quick increase. Importantly, there is no steady-state solution for the flow within this range of the Ion-slip parameter. The axial flow exhibits multiple contours, and the secondary flow's solution structure consists of asymmetric ten-vortex streamlines, as depicted in Figure 4.23b (Case-IV). The strength of both flows remains consistent for all values of the Ion-slip parameter α after a specific range of the Ion-slip parameter.

Case-V: $\delta = 0.5, D_n = 800$

In Figure 4.23a (Case-V), the solution curve of the Ion-slip parameter (α) vs. the dimensionless flux (Q) spans the entire range of α ($\alpha \geq 0$). The behaviour of the solution curve is characterized by an initial rapid decrease in flux within the range $0 \leq \alpha \leq 0.8$, followed by a rapid increase within the range $0.8 \leq \alpha \leq 10$, and finally a slow increase. A steady solution is observed after a specific value of α . In this case, the secondary flow's solution structure consists of symmetric four-vortex streamlines, while the axial flow exhibits single contours (Fig. 4.23b, Case-V). Interestingly, very little variation is observed in the strength of both flows for all values of the Ion-slip parameter within this range.

Chapter 5

Magneto-hydrodynamic Non-Isothermal Fluid Flow through a Rotating Curved Duct with Magnetic Field

The study examines fully developed, steady, non-isothermal, viscous, incompressible fluid flow. This flow occurs within a rotating curved duct while being subjected to a magnetic field, with Hall and Ion-slip currents taken into account. The duct configuration includes outer walls subject to heating, inner walls subject to cooling, and upper and lower walls treated as adiabatic boundaries. This arrangement leads to the generation of a non-isothermal flow within the curved duct. A pressure gradient force (Dean Force) is applied along centreline of the duct. The Centrifugal and Coriolis forces have been created due to the duct's curvature and system's rotation. Acting forces over the fluid flow are gravitational force, pressure gradient, Centrifugal, Coriolis, and gravitational force. The combined effect of these forces provides to accelerate the flow. The spectral method is used numerically to carry out the solution of the governing equation as the primary tool. Additionally, as auxiliary tools, the Chebyshev polynomial, Newton-Raphson, Collocation methods, and Arc-length techniques are employed. The results have been calculated using the arc-length approach at any location along the solution curve's critical zone. Investigating the impact of the magnetic, Hall, and ion-slip parameters on the velocity and temperature distribution of a non-isothermal fluid flow that flows through a curved square or rectangular duct with a two-aspect ratio in a rotating system is the main goal of this study.

5.1 Introduction

In an engineering application, the study of fluid flow through a non-isothermal curved duct has the utmost importance. The magnetic systems of rotating mechanisms also have a significant impact in the electromagnetic field. In the presence of a magnetic field, Hall and ion-slip currents also have an impact on the electrically conducting fluid. Regarding fully developed fluid flow in a curved duct, a pile of studies has been conducted throughout the long span of time.

Great Mathematician Dean (1927, 1928), a pioneering author, demonstrated how a pair of counter-rotating vortices flow in a curved pipe. The flow of a viscous incompressible fluid under a constant pressure gradient force is dependent on a parameter $D_n = \frac{G d^3}{\mu v} \sqrt{\frac{2d}{L}}$, also known as the Dean Number according to his name. The flow condition within the curved duct is commonly referred to as Dean's hydro-dynamical instability. The additional vortices

that manifest within this flow are often termed Dean's vortices. This type of flow is also recognized as Dean Flow.

Throughout the subsequent decades, a substantial body of research was dedicated to the theoretical and experimental exploration of fluid flow through both curved and straight ducts, with some studies incorporating systems featuring rotation. Notable researchers in this field include Berger et al. (1983), Nandakumar and Masliyah (1982, 1986), Winters (1987), Yanase et al. (1989, 2002, 2005), Ishigaki (1996), Yamamoto et al. (1999, 2000, 2006), Chandratilleke et al. (2001, 2003, 2012, 2013), Wang and Yang (2003, 2004), and numerous others who have contributed significantly to our understanding of fluid flow in ducts. The source provides a concise overview of several studies focused on curved duct flow. In the context of curved pipes, Berger et al. (1983) conducted research on fully developed flow, exploring both stable and unstable conditions. This investigation encompassed different geometries, wall characteristics, fluid properties, and Dean numbers to assess their respective importance in the context of curved duct flow. Nandakumar and Masliyah (1982, 1986) delved into the study of heat-transferable vortex flow within coiled and curved pipes, considering both whirling flow and steady laminar flow in ducts with square cross-sections. Winters (1987) employed a complex structure featuring a multitude of symmetric and asymmetric solutions to explore laminar bifurcation flow in a curved tube characterized by a rectangular cross-section. Ishigaki (1996) delved into the study of flow patterns and frictional forces in small-curvature circular pipes, both in co-rotating and counter-rotating configurations. Selmi et al. (1994, 1999) conducted research to investigate the impact of Coriolis and centrifugal forces on pressure-driven two-dimensional flow within a rotating curved duct featuring a rectangular cross-section. Yanase et al. (1989) quantitatively examined the stability of dual solutions, namely the 2-vortex and 4-vortex solutions, within a slightly curved tube featuring a circular cross-section. This investigation spanned a wide range of Dean Numbers. Yamamoto et al. (1999, 2000) conducted observations of flow within a rotating system, focusing on both a square-curved duct and a circular pipe with a helical cross-section. The flow they investigated was viscous, incompressible, and continuous. Zhang et al. (2001) explored the combined effects of Coriolis and centrifugal forces on isothermal flows. Their study was conducted in a curved duct with a rectangular cross-section that exhibited rotational characteristics. Yanase et al. (2002) delved into the examination of viscous incompressible laminar flow within a rectangular curved duct, covering a wide range of the extended aspect ratio from 1 to 12. Wang and Yang (2003, 2004) carried out a comprehensive examination, combining numerical simulations and experimental investigations, on fully developed free and forced convection flows within a rotating curved duct characterized by a square cross-section.

Yamamoto et al. (2006) employed a visualization technique in their experimental assessment to study the characteristics of secondary flow within a curved pipe featuring a

square cross-section. Yanase et al. (2008) conducted a comprehensive analysis of traveling-wave solutions, comparing the spectral approach with the two-dimensional analysis of experimental studies focusing on the flow within a curved square duct. Wang and Liu (2007) embarked on an investigation that delved into the effects of curvature, initial conditions, stability, instability, and the structure of the fully developed bifurcation of forced convection flow. This study was carried out within a curved square duct characterized by a micro-channel and a small curvature ratio of $5E-06$. Subsequently, they conducted a numerical investigation of the fully developed forced convection bifurcation structure in a tightly coiling square cross-section duct with a curvature ratio of 0.5, focusing on the high Dean Number region. Norouzi et al. (2009) concentrated on understanding how primary and secondary normal stress differences impacted forced convection heat transfer in the context of viscoelastic fluid flow within curved ducts. Liu and Wang (2009) delved into the physical factors that give rise to variable structure flow within fully developed forced convection curved ducts characterized by a rectangular cross-section. Fellouah et al. (2010) employed both experimental and numerical methods to investigate the influence of fluid rheology on Dean instability in power-law and Bingham fluids. They conducted these studies within a curved rectangular duct. Chandratilleke et al. (2003, 2012, 2013) explored laminar flow behaviour and related thermal factors to understand the formation of secondary vortices within fluid flow along curved passageways. Their research also included examinations of the results of secondary flow experiments conducted under different aspect ratios. Wu et al. (2013) used the spectral method to examine the secondary flow of streamlines within a curved square duct. Kun et al. (2014) employed ultrasonic Doppler velocimetry and microphones to investigate both laminar and turbulent flows of pseudoplastic fluids within a curved square duct characterized by significant curvature. Razavi et al. (2015) conducted research in a rotating curved duct featuring a square cross-section. They explored the effects of the force ratio, Dean Number, and dimensionless heat flux at the wall on the generation of entropy. This was achieved by applying the second law analysis to forced convection laminar flow. Li et al. (2016) explored fully developed three-dimensional flow, both numerically and physically, within a curved rectangular duct. This duct featured a configuration with spiral, double circular, and involutes line curvatures.

In addition, the researchers briefly examined the influence of Reynolds number, aspect ratio, and various curvatures on Dean Instability. This investigation aimed to precisely identify the centre of the secondary base vortices. In a separate study, Li et al. (2017) conducted a numerical investigation of pressure-driven, fully developed turbulent viscous incompressible fluid flow within curved rectangular ducts.

It's worth noting that, to the best of our knowledge, no research on non-isothermal magneto-hydrodynamic (MHD) fluid flow in curved ducts with Hall and ion-slip currents has been identified in available sources online. Given that much of the universe consists of highly

charged particles and is enveloped by a magnetic field, the innovative concept of incorporating Hall and ion-slip currents into MHD flow within a rotating curved duct in the presence of a magnetic field holds significant importance and potential applications in various engineering and industrial processes. As a result, our goal is to examine the

1. *Non-Isothermal MHD Fluid Flow along the Centre Line in a Rotating Curved Square Duct with Hall and Ion-slip Current.*
2. *Hall and Ion-slip Current Effects on Non-Isothermal Steady Flow through a Rotating Curved Rectangular Duct with Aspect Ratio of 2.*
3. *Non-Isothermal Fluid Flow through a Rotating Curved Duct with Aspect Ratio of 3 in the Presence of Magnetic Field, Hall, and Ion-slip Currents*

The numerical solution is computed by using the spectral approach as the primary tool, and the Chebyshev polynomial, Collocation method, and Newton-Raphson method as supplemental tools. Any point in the crucial zone on the solution curve has been calculated using the arc-length method.

5.2 Mathematical Formulation

This study has been thinking about the two-dimensional flow of a fully developed, viscous, incompressible fluid through a curved duct that rotates around its vertical y -axis. It has been made the assumption that the radial and centreline directions of the duct represent the x - and y -axes respectively. Let L be the duct's curvature's radius and C the cross-sectional centre of the duct. The width and height of the duct cross-section have been taken $2d$ and $2h$. It is assumed that the inner wall of the duct is cooled and the outer wall is heated so that the duct flow becomes to be a non-isothermal state. The outer wall temperature is taken as $T_0 + \Delta T$ and the inner wall is $T_0 - \Delta T$ where $\Delta T > 0$.

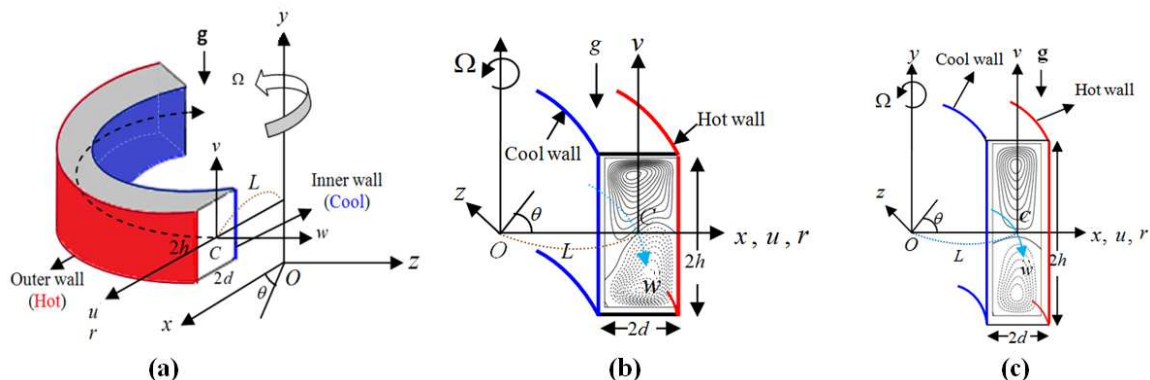


Figure 5.1: Coordinate system of Curved duct with non-isothermal flow with
 (a) Aspect ratio 1 (square cross-section)
 (b) Aspect ratio 2 (rectangular cross-section) and
 (c) Aspect ratio 3 (rectangular cross-section)

A pressure gradient force $G = -\frac{\partial p}{\partial z}$ has been applied as an external force along the centreline direction of the duct. The Lorentz force arises from the interaction of the electric field and the magnetic field. This Lorentz force is further influenced and modified by the presence of Hall and ion-slip currents. Consequently, the flow within the duct experiences the combined effects of the pressure gradient force and the Lorentz force. Additionally, the flow is accelerated due to the collective influence of the Coriolis forces and Centrifugal forces. These forces are a result of the system's rotation and the curvature of the duct. Simultaneously, a gravitational force, denoted as $\mathbf{g} = (0, g, 0)$, acts on the fluid flow within the duct, contributing to the overall dynamics of the system. The coordinate system with the relevant notation is shown in Fig. 5.1.

Due to the application of hall and Ion-slip current, the generalized Ohm's law is described as follows:

$$\mathbf{J} = \sigma\mu_e (\mathbf{q} \wedge \mathbf{B}) - \frac{m}{B_0} (\mathbf{J} \wedge \mathbf{B}) + \frac{m\alpha}{B_0^2} (\mathbf{J} \wedge \mathbf{B}) \wedge \mathbf{B}$$

Here, $\omega_e \tau_e = m$ where ω_e, τ_e are cyclotron frequency and electron collision time.

Under these considerations, the above governing equations are simplified in terms of cylindrical coordinates (r, θ, y) as follows:

Continuity Equation:

$$u \frac{\partial u}{\partial r} + v \frac{\partial v}{\partial y} + \frac{u}{r} = 0 \quad (5.2.1)$$

Momentum Equations:

$$u \frac{\partial u}{\partial r} + v \frac{\partial u}{\partial y} - \frac{w^2}{r} = -\frac{1}{\rho} \frac{\partial p}{\partial r} + v \left(\frac{\partial^2 u}{\partial r^2} + \frac{1}{r} \frac{\partial u}{\partial r} + \frac{\partial^2 u}{\partial y^2} - \frac{u}{r^2} \right) + 2w\Omega_0 + \frac{\sigma\mu_e B_0^2}{\rho} \left[\frac{mw - u(1+m\alpha)}{(1+m\alpha)^2 + m^2} \right] \quad (5.2.2)$$

$$u \frac{\partial v}{\partial r} + v \frac{\partial v}{\partial y} = -\frac{1}{\rho} \frac{\partial p}{\partial y} + v \left(\frac{\partial^2 v}{\partial r^2} + \frac{1}{r} \frac{\partial v}{\partial r} + \frac{\partial^2 v}{\partial y^2} \right) + \beta g T \quad (5.2.3)$$

$$u \frac{\partial w}{\partial r} + v \frac{\partial w}{\partial y} + \frac{uw}{r} = -\frac{1}{\rho} \frac{1}{r} \frac{\partial p}{\partial \theta} + v \left(\frac{\partial^2 w}{\partial r^2} + \frac{1}{r} \frac{\partial w}{\partial r} + \frac{\partial^2 w}{\partial y^2} - \frac{w}{r^2} \right) - 2u\Omega_0 - \frac{\sigma\mu_e B_0^2}{\rho} \left[\frac{mu + (1+m\alpha)w}{(1+m\alpha)^2 + m^2} \right] \quad (5.2.4)$$

Energy Equation:

$$u \frac{\partial T}{\partial r} + v \frac{\partial T}{\partial y} = \frac{k}{\rho C_p} \left[\frac{\partial^2 T}{\partial r^2} + \frac{1}{r} \frac{\partial T}{\partial r} + \frac{\partial^2 T}{\partial y^2} \right] \quad (5.2.5)$$

where, $r = L + x$ is the radial variable, θ is the circumferential angle, and y is the vertical variable, $u, v,$ and w are the corresponding velocity components, p is the dimensional pressure. And the symbols $\rho, \nu, \beta, k, C_p,$ and g refer to the density, kinematic viscosity, coefficient of thermal expansion, thermal conductivity, specific heat at constant pressure

and gravity respectively. The coordinate (r, θ, y) has been changed to the non-dimensional rectangular coordinate (x', z', y') under the following transform of variables

$$r = L + x'd, \quad y = hy', \quad \text{and} \quad L\theta = z'd$$

Here, the non-dimensional variables are introduced by using the characteristic length d and the kinematic viscosity ν so that the non-dimensional form of the velocity U_0 is defined by $\frac{v}{d}$. The other non-dimensional variables are assumed as

$$x' = \frac{x}{d}; \quad \bar{y} = \frac{y}{d}; \quad z' = \frac{z}{d}; \quad u' = \frac{d}{\nu} u; \quad v' = \frac{d}{\nu} v; \quad w' = \frac{d\sqrt{2\delta}}{\nu} w; \quad p' = \frac{d^2}{\rho\nu^2} p \quad \text{and} \quad T' = \frac{T}{\Delta T}$$

Thus the transform equations $r = L + x'd$ and $L\theta = z'd$ (i.e. $r = L + x$ and $L\theta = z$) are used into the above equations to transform its rectangular coordinate form, where x' , \bar{y} and z' are the non-dimensional radial, vertical and axial coordinates respectively and δ is the dimensionless curvature of curve duct which is defined by $\delta = \frac{d}{L}$. Here u', v', w' are the dimensionless velocity components in the direction of x', \bar{y} and z' , also p' is the dimensionless pressure. Using the above dimensionless quantities into the equations (5.2.1)-(5.2.5) and removing the prime over the variables, the following equations are obtained as follows:

Continuity Equation:

$$\frac{\partial u}{\partial x} + \frac{\partial v}{\partial \bar{y}} + \frac{\delta}{1+x\delta} u = 0 \quad (5.2.6)$$

Momentum Equations:

$$u \frac{\partial u}{\partial x} + v \frac{\partial u}{\partial \bar{y}} - \frac{w^2}{2(1+x\delta)} = -\frac{\partial p}{\partial x} + \left(\frac{\partial^2 u}{\partial x^2} + \frac{\delta}{(1+x\delta)} \frac{\partial u}{\partial x} + \frac{\partial^2 u}{\partial \bar{y}^2} - \frac{\delta^2 u}{(1+x\delta)^2} \right) + \frac{T_r}{2} w + M \left(\frac{1}{\sqrt{2\delta}} \frac{mw - (1+m\alpha)u}{(1+m\alpha)^2 + m^2} \right) \quad (5.2.7)$$

$$u \frac{\partial v}{\partial x} + v \frac{\partial v}{\partial \bar{y}} = -\frac{\partial p}{\partial \bar{y}} + \left(\frac{\partial^2 v}{\partial x^2} + \frac{\delta}{1+x\delta} \frac{\partial v}{\partial x} + \frac{\partial^2 v}{\partial \bar{y}^2} \right) + G_r T \quad (5.2.8)$$

$$u \frac{\partial w}{\partial x} + v \frac{\partial w}{\partial \bar{y}} + \frac{\delta}{1+x\delta} uw = \frac{D_n}{1+x\delta} \frac{\partial^2 w}{\partial x^2} + \frac{\delta}{1+x\delta} \frac{\partial w}{\partial x} + \frac{\partial^2 w}{\partial \bar{y}^2} - \frac{\delta^2}{(1+x\delta)^2} w - \delta T_r u - M \left(\frac{\sqrt{2\delta} mu + (1+m\alpha)w}{(1+m\alpha)^2 + m^2} \right) \quad (5.2.9)$$

Energy Equation:

$$u \frac{\partial T}{\partial x} + v \frac{\partial T}{\partial \bar{y}} = \frac{1}{P_r} \left[\frac{\partial^2 T}{\partial x^2} + \frac{\delta}{1+x\delta} \frac{\partial T}{\partial x} + \frac{\partial^2 T}{\partial \bar{y}^2} \right] \quad (5.2.10)$$

where, $D_n = \frac{G d^3}{\mu \nu} \sqrt{\frac{2d}{L}}$ refers to the Dean number, $T_r = \frac{2d^2 \sqrt{2\delta}}{\delta \nu} \Omega_0$ refers to the Taylor

number ; $M = \frac{d^2 \sigma \mu_e B_0^2}{\rho \nu}$ refers to the Magnetic parameter $G_r = \frac{d^3 \beta g \Delta T}{\nu^2}$ is the Grashof

Number,

$P_r = \frac{v\rho C_p}{k}$ is the Prandtl Number, m refers to the Hall parameter and α refers to the Ion-slip parameter

Again by using the sectional stream function $u = \frac{1}{1+x\delta} \frac{\partial \psi}{\partial y}$ and $v = -\frac{1}{1+x\delta} \frac{\partial \psi}{\partial x}$, and using the other one transformation $y = hy'$ which gives a unique variable y' such that $\bar{y} = ly'$, where $l = h/d$ is the aspect ratio of the duct. Thereafter remove prime on this variable for the sake simplicity, it has been found the following equations:

Central line (axial) direction of Momentum equation:

$$\begin{aligned} \frac{1}{l} \left(\frac{\partial \psi}{\partial y} \frac{\partial w}{\partial x} - \frac{\partial \psi}{\partial x} \frac{\partial w}{\partial y} \right) + \delta \frac{\partial w}{\partial x} + D_n + (1+x\delta) \left[\left(\frac{\partial^2}{\partial x^2} + \frac{1}{l^2} \frac{\partial^2}{\partial y^2} \right) w - \frac{\delta^2}{(1+x\delta)^2} w \right] - \frac{\delta}{1+x\delta} w \frac{1}{l} \frac{\partial \psi}{\partial y} - \frac{\delta}{l} T_r \frac{\partial \psi}{\partial y} \\ - \frac{M}{(1+m\alpha)^2 + m^2} \left[\frac{1}{l} \sqrt{2\delta} m \frac{\partial \Psi}{\partial y} + (1+x\delta)(1+m\alpha)w \right] = 0 \end{aligned} \quad (5.2.11)$$

Secondary direction of Momentum equation:

$$\begin{aligned} \frac{1}{l^2} \frac{\partial \psi}{\partial y} \frac{\partial^3 \psi}{\partial x \partial y^2} + \frac{1}{l^2} \frac{\partial \psi}{\partial x} \frac{\partial^3 \psi}{\partial y^3} - \frac{\partial \psi}{\partial y} \frac{\partial^3 \psi}{\partial x^3} + \frac{\partial \psi}{\partial x} \frac{\partial^3 \psi}{\partial y \partial x^2} + l(1+\delta x) \left(\frac{\partial^4 \psi}{\partial x^4} + \frac{2}{l^2} \frac{\partial^4 \psi}{\partial y^2 \partial x^2} + \frac{1}{l^4} \frac{\partial^4 \psi}{\partial y^4} \right) + \frac{3\delta}{1+\delta x} \frac{\partial \psi}{\partial y} \frac{\partial^2 \psi}{\partial x^2} \\ - \frac{\delta}{1+\delta x} \frac{\partial \psi}{\partial x} \frac{\partial^2 \psi}{\partial y \partial x} + \frac{1}{l^2} \frac{2\delta}{1+\delta x} \frac{\partial \psi}{\partial y} \frac{\partial^2 \psi}{\partial y^2} - 2\delta l \frac{\partial^3 \psi}{\partial x^3} - \frac{2\delta}{l} \frac{\partial^3 \psi}{\partial x \partial y^2} - \frac{3\delta^2}{(1+\delta x)^2} \frac{\partial \psi}{\partial x} \frac{\partial \psi}{\partial y} + \frac{3\delta^2 l}{1+\delta x} \frac{\partial^2 \psi}{\partial x^2} \\ - \frac{M(1+\delta x)(1+m\alpha)}{(1+m\alpha)^2 + m^2} \frac{1}{l} \frac{\partial^2 \psi}{\partial y^2} + (1+\delta x)w \frac{\partial w}{\partial y} + (1+\delta x)^2 \frac{T_r}{2} \frac{\partial w}{\partial y} - \frac{3\delta^3}{(1+\delta x)^2} l \frac{\partial \psi}{\partial x} \\ + \frac{M}{(1+m\alpha)^2 + m^2} \frac{m}{\sqrt{2\delta}} (1+x\delta)^2 \frac{\partial w}{\partial y} - l G_r (1+x\delta)^2 \frac{\partial T}{\partial x} = 0 \end{aligned} \quad (5.2.12)$$

Energy equation:

$$\frac{\partial \psi}{\partial y} \frac{\partial T}{\partial x} - \frac{\partial \psi}{\partial x} \frac{\partial T}{\partial y} = \frac{l(1+x\delta)}{P_r} \left[\frac{\partial^2 T}{\partial x^2} + \frac{1}{l^2} \frac{\partial^2 T}{\partial y^2} + \frac{\delta}{(1+x\delta)} \frac{\partial T}{\partial x} \right] \quad (5.2.13)$$

Boundary conditions for w and ψ are used as

$$w(\pm 1, y) = w(x, \pm 1) = \psi(\pm 1, y) = \psi(x, \pm 1) = \frac{\partial \psi}{\partial x}(\pm 1, y) = \frac{\partial \psi}{\partial y}(x, \pm 1) = 0 \quad (5.2.14a)$$

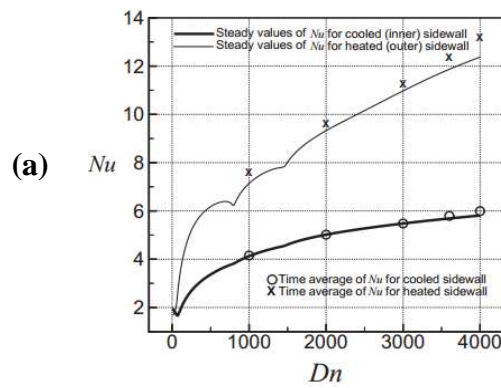
and temperature T at the wall is considered constant

$$T(1, y) = 1, \quad T(-1, y) = -1, \quad T(x, \pm 1) = x \quad (5.2.14b)$$

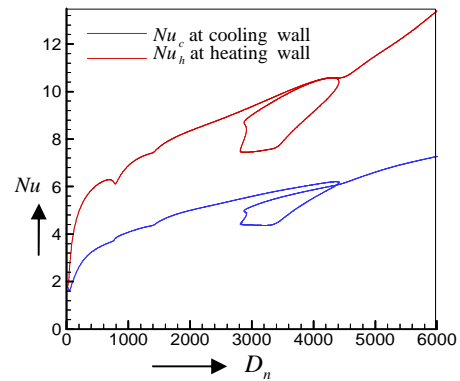
5.3 Validation Test of the Numerical Results

In Chapter-4, Section 4.4, the validations of the present numerical simulations are verified by comparing it with the previously published experimental result for the secondary flow of the velocity. Additionally, another two comparisons are displayed in Fig.5.2(a) and

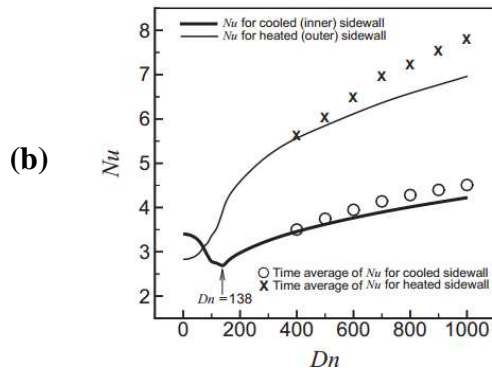
Fig.5.2(b) by the solution curves of the Dean Number versus Nusselt number for the square and rectangular duct respectively. These figures depict the behaviour of the Nusselt number for the dean number increases from zero. R. N. Mandal (2006) showed in his PhD thesis that the solution curve of the Dean Number versus Nusselt Number for the square cross-section of the duct with the curvature at $\delta = 0.1$, which is shown in Fig.5.2a(i) and Fig.5.2b(i) illustrates the solution curve done by Yanase et al. (2006) for the rectangular duct cross-section. The present numerical solutions Fig.5.2a(ii) and Fig.5.2b(ii) are compared with the solution curve in Fig.5.2a(i) and Fig.5.2b(i) for the square and rectangular cross-section of the duct respectively in the absence of Hall and Ion-slip current.



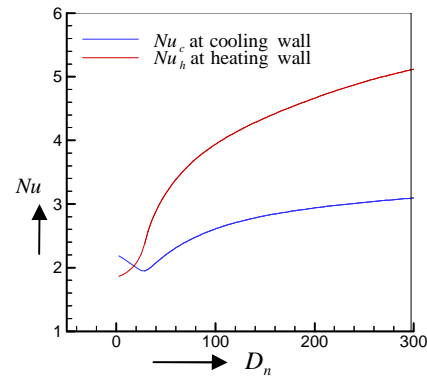
(i) **R. N. Mandal PhD thesis (2006):** Solution curve of the Dean Number vs Nusselt Number at the curvature $\delta = 0.1$ in the 1st steady -state solution curve for square duct.



(ii) **Present Numerical Result:** Solution curve of the Dean Number vs Nusselt Number at the curvature $\delta = 0.1$ for square duct. (In the absence of Hall and Ion-slip current)



(i) **Yanase et al. (2006) Result** (for rectangular duct): Solution curve of the Dean Number vs Nusselt Number.



(ii) **Present Numerical Result** (for rectangular duct): Solution curve of the Dean Number vs Nusselt Number. (In the absence of Hall and Ion-slip current)

Figure 5.2: Comparison of the present numerical results with previous published results by the solution curves of the temperature

On the basis of both quantitative and qualitative comparisons, it can be seen in Fig. 5.2(a)-(b) that the present findings are remarkably similar to those of the published experiment. It follows that our numerical results have a respectable correlation with the experimental data.

5.4 Curved Square Duct for Non-Isothermal Flow:

Non-Isothermal Magneto-hydrodynamic Fluid Flow along the Centreline in a Rotating Curved Square Duct with Hall and Ion-slip Current

This research is regarded as an investigation of a fully developed, non-isothermal, viscous, incompressible laminar fluid flow that passes through the centreline of a rotating square curved duct in the presence of a magnetic field with Hall and Ion-slip current. This non-isothermal duct is produced by keeping the inner wall cool and the outside wall hot; the upper and lower walls are assumed to be adiabatic. Due to the duct's aspect ratio being assumed to be $l=1$, the cross-section of the duct appears perfectly square. In addition to the pressure gradient force (specifically Dean number effects) that has been applied along the duct's centreline, the gravitational force operates externally on the flow. Centrifugal force and Coriolis force are affected on the fluid flow as a result of the system's rotation and the duct's curvature. The spectral method is utilized to perform the calculations as a main tool, whereas the Chebyshev polynomial, Newton-Raphson method, Collocation method, and Arc-length method serve as auxiliary tools. The graphic presentation describes the relationship between the flux with the Grashof number (G_r), Taylor number (T_r), and Dean number (D_n). Also, their related structures of the temperature and velocity distribution at various cross-sections of the curved duct are examined. Showing the impact of the Hall parameter (m), magnetic parameter (M) and Ion-slip parameter (α) on the flow characteristics of this rotationally curved square duct is the main goal of this study. The new results have been presented for the three cases of Dean Number such as Case-I: $D_n = 1000$, Case-II: $D_n = 3000$, and Case-III: $D_n = 5000$ with varying curvature, while the rotational parameter is set at $T_r = 20$. In this case, it is assumed that G_r , D_n , T_r , M , m , and α are varied while the duct's curvature varies from $\delta=0.01$ to 0.5 .

5.4.1 Grid Spaces Accuracy

Grid space accuracy needs to be discussed before implementing the FORTRAN program. The equations are solved for many combinations of the truncation numbers. It is presumed that in order to make the calculations simple and the solutions reasonably accurate for the choice of \bar{M} and \bar{N} are equal, due to the square cross-section of the duct. The flux Q , mean Nusselt number at the heating wall Nu_h and cooling wall Nu_c have been calculated for several pairs of truncation numbers such as $(\bar{M}, \bar{N}) = (16, 16)$, $(18, 18)$, $(20, 20)$ and $(22, 22)$, which is shown in Table-4. From this table, it can be decided that the sufficient accuracy of the numerical solutions has occurred at $(\bar{M}, \bar{N}) = (20, 20)$.

\bar{M}	\bar{N}	Q	Nu_c	Nu_h
16	16	338.8427092101321	3.976475019009116	7.262095071416873
18	18	338.8161925588088	4.107726384434951	7.312240346344643
20	20	338.8164840696670	4.150574491500325	7.253072293037905
22	22	338.8169680135140	4.099858655172923	7.235930319328718

Table-4: Fluxes and mean Nusselt number for several pairs of truncation numbers \bar{M} and \bar{N} at fixed values of $\delta=0.1$, $D_n = 1000$, $G_r = 100$, $T_r = 20$, $M = 0$, $m = 0$ and $\alpha=0$.

5.4.2 Results and Discussion

The study involves the investigation of fully developed flow in a rotating curve square duct. The effects of various parameters such as Grashof number (G_r), rotation parameter (T_r) and Dean Number (D_n) were examined, and the primary focus of the research was on how parameters like the Hall parameter (m), magnetic parameter (M), and Ion-slip parameter (α) affect fluid velocity and temperature. The study considered three different cases with varying Dean Numbers (D_n) and a duct curvature of $\delta = 0.1$, along with a Prandtl number (P_r) of 7.0. The findings were presented in the form of solution curves, which were indicated by arrows (\dashrightarrow) or (\dashleftarrow), depending on their direction. Each square box represented the cross-section of the duct at a specific point on the solution curve, with the right side indicating the outer boundary of the duct. Solid lines denoted anti-clockwise flow (positive direction), while dotted lines indicated clockwise flow (negative direction) for the secondary flow. For temperature distribution, solid lines represented the temperature at the heated wall, while dotted lines represented the temperature at the cooling wall. The calculations were performed using a FORTRAN program with specified increments for various parameters. This research aimed to provide insights into the behaviour of fluid flow and temperature distribution in a rotating curved duct under the influence of different parameters, helping to understand the impact of rotation, Dean Number, and other variables on the flow patterns and thermal characteristics.

A. Effects of Grashof Number (G_r) on the Fluid Flow and Temperature

The increase in rotation leads to a balance between the Coriolis force and the centrifugal force, resulting in approximately symmetrical flow patterns. In this experiment, the flow of the fluid is influenced by the external gravitational force, which causes the flow pattern to become asymmetric.

The impact of the Grashof number on the secondary velocities (radial and axial flows) and temperature is demonstrated in Fig. 5.3a-b. In Fig. 5.3a, the solution curve for the Grashof Number (G_r) versus (i) the flux (Q) and (ii) the mean Nusselt Number (Nu) at both the heated and cooled walls is displayed. This is done for fixed parameters, including $D_n=500$, $T_r=20$, $P_r=7.0$, $M=0$, $m=0$ and $\alpha=0$, with the duct's curvature set at $\delta=0.1$.

In Figure 5.3a (i), a single-branch solution curve is identified within all Grashof number ranges ($G_r > 0$). It is evidently characterized as an increasing function, signifying a gradual increase in flux with higher Grashof number values. Meanwhile, concerning temperature, it is observed that the Nusselt number values at the heated wall consistently exceed those at the cooled wall. The temperature deviation gradually reduces as the Grashof number increases. Fig. 5.3b presents the flow structures corresponding to the solution curves outlined in Fig. 5.3a. Under the influence of gravity, the initially symmetrical scenario

gradually transitions into an asymmetric one. With increasing Grashof number, the positive flow predominates over the negative rotational radial flow.

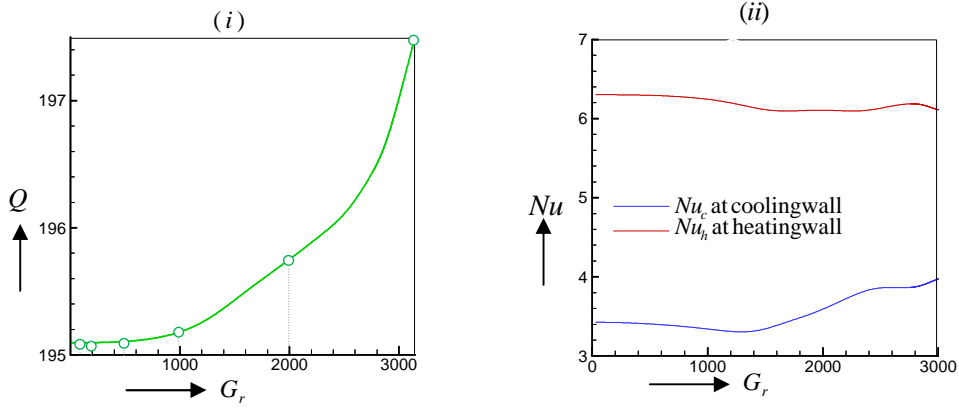


Figure 5.3a: Solution curve: Grashof number G_r versus (i) flux Q (ii) Mean Nusselt number Nu at the heating and cooling wall for fixed $\delta=0.1$, $D_n = 500$, $T_r = 20$, $P_r = 7$, $M = 0$, $m = 0$ and $\alpha=0$

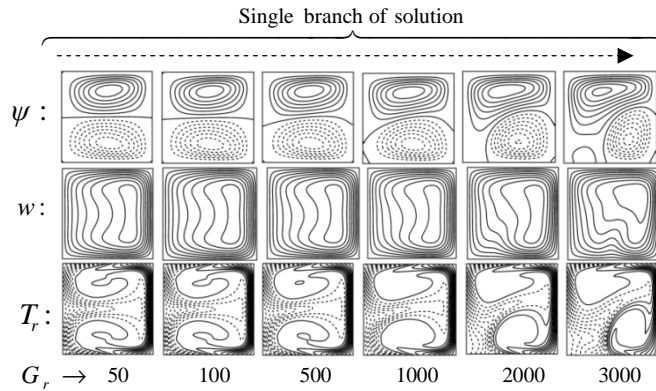


Figure 5.3b: Streamlines ψ (upper), axial contour flow w (lower) and Temperature profile T (bottom) in accordance with the solution curve in Fig. 5.3a

B. Effects of Taylor Number (T_r) on the Fluid Flow and Temperature

For the given fixed parameters, where $D_n=1000$, $G_r = 100$, $P_r = 7.0$, $M=0$, $m=0$, and $\alpha=0$, Figure 5.4a illustrates the relationship between the Taylor Number (T_r) and (i) fluid flux (Q) for velocity and (ii) the average Nusselt number (Nu) at the heated and cooled walls in a duct with a curvature of $\delta=0.1$. In Figure 5.4b, the corresponding velocity and temperature distribution patterns at different T_r values are presented. Within the valid range of Taylor numbers, a single-branch solution curve is identified. This curve can be subdivided into two distinct regions: one spanning $-274.66 < T_r < -261.20$, where the flux increases as T_r increases, and the other for $T_r > -261.20$, where the flux decreases as T_r increases. The solution curve is constrained by $Tr = -274.66$ for negative rotation, where the flux achieves its peak value of 427.8 at $T_r = -261.2$, coinciding with the emergence of up to six secondary flow vortices. Concerning temperature distribution, the Nusselt numbers at the heating wall are consistently lower than those at the cooling wall for $-274.66 < T_r < -261.20$. This

temperature deviation gradually diminishes with increasing T_r within this range but exhibits a reverse trend beyond it. When $T_r = 0$ (indicating a non-rotating system), the secondary flow streamlines exhibit asymmetric, two-solution vortices. As T_r increases in the positive direction, the strength of the flow patterns gradually weakens. In contrast, negative T_r values create a critical zone, giving rise to six asymmetric vortex structures. In all cases, as T_r increases, the asymmetric conditions gradually transition to a more symmetric configuration, signifying a decrease in asymmetry with increasing T_r . Notably, the temperature at the cooling wall becomes increasingly influenced by the heating wall as T_r increases.

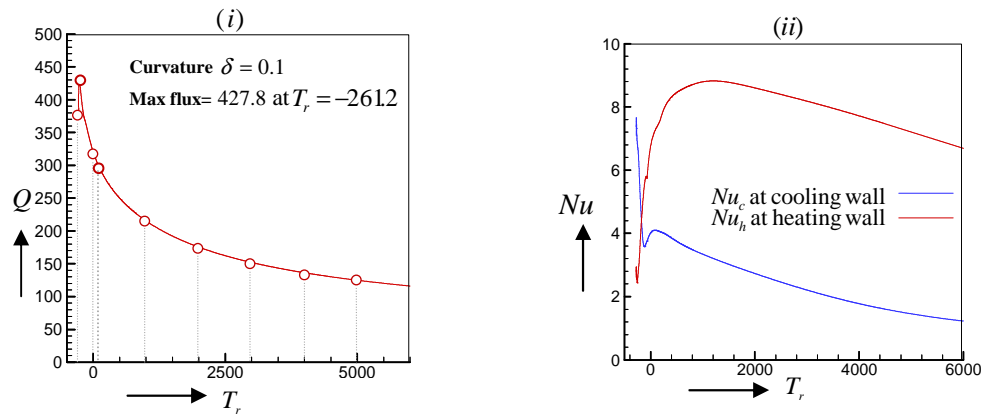


Figure 5.4a: Solution curve: Taylor number T_r versus (i) flux Q (ii) Mean Nusselt number Nu at the heating and cooling wall for fixed $\delta=0.1$, $D_n = 1000$, $G_r = 100$, $P_r = 7$, $M = 0$, $m = 0$ and $\alpha=0$

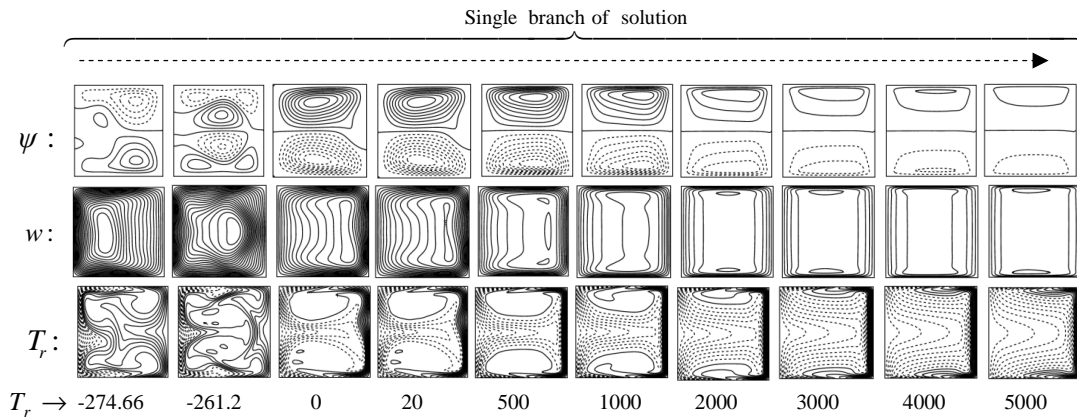


Figure 5.4b: Streamlines ψ (upper), axial contour flow w (lower) and Temperature profile T (bottom) in accordance with the solution curve in Fig. 5.4a

C. Effect of Dean Number (D_n) on the Fluid Flow and Temperature

At fixed values of $G_r=100$, $T_r =20$, $P_r = 7.0$, $M=0$, $m=0$, and $\alpha=0$, Figure 5.5a portrays the solution curve of the Dean Number (D_n) concerning two vital aspects: (i) fluid flux (Q) for velocity and (ii) the average Nusselt number at the heated and cooled walls within a curved duct characterized by $\delta=0.1$. Figure 5.5b is divided into three subplots, providing an enlarged view of specific segments of the solution curve highlighted in Figure 5.5a(i) by rectangular boxes.

This analysis reveals the presence of five distinct branches in the steady-state solution curves. These branches are represented by distinct colours: black, red, purple, green, and blue, designating the first, second, third, fourth, and fifth branches of the steady-state solution curve, respectively. In each branch, the fluxes increase in tandem with D_n . Notably, as D_n increases, the Nusselt number values at the heating wall surpass those at the cooling wall when D_n is greater than zero. This deviation becomes more pronounced with higher Dean Number values.

In Figure 5.5c, the corresponding flow structures of temperature and velocity distributions at various positions along T_r are presented. Each branch of the steady-state solution curve exhibits secondary flows characterized by a pair of counter-rotating vortices. For lower D_n values, positive rotational flow dominates over negative rotational flow, but this situation reverses for higher D_n values. As D_n increases for both velocity and temperature distributions, the flow pattern's intensity gradually strengthens. Importantly, all branches of the steady-state solution exhibit an asymmetric flow structure. The flow tends to peak near the duct's outer wall for axial flow. At higher Dean Number values, the temperature distribution takes on a chaotic appearance, adding to the complexity of the observed flow patterns.

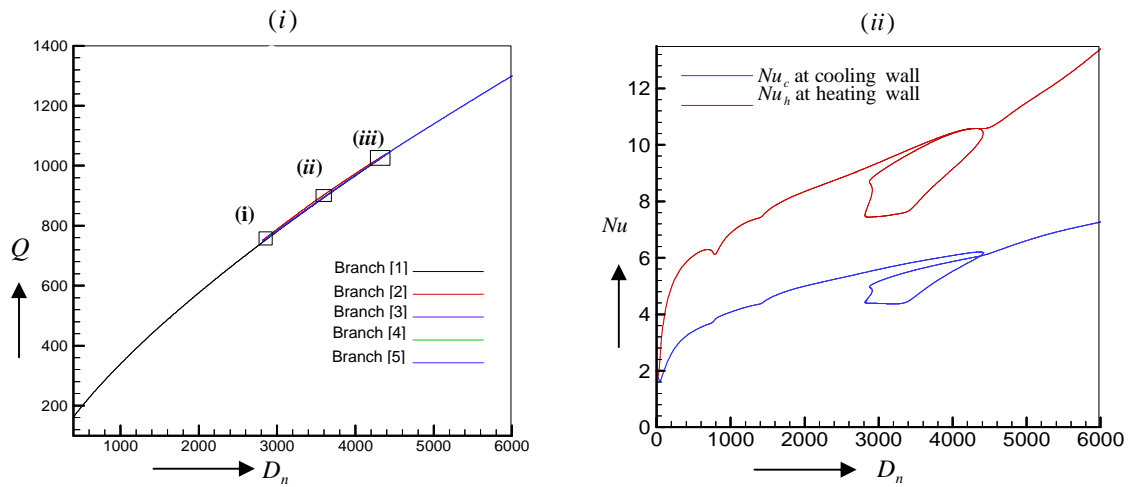


Figure 5.5a: Solution curve: Dean Number D_n versus (i) flux Q (ii) Mean Nusselt number Nu at the heating and cooling wall for fixed $\delta=0.1$, $T_r=20$, $G_r=100$, $P_r=7$, $M=0$, $m=0$ and $\alpha=0$.

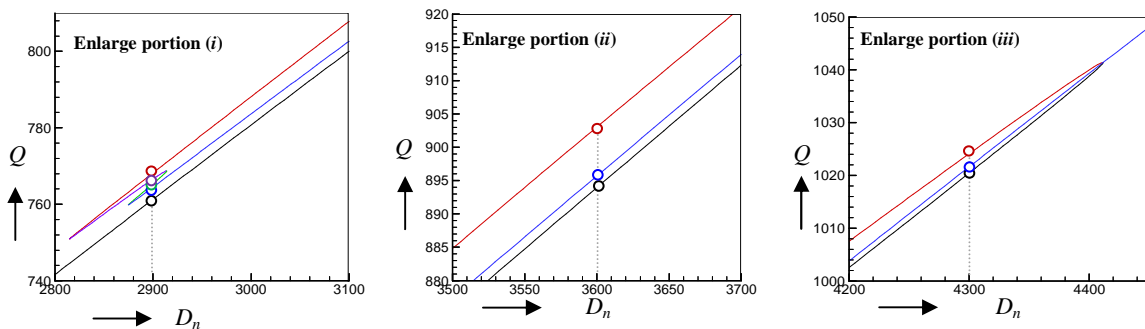


Figure 5.5b: Magnifying figures marked by the dashed box on Fig.5.5a

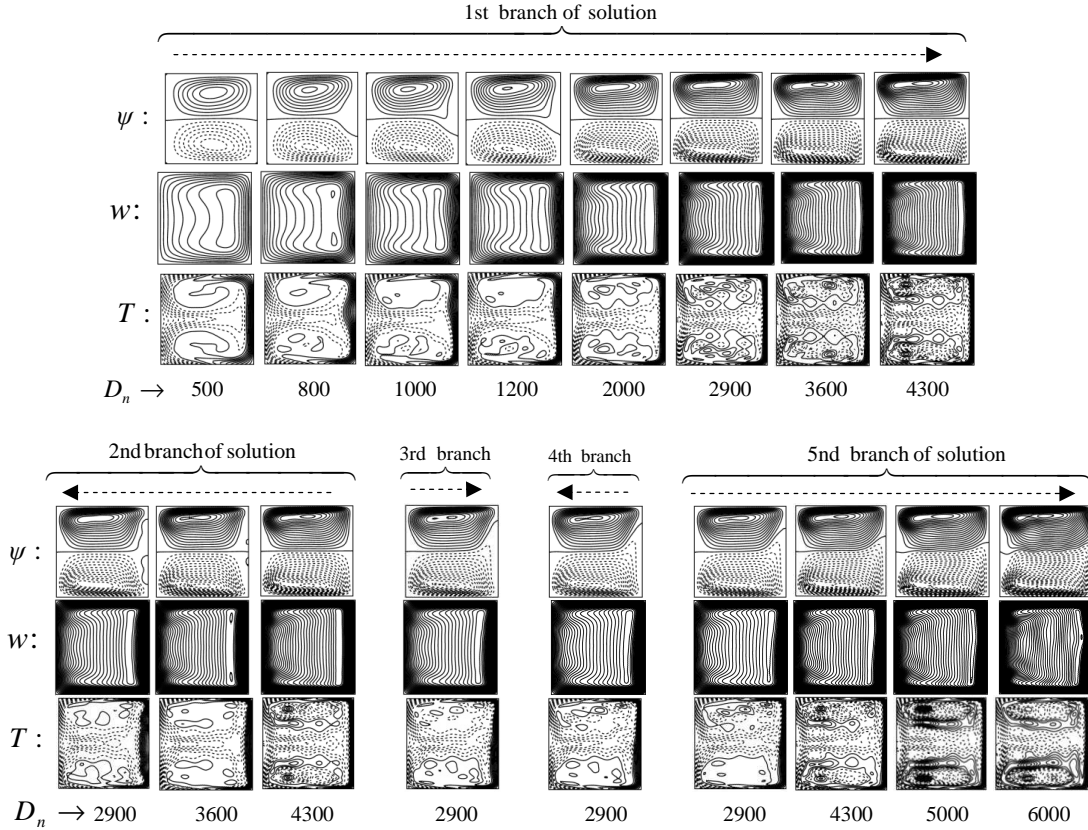


Figure 5.5c: Streamlines ψ (upper), axial contour flow w (lower) and Temperature profile T (bottom) in accordance with the solution curve in Fig. 5.5a

D. Effects of Magnetic Parameter (M) on the Fluid Flow and Temperature

At prescribed values of $G_r = 100$, $T_r = 20$, $P_r = 7.0$, $m = 0$, and $\alpha = 0$, Figure 5.6a illustrates the solution curve for the Magnetic parameter (M) in relation to (i) fluid flux (Q) for velocity and (ii) the average Nusselt number at the heated and cooled walls within a curved duct with $\delta = 0.1$. Notably, this analysis is carried out for three distinct Dean Number (D_n) values, specifically $D_n = 1000, 3000$, and 5000 .

Across all cases of Dean Number, these solution curves exhibit a consistent trend of decline as the magnetic parameter, M , increases. This suggests that there is a drop in fluid flux as the magnetic parameters become more prominent. In Case III, specifically at $D_n = 5000$, a unique finding emerges where two distinct solution curves are identified. The first solution curve is confined within $0 \leq M \leq 29.2722$ and displays an increase in flux as Dean Number rises. Additionally, in the temperature context, the Nusselt number values at the heating wall surpass those at the cooling wall. A noteworthy observation is that the temperature deviation gradually approaches zero beyond a certain threshold value of M .

Figure 5.6b(i)-(iv) complements this analysis by presenting the velocity profile and temperature distribution structures at various magnetic parameter values. As M increases in the context of velocity distribution, the flow pattern's strength gradually weakens. Negative flow predominates over the positively directed secondary flow, and the axial flow contour

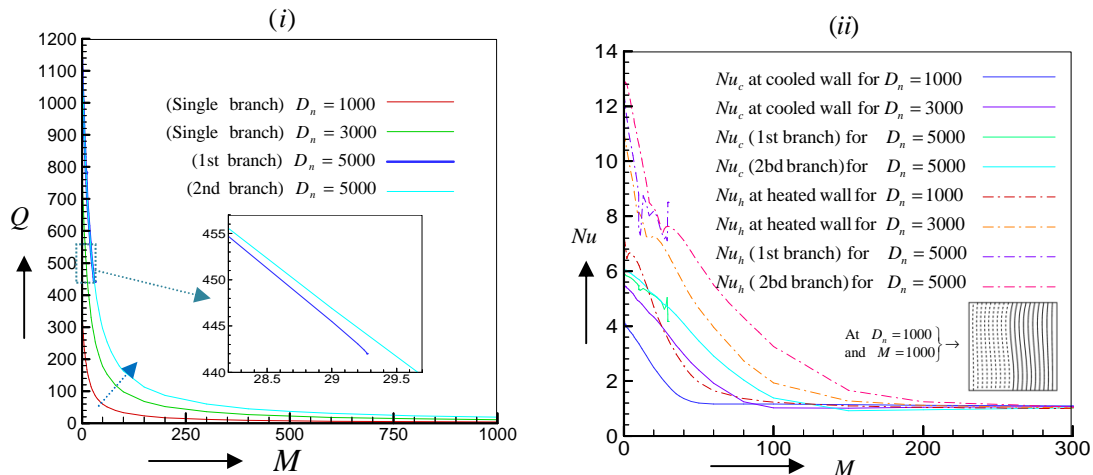


Figure 5.6a: Solution curve: Magnetic parameter M versus (i) flux Q (ii) Mean Nusselt number Nu at the heating and cooling wall for fixed $\delta=0.1$, $G_r = 100$, $T_r = 20$, $P_r = 7$, $m = 0$ and $\alpha=0$ where $D_n = 1000, 3000$ and 5000

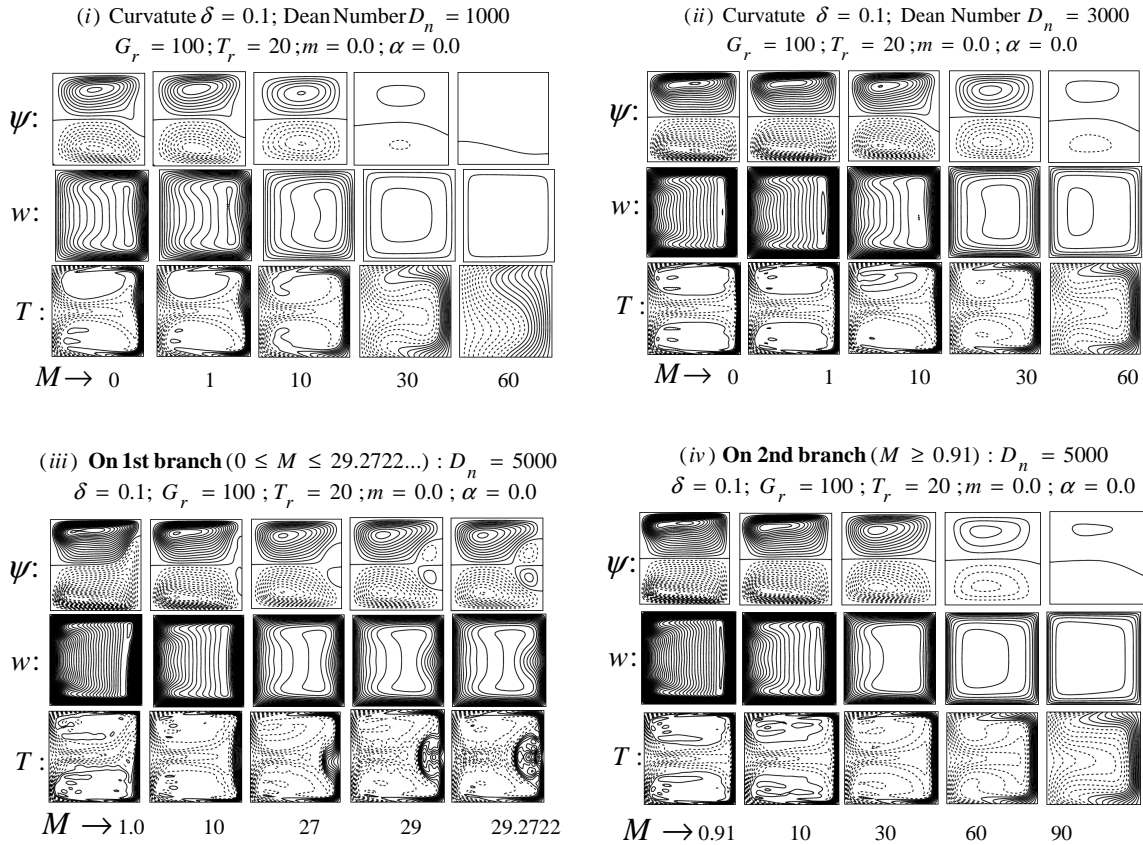


Figure 5.6b : Streamlines ψ (upper), axial contour flow w (lower) and Temperature profile T (bottom) in accordance with the solution curve in Fig. 5.6a

shifts closer to the duct's centre. Comparing the density of the velocity structure, it is noted that for $D_n = 1000$, it is weaker than for $D_n = 3000$ within a specific range around $M = 60$. Concerning temperature, the cooling wall temperature exerts a dominant influence over the heating wall temperature, and this dominance diminishes with increasing M for all Dean Number cases. However, a unique observation is made at $D_n = 5000$ in the first branch of

Case III, where the asymmetry condition transforms into a more symmetric form with the increase of M . Furthermore, the initially asymmetric two-vortex flow evolves into a nearly symmetric four-vortex flow as the magnetic parameter increases. Notably, additional Dean vortices are not generated as M exceeds 29.273. Within the range $0 < M < 29.2722$, up to four counter-rotating vortices are observed for the secondary flow. Meanwhile, in the second branch, the effects of M on velocity and temperature distribution exhibit the expected behaviour of M when M exceeds 0.91.

E. Effects of Hall Parameter (m) on the Fluid Flow and Temperature

At fixed parameters, including $G_r = 100$, $T_r = 20$, $P_r = 7.0$, $M = 1.0$, and $\alpha = 0$, Figure 5.7a illustrates the solution curve of the Hall parameter (m) in relation to (i) fluid flux (Q) for velocity and (ii) the average Nusselt number (Nu) at the heated and cooled walls within a curved duct with $\delta = 0.1$. The analysis is conducted for three distinct Dean Number (D_n) values: $D_n = 1000$, 3000, and 5000.

For all cases of Dean Number, it is observed that the flux experiences an increase with a rise in the Hall parameter, specifically within a certain range, approximately $0 \leq m \leq 3$. Beyond this range, the increase in the Hall parameter has a relatively minor effect on flux. A steady-state solution is achieved after surpassing a specific threshold value of m in all Dean Number cases. Notably, the maximum flux is found when m exceeds approximately 6. Numerically, this peak flux value is determined as 338.80, 780.07, and 1135.90 at Dean Numbers of 1000, 3000, and 5000, respectively. This finding confirms that the flux increases as the Dean Number rises. In the context of temperature [Figure 5.7a(ii)], the Nusselt number values at the heating wall are consistently higher than those at the cooling wall. Importantly, the temperature deviation remains relatively constant, showing no significant change with increasing Hall parameter, m .

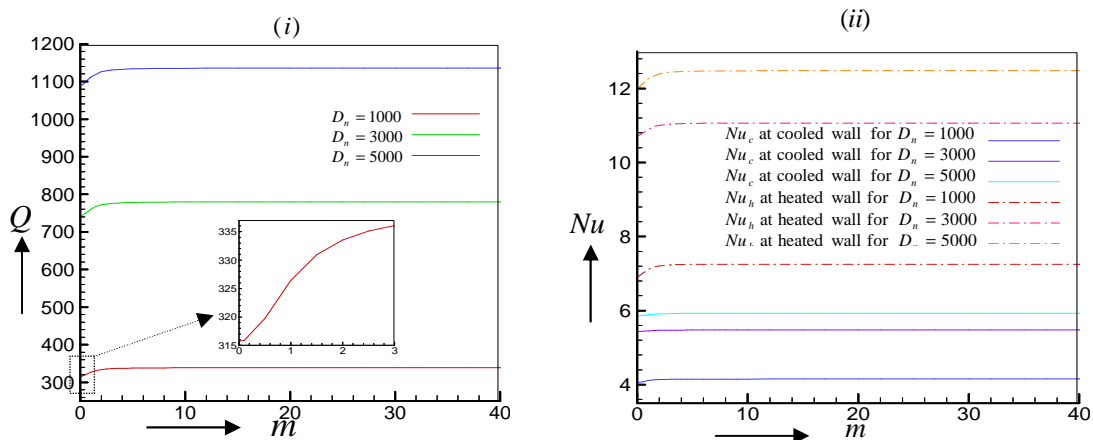


Figure 5.7a: Solution curve: Hall parameter m versus (i) flux Q (ii) Mean Nusselt number Nu at the heating and cooling wall for fixed $\delta = 0.1$, $G_r = 100$, $T_r = 20$, $P_r = 7$, $M = 1$ and $\alpha = 0$ whereas $D_n = 1000$, 3000 and 5000

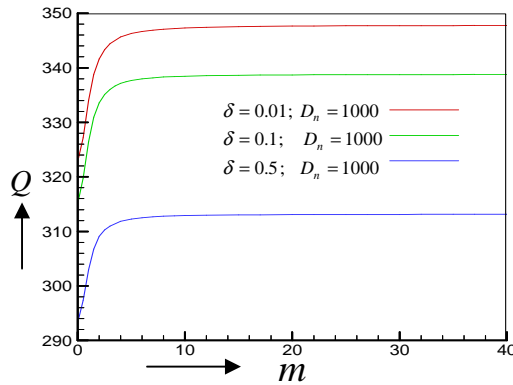


Figure 5.7b: Solution curve: Hall parameter m versus (i) flux Q (ii) Mean Nusselt number Nu at the heating and cooling wall for fixed $D_n=1000$, $G_r = 100$, $T_r=20$, $P_r = 7$, $M = 1$ and $\alpha=0$ where $\delta=0.01, 0.1$ and 0.5

In Figure 5.7b, the solution curve for the Hall parameter (m) vs. flux is presented for a constant set of parameters, including $D_n=1000$, $G_r=100$, $T_r=20$, $P_r=7.0$, $M=1.0$, and $\alpha = 0$. This curve is depicted for different values of duct curvature, specifically $\delta=0.01, 0.1$, and 0.5 . An interesting observation is made, indicating that as the duct's curvature increases, the flux decreases. This trend suggests a correlation between duct curvature and the resulting flux.

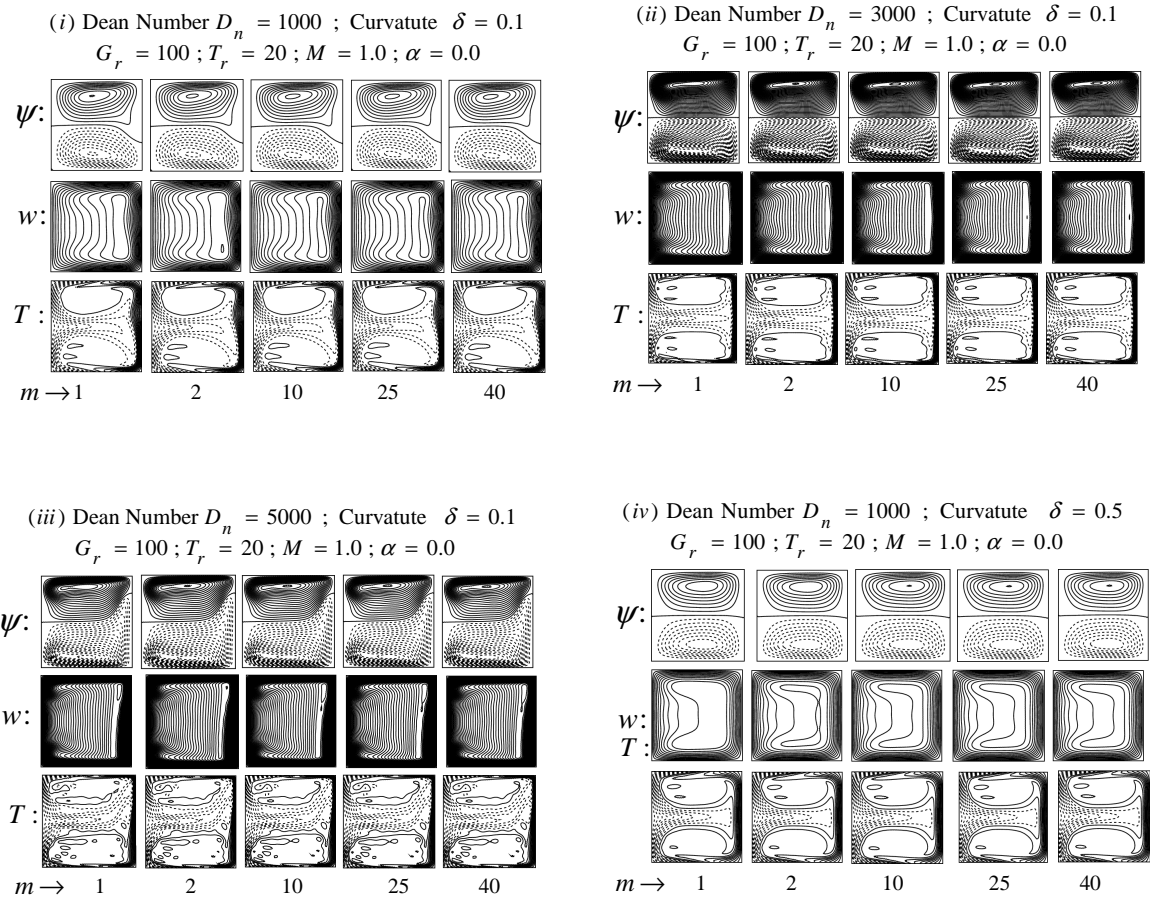


Figure 5.7c: Streamlines ψ (upper), axial contour flow w (lower) and Temperature profile T (bottom) in accordance with the solution curve in Fig. 5.7a-b

Figure 5.7c(i)-(iii) complements the analysis by showcasing the temperature and velocity distribution structures at various points along the Hall parameter (m) corresponding to the solution curve in Figure 5.7a. It is noted that the strength and structures of the flow pattern remain consistent, showing no significant change with increasing Hall parameter (m). Regarding temperature distribution, the dominating influence of the cooling wall temperature over the heating wall temperature remains unchanged with variations in the Hall parameter (m) for all Dean Number cases. Furthermore, upon comparing the figures in Figure 5.7c(i) with Figure 5.7c(iv), it becomes evident that the structures of the velocity and temperature distribution with a larger duct curvature at $\delta=0.5$ appear weaker compared to those with a smaller duct curvature at $\delta=0.1$. This observation highlights the impact of duct curvature on the resulting flow patterns and temperature distribution, indicating that a higher curvature results in less pronounced flow structures.

F. Effects of Ion-slip parameter (α) on the Fluid Flow and Temperature

In Figure 5.8a, the solution curve for the Ion-slip parameter (α) in relation to (i) fluid flux (Q) for velocity and (ii) the average Nusselt number (Nu) at the heated and cooled walls is presented. This is based on fixed parameters, including $G_r = 100$, $T_r = 20$, $P_r = 7.0$, $M = 1.0$, and $m = 5.0$, while the duct's curvature is $\delta = 0.1$. The analysis covers three different Dean Number cases: $D_n = 1000$, 3000, and 5000.

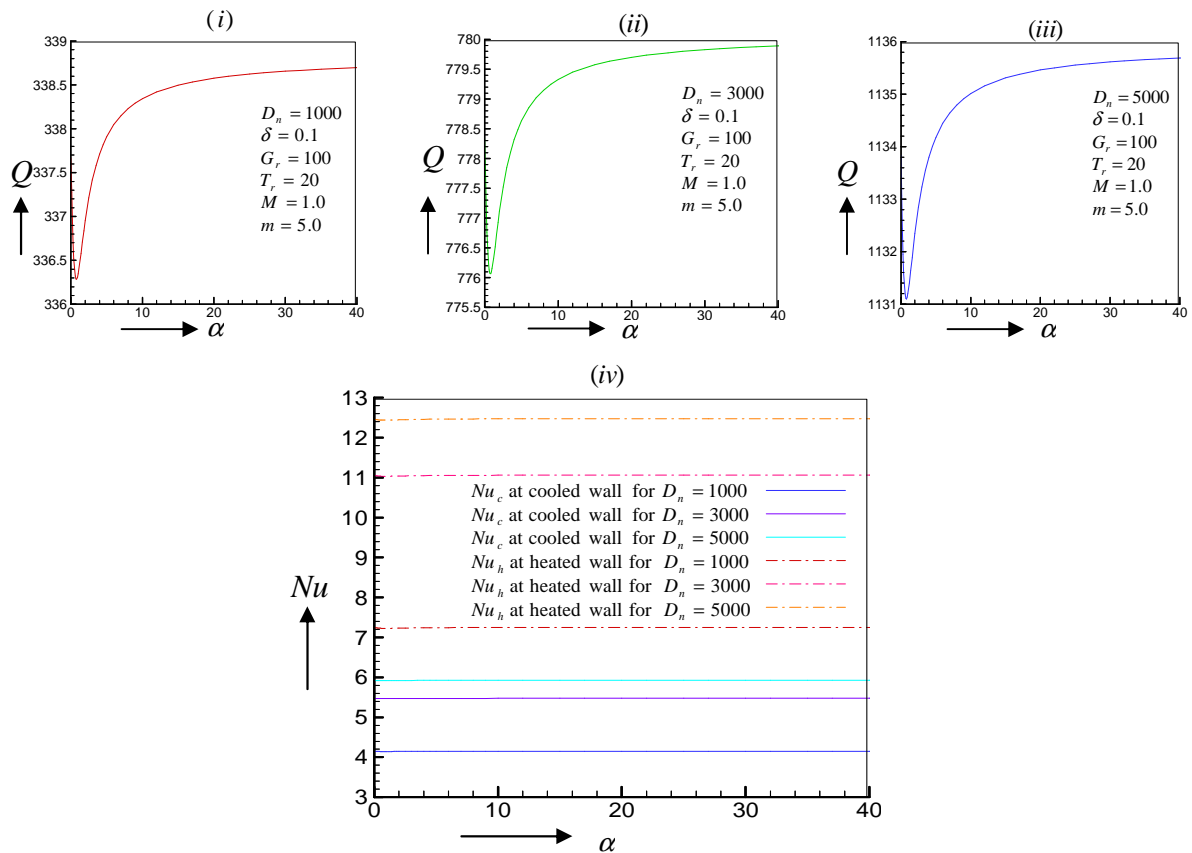


Figure 5.8a: Solution curve: Ion-slip parameter α versus flux Q for the velocity at the Dean Number (i) $D_n = 1000$ (ii) $D_n = 3000$ (iii) $D_n = 5000$ and (iv) Ion-slip parameter α versus Nu at the heating and cooling wall for fixed $\delta = 0.1$, $G_r = 100$, $T_r = 20$, $P_r = 7$, $M = 1$ and $m = 5$

An interesting trend is observed where the flux experiences a decrease in a limited range for $\alpha < 0.8$, followed by a rapid increase as α increases further. Beyond a certain threshold value of α , a steady-state solution is reached for all three Dean Number cases. The maximum fluxes are identified at Dean Numbers of 5000, 3000, and 1000, with values of 1135.83, 780.01, and 338.76, respectively. This finding reaffirms the relationship between an increase in Dean Number and an increase in flux. Concerning the Nusselt number, it remains higher at the heating wall compared to the cooling wall for temperature distribution. The deviation of the temperature does not change significantly with variations in α .

Figure 5.8*b* extends the analysis by illustrating the Ion-slip parameter (α) vs. flux (Q) solution curve for fixed parameters, similar to those in Figure 5.8*a*, but with different duct curvatures: $\delta=0.01, 0.1, \text{ and } 0.5$. It is observed that as the duct's curvature increases, the flux tends to decrease. Figures 5.8*c*(i)-(iii) display the velocity and temperature distribution structures at various points along the Ion-slip parameter (α) that correspond to the solution curves in Figure 5.8*a*. It is worth noting that the strength and structures of the flow pattern show negligible changes with increasing α . In terms of temperature distribution, the dominance of the cooling wall temperature over the heating wall temperature remains consistent, and this effect doesn't vary with changes in α for all Dean Number cases. Similarly, the strength and structures of the flow pattern do not show significant alterations with an increase in duct curvature. Comparing figures in Figure 5.8*c*(i) with Figure 5.8*c*(iv), it becomes evident that the velocity and temperature distribution structures with a larger duct curvature at $\delta=0.5$ appear weaker than those with a smaller curvature at $\delta=0.1$, reinforcing the influence of duct curvature on flow patterns.

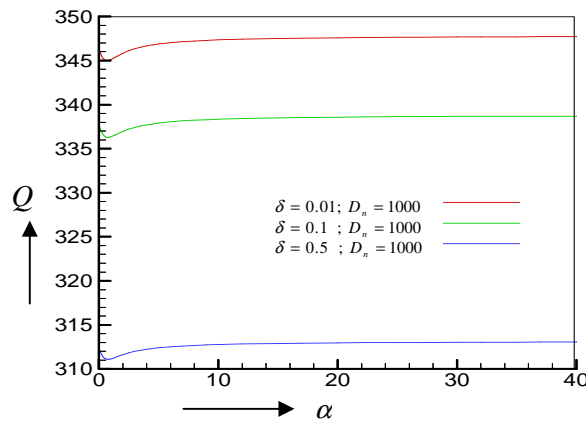


Figure 5.8*b*: Solution curve: Ion-slip parameter α versus flux Q for fixed $D_n = 1000$, $G_r = 100$, $T_r = 20$, $P_r = 7$, $M = 1$ and $m = 5$ where $\delta = 0.01, 0.1$ and 0.5

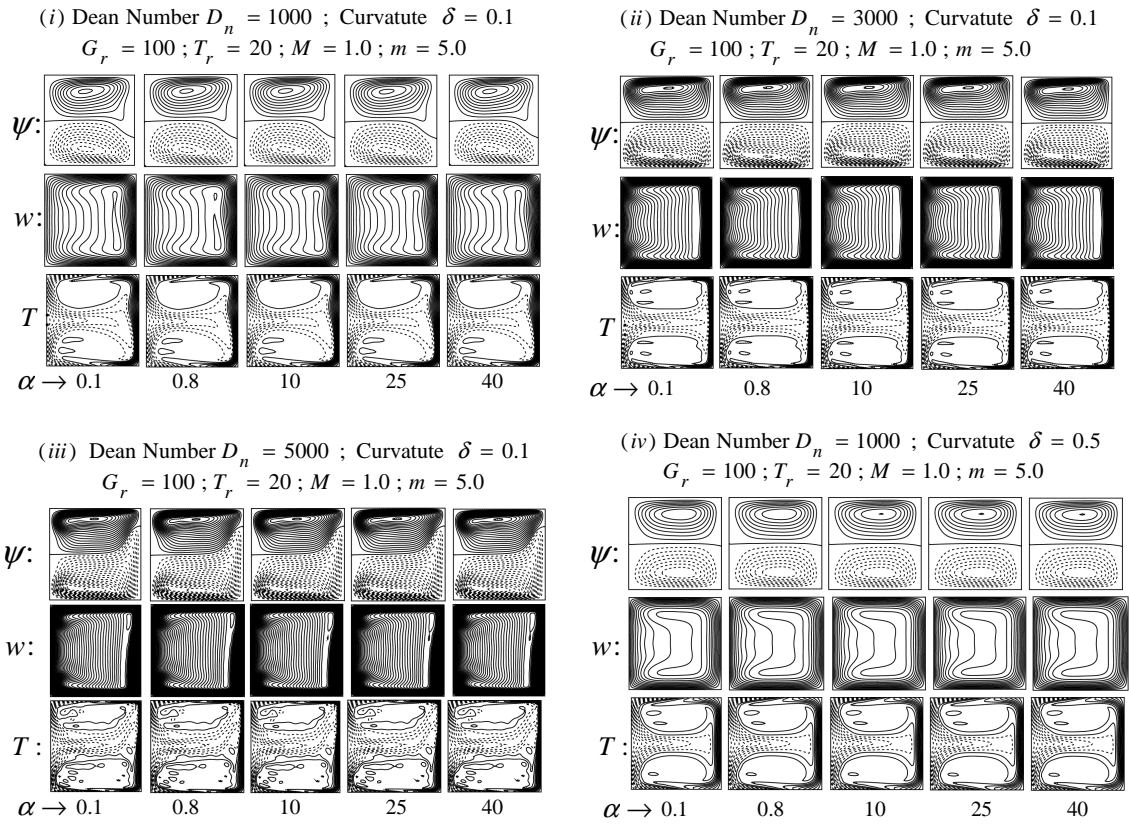


Figure 5.8c: Streamlines ψ (upper), axial contour flow w (lower) and Temperature profile T (bottom) in accordance with the solution curve in Fig. 5.8a-b

5.5 Curved Rectangular Duct for Non-Isothermal Fluid Flow (Aspect Ratio 2):

Hall and Ion-slip Current Effects on Non-Isothermal Steady Flow through a Rotating Curved Rectangular Duct with Aspect Ratio 2

A fully developed non-isothermal, viscous, steady flow passes through a rotating curving duct with a rectangular cross-section that has been explored in this study in the presence of a magnetic field with Hall and Ion-slip current. The duct has been formed as a non-isothermal by keeping the outer heating wall, inner cooling wall, and upper and lower walls adiabatic. The aspect ratio of the duct is taken 'two' so that the duct cross-section is viewed as rectangular. Along the duct's midline, a pressure gradient force (Dean Force) has been applied. As an external force, the gravitational, Lorentz, centrifugal, and Coriolis forces influence on the fluid flow. The Centrifugal and Coriolis forces have been created due to the system's rotation and duct's curvature. The numerical solutions are carried out using the spectral method as the primary tool. In addition, the Chebyshev polynomial, Newton-Raphson, Collocation, and Arc-length methods are used as secondary tools. The main focus is on investigating the effects of the magnetic parameter (M), Hall parameter (m), and Ion-slip parameter (α) on the velocity and temperature distribution of the non-isothermal fluid flow passing through the curved rectangular duct with an aspect ratio of two in a rotating system. This investigation has been carried out for the four cases of curvature (δ) and Dean Number (D_n) such as Case-I: $\delta = 0.01$, $D_n = 500$ Case-II: $\delta = 0.1$, $D_n = 500$, Case-III: $\delta = 0.5$, $D_n = 500$ and Case-IV: $\delta = 0.5$, $D_n = 1000$. It is considered here that D_n, G_r, T_r, M, m and α are varied, while curvature of the duct δ ranges from 0.01 to 0.5.

5.5.1 Grid Spaces Accuracy

For several pairs of truncation numbers, the equations are solved to find the grid space accuracy. It is presumed that in order to make the calculations simple and the solutions reasonably accurate, it is assumed that the value of \bar{N} is twice of \bar{M} . The values of the flux Q , mean Nusselt number at the heating wall Nu_h and cooling wall Nu_c have been furnished for several pairs of truncation numbers such as $(\bar{M}, \bar{N}) = (7, 14), (8, 16), (9, 18), (10, 20),$ and $(11, 22)$, which is shown in Table-5. It has been seen from this table that the numerical solutions can be found sufficient accuracy at $(\bar{M}, \bar{N}) = (10, 20)$.

\bar{M}	\bar{N}	Q	Nu_c	Nu_h
07	14	296.9929324335965	3.194661434357543	5.382577053844398
08	16	296.1440867269804	3.634386655368639	5.507305127743999
09	18	297.5147703732567	3.578849034794546	5.670558453687153
10	20	297.6505647639801	3.334674372681358	5.842032867239069
11	22	297.5520924528217	3.598868974689484	5.711389952152222

Table-5: Fluxes Q and mean Nusselt number Nu for distinct pairs of truncation numbers \bar{M} and \bar{N} for fixed $\delta=0.1, D_n = 500, G_r = 100, T_r = 20, P_r = 7, M = 0, m = 0$ and $\alpha=0$.

5.5.2 Results and Discussion

The study of flow characteristics in curved ducts has involved a comprehensive analysis of the Grashof number (G_r), Taylor number (T_r), and Dean number (D_n) at a curvature factor of 0.1. This investigation aimed to gain insights into the physical implications of the curvature. Furthermore, these findings were cross-referenced with results from prior studies. In an extension of this research, we delved into the impact of additional parameters, specifically the magnetic parameter (M), Hall parameter (m), and Ion-slip parameter (α), on both fluid flow and temperature. Utilizing solution curves, we illustrated the corresponding flow vortex structures for four distinct cases of curvature, each associated with different Dean Numbers: Case-I: $\delta=0.01$, $D_n = 500$, Case-II: $\delta=0.1$, $D_n = 500$, Case-III: $\delta=0.5$, $D_n = 500$, and Case-IV: $\delta=0.5$, $D_n = 1000$.

A. Effects of Grashof Number (G_r) on the fluid flow and Temperature

The curved duct's rotation leads to a balance between the Centrifugal force and the Coriolis force, resulting in an approximately symmetric flow structure. However, the presence of an external gravitational force exerts an additional influence on the fluid flow, causing the flow pattern to become asymmetric.

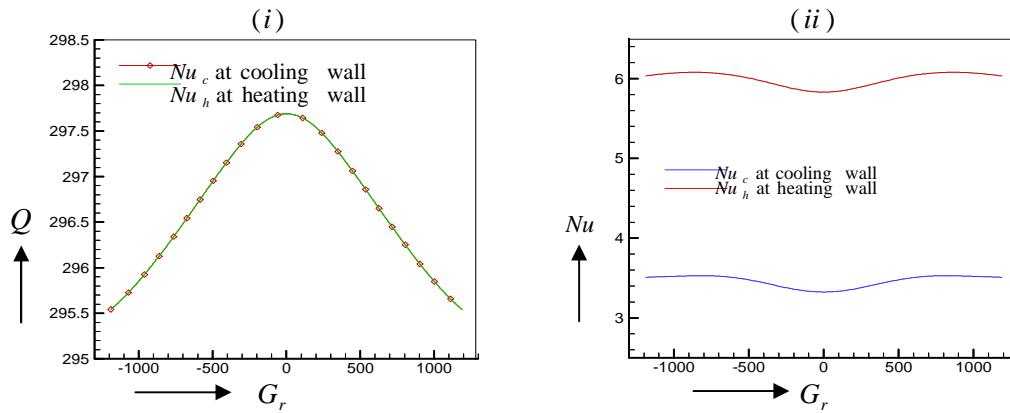


Figure 5.9a: Solution Curve: Grashof number G_r versus (i) Flux Q
 (ii) Mean Nusselt number Nu at the heating and cooling wall for fixed
 $\delta=0.1$, $D_n=500$, $T_r=20$, $P_r=7$, $M=0$, $m=0$ and $\alpha=0$

Figure 5.9a-b illustrates the effects of the Grashof number on both radial and axial flows, as well as temperature, with fixed values of $\delta=0.1$, $D_n = 500$, $T_r = 20$, $P_r = 7$, $M = 0$, $m = 0$ and $\alpha=0$. Figure 5.9a provides solution curves for the Grashof Number (G_r) with respect to (i) Flux (Q) and (ii) Mean Nusselt number (Nu) at both the cooling and heating walls.

In Figure 5.9a, multiple branches of curves are visible for flux, yet all these branches remain within the range $-1188.76 \leq G_r \leq 1190.17$ along the same path. Only the 1st and 2nd branches are activated in Figure 5.9a. Notably, the solution curves for flux and temperature exhibit a symmetric pattern around the vertical line at $G_r = 0$. The peak flux value is observed at G_r

$=0$, and it gradually decreases with an increase in $|G_r|$. In Figure 5.9a (ii), temperature deviations on both walls concerning the Grashof number are displayed. It is noteworthy that the Nusselt numbers at the cooling wall are lower compared to the heating wall. The temperature deviation, or mean Nusselt number, gradually decreases with a slow increment in G_r .

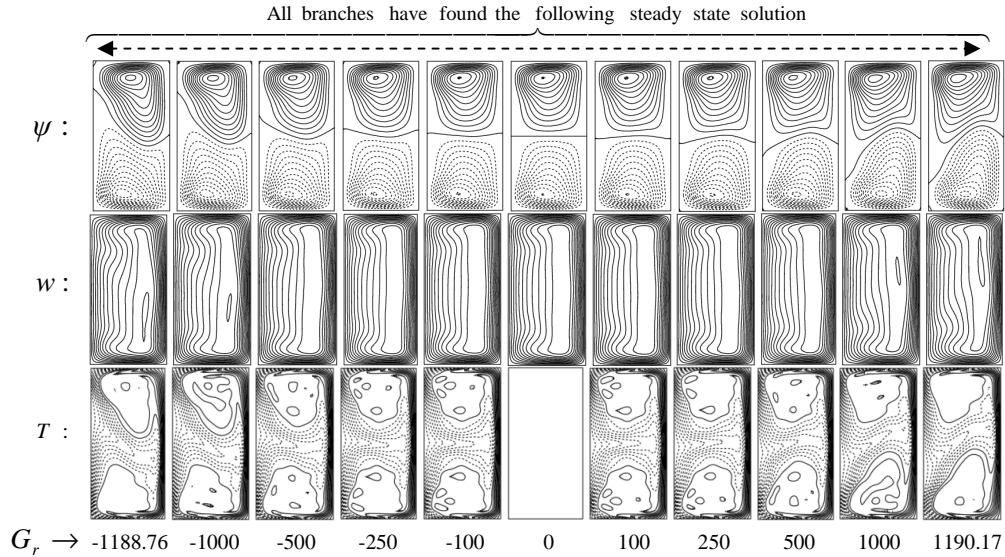


Figure 5.9b: Streamlines ψ (top), axial Contour flow w (middle) and Temperature profile T (bottom) in accordance with the solution curve in Fig. 5.9a

Figure 5.9b illustrates the corresponding velocity and temperature flow patterns at various distinct Grashof number points. At $G_r=0$, two symmetric vortex flows are observed in the secondary flow, while a straightforward contour is seen in the axial flow. The majority of the flow is concentrated near the top and bottom for the secondary velocity and closer to the outer wall for the axial velocity. The temperature distribution is not present at $G_r=0$ but becomes active with increasing Grashof numbers. Across all G_r values, the cooling wall temperature flow dominates over the heating wall. However, asymmetrical temperature structures gradually intensify as positive G_r values increase. In contrast, these structures become asymmetrical but in the opposite direction as G_r moves in a negative direction. This asymmetry is a result of the gravitational influence on the system.

B. Effects of Taylor Number (T_r) on the fluid flow and Temperature

Regarding the impact of rotation parameters (T_r) on the flow, it's important to note that a positive T_r indicates the rotational direction of the system coincides with the directions of the duct flow, which is termed co-rotation. On the other hand, for negative T_r , the rotational direction of the system opposes the directions of the duct flow, known as counter-rotation. Figure 5.10a illustrates the solution curve of the Taylor Number (T_r) concerning (i) Flux (Q) and (ii) Mean Nusselt number (Nu) at both the cooling and heating walls. These results are presented for fixed values of $\delta=0.1$, $D_n = 500$, $G_r = 100$, $P_r = 7$, $M = 0$, $m = 0$ and $\alpha=0$.

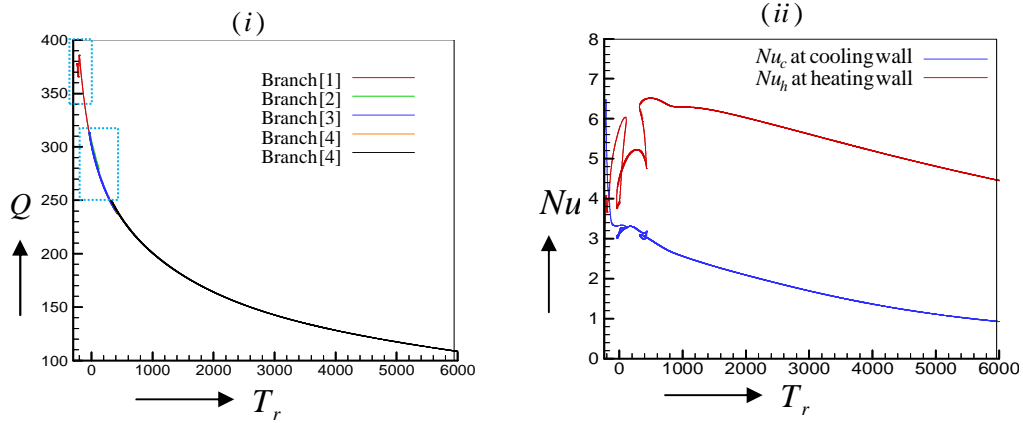


Fig. 5.10a: Solution Curve: Taylor number T_r versus (i) Flux Q (ii) Mean Nusselt number Nu at the heating and cooling wall for fixed $\delta=0.1$, $D_n=500$, $G_r=100$, $P_r=7$, $M=0$, $m=0$ and $\alpha=0$.

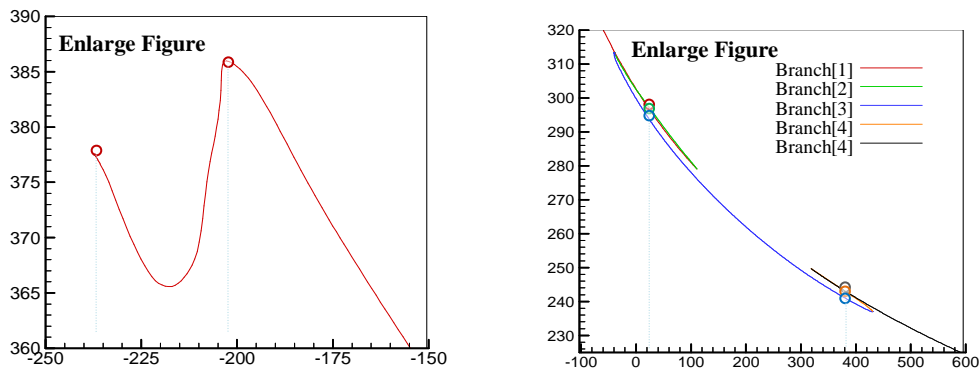


Figure 5.10b: Magnifying figure marked by the dashed box on Fig. 5.10a

Figure 5.10b provides an enlarged view of a specific portion highlighted by dotted rectangular boxes in Figure 5.10a (i). In Figure 5.10c, the flow structure of velocity and temperature distribution is presented at various distinct points of the Taylor Number (T_r). At the peak point on the solution curve, where the flux is 385.97, six vortices with asymmetric structures in the secondary flow are observed. Moving in the positive direction, five bifurcation solution curves are evident, creating a bifurcation zone within the range $-40.32 \leq T_r \leq 430.43$. All these curves exhibit a decreasing trend, indicating a gradual decrease in flux with increasing T_r . However, in the negative direction, a critical zone is reached, and the Taylor number cannot exceed $T_r = -237.44$. In these flow patterns, the primary characteristics include the concentration of flow near the top and bottom for secondary velocity and near the outer wall for axial velocity, with the centre of contours positioned in the middle of the duct. The axial flow contours maintain a simple shape. Positive-directed secondary flow predominates over the negative flow, particularly evident near the 2nd and 3rd branches of the solution curve. The strength of the flow patterns gradually weakens with increasing T_r . Across all cases, the initial asymmetrical conditions transform into a more symmetric form as T_r increases, signifying a reduction in asymmetry. Regarding temperature, the Nusselt number values at the heating wall are initially lower than those at the cooling wall within a limited range, after which this effect reverses. On average, temperature deviations gradually decrease with increasing T_r .

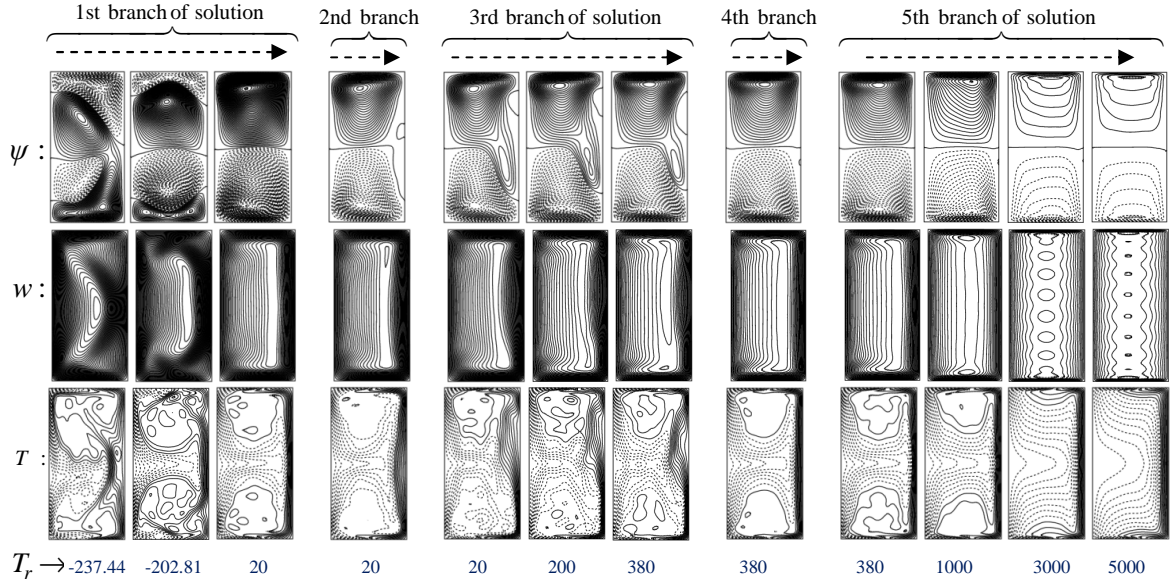


Figure 5.10c: Streamlines ψ (top), axial Contour flow w (middle) and Temperature profile T (bottom) in accordance with the solution curve in Fig. 5.10a

C. Effect of Dean Number (D_n) on the fluid flow and Temperature

Figures 5.11a (i)-(iii) depict the solution curve of Dean Number (D_n) concerning velocity flux (Q) and Figures 5.11a (iv)-(vi) display the solution curve of D_n with respect to the mean Nusselt number (Nu) at both the heated and cooled walls for temperature distribution. These illustrations are provided for three different curvatures: $\delta=0.01$, $\delta=0.1$, and $\delta=0.5$. The parameters $T_r=20$, $G_r=100$, $P_r=7$, $M=0$, $m=0$, and $\alpha=0$ are kept constant.

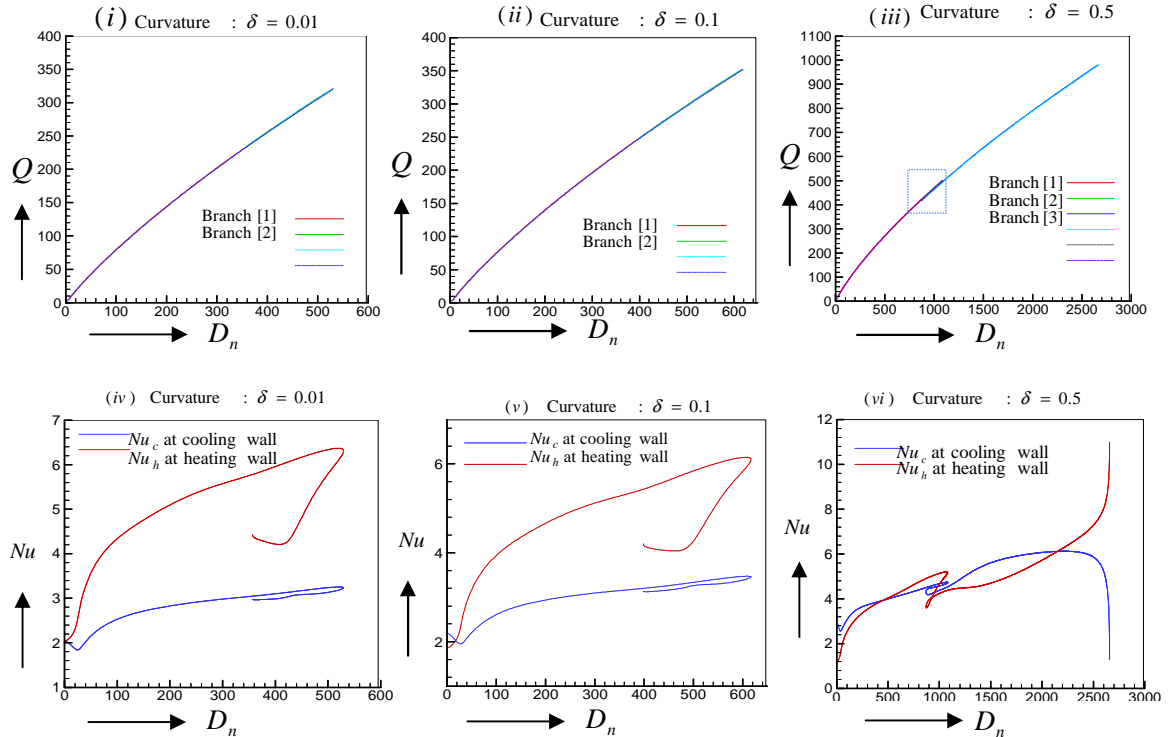


Figure 5.11a: Solution Curve: (i)-(iii) Dean Number D_n versus Flux Q (iv)-(vi) Dean Number D_n versus Mean Nusselt number Nu at the heating and cooling wall for fixed $\delta=0.1$, $G_r = 100$, $P_r = 7$, $M = 0$, $m=0$ and $\alpha = 0$.

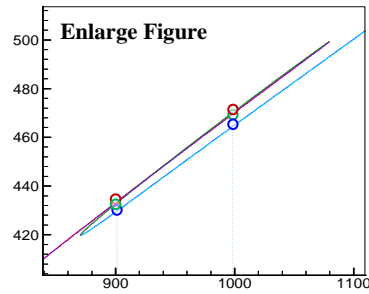
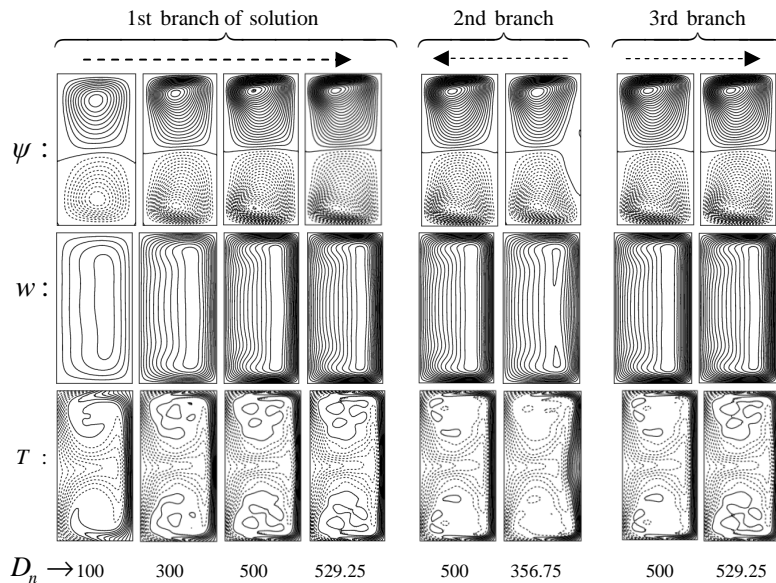
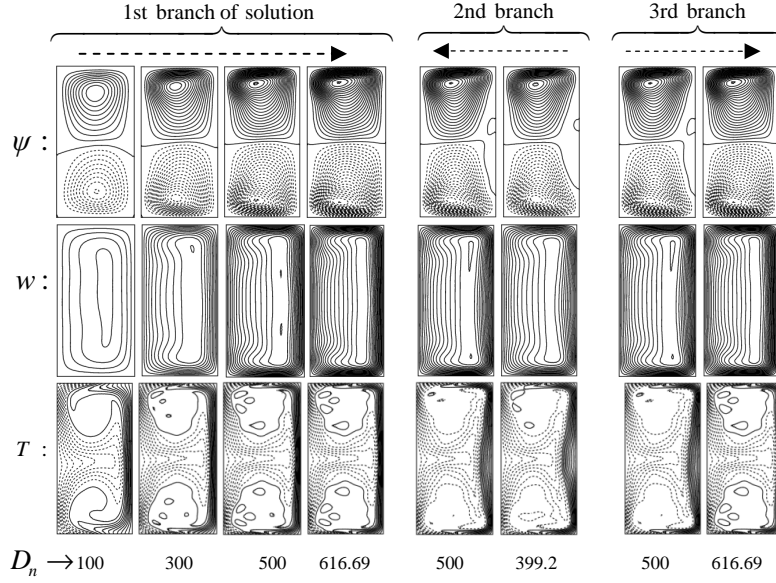


Figure 5.11b: Magnifying figure marked by the dashed box on Fig. 5.11.a(iii)

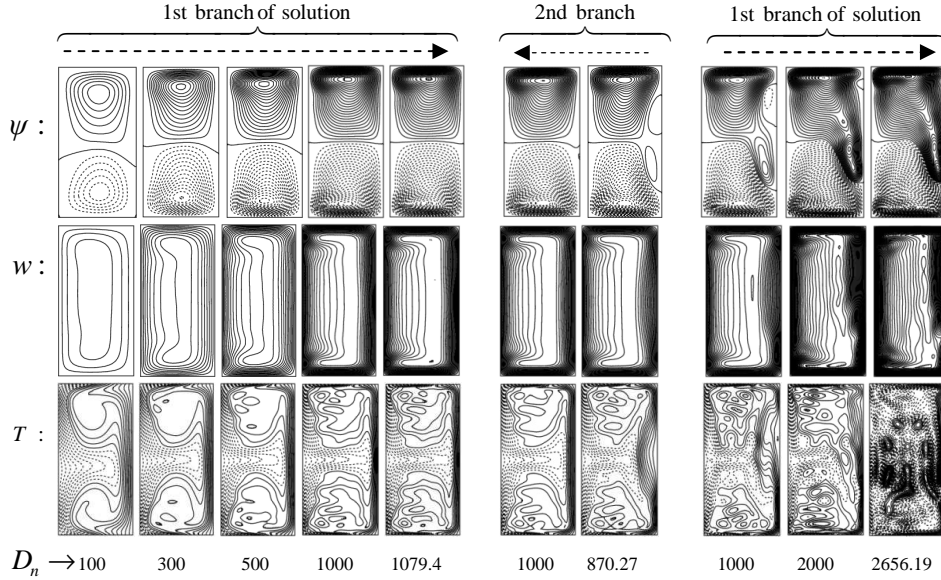
In Figure 5.11b, It has been seen the enlarged figures of a specific portion marked by dotted rectangular boxes in Figure 5.11a (iii). When examining the velocity distribution, two bifurcation branches of the solution curve are identified for $\delta=0.01$ and $\delta=0.1$, while three branches of the solution curve are observed for $\delta=0.5$. Bifurcation branches are distinguished by different colors. The solution curves cover a wide range of Dean Numbers, specifically $0 < D_n \leq 529.25$ for $\delta=0.01$, $0 < D_n \leq 616.69$ for $\delta=0.1$, and $0 < D_n \leq 2656.19$ for $\delta=0.5$. It's notable from Figure 5.11a (i), (ii), and (iii) that the maximum flux occurs at $D_n = 529.25$ for $\delta=0.01$ (320.4), at $D_n = 616.69$ for $\delta=0.1$ (351.83), and at $D_n = 2656.19$ for $\delta=0.5$ (978.41). This suggests that the flux increases as the duct's curvature increases. In general, across all cases, fluxes increase with higher values of D_n . Figure 5.11c showcases the flow structure of velocity and temperature distribution at various D_n points. In all cases, asymmetric vortex solutions are observed in radial flow, axial flow exhibits a simple contour, and temperature distribution maintains a typical pattern as D_n increases. Positive rotational flow dominates over negative rotational flow, particularly near the duct's outer wall for radial velocity. The temperature distribution becomes chaotic with larger Dean Numbers and greater curvature. The density of the velocity distribution gradually strengthens at higher Dean Numbers.



(i) : Solution structures for $\delta = 0.01$, $G_r = 100$, $T_r = 20$, $P_r = 7$, $M = 0$, $m = 0$ and $\alpha = 0$



(ii) : Solution structures for $\delta = 0.1$, $G_r = 100$, $T_r = 20$, $P_r = 7$, $M = 0$, $m = 0$ and $\alpha = 0$



(iii) : Solution structures for $\delta = 0.5$, $G_r = 100$, $T_r = 20$, $P_r = 7$, $M = 0$, $m = 0$ and $\alpha = 0$

Figure 5.11c (i)-(iii): Streamlines ψ (top), axial Contour flow w (middle) and Temperature profile T (bottom) in accordance with the solution curve in Fig. 5.11a

D. Effects of Magnetic Parameter (M) on the fluid flow and Temperature

Figure 5.12a illustrates the solution curve of the magnetic parameter (M) with respect to (i) velocity flux (Q) and (ii) mean Nusselt number (Nu) at the heated and cooled walls for temperature distribution. This is examined across three cases: as Case-I: $\delta=0.01$, $D_n = 500$, Case-II: $\delta=0.1$, $D_n = 500$, and Case-III: $\delta=0.5$, $D_n = 1000$., with fixed values of $T_r=20$, $G_r=100$, $P_r=7$, $m=1$ and $\alpha=0$. In all three cases, the solution curves exhibit two branches: one branch where the steady solution remains stable for all values of the magnetic parameter (M), and another branch featuring a stable steady solution within the approximate range of $0 \leq M \leq 5.7$, $0 \leq M \leq 4.63$, and $0 \leq M \leq 5.45$ for Cases I, II, and III, respectively.

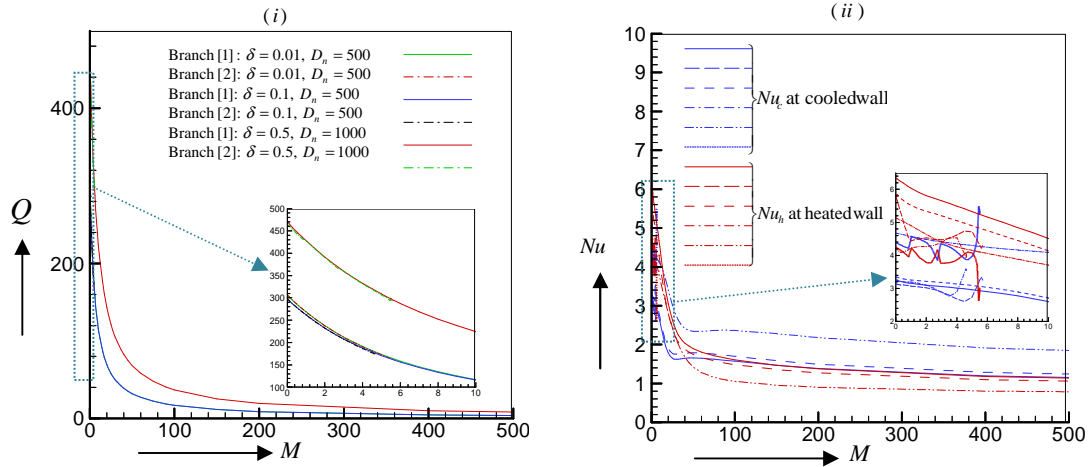
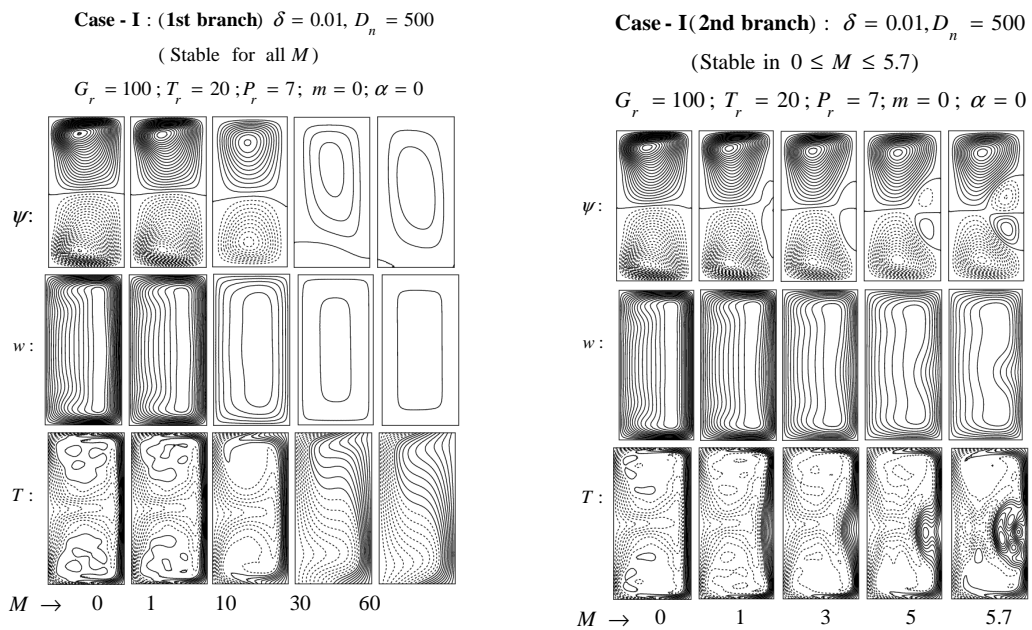


Figure 5.12a: Solution Curve: Magnetic parameter M versus (i) Flux Q
 (ii) Mean Nusselt number Nu at the heating and cooling wall for the Case-I : $\delta=0.01$,
 $D_n = 500$; Case-II : $\delta=0.1, D_n = 500$; Case-III : $\delta=0.5, D_n = 1000$;
 with fixed $G_r = 100$, $T_r = 20$, $P_r = 7$, $m=0$ and $\alpha = 0$.

The behaviour of the flux is notable in relation to the magnetic parameter (M). It exhibits a rapid decrease as M increases, and after reaching a specific critical value, the solution stabilizes into a steady state. From Figure 5.12a (ii), it's evident that the non-isothermal flow gradually transitions towards an isothermal state for a significant value of the magnetic parameter. Figures 5.12b, representing Case-I to Case-III, show the flow structures of velocity and temperature distribution corresponding to the solution curve in Figure 5.12a at



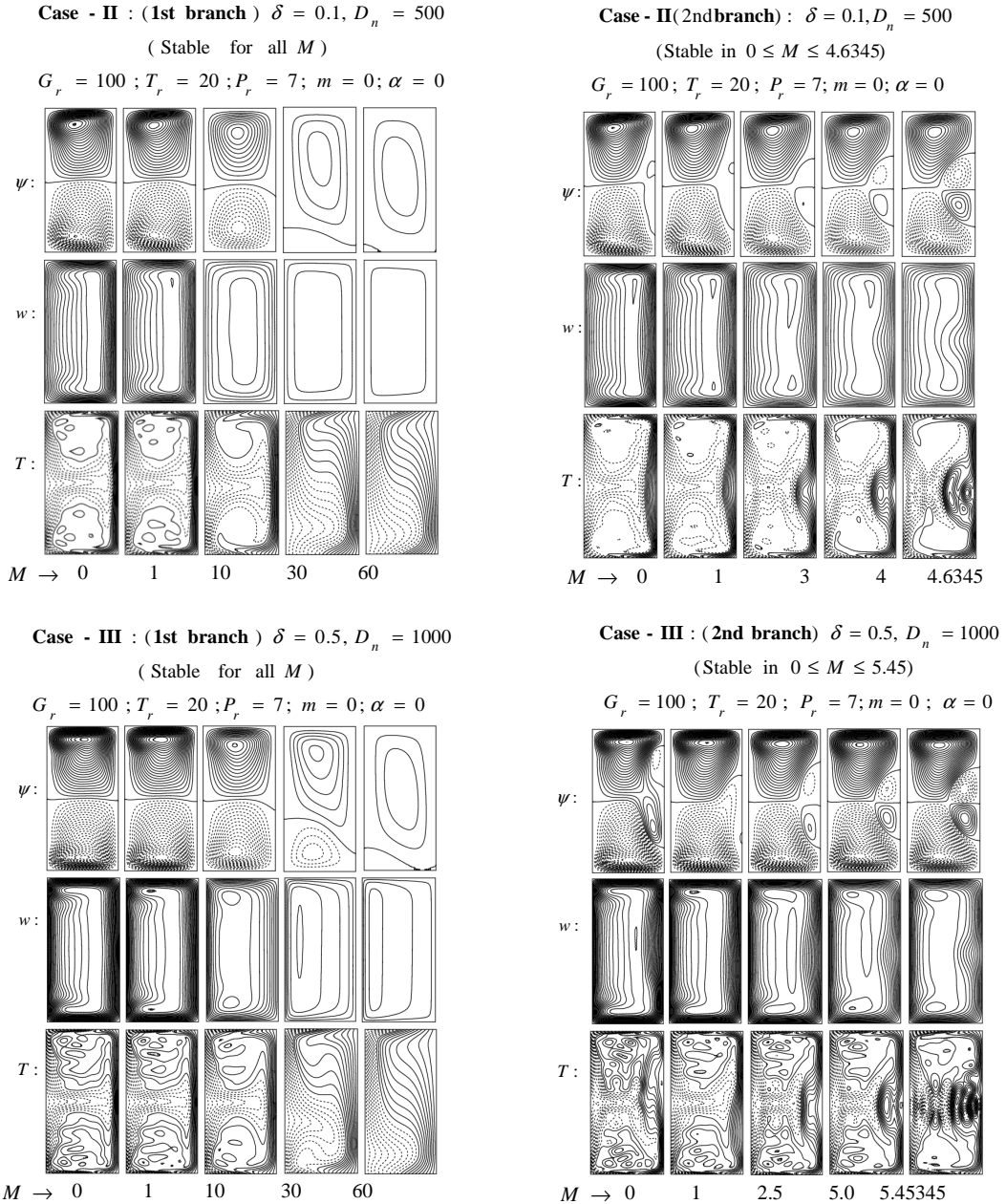


Figure 5.12b: Streamlines ψ (top), axial Contour flow w (middle) and Temperature profile T (bottom) in accordance with the solution curve in Fig. 5.12a

various distinct points of the magnetic parameter. For all cases in the first branch, two streamline vortices in radial flow are observed, and the axial flow contours gradually weaken as M increases. The positive-directed secondary flow (solid streamline) dominates over the negative flow with increasing M . The centre of the axial flow contour shifts towards the centre of the duct for Case-I and Case-II, but in Case-III, this centre shifts toward the inner wall. In the second branch, a two-vortex structure of radial flow is initially observed, and it generates two additional vortices near the outer wall of the duct as M increases within the respective ranges of $M \leq 5.7$, $M \leq 4.6345$, and $M \leq 5.45345$ for Cases I, II, and III. However, the contours of the axial flow remain simple, and the temperature distribution maintains its typical pattern as M increases.

E. Effects of Hall Parameter (m) on the fluid flow and Temperature

Figure 5.13a displays the solution curve of the Hall parameter (m) concerning (i) velocity flux (Q) and (ii) mean Nusselt number (Nu) at the heated and cooled walls for temperature distribution in four cases such as Case-I: $\delta=0.01, D_n = 500$, Case-II: $\delta=0.1, D_n = 500$, Case-III: $\delta=0.5, D_n = 500$ and Case-IV: $\delta=0.5, D_n = 1000$. Fixed values include $T_r = 20, G_r = 100, P_r = 7, M=4$, and $\alpha=0$. In each of these cases, there is a single branch in the solution curve, and the steady solution remains stable for all values of the Hall parameter (m). The flux experiences a rapid increase as the Hall parameter (m) increases, and after reaching a significant value, a steady-state solution is achieved in all instances. As indicated in Figure 5.13a (ii), the non-isothermal flow does not transform into an isothermal state for any value of the Hall parameter. Additionally, it's worth noting that the numerical results show that the maximum flux gradually decreases with an increase in curvature. This underscores that the flux increases with an increase in the Dean Number.

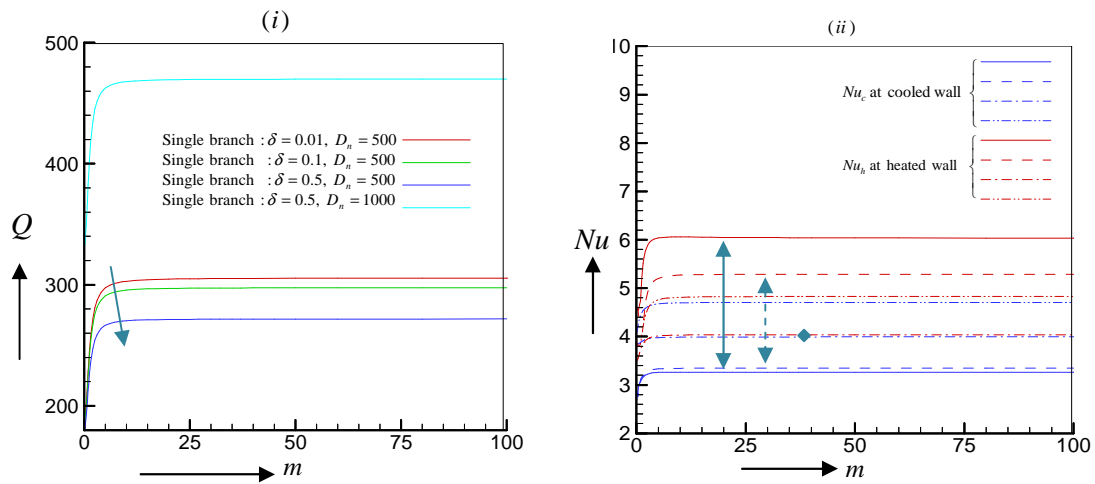


Figure 5.13a: Solution Curve: Hall parameter m versus (i) Flux Q (ii) Mean Nusselt number Nu at the heating and cooling wall for the Case-I: $\delta=0.01, D_n = 500$; Case-II: $\delta=0.1, D_n = 500$; Case-III: $\delta=0.5, D_n = 1000$; with fixed $G_r = 100, T_r = 20, P_r = 7, M=4$ and $\alpha = 0$.

Figures 5.13b (represents Case-I to Case-III) depict the flow structures of velocity and temperature distribution corresponding to the solution curve presented in Figure 5.13a at various distinct points of the Hall parameter. It's evident that the structures of velocity and temperature distribution undergo minor changes as the Hall parameter increases. In Cases I and II, the negative-directed secondary flow (dashed streamline) dominates over the positive flow as the Hall parameter (m) increases. Conversely, in Cases III and IV, it is observed that the positive-directed secondary flow (dotted streamline) dominates over the negative flow. The strength of the flow patterns, both in velocity and temperature, becomes notably stronger within a specific range of Hall parameters, approximately within the range of $0 \leq m \leq 8$. Afterward, there is a slight change in the pattern with further increases in the Hall parameter.

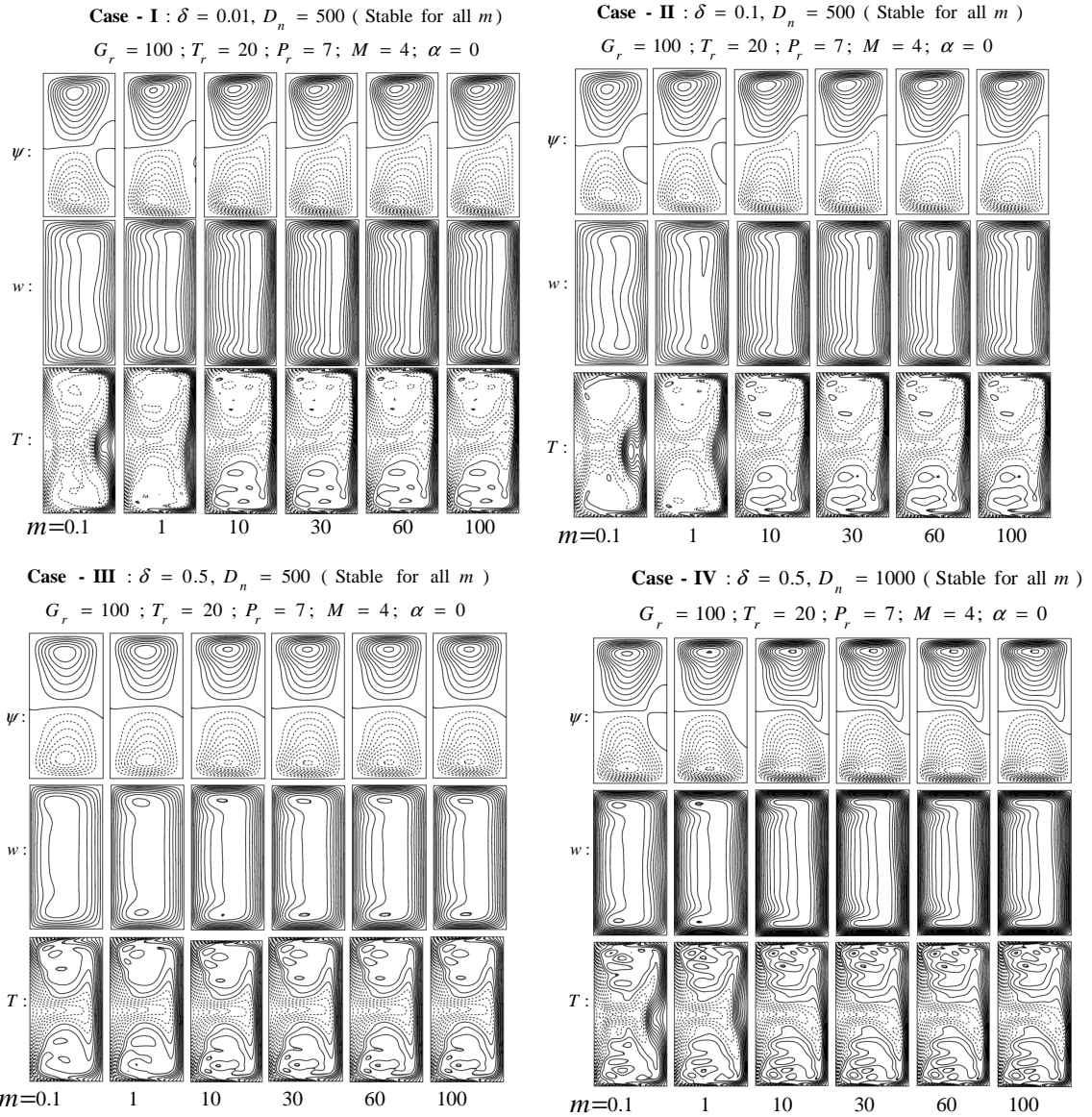


Figure 5.13b: Streamlines ψ (top), axial Contour flow w (middle) and Temperature profile T (bottom) in accordance with the solution curve in Fig. 5.13a

F. Effects of Ion-slip Parameter (α) on the fluid flow and Temperature

Figure 5.14a presents the solution curve of the Ion-slip parameter (α) in relation to (i) velocity flux (Q) and (ii) mean Nusselt number (Nu) at the heated and cooled walls for temperature distribution. This analysis is conducted for four distinct scenarios: as Case-I: $\delta=0.01, D_n = 500$, Case-II: $\delta=0.1, D_n = 500$, Case-III: $\delta=0.5, D_n = 500$ and Case-IV: $\delta=0.5, D_n = 1000$. Fixed values for this investigation include $T_r = 20, G_r = 100, P_r = 7, M = 4$, and $m=1$. In each of these scenarios, there is a single branch in the solution curve, and the steady solution remains stable for all values of the Ion-slip parameter (α). The flux experiences a rapid increase within a short range of the Ion-slip parameter, and after reaching a specific critical value of α , a steady-state solution is achieved.

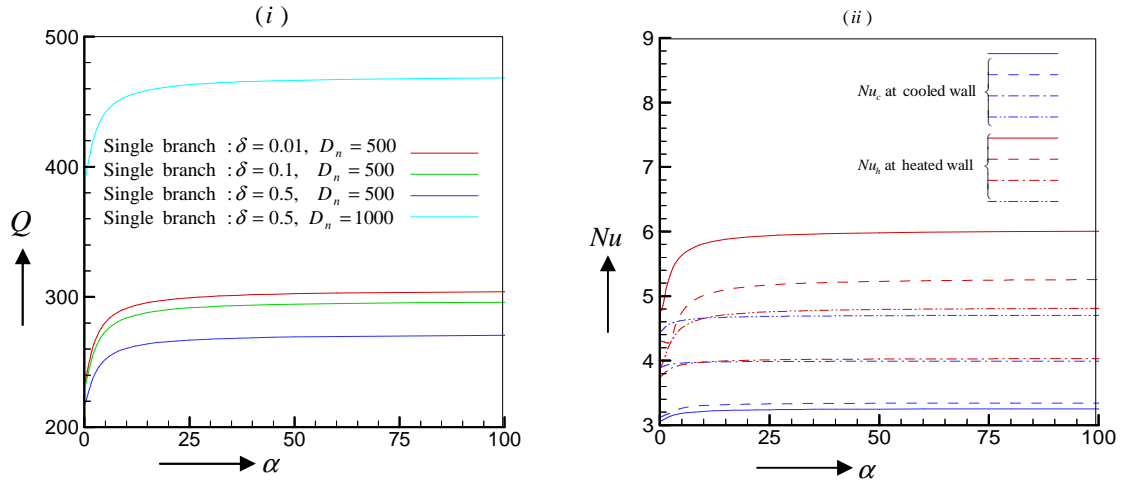
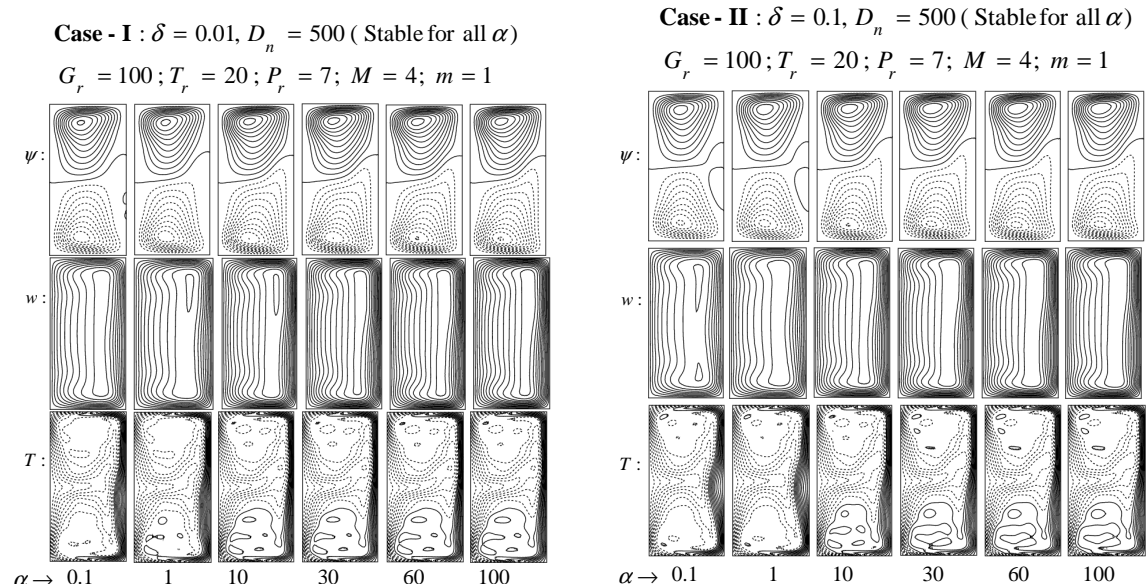


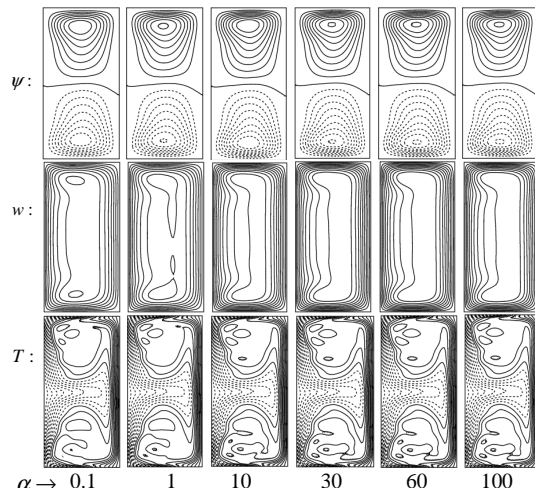
Figure 5.14a: Solution Curve: Ion-slip parameter α versus (i) Flux Q
(ii) Mean Nusselt number Nu at the heating and cooling wall for the
Case-I : $\delta=0.01, D_n = 500$; Case-II : $\delta=0.1, D_n = 500$; Case-III : $\delta=0.5,$
 $D_n = 1000$; with fixed $G_r=100, T_r = 20, P_r = 7, M=4$ and $m = 1$.

Figure 5.14a (ii) clearly indicates that the non-isothermal flow does not transition into an isothermal state for any value of the Ion-slip parameter. In addition, the numerical results demonstrate that the maximum flux gradually decreases with an increase in the curvature. Furthermore, it confirms that the flux increases with higher values of the Dean Number. Figures 5.14b, denoted as Case-I to Case-IV, depict the flow structures of velocity and temperature distribution corresponding to the solution curve presented in Figure 5.14a at various distinct points along the Ion-slip parameter. These figures reveal that the structures of velocity and temperature distributions exhibit minor changes with an increase in the Ion-slip parameter. The effects of the Ion-slip parameter on the velocity and temperature distributions mirror the effects of the Hall parameter, as previously described.



Case - III : $\delta = 0.5, D_n = 500$ (Stable for all α)

$G_r = 100; T_r = 20; P_r = 7; M = 4; m = 1$



Case - IV : $\delta = 0.5, D_n = 1000$ (Stable for all α)

$G_r = 100; T_r = 20; P_r = 7; M = 4; m = 1$

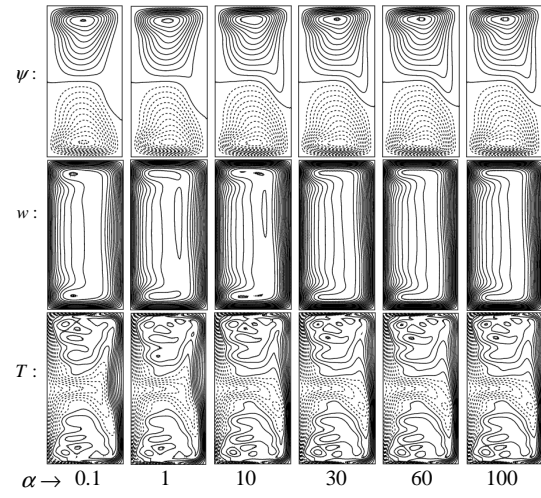


Figure 5.14b: Streamlines ψ (top), axial Contour flow w (middle) and Temperature profile T (bottom) in accordance with the solution curve in Fig. 5.14a

5.6 Curved Rectangular Duct for Non-Isothermal Fluid Flow (Aspect Ratio 3):

Non-Isothermal Fluid Flow through a Rotating Curved Duct with Aspect Ratio of 3 in the Presence of Magnetic Field, Hall, and Ion-slip Currents

In this study, the effects of Hall and ion-slip currents on the flow are investigated, when a fully developed non-isothermal, steady viscous, incompressible fluid flows through the centreline of a curved duct of a relatively large aspect ratio (3) in the presence of a magnetic field with rotation. This duct is generated non-isothermal by keeping the heated outer wall and cooled inner wall; the lower and upper walls are taken adiabatic. The gravitational force, pressure gradient force, Lorentz force, Coriolis force, and centrifugal force act on the flow as an external force. These forces are produced in that order by the effects of gravity, pressure exerted on the flow, magnetic field with Hall and Ion-slip current, rotation, and duct curvature. The pressure gradient forces (or Dean Forces) are applied along the duct's centreline. Therefore, due to the combined action of these forces, the flow is accelerated along the centreline direction of the curved duct. The spectral approach is used as the main tool to carry out the numerical solutions. In contrast, the Newton-Raphson, Chebyshev polynomial, Arc-length and Collocation methods are used as supporting tools. The solution curve for the flux versus above-mentioned parameter is used to investigate the effects of the parameters Grashof number (G_r), Taylor number (T_r), Dean Number (D_n), magnetic parameter (M), Hall parameter (m), and Ion-slip parameter (α) on the flow of the velocity and temperature profiles, and their corresponding flow structures are examined at various cross-sections on the curved duct. The results have been presented under several values of M , m , and at Dean Number $D_n = 300$ curvature of the duct $\delta = 0.1$, and with the Taylor number is at $T_r = 20$.

5.6.1 Grid Spaces Accuracy

Prior to execute the FORTRAN program, it is required to discuss grid space accuracy. To achieve good accuracy, it is assumed that the value of \bar{N} is three times that of \bar{M} . Several pairs of the truncation numbers (\bar{M}, \bar{N}) such as (08, 28), (09, 27), (10, 30) and (11, 33) are used to solve the equations. The flux Q , mean Nusselt number at the heating wall Nu_h and cooling wall Nu_c have been calculated for the above mentioned pairs of truncation number (\bar{M}, \bar{N}) in Table-6. The reasonable accuracy of the numerical solutions can be found at (\bar{M}, \bar{N})=(10,30).

\bar{M}	\bar{N}	Q	Nu_c	Nu_h
08	24	357.2666413022296	3.582898511659145	5.274281332623154
09	27	357.4344730996830	3.475725455807831	5.361503057468419
10	30	357.9893487357052	3.465119587366944	5.662430447047709
11	33	359.0095108103720	3.496575983295057	5.435040381200298

Table-6: Fluxes Q and mean Nusselt number Nu_c and Nu_h for distinct pairs of truncation numbers \bar{M} and \bar{N} for fixed $\delta=0.1$, $D_n = 1000$, $G_r = 100$, $T_r = 20$, $P_r = 7$, $M = 0$, $m = 0$ and $\alpha=0$.

5.6.2 Results and Discussion

The characteristics of the flow patterns were initially studied while maintaining fixed values for the magnetic parameter (M), Hall parameter (m), and Ion-slip parameter (α) at zero, in order to investigate the effects of the Grashof number (G_r), Taylor number (T_r), and Dean number (D_n) on the flow. This examination was conducted with an aspect ratio $l=3$. Additionally, these findings have been compared with that had already been published. The solution curve has demonstrated the impact of several parameters the magnetic, Hall, and Ion-slip on fluid flow. Their respective flow structures at various places are shown when Taylor number is at $T_r=20$, Prandtl number is at $P_r=7$, the duct's curvature is at $\delta=0.1$, and Dean number is at $D_n=300$. The direction of the solution curve is denoted by the dashed arrow notation ($---\blacktriangleright$) above the flow structures. In the figures, the external side of the curved duct is indicated by the right side of each duct box. In the context of the velocity profile, the solid lines represent the anti-clockwise direction of the flow, which corresponds to positive-directed flow ($\psi>0$). Conversely, the dotted lines represent the clockwise or negative-directed flow ($\psi<0$) for the velocity distribution. Regarding the temperature profile, solid lines indicate regions where the temperature (T) is greater than zero, typically corresponding to the temperature at the heated fence. Conversely, the dotted lines represent regions where the temperature is less than zero, often associated with the temperature at the cooled fence. To create these profiles, increments of $\Delta w=10$ for velocity, $\Delta\psi=0.8$ for stream function, and $\Delta T=0.1$ for temperature were employed in the program.

A. Effects of Grashof Number (G_r) on the Fluid Velocity and Temperature

The influence of the Grashof number (G_r) on secondary velocity (radial and axial) and temperature is illustrated in Figure 5.15a-b. Figure 5.15a presents the solution curve of the Grashof Number (G_r) in relation to (i) velocity flux (Q) and (ii) mean Nusselt Number (Nu) at the heated and cooled walls. These results are presented with fixed values of $\delta=0.1$, $D_n=300$, $T_r=20$, $P_r=7.0$, $M=0$, $m=0$ and $\alpha=0$. In the context of velocity flux, a single branch of the solution curve is identified, bounded within the range of $-1170.75 \leq G_r \leq 1166$. Figure 5.15b displays the flow structures of temperature and velocity profiles at various Grashof number points. For secondary flow, two symmetric vortex flows are observed at $G_r=0$, but no temperature distribution is generated at this point. In contrast, a simple contour is found for the axial flow. Most of the flow is concentrated near the top and bottom of the duct. The structure of the solution is influenced by the increasing Grashof number, causing both positive and negative flows to grow, resulting in asymmetric flow structures. This asymmetry is attributed to the force of gravity. Additionally, it's noteworthy that the Nusselt number at the heating wall is higher than that at the cooling wall. The temperature deviation undergoes gradual changes with an increase in G_r .

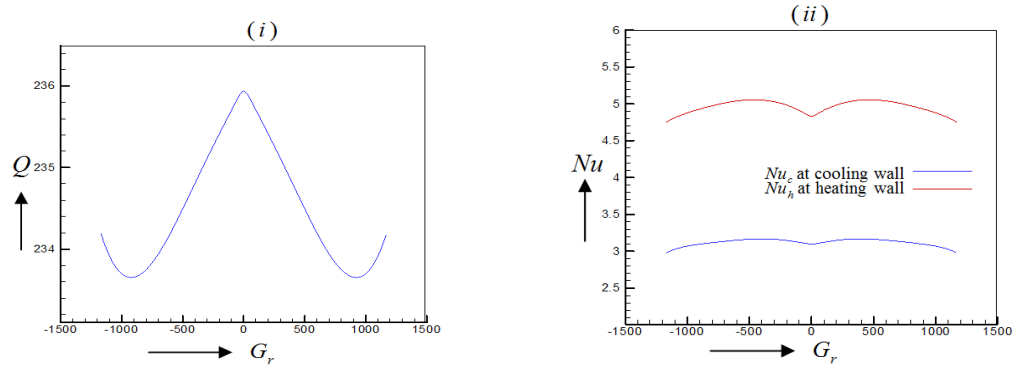


Figure 5.15a: Solution curve: Grashof Number \bar{G}_r versus (i) flux Q (ii) Mean Nusselt number Nu at the heating and cooling wall for fixed $\delta=0.1$, $T_r=20$, $D_n=300$, $P_r=7$, $M=0$, $m=0$ and $\alpha=0$.

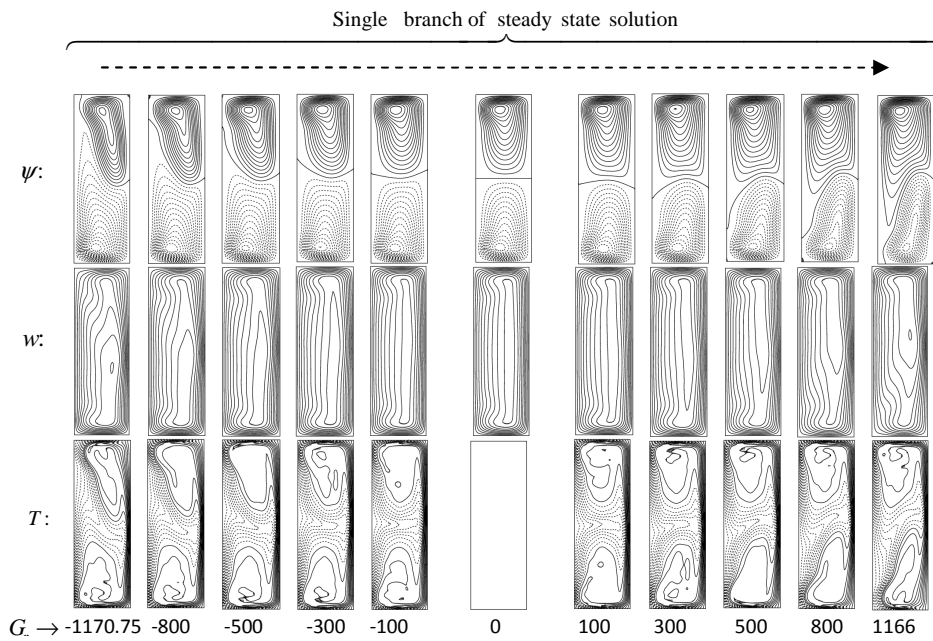


Figure 5.15b: Streamlines ψ (top), axial Contour flow w (middle) and Temperature profile T (bottom) in accordance with the solution curve in Fig.5.15a.

B. Effects of Taylor Number (T_r) on the Fluid Velocity and Temperature

The impact of the Taylor number (T_r) on secondary velocity (radial and axial flows) and temperature is presented in Figure 5.16a-b. Figure 5.16a displays the solution curve of the Taylor Number (T_r) with respect to (i) velocity flux (Q) and (ii) mean Nusselt Number (Nu) at the heated and cooled walls. These results are presented with fixed values of $\delta=0.1$, $D_n=300$, $G_r=100$, $P_r=7.0$, $M=0$, $m=0$ and $\alpha=0$

It is observed that the solution curve is bounded in the negative direction of T_r , and for positive T_r , it represents a decreasing function, indicating that the flux gradually decreases with increasing T_r . In Figure 5.16b, the flow structures of temperature and velocity profiles

are depicted at various points along the Taylor number. For secondary flow, both two-vortex and four-vortex structures have been identified. The strength of the flow pattern gradually weakens with an increase in positive T_r . However, in the negative direction of T_r , a critical zone is observed. Within this critical zone (approximately $-174.62 < T_r \leq -120$), four asymmetric vortex structures are generated on the solution curve. For the axial flow, simple contours are found. The structure of the temperature distribution is presented in the third row of Figure 5.16b. Notably, for positive T_r , the values of the Nusselt number at the heating wall are lower than those at the cooling wall. The cooling wall's temperature dominates over the heating wall as T_r increases in the positive direction. The strength of the flow pattern gradually weakens with an increase in positive T_r .

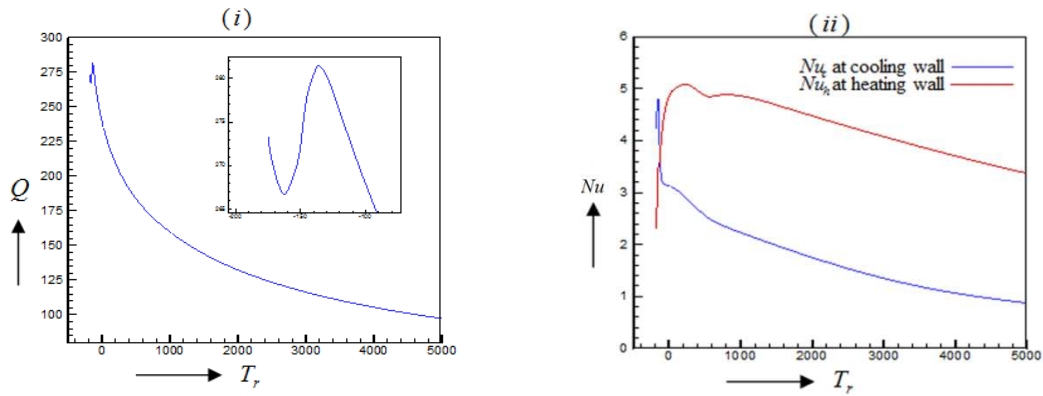


Figure 5.16a: Solution curve: Taylor Number T_r versus (i) flux Q (ii) Mean Nusselt number Nu at the heating and cooling wall for fixed $\delta=0.1$, $G_r = 100$, $D_n = 300$, $P_r = 7$, $M = 0$, $m = 0$ and $\alpha=0$.

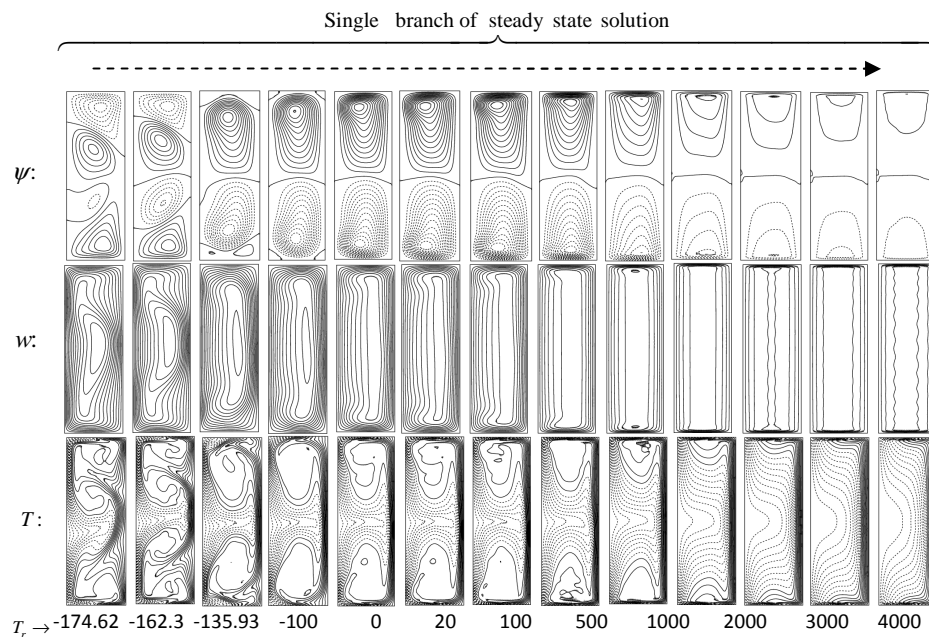


Figure 5.16b: Streamlines ψ (top), axial Contour flow w (middle) and Temperature profile T (bottom) in accordance with the solution curve in Fig.5.16a.

C. Effect of Dean Number (D_n) on the Fluid Velocity and Temperature

The influence of the Dean Number (D_n) on secondary velocity (radial and axial flows) and temperature is depicted in Figure 5.17a-b. Figure 5.17a displays the solution curve of the Dean Number (D_n) concerning (i) velocity flux (Q) and (ii) mean Nusselt Number (Nu) at the heated and cooled walls. These results are presented with fixed values of $\delta=0.1$, $T_r=20$, $G_r=100$, $P_r=7.0$, $M=0$, $m=0$ and $\alpha=0$.

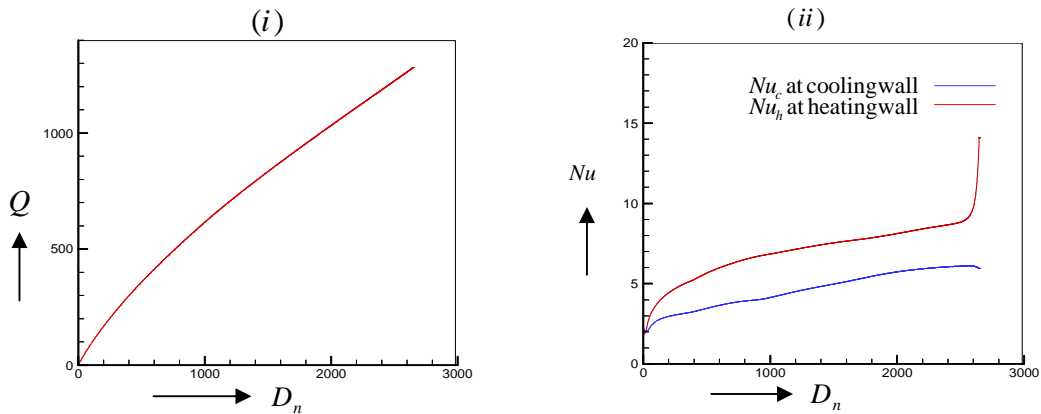


Figure 5.17a: Solution curve: Dean Number D_n versus (i) flux Q (ii) Mean Nusselt number Nu at the heating and cooling wall for fixed $\delta=0.1$, $T_r=20$, $G_r=100$, $P_r=7$, $M=0$, $m=0$ and $\alpha=0$.

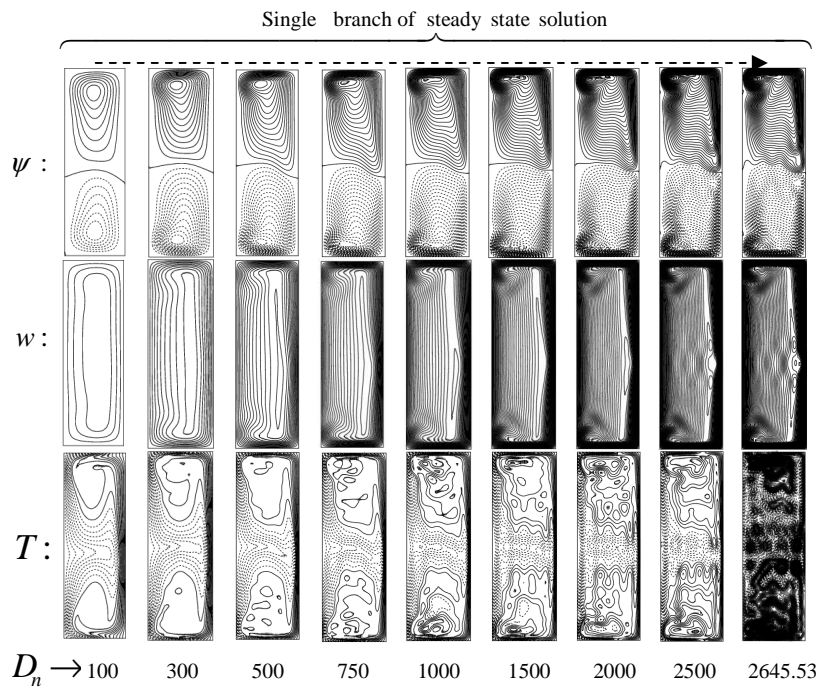


Figure 5.17b: Streamlines ψ (top), axial Contour flow w (middle) and Temperature profile T (bottom) in accordance with the solution curve in Fig.5.17a.

A single branch of the solution curve is observed, spanning a wide range of Dean Numbers. This curve represents an increasing function, signifying that the flux gradually increases with an increase in D_n . However, the steady solution ceases to exist when a high-pressure gradient force is exerted on the flow, approximately at $D_n > 2645.53$. The maximum flux is

found at $D_n=2645.527$, reaching a value of 1282.12. Figure 5.17b showcases the flow structures of velocity and temperature profiles at various points along the Dean number corresponding to the solution curve in Figure 5.17a. As the Dean Number increases, asymmetric vortex solutions become evident. The strength of velocity progressively intensifies. In terms of temperature, it's observed that the Nusselt number values at the heating wall exceed those at the cooling wall. This deviation becomes more pronounced for large values of D_n , and at such magnitudes, the temperature distribution becomes chaotic.

D. Effects of Magnetic Parameter (M) on the Fluid Velocity and Temperature

The effects of the magnetic parameter on the secondary (radial and axial flows) velocity and on the temperature are illustrated in Fig. 5.18a-b. The solution curve of the magnetic parameter (M) versus (i) the flux (Q) and (ii) mean Nusselt Number (Nu) at the heated wall and at the cooled wall are shown in Fig.5.18a for fixed valued of $\delta=0.1$, $T_r=20$, $D_n=300$, $G_r=100$, $P_r=7.0$, $m=0$ and $\alpha=0$. These solution curves are the decreasing function therefore, it can be concluded that flux decreases with the increase of magnetic parameter and after a specific value of M ; it has a steady-state solution. For the temperature distribution, the values of the Nusselt number at the heating wall are higher than with the cooling wall until a certain value of M , and thereafter it has a reversed effect. The structures of vortex flow, contours of axial flow and temperature distribution have been demonstrated in Fig.5.18b corresponding to the solution curve of Fig.5.18a (i)-(ii) at several points of the magnetic parameter. In this case, two vortices streamline the secondary flow, and simple axial flow contours have been present for all values of M . As M increases, these flows rapidly degenerate into weak patterns. The positive directed secondary flow (solid line) dominates the negative directed secondary flow (dotted line), and this tendency grows as M increases. The centre of the axial flow contour has moved closer to the duct's centre. It has been noted from the solution curve shown in Fig. 5.18a(ii) and the temperature structure in the third row of Fig. 5.18b that the non-isothermal flow gradually transforms to the isothermal state for a particularly large value of the magnetic parameter.

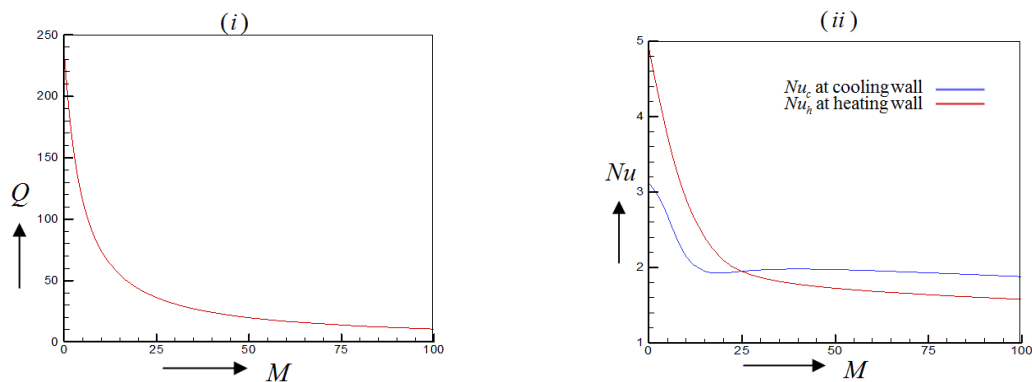


Figure 5.18a: Solution curve: Magnetic parameter M versus (i) flux Q (ii) Mean Nusselt number Nu at the heating and cooling wall for fixed $\delta=0.1$, $D_n=300$, $T_r=20$, $G_r=100$, $P_r=7$, $m=0$ and $\alpha=0$.

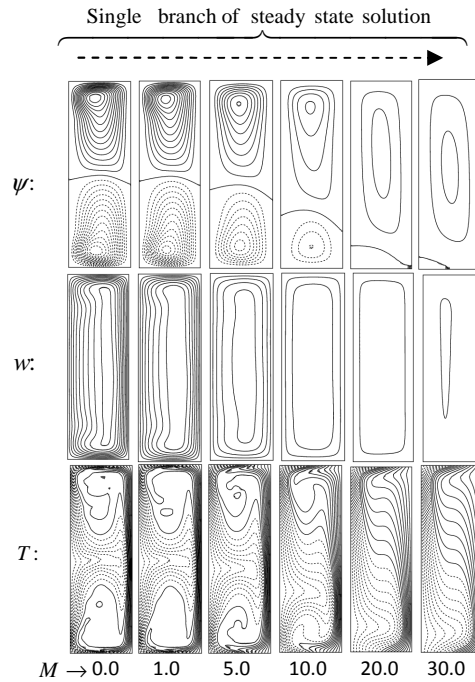


Figure 5.18b: Streamlines ψ (top), axial Contour flow w (middle) and Temperature profile T (bottom) in accordance with the solution curve in Fig.5.18a.

E. Effects of Hall Parameter (m) on the Fluid Velocity and Temperature

The effects of the Hall parameter (m) on secondary velocity (radial and axial flows) and temperature are depicted in Figure 5.19a-b. Figure 5.19a presents the solution curve of the Hall parameter (m) in relation to (i) velocity flux (Q) and (ii) mean Nusselt Number (Nu) at the heated and cooled walls. These results are presented with fixed values of $\delta=0.1$, $T_r=20$, $D_n=300$, $G_r=100$, $P_r=7.0$, $M=5$ and $\alpha=0$.

For all values of the Hall parameter (m), the solution curve consists of a single branch. The flux experiences rapid increases within a short range, specifically within $0 < m < 5$. After a specific value of m is reached, a steady-state solution is established for the velocity distribution. Figure 5.19b displays the structures of vortex flow, contours of axial flow, and temperature distribution at various points along the Hall parameter corresponding to the solution curve in Figure 5.19a (i)-(ii). For secondary flow, two vortices are consistently observed, and the axial flow maintains simple contours for all values of m . The flow pattern experiences slight changes as m increases. Throughout the range of $0 < m < 5$, the Hall parameter leads to a gradual increase in the flow's strength, after which the flow pattern remains constant. In terms of temperature, it's noteworthy that the cooling wall temperature consistently dominates over the heating wall temperature, and this dominating effect remains constant with changes in m for all cases of Dean Number. Nevertheless, gravity's influence contributes to an asymmetrical shape in the temperature distribution.

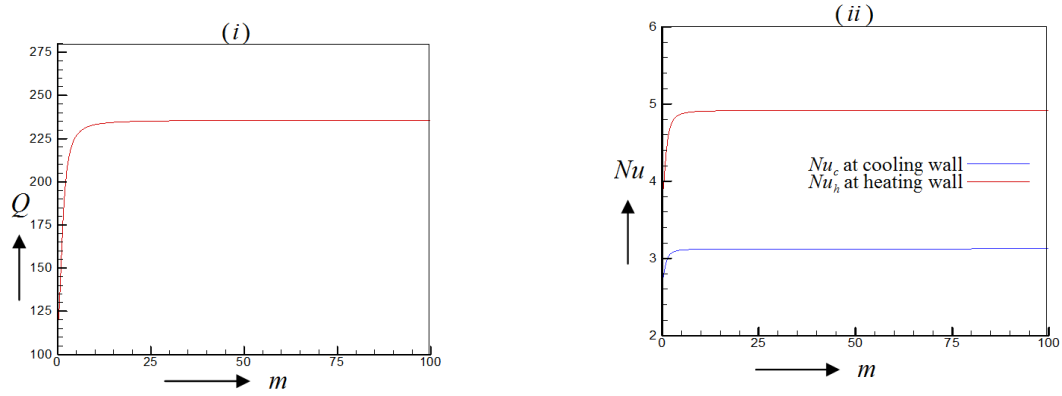


Figure 5.19a: Solution curve: Hall parameter m versus (i) flux Q (ii) Mean Nusselt number Nu at the heating and cooling wall for fixed $\delta=0.1$, $D_n = 300$, $T_r = 20$, $G_r = 100$, $P_r = 7$, $M = 5$ and $\alpha=0$.

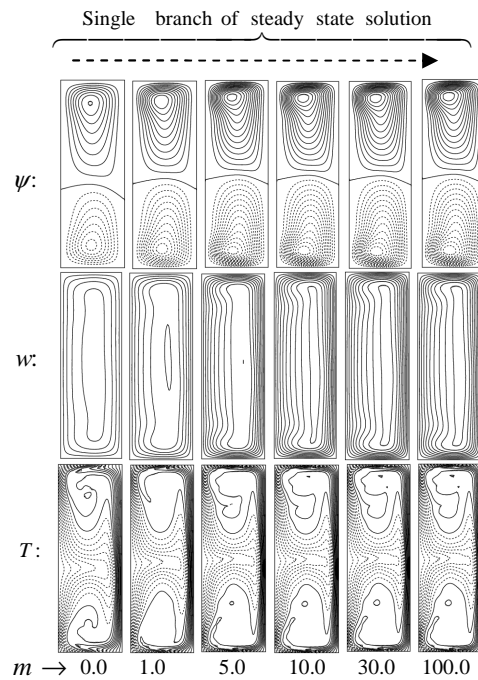


Figure 5.19b: Streamlines ψ (top), axial Contour flow w (middle) and Temperature profile T (bottom) in accordance with the solution curve in Fig.5.19a.

F. Effects of Ion-slip Parameter (α) on the Fluid Velocity and Temperature

The effects of the Ion-slip parameter (α) on secondary velocity (radial and axial flows) and temperature are illustrated in Figure 5.20a-b. Figure 5.20a presents the solution curve of the Ion-slip parameter (α) concerning (i) velocity flux (Q) and (ii) mean Nusselt Number (Nu) at the heated and cooled walls. These results are presented with fixed values of $\delta= 0.1$, $T_r=20$, $D_n=300$, $G_r=100$, $P_r = 7.0$, $M=5$ and $m=1$.

The solution curve exhibits a single branch for all values of the Ion-slip parameter. Within a relatively narrow range of the Ion-slip parameter, approximately $0 < \alpha < 25$, the flux experiences a sharp increase. Afterward, the increase becomes gradual, and eventually, a steady state is reached after a specific value of α . Figure 5.20b showcases the structures of vortex flow, contours of axial flow, and temperature distribution at various points along the

Ion-slip parameter corresponding to the solution curve in Figure 5.20a (i)-(ii). Simple contours are consistently found for the axial flow, and two vortex streamlines of secondary flow are present for all values of α . The increase in α leads to slight alterations in the flow patterns. The positive flow dominates over the negative-directed secondary flow (solid streamline) for all values of α . Within the range of $0 < \alpha < 5$, the flow strength gradually intensifies, and afterward, it remains constant. It is worth noting from the solution curve in Figure 5.20a (ii) and the temperature structure in the third row of Figure 5.20b that an increase in the Ion-slip parameter does not result in a transition from non-isothermal flow to an isothermal state. However, the influence of gravity contributes to an asymmetrical shape in the temperature distribution.

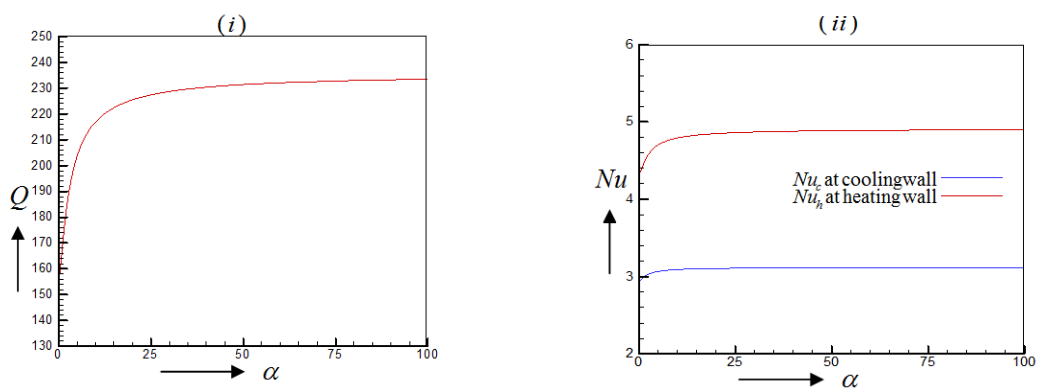


Figure 5.20a: Solution curve: Ion-slip parameter α versus (i) flux Q (ii) Mean Nusselt number Nu at the heating and cooling wall for fixed $\delta=0.1$, $D_n = 300$, $T_r = 20$, $G_r = 100$, $P_r = 7$, $M = 5$ and $m=1$.

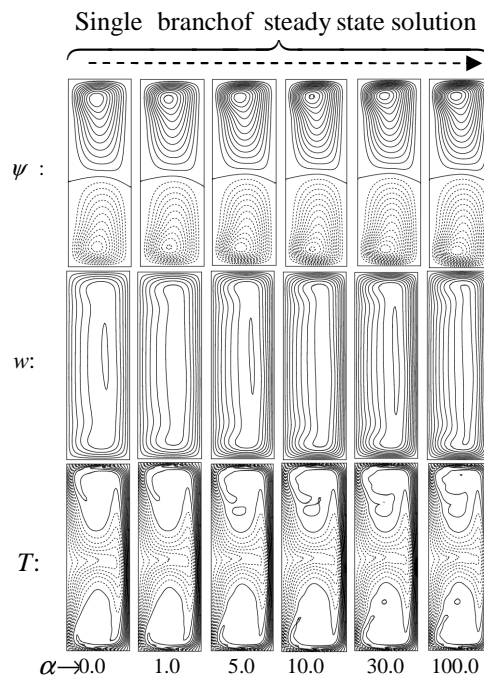


Figure 5.20b: Streamlines ψ (top), axial Contour flow w (middle) and Temperature profile T (bottom) in accordance with the solution curve in Fig.5.20a.

Chapter 6

Straight Duct Flow

6.1 Basic Governing Equations

Continuity equation:

$$\nabla \cdot \mathbf{q} = 0 \quad (6.1)$$

Momentum equation:

$$\frac{\partial \mathbf{q}}{\partial t} + (\mathbf{q} \cdot \nabla) \mathbf{q} = \mathbf{F} - \frac{1}{\rho} \nabla p - \nu \nabla^2 \mathbf{q} + \frac{1}{\rho} (\mathbf{J} \wedge \mathbf{B}) - 2(\boldsymbol{\Omega} \wedge \mathbf{q}) + \beta \mathbf{g} T \quad (6.2)$$

Energy equation

$$\frac{\partial T}{\partial t} + (\mathbf{q} \cdot \nabla) T = \frac{k}{\rho C_p} \nabla^2 T \quad (6.3)$$

Ohm's Law:

$$\mathbf{J} = \sigma(\mathbf{E} + \mathbf{q} \wedge \mathbf{B})$$

Due to the action of Hall and ion slip current on the fluid, Ohm's law is generalized as

$$\mathbf{J} = \sigma \mu_e (\mathbf{q} \wedge \mathbf{B}) - \frac{m}{B_0} (\mathbf{J} \wedge \mathbf{B}) + \frac{m\alpha}{B_0^2} (\mathbf{J} \wedge \mathbf{B}) \wedge \mathbf{B} \quad (6.4)$$

6.1.1 Momentum Equation with Hall and Ion-slip Currents through a Rotating Square Duct.

Let us consider viscous, laminar, incompressible, two-dimensional, MHD fluid flow through the straight duct has been placed in a rotating coordinate system, which is rotated with an angular velocity Ω around its vertical z -axis and x, y -axes are perpendicular to it. Due to square duct flow, the governing equations are considered as in terms of Cartesian coordinate system. Let \mathbf{q} velocity whose components are u, v and w , which directed along the directions of x, y and z respectively and $\mathbf{g} = (0, 0, g)$ is the gravitational vector. The geometrical configuration with curved duct is shown in Fig. 6.1:

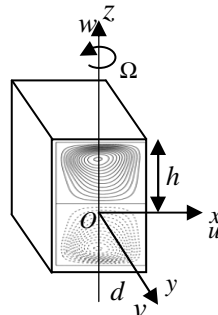


Fig.6.1: Geometrical model of straight duct

Suppose the straight duct rotates about its vertical z -axis,

But $\nabla \cdot \boldsymbol{\Omega} = 0$ gives that $\frac{\partial \Omega_z}{\partial z} = 0$

Or, $\Omega_z = \text{constant} = \Omega_0$ (say)

$$\therefore \boldsymbol{\Omega} = (0, 0, \Omega_0) = \hat{k} \Omega_0$$

Consider the centreline direction of the duct is taken as along y -axis, and the direction of the magnetic force is transverse to y -axis, which is along z -axis. Therefore the magnetic field vector is defined as $\mathbf{B} = (0, 0, B_z)$.

Similarly $\nabla \cdot \mathbf{B} = 0$ Or, $\frac{\partial B_z}{\partial z} = 0$

Or, $B_z = \text{constant} = B_0$ (say)

$$\therefore \mathbf{B} = (0, 0, B_0)$$

Again the current density vector is $\mathbf{J} = (J_x, J_y, J_z)$.

Consider the direction of propagation is considered along x - and y -axis and does not have any variation along z -axis.

i.e. $\frac{\partial J_z}{\partial z} = 0$

Or, $J_z = \text{constant} = 0$ (say)

$$\therefore \mathbf{J} = (j_x, j_y, 0)$$

Now, $\mathbf{q} = \hat{i}u + \hat{j}v + \hat{k}w$

$$\therefore \mathbf{q} \cdot \nabla = (\hat{i}u + \hat{j}v + \hat{k}w) \cdot \left(\hat{i} \frac{\partial}{\partial x} + \hat{j} \frac{\partial}{\partial y} + \hat{k} \frac{\partial}{\partial z} \right) = u \frac{\partial}{\partial x} + v \frac{\partial}{\partial y} + w \frac{\partial}{\partial z}$$

$$\begin{aligned} \therefore (\mathbf{q} \cdot \nabla) \mathbf{q} &= \left(u \frac{\partial}{\partial x} + v \frac{\partial}{\partial y} + w \frac{\partial}{\partial z} \right) \cdot (\hat{i}u + \hat{j}v + \hat{k}w) \\ &= \hat{i} \left(u \frac{\partial u}{\partial x} + v \frac{\partial u}{\partial y} + w \frac{\partial u}{\partial z} \right) + \hat{j} \left(u \frac{\partial v}{\partial x} + v \frac{\partial v}{\partial y} + w \frac{\partial v}{\partial z} \right) + \hat{k} \left(u \frac{\partial w}{\partial x} + v \frac{\partial w}{\partial y} + w \frac{\partial w}{\partial z} \right) \end{aligned}$$

$$\nabla^2 = \frac{\partial^2}{\partial x^2} + \frac{\partial^2}{\partial y^2} + \frac{\partial^2}{\partial z^2}$$

$$\begin{aligned} \therefore \nabla^2 \mathbf{q} &= \left(\frac{\partial^2}{\partial x^2} + \frac{\partial^2}{\partial y^2} + \frac{\partial^2}{\partial z^2} \right) \cdot (\hat{i}u + \hat{j}v + \hat{k}w) \\ &= \hat{i} \left(\frac{\partial^2 u}{\partial x^2} + \frac{\partial^2 u}{\partial y^2} + \frac{\partial^2 u}{\partial z^2} \right) + \hat{j} \left(\frac{\partial^2 v}{\partial x^2} + \frac{\partial^2 v}{\partial y^2} + \frac{\partial^2 v}{\partial z^2} \right) + \hat{k} \left(\frac{\partial^2 w}{\partial x^2} + \frac{\partial^2 w}{\partial y^2} + \frac{\partial^2 w}{\partial z^2} \right) \end{aligned}$$

$$\text{Again } \boldsymbol{\Omega} \times \mathbf{q} = \begin{pmatrix} \hat{i} & \hat{j} & \hat{k} \\ 0 & 0 & \Omega_0 \\ u & v & w \end{pmatrix} = -\Omega_0 v \hat{i} + \Omega_0 u \hat{j}$$

Also $\mathbf{F} = \hat{i}F_1 + \hat{j}F_2 + \hat{k}F_3$

$$\text{Now } \mathbf{q} \wedge \mathbf{B} = \begin{pmatrix} \hat{i} & \hat{j} & \hat{k} \\ u & v & w \\ 0 & 0 & B_0 \end{pmatrix} = vB_0 \hat{i} - uB_0 \hat{j}$$

$$\mathbf{J} \wedge \mathbf{B} = \begin{pmatrix} \hat{i} & \hat{j} & \hat{k} \\ J_x & J_y & 0 \\ 0 & 0 & B_0 \end{pmatrix} = \hat{i}(J_y B_0) - \hat{j}(J_x B_0) = J_y B_0 \hat{i} - J_x B_0 \hat{j}$$

$$(\mathbf{J} \wedge \mathbf{B}) \wedge \mathbf{B} = \begin{pmatrix} \hat{i} & \hat{j} & \hat{k} \\ J_y B_0 & -J_x B_0 & 0 \\ 0 & 0 & B_0 \end{pmatrix} = (-J_x B_0^2) \hat{i} - (J_y B_0^2) \hat{j} = -J_x B_0^2 \hat{i} - J_y B_0^2 \hat{j}$$

Thus generalized Ohm's law $\mathbf{J} = \sigma \mu_e (\mathbf{q} \wedge \mathbf{B}) - \frac{m}{B_0} (\mathbf{J} \wedge \mathbf{B}) + \frac{m\alpha}{B_0^2} (\mathbf{J} \wedge \mathbf{B}) \wedge \mathbf{B}$ becomes

$$J_x \hat{i} + J_y \hat{j} + J_z \hat{k} = \sigma \mu_e (vB_0 \hat{i} - uB_0 \hat{j}) - \frac{m}{B_0} (J_y B_0 \hat{i} - J_x B_0 \hat{j}) + \frac{m\alpha}{B_0^2} (-J_x B_0^2 \hat{i} - J_y B_0^2 \hat{j})$$

Therefore

$$\left. \begin{aligned} J_x &= \sigma \mu_e v B_0 - m J_y - m \alpha J_x \\ J_y &= -\sigma \mu_e u B_0 + m J_x - m \alpha J_y \\ J_z &= 0 \end{aligned} \right\} \text{ Or, } \left. \begin{aligned} (1+m\alpha)J_x + mJ_y &= \sigma \mu_e v B_0 \\ (1+m\alpha)J_y - mJ_x &= -\sigma \mu_e u B_0 \\ J_z &= 0 \end{aligned} \right\} \quad (6.5)$$

To find the value of J_x and J_y , multiply 1st equation of (6.5) by m and multiply 2nd equation of (6.5) by $(1+m\alpha)$ and then adding them, it becomes

$$m(1+m\alpha)J_x + m^2 J_y + (1+m\alpha)^2 J_y - m(1+m\alpha)J_x = \sigma \mu_e v B_0 m - \sigma \mu_e u B_0 (1+m\alpha)$$

$$\text{Or, } [m^2 + (1+m\alpha)^2] J_y = \sigma \mu_e B_0 [vm - u(1+m\alpha)]$$

$$\text{Or, } J_y = \frac{[mv - (1+m\alpha)u]}{[(1+m\alpha)^2 + m^2]} \sigma \mu_e B_0$$

Again multiply 1st equation of (6.5) by $(1+m\alpha)$ and 2nd equation of (6.5) by m then subtracting, it becomes

$$(1+m\alpha)^2 J_x + m(1+m\alpha)J_y - [m(1+m\alpha)J_y - m^2 J_x] = \sigma \mu_e v B_0 (1+m\alpha) + m \sigma \mu_e u B_0$$

$$\text{Or, } (1+m\alpha)^2 J_x + m^2 J_x = \sigma \mu_e v B_0 (1+m\alpha) + m \sigma \mu_e u B_0$$

$$\text{Or, } [(1+m\alpha)^2 + m^2] J_x = \sigma \mu_e v B_0 (1+m\alpha) + m \sigma \mu_e u B_0$$

$$\text{Or, } [(1+m\alpha)^2 + m^2] J_x = [v(1+m\alpha) + mu] \sigma \mu_e B_0$$

$$\therefore J_x = \frac{mu + (1+m\alpha)v}{(1+m\alpha)^2 + m^2} \sigma \mu_e B_0$$

Therefore $\mathbf{J} \wedge \mathbf{B} = J_y B_0 \hat{i} - J_x B_0 \hat{j}$

$$\begin{aligned} \text{Or, } \frac{1}{\rho} (\mathbf{J} \times \mathbf{B}) &= \frac{B_0 J_y}{\rho} \hat{i} - \frac{B_0 J_x}{\rho} \hat{j} \\ &= \frac{\sigma \mu_e B_0^2}{\rho} \left[\frac{mv - (1+m\alpha)u}{(1+m\alpha)^2 + m^2} \right] \hat{i} - \frac{\sigma \mu_e B_0^2}{\rho} \left[\frac{v(1+m\alpha) + mu}{(1+m\alpha)^2 + m^2} \right] \hat{j} \end{aligned}$$

Now,

$$\begin{aligned}
& \frac{\partial}{\partial t} (\hat{i}u + \hat{j}v + \hat{k}w) + \hat{i} \left(u \frac{\partial u}{\partial x} + v \frac{\partial u}{\partial y} + w \frac{\partial u}{\partial z} \right) + \hat{j} \left(u \frac{\partial v}{\partial x} + v \frac{\partial v}{\partial y} + w \frac{\partial v}{\partial z} \right) + \hat{k} \left(u \frac{\partial w}{\partial x} + v \frac{\partial w}{\partial y} + w \frac{\partial w}{\partial z} \right) \\
&= (\hat{i}F_1 + \hat{j}F_2 + \hat{k}F_3) - \frac{1}{\rho} \left(\hat{i} \frac{\partial p}{\partial x} + \hat{j} \frac{\partial p}{\partial y} + \hat{k} \frac{\partial p}{\partial z} \right) \\
&+ \hat{i} v \left(\frac{\partial^2 u}{\partial x^2} + \frac{\partial^2 u}{\partial y^2} + \frac{\partial^2 u}{\partial z^2} \right) + \hat{j} v \left(\frac{\partial^2 v}{\partial x^2} + \frac{\partial^2 v}{\partial y^2} + \frac{\partial^2 v}{\partial z^2} \right) + \hat{k} v \left(\frac{\partial^2 w}{\partial x^2} + \frac{\partial^2 w}{\partial y^2} + \frac{\partial^2 w}{\partial z^2} \right) \\
&- (-\Omega_0 v \hat{i} + \Omega_0 u \hat{j}) \\
&+ \frac{\sigma \mu_e B_0^2}{\rho} \left[\frac{mv - (1+m\alpha)u}{(1+m\alpha)^2 + m^2} \right] \hat{i} - \frac{\sigma \mu_e B_0^2}{\rho} \left[\frac{mu + (1+m\alpha)v}{(1+m\alpha)^2 + m^2} \right] \hat{j} + \beta g T \hat{k}
\end{aligned}$$

And equating the \hat{i} th, \hat{j} th and \hat{k} th component, it becomes

$$\begin{aligned}
\frac{\partial u}{\partial t} + \left(u \frac{\partial u}{\partial x} + v \frac{\partial u}{\partial y} + w \frac{\partial u}{\partial z} \right) &= F_1 - \frac{1}{\rho} \frac{\partial p}{\partial x} + v \left(\frac{\partial^2 u}{\partial x^2} + \frac{\partial^2 u}{\partial y^2} + \frac{\partial^2 u}{\partial z^2} \right) + 2\Omega_0 v + \frac{\sigma \mu_e B_0^2}{\rho} \left[\frac{mv - (1+m\alpha)u}{(1+m\alpha)^2 + m^2} \right] \\
\frac{\partial v}{\partial t} + \left(u \frac{\partial v}{\partial x} + v \frac{\partial v}{\partial y} + w \frac{\partial v}{\partial z} \right) &= F_2 - \frac{1}{\rho} \frac{\partial p}{\partial y} + u \left(\frac{\partial^2 v}{\partial x^2} + \frac{\partial^2 v}{\partial y^2} + \frac{\partial^2 v}{\partial z^2} \right) - 2\Omega_0 u - \frac{\sigma \mu_e B_0^2}{\rho} \left[\frac{mu + (1+m\alpha)v}{(1+m\alpha)^2 + m^2} \right] \\
\frac{\partial w}{\partial t} + \left(u \frac{\partial w}{\partial x} + v \frac{\partial w}{\partial y} + w \frac{\partial w}{\partial z} \right) &= F_3 - \frac{1}{\rho} \frac{\partial p}{\partial z} + u \left(\frac{\partial^2 w}{\partial x^2} + \frac{\partial^2 w}{\partial y^2} + \frac{\partial^2 w}{\partial z^2} \right) + \beta g T
\end{aligned}$$

Again for the Energy equation,

$$(\mathbf{q} \cdot \nabla)T = u \frac{\partial T}{\partial x} + v \frac{\partial T}{\partial y} + w \frac{\partial T}{\partial z} \quad \text{and} \quad \nabla^2 T = \frac{\partial^2 T}{\partial x^2} + \frac{\partial^2 T}{\partial y^2} + \frac{\partial^2 T}{\partial z^2}$$

Hence the governing equations in terms of Cartesian coordinate system are as follows:

Continuity Equation:

$$\frac{\partial u}{\partial x} + \frac{\partial v}{\partial y} + \frac{\partial w}{\partial z} = 0 \tag{6.6a}$$

Momentum Equation

$$\frac{\partial u}{\partial t} + \left(u \frac{\partial u}{\partial x} + v \frac{\partial u}{\partial y} + w \frac{\partial u}{\partial z} \right) = F_1 - \frac{1}{\rho} \frac{\partial p}{\partial x} + v \left(\frac{\partial^2 u}{\partial x^2} + \frac{\partial^2 u}{\partial y^2} + \frac{\partial^2 u}{\partial z^2} \right) + 2\Omega_0 v + \frac{\sigma \mu_e B_0^2}{\rho} \left[\frac{mv - (1+m\alpha)u}{(1+m\alpha)^2 + m^2} \right] \tag{6.6b}$$

$$\frac{\partial v}{\partial t} + \left(u \frac{\partial v}{\partial x} + v \frac{\partial v}{\partial y} + w \frac{\partial v}{\partial z} \right) = F_2 - \frac{1}{\rho} \frac{\partial p}{\partial y} + u \left(\frac{\partial^2 v}{\partial x^2} + \frac{\partial^2 v}{\partial y^2} + \frac{\partial^2 v}{\partial z^2} \right) - 2\Omega_0 u - \frac{\sigma \mu_e B_0^2}{\rho} \left[\frac{mu + (1+m\alpha)v}{(1+m\alpha)^2 + m^2} \right] \tag{6.6c}$$

$$\frac{\partial w}{\partial t} + \left(u \frac{\partial w}{\partial x} + v \frac{\partial w}{\partial y} + w \frac{\partial w}{\partial z} \right) = F_3 - \frac{1}{\rho} \frac{\partial p}{\partial z} + u \left(\frac{\partial^2 w}{\partial x^2} + \frac{\partial^2 w}{\partial y^2} + \frac{\partial^2 w}{\partial z^2} \right) + \beta g T \tag{6.6d}$$

Energy Equation

$$\frac{\partial T}{\partial t} + u \frac{\partial T}{\partial x} + v \frac{\partial T}{\partial y} + w \frac{\partial T}{\partial z} = \frac{k}{\rho C_p} \left(\frac{\partial^2 T}{\partial x^2} + \frac{\partial^2 T}{\partial y^2} + \frac{\partial^2 T}{\partial z^2} \right) \tag{6.6e}$$

6.2 Governing Equations for Straight Duct Regarding to Current Study

6.2.1 Transforming Coordinate Variables in Governing Equations:

Consider a thermally fully developed, viscous, incompressible, two-dimensional, MHD fluid flow through a curved duct of height $2h$ and width $2d$ so that the aspect ratio of this duct is $l = h/d$. To compare our obtained results with the previously published results on the curved duct flow, it is required to interchange the coordinate axes y and z from each other of the rectangular Cartesian coordinate system. In this case, the duct system is rotated around its vertical y -axis with an angular velocity Ω .

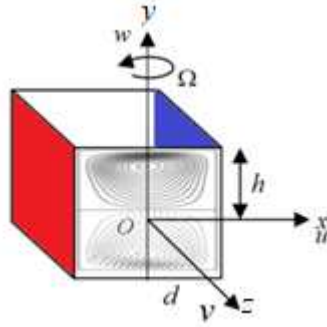


Fig.6.2: Geometrical model of the present straight square duct

To get the modified governing equations, It is required to interchange the variables y and z , and the velocity component v and w each other in the equations from (6.6a) to (6.6e).

Thus the modified governing equation for incompressible fluid is

Continuity Equation:

$$\frac{\partial u}{\partial x} + \frac{\partial w}{\partial z} + \frac{\partial v}{\partial y} = 0 \quad (6.7a)$$

Momentum Equation

$$\frac{\partial u}{\partial t} + \left(u \frac{\partial u}{\partial x} + w \frac{\partial u}{\partial z} + v \frac{\partial u}{\partial y} \right) = F_1 - \frac{1}{\rho} \frac{\partial p}{\partial x} + \nu \left(\frac{\partial^2 u}{\partial x^2} + \frac{\partial^2 u}{\partial z^2} + \frac{\partial^2 u}{\partial y^2} \right) + 2\Omega_0 w + \frac{\sigma \mu_e B_0^2}{\rho} \left[\frac{mw - (1+m\alpha)u}{(1+m\alpha)^2 + m^2} \right] \quad (6.7b)$$

$$\frac{\partial w}{\partial t} + \left(u \frac{\partial w}{\partial x} + w \frac{\partial w}{\partial z} + v \frac{\partial w}{\partial y} \right) = F_2 - \frac{1}{\rho} \frac{\partial p}{\partial z} + \nu \left(\frac{\partial^2 w}{\partial x^2} + \frac{\partial^2 w}{\partial z^2} + \frac{\partial^2 w}{\partial y^2} \right) - 2\Omega_0 u - \frac{\sigma \mu_e B_0^2}{\rho} \left[\frac{mu + (1+m\alpha)w}{(1+m\alpha)^2 + m^2} \right] \quad (6.7c)$$

$$\frac{\partial v}{\partial t} + \left(u \frac{\partial v}{\partial x} + w \frac{\partial v}{\partial z} + v \frac{\partial v}{\partial y} \right) = F_3 - \frac{1}{\rho} \frac{\partial p}{\partial y} + \nu \left(\frac{\partial^2 v}{\partial x^2} + \frac{\partial^2 v}{\partial z^2} + \frac{\partial^2 v}{\partial y^2} \right) + \beta g T \quad (6.7d)$$

Energy Equation

$$\frac{\partial T}{\partial t} + u \frac{\partial T}{\partial x} + w \frac{\partial T}{\partial z} + v \frac{\partial T}{\partial y} = \frac{k}{\rho C_p} \left(\frac{\partial^2 T}{\partial x^2} + \frac{\partial^2 T}{\partial z^2} + \frac{\partial^2 T}{\partial y^2} \right) \quad (6.7e)$$

Now it is assumed that the body force is absent and all the variables are independent of z except p due to the fully developed flow.

i.e. $(F_1, F_2, F_3) = (0, 0, 0)$ & $\frac{\partial A_1}{\partial z} = 0$ but $\frac{\partial p}{\partial z} \neq 0$ where, $A_1 =$ fluid variables. Therefore the above equations are reduces to the following form:

Continuity Equation:

$$\frac{\partial u}{\partial x} + \frac{\partial v}{\partial y} = 0 \quad (6.8a)$$

Momentum Equation

$$\frac{\partial u}{\partial t} + u \frac{\partial u}{\partial x} + v \frac{\partial u}{\partial y} = -\frac{1}{\rho} \frac{\partial p}{\partial x} + \nu \left(\frac{\partial^2 u}{\partial x^2} + \frac{\partial^2 u}{\partial y^2} \right) + 2\Omega_0 w + \frac{\sigma \mu_e B_0^2}{\rho} \left[\frac{mw - (1+m\alpha)u}{(1+m\alpha)^2 + m^2} \right] \quad (6.8b)$$

$$\frac{\partial v}{\partial t} + u \frac{\partial v}{\partial x} + v \frac{\partial v}{\partial y} = -\frac{1}{\rho} \frac{\partial p}{\partial y} + \nu \left(\frac{\partial^2 v}{\partial x^2} + \frac{\partial^2 v}{\partial y^2} \right) + \beta g T \quad (6.8c)$$

$$\frac{\partial w}{\partial t} + u \frac{\partial w}{\partial x} + v \frac{\partial w}{\partial y} = -\frac{1}{\rho} \frac{\partial p}{\partial z} + \nu \left(\frac{\partial^2 w}{\partial x^2} + \frac{\partial^2 w}{\partial y^2} \right) - 2\Omega_0 u - \frac{\sigma \mu_e B_0^2}{\rho} \left[\frac{mu + (1+m\alpha)w}{(1+m\alpha)^2 + m^2} \right] \quad (6.8d)$$

Energy Equation

$$\frac{\partial T}{\partial t} + u \frac{\partial T}{\partial x} + v \frac{\partial T}{\partial y} = \frac{k}{\rho C_p} \left(\frac{\partial^2 T}{\partial x^2} + \frac{\partial^2 T}{\partial y^2} \right) \quad (6.8e)$$

Non-Dimensional Analysis:

To make dimensionless form of the governing equations (6.8a)-(6.8e), use respective length d and the kinematic viscosity ν , the non-dimensional uniform velocity is defined by

$U_0 = \frac{\nu}{d}$. And it has been introduced some dimensionless quantities

$$\begin{aligned} x' &= \frac{x}{d} & \bar{y} &= \frac{y}{d} & z' &= \frac{z}{d} & u' &= \frac{d}{\nu} u & v' &= \frac{d}{\nu} v; \\ w' &= \frac{d}{\nu} w & t' &= \frac{\nu}{d^2} t & p' &= \frac{d^2}{\rho \nu^2} p & \text{and} & T' &= \frac{T}{\Delta T} \end{aligned}$$

where x', \bar{y} and z' are the non-dimensional horizontal, vertical and axial coordinates respectively; u', v', w' are the non-dimensional velocity components in the direction of x', \bar{y} and z' respectively; t' is the non-dimensional time; T' is the non-dimensional temperature and p' is also the dimensionless pressure.

Now we calculate necessary terms which are involved in the equations (6.8a)-(6.8e).

$$\begin{aligned} x &= d x'; & y &= d \bar{y}; & z &= d z' & \partial x &= d \partial x'; & \partial y &= d \partial \bar{y}; & \partial z &= d \partial z' \\ t &= \frac{d^2}{\nu} t' & & & & & \partial t &= \frac{d^2}{\nu} \partial t' \\ u &= \frac{\nu}{d} u'; & v &= \frac{\nu}{d} v'; & w &= \frac{\nu}{d} w' & \partial u &= \frac{\nu}{d} \partial u'; & \partial v &= \frac{\nu}{d} \partial v'; & \partial w &= \frac{\nu}{d} \partial w' \\ p &= \frac{\rho \nu^2}{d^2} p'; & T &= \Delta T T' & & & \partial p &= \frac{\rho \nu^2}{d^2} \partial p'; & \partial T &= \Delta T \partial T' \end{aligned}$$

$$\begin{aligned}
\frac{\partial u}{\partial t} &= \frac{v^2}{d^3} \frac{\partial u'}{\partial t'} & \frac{\partial v}{\partial y} &= \frac{v}{d^2} \frac{\partial v'}{\partial \bar{y}} \\
\frac{\partial v}{\partial t} &= \frac{v^2}{d^3} \frac{\partial v'}{\partial t'} & \frac{\partial p}{\partial y} &= \frac{\rho v^2}{d^3} \frac{\partial p'}{\partial \bar{y}} \\
\frac{\partial w}{\partial t} &= \frac{v^2}{d^3} \frac{\partial w'}{\partial t'} & \frac{\partial p}{\partial z} &= \frac{\rho v^2}{d^3} \frac{\partial p'}{\partial z'} \\
\frac{\partial w}{\partial y} &= \frac{v}{d^2} \frac{\partial w'}{\partial \bar{y}} & \frac{\partial^2 T}{\partial r^2} &= \frac{\partial}{\partial r} \left(\frac{\partial T}{\partial r} \right) = \frac{\partial}{\partial r} \left(\frac{\Delta T}{d} \frac{\partial T'}{\partial x'} \right) = \frac{\Delta T}{d^2} \frac{\partial^2 T'}{\partial x'^2} \\
\frac{\partial T}{\partial t} &= \frac{v}{d^2} \Delta T \frac{\partial T'}{\partial t'} & \frac{\partial^2 T}{\partial y^2} &= \frac{\partial}{\partial \bar{y}} \left(\frac{\partial T}{\partial \bar{y}} \right) = \frac{\partial}{\partial \bar{y}} \left(\frac{\Delta T}{d} \frac{\partial T'}{\partial \bar{y}} \right) = \frac{\Delta T}{d^2} \frac{\partial^2 T'}{\partial \bar{y}^2} \\
\frac{\partial T}{\partial x} &= \frac{\Delta T}{d} \frac{\partial T'}{\partial x'} \\
\frac{\partial T}{\partial y} &= \frac{\Delta T}{d} \frac{\partial T'}{\partial \bar{y}}
\end{aligned}$$

Put these terms into the equations (6.8a)-(6.8e).

From continuity equation (6.8a), yields

$$\begin{aligned}
\frac{v}{d^2} \frac{\partial u'}{\partial x'} + \frac{v}{d^2} \frac{\partial v'}{\partial \bar{y}} &= 0 \\
\therefore \frac{\partial u'}{\partial x'} + \frac{\partial v'}{\partial \bar{y}} &= 0
\end{aligned}$$

u- Momentum equation (6.8b), yields

$$\begin{aligned}
\frac{v^2}{d^3} \frac{\partial u'}{\partial t'} + \frac{v}{d} u' \frac{v}{d^2} \frac{\partial u'}{\partial x'} + \frac{v}{d} v' \frac{v}{d^2} \frac{\partial u'}{\partial \bar{y}} &= -\frac{1}{\rho} \frac{\rho v^2}{d^3} \frac{\partial p'}{\partial x'} + v \left(\frac{v}{d^3} \frac{\partial^2 u'}{\partial x'^2} + \frac{v}{d^3} \frac{\partial^2 u'}{\partial \bar{y}^2} \right) \\
&+ 2 \frac{v}{d} w' \Omega_0 + \frac{1}{\rho} \frac{\sigma \mu_e B_0^2}{(1+m\alpha)^2 + m^2} \left(m \frac{v}{d} w' - (1+m\alpha) \frac{v}{d} u' \right) \\
\text{Or, } \frac{v^2}{d^3} \left(\frac{\partial u'}{\partial t'} + u' \frac{\partial u'}{\partial x'} + v' \frac{\partial u'}{\partial \bar{y}} \right) &= -\frac{v^2}{d^3} \frac{\partial p'}{\partial x'} + \frac{v^2}{d^3} \left(\frac{\partial^2 u'}{\partial x'^2} + \frac{\partial^2 u'}{\partial \bar{y}^2} \right) + \frac{2v}{d} w' \Omega_0 + \frac{v}{d} \frac{\sigma \mu_e B_0^2}{\rho} \left(\frac{mw' - (1+m\alpha)u'}{(1+m\alpha)^2 + m^2} \right) \\
\text{Or, } \frac{\partial u'}{\partial t'} + u' \frac{\partial u'}{\partial x'} + v' \frac{\partial u'}{\partial \bar{y}} &= -\frac{\partial p'}{\partial x'} + \left(\frac{\partial^2 u'}{\partial x'^2} + \frac{\partial^2 u'}{\partial \bar{y}^2} \right) + \frac{d^3}{v^2} \times \frac{2v}{d} \Omega_0 w' + \frac{d^3}{v^2} \times \frac{v}{d} \frac{\sigma \mu_e B_0^2}{\rho} \left(\frac{mw' - (1+m\alpha)u'}{(1+m\alpha)^2 + m^2} \right) \\
\text{Or, } \frac{\partial u'}{\partial t'} + u' \frac{\partial u'}{\partial x'} + v' \frac{\partial u'}{\partial \bar{y}} &= -\frac{\partial p'}{\partial x'} + \left(\frac{\partial^2 u'}{\partial x'^2} + \frac{\partial^2 u'}{\partial \bar{y}^2} \right) + \frac{2d^2}{v} \Omega_0 w' + \frac{d^2}{v} \frac{\sigma \mu_e B_0^2}{\rho} \left(\frac{mw' - (1+m\alpha)u'}{(1+m\alpha)^2 + m^2} \right) \\
\text{Or, } \Rightarrow \frac{\partial u'}{\partial t'} + u' \frac{\partial u'}{\partial x'} + v' \frac{\partial u'}{\partial \bar{y}} &= -\frac{\partial p'}{\partial x'} + \left(\frac{\partial^2 u'}{\partial x'^2} + \frac{\partial^2 u'}{\partial \bar{y}^2} \right) + \frac{2d^2}{v} \Omega_0 w' + \frac{d^2 \sigma \mu_e B_0^2}{\rho v} \left(\frac{mw' - (1+m\alpha)u'}{(1+m\alpha)^2 + m^2} \right) \\
\therefore \frac{\partial u'}{\partial t'} + u' \frac{\partial u'}{\partial x'} + v' \frac{\partial u'}{\partial \bar{y}} &= -\frac{\partial p'}{\partial x'} + \frac{\partial^2 u'}{\partial x'^2} + \frac{\partial^2 u'}{\partial \bar{y}^2} + T_r w' + \frac{M}{(1+m\alpha)^2 + m^2} (mw' - (1+m\alpha)u')
\end{aligned}$$

where, $T_r = \frac{2d^2}{v} \Omega_0$ is the Taylor number and $M = \frac{d^2 \sigma \mu_e B_0^2}{\rho v}$ is the Magnetic parameter.

v-Momentum equation (6.8c), gives

$$\frac{v^2}{d^3} \frac{\partial v'}{\partial t'} + \frac{v}{d} u' \frac{v}{d^2} \frac{\partial v'}{\partial x'} + \frac{v}{d} v' \frac{v}{d^2} \frac{\partial v'}{\partial \bar{y}} = -\frac{1}{\rho} \frac{\rho v^2}{d^3} \frac{\partial p'}{\partial \bar{y}} + v \left(\frac{v}{d^3} \frac{\partial^2 v'}{\partial x'^2} + \frac{v}{d^3} \frac{\partial^2 v'}{\partial \bar{y}^2} \right) + \beta g \Delta T T'$$

$$\Rightarrow \frac{v^2}{d^3} \frac{\partial v'}{\partial t'} + \frac{v^2}{d^3} u' \frac{\partial v'}{\partial x'} + \frac{v^2}{d^3} v' \frac{\partial v'}{\partial y} = -\frac{v^2}{d^3} \frac{\partial p'}{\partial y} + \frac{v^2}{d^3} \left(\frac{\partial^2 v'}{\partial x'^2} + \frac{\partial^2 v'}{\partial y^2} \right) + \beta g \Delta T T'$$

$$\text{Or, } \frac{\partial v'}{\partial t'} + u' \frac{\partial v'}{\partial x'} + v' \frac{\partial v'}{\partial y} = -\frac{\partial p'}{\partial y} + \left(\frac{\partial^2 v'}{\partial x'^2} + \frac{\partial^2 v'}{\partial y^2} \right) + \frac{d^3 \beta g \Delta T}{v^2} T'$$

$$\therefore \frac{\partial v'}{\partial t'} + u' \frac{\partial v'}{\partial x'} + v' \frac{\partial v'}{\partial y} = -\frac{\partial p'}{\partial y} + \frac{\partial^2 v'}{\partial x'^2} + \frac{\partial^2 v'}{\partial y^2} + G_r T'$$

where $G_r = \frac{d^3 \beta g \Delta T}{v^2}$ is the Grashof Number.

w- Momentum equation (6.8d) gives

$$\frac{v^2}{d^3} \frac{\partial w'}{\partial t'} + \frac{v}{d} u' \frac{\partial w'}{\partial x'} + \frac{v}{d} v' \frac{\partial w'}{\partial y} = -\frac{1}{\rho} \frac{\rho v^2}{d^3} \frac{\partial p'}{\partial z'} + v \left(\frac{v}{d^3} \frac{\partial^2 w'}{\partial x'^2} + \frac{v}{d^3} \frac{\partial^2 w'}{\partial y^2} \right) - 2 \frac{v}{d} u' \Omega_0 - \frac{\sigma \mu_e B_0^2}{\rho [(1+m\alpha)^2 + m^2]} \left(\frac{mv}{d} u' + \frac{v(1+m\alpha)}{d} w' \right)$$

$$\text{Or, } \frac{v^2}{d^3} \left(\frac{\partial w'}{\partial t'} + u' \frac{\partial w'}{\partial x'} + v' \frac{\partial w'}{\partial y} \right) = -\frac{1}{\rho} \frac{\rho v^2}{d^3} \frac{\partial p'}{\partial z'} + \frac{v^2}{d^3} \left(\frac{\partial^2 w'}{\partial x'^2} + \frac{\partial^2 w'}{\partial y^2} \right) - 2 \frac{v}{d} u' \Omega_0 - \frac{\sigma \mu_e B_0^2}{\rho [(1+m\alpha)^2 + m^2]} \times \frac{v}{d} [mu' + (1+m\alpha)w']$$

$$\text{Or, } \left(\frac{\partial w'}{\partial t'} + u' \frac{\partial w'}{\partial x'} + v' \frac{\partial w'}{\partial y} \right) = -\frac{\partial p'}{\partial z'} + \left(\frac{\partial^2 w'}{\partial x'^2} + \frac{\partial^2 w'}{\partial y^2} \right) - \frac{2v}{d} \Omega_0 u' \times \frac{d^3}{v^2} - \frac{\sigma \mu_e B_0^2}{\rho [(1+m\alpha)^2 + m^2]} \times \frac{v}{d} \times \frac{d^3}{v^2} [mu' + (1+m\alpha)w']$$

$$\text{Or, } \frac{\partial w'}{\partial t'} + u' \frac{\partial w'}{\partial x'} + v' \frac{\partial w'}{\partial y} = -\frac{\partial p'}{\partial z'} + \left(\frac{\partial^2 w'}{\partial x'^2} + \frac{\partial^2 w'}{\partial y^2} \right) - \frac{2d^2}{v} \Omega_0 u' - \frac{d^2 \sigma \mu_e B_0^2}{\rho v [(1+m\alpha)^2 + m^2]} [mu' + (1+m\alpha)w']$$

$$\therefore \frac{\partial w'}{\partial t'} + u' \frac{\partial w'}{\partial x'} + v' \frac{\partial w'}{\partial y} = D_n + \frac{\partial^2 w'}{\partial x'^2} + \frac{\partial^2 w'}{\partial y^2} - T_r u' - \frac{M}{(1+m\alpha)^2 + m^2} [mu' + (1+m\alpha)w']$$

$D_n = -\frac{\partial p'}{\partial z'}$ or $-\frac{d^3}{\rho v^2} \frac{\partial p}{\partial z}$ or $\frac{d^3 G}{\rho v^2}$ is the Dean Number where, $P = -\frac{\partial p}{\partial z}$ is the pressure gradient

Again from Energy equation (6.8e)

$$\frac{\partial T}{\partial t} + u \frac{\partial T}{\partial x} + v \frac{\partial T}{\partial y} = \frac{k}{\rho C_p} \left(\frac{\partial^2 T}{\partial x^2} + \frac{\partial^2 T}{\partial y^2} \right)$$

$$\text{Or, } \frac{v}{d^2} \Delta T \frac{\partial T'}{\partial t'} + \frac{v}{d} u' \frac{\Delta T}{d} \frac{\partial T'}{\partial x'} + \frac{v}{d} v' \frac{\Delta T}{d} \frac{\partial T'}{\partial y} = \frac{k}{\rho C_p} \left(\frac{\Delta T}{d^2} \frac{\partial^2 T'}{\partial x'^2} + \frac{\Delta T}{d^2} \frac{\partial^2 T'}{\partial y^2} \right)$$

$$\text{Or, } \frac{v}{d^2} \Delta T \frac{\partial T'}{\partial t'} + \frac{v}{d^2} \Delta T u' \frac{\partial T'}{\partial x'} + \frac{v}{d^2} \Delta T v' \frac{\partial T'}{\partial y} = \frac{k}{\rho C_p} \frac{1}{d^2} \Delta T \left[\frac{\partial^2 T'}{\partial x'^2} + \frac{\partial^2 T'}{\partial y^2} \right]$$

$$\text{Or, } \frac{\partial T'}{\partial t'} + u' \frac{\partial T'}{\partial x'} + v' \frac{\partial T'}{\partial y'} = \frac{k}{\rho C_p} \frac{d^2}{d^2} \frac{\Delta T}{d^2} \left[\frac{\partial^2 T'}{\partial x'^2} + \frac{\partial^2 T'}{\partial y'^2} \right]$$

$$\text{Or, } \frac{\partial T'}{\partial t'} + u' \frac{\partial T'}{\partial x'} + v' \frac{\partial T'}{\partial y'} = \frac{k}{\nu \rho C_p} \left[\frac{\partial^2 T'}{\partial x'^2} + \frac{\partial^2 T'}{\partial y'^2} \right]$$

$$\therefore \frac{\partial T'}{\partial t'} + u' \frac{\partial T'}{\partial x'} + v' \frac{\partial T'}{\partial y'} = \frac{1}{P_r} \left[\frac{\partial^2 T'}{\partial x'^2} + \frac{\partial^2 T'}{\partial y'^2} \right], \quad \text{where, } P_r = \frac{\nu \rho C_p}{k} \text{ is the Prandtl Number.}$$

Now dropping the primes on the variables, it can be written as the above equations into its non-dimensional form as follows:

Continuity equation

$$\frac{\partial u}{\partial x} + \frac{\partial v}{\partial y} = 0 \quad (6.9a)$$

Momentum Equation

$$\frac{\partial u}{\partial t} + u \frac{\partial u}{\partial x} + v \frac{\partial u}{\partial y} = -\frac{\partial p}{\partial x} + \left(\frac{\partial^2 u}{\partial x^2} + \frac{\partial^2 u}{\partial y^2} \right) + T_r w + \frac{M}{(1+m\alpha)^2 + m^2} (mw - (1+m\alpha)u) \quad (6.9b)$$

$$\frac{\partial v}{\partial t} + u \frac{\partial v}{\partial x} + v \frac{\partial v}{\partial y} = -\frac{\partial p}{\partial y} + \left(\frac{\partial^2 v}{\partial x^2} + \frac{\partial^2 v}{\partial y^2} \right) + G_r T \quad (6.9c)$$

$$\frac{\partial w}{\partial t} + u \frac{\partial w}{\partial x} + v \frac{\partial w}{\partial y} = D_n + \left(\frac{\partial^2 w}{\partial x^2} + \frac{\partial^2 w}{\partial y^2} \right) - T_r u - \frac{M}{(1+m\alpha)^2 + m^2} [mu + (1+m\alpha)w] \quad (6.9d)$$

Energy equation

$$\frac{\partial T}{\partial t} + u \frac{\partial T}{\partial x} + v \frac{\partial T}{\partial y} = \frac{1}{P_r} \left(\frac{\partial^2 T}{\partial x^2} + \frac{\partial^2 T}{\partial y^2} \right) \quad (6.9e)$$

Now let us consider the stream function $u = \frac{\partial \psi}{\partial y}$ and $v = -\frac{\partial \psi}{\partial x}$, These are the secondary velocity in terms of stream function ψ which satisfies the continuity equation (6.9a).

$$\text{To verify L.H.S.} = \frac{\partial}{\partial x} \left(\frac{\partial \psi}{\partial y} \right) + \frac{\partial}{\partial y} \left(-\frac{\partial \psi}{\partial x} \right) = \frac{\partial^2 \psi}{\partial x \partial y} - \frac{\partial^2 \psi}{\partial x \partial y} = 0 = \text{R.H.S.}$$

Now by using these stream functions in to (7.2.3)- (7.2.4), it becomes

From equation (6.9b)

$$\frac{\partial u}{\partial t} + u \frac{\partial u}{\partial x} + v \frac{\partial u}{\partial y} = -\frac{\partial p}{\partial x} + \left(\frac{\partial^2 u}{\partial x^2} + \frac{\partial^2 u}{\partial y^2} \right) + T_r w + \frac{M}{(1+m\alpha)^2 + m^2} (mw - (1+m\alpha)u)$$

$$\text{Or, } \frac{\partial}{\partial t} \left(\frac{\partial \psi}{\partial y} \right) + \frac{\partial \psi}{\partial y} \frac{\partial}{\partial x} \left(\frac{\partial \psi}{\partial y} \right) + \left(-\frac{\partial \psi}{\partial x} \right) \frac{\partial}{\partial y} \left(\frac{\partial \psi}{\partial y} \right)$$

$$= -\frac{\partial p}{\partial x} + \frac{\partial^2}{\partial x^2} \left(\frac{\partial \psi}{\partial y} \right) + \frac{\partial^2}{\partial y^2} \left(\frac{\partial \psi}{\partial y} \right) + T_r w + \frac{M}{(1+m\alpha)^2 + m^2} \left(mw - (1+m\alpha) \frac{\partial \psi}{\partial y} \right)$$

$$\therefore \frac{\partial^2 \psi}{\partial t \partial y} + \frac{\partial \psi}{\partial y} \frac{\partial^2 \psi}{\partial x \partial y} - \frac{\partial \psi}{\partial x} \frac{\partial^2 \psi}{\partial y^2} = -\frac{\partial p}{\partial x} + \frac{\partial^3 \psi}{\partial x^2 \partial y} + \frac{\partial^3 \psi}{\partial y^3} + T_r w + \frac{M}{(1+m\alpha)^2 + m^2} \left(mw - (1+m\alpha) \frac{\partial \psi}{\partial y} \right)$$

$$\frac{\partial v}{\partial t} + u \frac{\partial v}{\partial x} + v \frac{\partial v}{\partial y} = -\frac{\partial p}{\partial y} + \frac{\partial^2 v}{\partial x^2} + \frac{\partial^2 v}{\partial y^2} + G_r T \quad (6.9c)$$

From equation (6.9c):

$$\begin{aligned} \frac{\partial v}{\partial t} + u \frac{\partial v}{\partial x} + v \frac{\partial v}{\partial \bar{y}} &= - \frac{\partial p}{\partial \bar{y}} + \left(\frac{\partial^2 v}{\partial x^2} + \frac{\partial^2 v}{\partial \bar{y}^2} \right) + G_r T \\ \text{Or, } \frac{\partial}{\partial t} \left(- \frac{\partial \psi}{\partial x} \right) + \frac{\partial \psi}{\partial \bar{y}} \frac{\partial}{\partial x} \left(- \frac{\partial \psi}{\partial x} \right) + \left(- \frac{\partial \psi}{\partial x} \right) \frac{\partial}{\partial \bar{y}} \left(- \frac{\partial \psi}{\partial x} \right) &= - \frac{\partial p}{\partial \bar{y}} + \frac{\partial^2}{\partial x^2} \left(- \frac{\partial \psi}{\partial x} \right) + \frac{\partial^2}{\partial \bar{y}^2} \left(- \frac{\partial \psi}{\partial x} \right) + G_r T \\ \therefore - \frac{\partial^2 \psi}{\partial t \partial x} - \frac{\partial \psi}{\partial \bar{y}} \frac{\partial^2 \psi}{\partial x^2} + \frac{\partial \psi}{\partial x} \frac{\partial^2 \psi}{\partial \bar{y} \partial x} &= - \frac{\partial p}{\partial \bar{y}} - \frac{\partial^3 \psi}{\partial x^3} - \frac{\partial^3 \psi}{\partial \bar{y}^2 \partial x} + G_r T \end{aligned}$$

From equation (6.9d):

$$\begin{aligned} \frac{\partial w}{\partial t} + u \frac{\partial w}{\partial x} + v \frac{\partial w}{\partial \bar{y}} &= D_n + \frac{\partial^2 w}{\partial x^2} + \frac{\partial^2 w}{\partial \bar{y}^2} - T_r u - \frac{M}{(1+m\alpha)^2 + m^2} [mu + (1+m\alpha)w] \\ \text{Or, } \frac{\partial w}{\partial t} + \frac{\partial \Psi}{\partial \bar{y}} \frac{\partial w}{\partial x} - \frac{\partial \Psi}{\partial x} \frac{\partial w}{\partial \bar{y}} &= D_n + \frac{\partial^2 w}{\partial x^2} + \frac{\partial^2 w}{\partial \bar{y}^2} - T_r \left(\frac{\partial \Psi}{\partial \bar{y}} \right) - \frac{M}{(1+m\alpha)^2 + m^2} \left[m \frac{\partial \Psi}{\partial \bar{y}} + (1+m\alpha)w \right] \\ \therefore \frac{\partial w}{\partial t} + \frac{\partial \Psi}{\partial \bar{y}} \frac{\partial w}{\partial x} - \frac{\partial \Psi}{\partial x} \frac{\partial w}{\partial \bar{y}} &= D_n + \frac{\partial^2 w}{\partial x^2} + \frac{\partial^2 w}{\partial \bar{y}^2} - T_r \frac{\partial \Psi}{\partial \bar{y}} - \frac{M}{(1+m\alpha)^2 + m^2} \left[m \frac{\partial \Psi}{\partial \bar{y}} + (1+m\alpha)w \right] \end{aligned}$$

From equation (6.9e):

$$\begin{aligned} \frac{\partial T}{\partial t} + u \frac{\partial T}{\partial x} + v \frac{\partial T}{\partial \bar{y}} &= \frac{1}{P_r} \left(\frac{\partial^2 T}{\partial x^2} + \frac{\partial^2 T}{\partial \bar{y}^2} \right) \\ \text{Or, } \frac{\partial T}{\partial t} + \frac{\partial \Psi}{\partial \bar{y}} \frac{\partial T}{\partial x} - \frac{\partial \Psi}{\partial x} \frac{\partial T}{\partial \bar{y}} &= \frac{1}{P_r} \left(\frac{\partial^2 T}{\partial x^2} + \frac{\partial^2 T}{\partial \bar{y}^2} \right) \\ \therefore \frac{\partial T}{\partial t} + \left(\frac{\partial \Psi}{\partial \bar{y}} \frac{\partial T}{\partial x} - \frac{\partial \Psi}{\partial x} \frac{\partial T}{\partial \bar{y}} \right) &= \frac{1}{P_r} \left(\frac{\partial^2 T}{\partial x^2} + \frac{\partial^2 T}{\partial \bar{y}^2} \right) \end{aligned}$$

Momentum equation

Radial u -component

$$\frac{\partial^2 \psi}{\partial t \partial \bar{y}} + \frac{\partial \psi}{\partial \bar{y}} \frac{\partial^2 \psi}{\partial x \partial \bar{y}} - \frac{\partial \psi}{\partial x} \frac{\partial^2 \psi}{\partial \bar{y}^2} = - \frac{\partial p}{\partial x} + \frac{\partial^3 \psi}{\partial x^2 \partial \bar{y}} + \frac{\partial^3 \psi}{\partial \bar{y}^3} + T_r w + \frac{M}{(1+m\alpha)^2 + m^2} \left(mw - (1+m\alpha) \frac{\partial \psi}{\partial \bar{y}} \right) \quad (6.10a)$$

Vertical v -component

$$- \frac{\partial^2 \psi}{\partial t \partial x} - \frac{\partial \psi}{\partial \bar{y}} \frac{\partial^2 \psi}{\partial x^2} + \frac{\partial \psi}{\partial x} \frac{\partial^2 \psi}{\partial \bar{y} \partial x} = - \frac{\partial p}{\partial \bar{y}} - \frac{\partial^3 \psi}{\partial x^3} - \frac{\partial^3 \psi}{\partial \bar{y}^2 \partial x} + G_r T \quad (6.10b)$$

Axial w -component

$$\frac{\partial w}{\partial t} + \frac{\partial \Psi}{\partial \bar{y}} \frac{\partial w}{\partial x} - \frac{\partial \Psi}{\partial x} \frac{\partial w}{\partial \bar{y}} = D_n + \frac{\partial^2 w}{\partial x^2} + \frac{\partial^2 w}{\partial \bar{y}^2} - T_r \frac{\partial \Psi}{\partial \bar{y}} - \frac{M}{(1+m\alpha)^2 + m^2} \left[m \frac{\partial \Psi}{\partial \bar{y}} + (1+m\alpha)w \right] \quad (6.10c)$$

To find the unique equation for streamlines of the secondary velocity, it needs to combine the tangential and vertical component of momentum equations. To do this differentiate the equation (6.9a) with respect to \bar{y} and equation (6.9b) with respect to x , and then subtract them.

Now by differentiating equation (6.9a), with respect to \bar{y} gives

$$\begin{aligned} \frac{\partial}{\partial \bar{y}} \left[\frac{\partial^2 \psi}{\partial t \partial \bar{y}} + \frac{\partial \psi}{\partial \bar{y}} \frac{\partial^2 \psi}{\partial x \partial \bar{y}} - \frac{\partial \psi}{\partial x} \frac{\partial^2 \psi}{\partial \bar{y}^2} = \frac{\partial}{\partial \bar{y}} \left[- \frac{\partial p}{\partial x} + \frac{\partial^3 \psi}{\partial x^2 \partial \bar{y}} + \frac{\partial^3 \psi}{\partial \bar{y}^3} + T_r w + \frac{M}{(1+m\alpha)^2 + m^2} \left(mw - (1+m\alpha) \frac{\partial \psi}{\partial \bar{y}} \right) \right] \right] \\ \text{Or, } \frac{\partial^3 \psi}{\partial t \partial \bar{y}^2} + \frac{\partial^2 \psi}{\partial \bar{y}^2} \frac{\partial^2 \psi}{\partial x \partial \bar{y}} + \frac{\partial \psi}{\partial \bar{y}} \frac{\partial^3 \psi}{\partial x \partial \bar{y}^2} - \frac{\partial^2 \psi}{\partial \bar{y} \partial x} \frac{\partial^2 \psi}{\partial \bar{y}^2} - \frac{\partial \psi}{\partial x} \frac{\partial^3 \psi}{\partial \bar{y}^3} \end{aligned}$$

$$= -\frac{\partial^2 p}{\partial y \partial x} + \frac{\partial^4 \psi}{\partial x^2 \partial y^2} + \frac{\partial^4 \psi}{\partial y^4} + T_r \frac{\partial w}{\partial y} + \frac{M}{(1+m\alpha)^2 + m^2} \left(m \frac{\partial w}{\partial y} - (1+m\alpha) \frac{\partial^2 \psi}{\partial y^2} \right) \quad (6.11a)$$

Again by differentiating equation (6.9b), with respect to x gives

$$\begin{aligned} \frac{\partial}{\partial x} \left[-\frac{\partial^2 \psi}{\partial t \partial x} - \frac{\partial \psi}{\partial y} \frac{\partial^2 \psi}{\partial x^2} + \frac{\partial \psi}{\partial x} \frac{\partial^2 \psi}{\partial y \partial x} \right] &= \frac{\partial}{\partial x} \left[-\frac{\partial p}{\partial y} - \frac{\partial^3 \psi}{\partial x^3} - \frac{\partial^3 \psi}{\partial y^2 \partial x} + G_r T \right] \\ \therefore \frac{\partial^3 \psi}{\partial t \partial x^2} - \frac{\partial^2 \psi}{\partial x \partial y} \frac{\partial^2 \psi}{\partial x^2} - \frac{\partial \psi}{\partial y} \frac{\partial^3 \psi}{\partial x^3} + \frac{\partial^2 \psi}{\partial x^2} \frac{\partial^2 \psi}{\partial y \partial x} + \frac{\partial \psi}{\partial x} \frac{\partial^3 \psi}{\partial y \partial x^2} &= -\frac{\partial^2 p}{\partial x \partial y} - \frac{\partial^4 \psi}{\partial x^4} - \frac{\partial^4 \psi}{\partial y^2 \partial x^2} + G_r \frac{\partial T}{\partial x} \end{aligned} \quad (6.11b)$$

Now subtracting equation (6.11b) from (6.11a) gives

$$\begin{aligned} \frac{\partial^3 \psi}{\partial t \partial y^2} + \frac{\partial^2 \psi}{\partial y^2} \frac{\partial^2 \psi}{\partial x \partial y} + \frac{\partial \psi}{\partial y} \frac{\partial^3 \psi}{\partial x \partial y^2} - \frac{\partial^2 \psi}{\partial y \partial x} \frac{\partial^2 \psi}{\partial y^2} - \frac{\partial \psi}{\partial x} \frac{\partial^3 \psi}{\partial y^3} \\ + \frac{\partial^3 \psi}{\partial t \partial x^2} + \frac{\partial^2 \psi}{\partial x \partial y} \frac{\partial^2 \psi}{\partial x^2} + \frac{\partial \psi}{\partial y} \frac{\partial^3 \psi}{\partial x^3} - \frac{\partial^2 \psi}{\partial x^2} \frac{\partial^2 \psi}{\partial y \partial x} - \frac{\partial \psi}{\partial x} \frac{\partial^3 \psi}{\partial y \partial x^2} \\ = -\frac{\partial^2 p}{\partial y \partial x} + \frac{\partial^4 \psi}{\partial x^2 \partial y^2} + \frac{\partial^4 \psi}{\partial y^4} + T_r \frac{\partial w}{\partial y} + \frac{M}{(1+m\alpha)^2 + m^2} \left(m \frac{\partial w}{\partial y} - (1+m\alpha) \frac{\partial^2 \psi}{\partial y^2} \right) \\ + \frac{\partial^2 p}{\partial x \partial y} + \frac{\partial^4 \psi}{\partial x^4} + \frac{\partial^4 \psi}{\partial y^2 \partial x^2} - G_r \frac{\partial T}{\partial x} \end{aligned}$$

By writing this in order wise

$$\begin{aligned} \frac{\partial}{\partial t} \left(\frac{\partial^2 \psi}{\partial x^2} + \frac{\partial^2 \psi}{\partial y^2} \right) &= \frac{\partial^4 \psi}{\partial x^4} + \frac{\partial^4 \psi}{\partial y^2 \partial x^2} + \frac{\partial^4 \psi}{\partial y^4} - \frac{\partial^2 \psi}{\partial y^2} \frac{\partial^2 \psi}{\partial x \partial y} - \frac{\partial \psi}{\partial y} \frac{\partial^3 \psi}{\partial x \partial y^2} + \frac{\partial^2 \psi}{\partial y \partial x} \frac{\partial^2 \psi}{\partial y^2} - \frac{\partial \psi}{\partial x} \frac{\partial^3 \psi}{\partial y^3} \\ &\quad - \frac{\partial^2 \psi}{\partial x \partial y} \frac{\partial^2 \psi}{\partial x^2} - \frac{\partial \psi}{\partial y} \frac{\partial^3 \psi}{\partial x^3} + \frac{\partial^2 \psi}{\partial x^2} \frac{\partial^2 \psi}{\partial y \partial x} + \frac{\partial \psi}{\partial x} \frac{\partial^3 \psi}{\partial y \partial x^2} + \frac{\partial^4 \psi}{\partial x^2 \partial y^2} \\ &\quad + T_r \frac{\partial w}{\partial y} + \frac{M}{(1+m\alpha)^2 + m^2} \left(m \frac{\partial w}{\partial y} - (1+m\alpha) \frac{\partial^2 \psi}{\partial y^2} \right) - G_r \frac{\partial T}{\partial x} \end{aligned}$$

$$\begin{aligned} \text{Or, } \frac{\partial}{\partial t} \left(\frac{\partial^2 \psi}{\partial x^2} + \frac{\partial^2 \psi}{\partial y^2} \right) &= \frac{\partial^4 \psi}{\partial x^4} + 2 \frac{\partial^4 \psi}{\partial x^2 \partial y^2} + \frac{\partial^4 \psi}{\partial y^4} - \frac{\partial \psi}{\partial y} \frac{\partial^3 \psi}{\partial x \partial y^2} - \frac{\partial \psi}{\partial x} \frac{\partial^3 \psi}{\partial y^3} \\ &\quad - \frac{\partial \psi}{\partial y} \frac{\partial^3 \psi}{\partial x^3} + \frac{\partial \psi}{\partial x} \frac{\partial^3 \psi}{\partial y \partial x^2} + T_r \frac{\partial w}{\partial y} + \frac{M}{(1+m\alpha)^2 + m^2} \left(m \frac{\partial w}{\partial y} - (1+m\alpha) \frac{\partial^2 \psi}{\partial y^2} \right) - G_r \frac{\partial T}{\partial x} \end{aligned}$$

Hence the central line (axial) direction of Momentum equation

$$\frac{\partial w}{\partial t} + \frac{\partial \psi}{\partial y} \frac{\partial w}{\partial x} - \frac{\partial \psi}{\partial x} \frac{\partial w}{\partial y} = D_n + \frac{\partial^2 w}{\partial x^2} + \frac{\partial^2 w}{\partial y^2} - T_r \frac{\partial \psi}{\partial y} - \frac{M}{(1+m\alpha)^2 + m^2} \left[m \frac{\partial \psi}{\partial y} + (1+m\alpha) w \right] \quad (6.12a)$$

Stream line for the secondary velocity of Momentum equation

$$\begin{aligned} \frac{\partial}{\partial t} \left(\frac{\partial^2 \psi}{\partial x^2} + \frac{\partial^2 \psi}{\partial y^2} \right) &= \frac{\partial^4 \psi}{\partial x^4} + 2 \frac{\partial^4 \psi}{\partial x^2 \partial y^2} + \frac{\partial^4 \psi}{\partial y^4} - \frac{\partial \psi}{\partial y} \frac{\partial^3 \psi}{\partial x \partial y^2} - \frac{\partial \psi}{\partial x} \frac{\partial^3 \psi}{\partial y^3} \\ &\quad - \frac{\partial \psi}{\partial y} \frac{\partial^3 \psi}{\partial x^3} + \frac{\partial \psi}{\partial x} \frac{\partial^3 \psi}{\partial y \partial x^2} + T_r \frac{\partial w}{\partial y} + \frac{M}{(1+m\alpha)^2 + m^2} \left(m \frac{\partial w}{\partial y} - (1+m\alpha) \frac{\partial^2 \psi}{\partial y^2} \right) - G_r \frac{\partial T}{\partial x} \end{aligned} \quad (6.12b)$$

And the Energy equation

$$\frac{\partial T}{\partial t} + \left(\frac{\partial \psi}{\partial y} \frac{\partial T}{\partial x} - \frac{\partial \psi}{\partial x} \frac{\partial T}{\partial y} \right) = \frac{1}{P_r} \left[\frac{\partial^2 T}{\partial x^2} + \frac{\partial^2 T}{\partial y^2} \right] \quad (6.12c)$$

It is now looking forward to put the transformation $y = hy'$.

Since the non-dimensional transformation $\bar{y} = \frac{y}{d} \Rightarrow y = d \bar{y}$

Therefore $d\bar{y} = h y' \Rightarrow \bar{y} = \frac{h}{d} y' \therefore \bar{y} = l y'$,

where $l = h/d$ is the aspect ratio of this duct. Hence, by using $\bar{y} = l y'$ in to the equations (6.12a)-(6.12c), and thereafter remove prime on this variable for the sake simplicity, it becomes

The central line (axial) direction of Momentum equation

$$\frac{\partial w}{\partial t} + \frac{1}{l} \frac{\partial \psi}{\partial y} \frac{\partial w}{\partial x} - \frac{1}{l} \frac{\partial \psi}{\partial x} \frac{\partial w}{\partial y} = D_n + \frac{\partial^2 w}{\partial x^2} + \frac{1}{l^2} \frac{\partial^2 w}{\partial y^2} - \frac{1}{l} T_r \frac{\partial \psi}{\partial y} - \frac{M}{(1+m\alpha)^2 + m^2} \left[\frac{1}{l} m \frac{\partial \psi}{\partial y} + (1+m\alpha)w \right]$$

$$\therefore \frac{\partial w}{\partial t} = D_n + \frac{\partial^2 w}{\partial x^2} + \frac{1}{l^2} \frac{\partial^2 w}{\partial y^2} + \frac{1}{l} \left(\frac{\partial \psi}{\partial x} \frac{\partial w}{\partial y} - \frac{\partial \psi}{\partial y} \frac{\partial w}{\partial x} \right) - \frac{1}{l} T_r \frac{\partial \psi}{\partial y} - \frac{M}{(1+m\alpha)^2 + m^2} \left[\frac{1}{l} m \frac{\partial \psi}{\partial y} + (1+m\alpha)w \right]$$

Stream line for the secondary velocity of Momentum equation

$$\begin{aligned} \frac{\partial}{\partial t} \left(\frac{\partial^2 \psi}{\partial x^2} + \frac{1}{l^2} \frac{\partial^2 \psi}{\partial y^2} \right) &= \frac{\partial^4 \psi}{\partial x^4} + \frac{2}{l^2} \frac{\partial^4 \psi}{\partial x^2 \partial y^2} + \frac{1}{l^4} \frac{\partial^4 \psi}{\partial y^4} - \frac{1}{l^3} \frac{\partial \psi}{\partial y} \frac{\partial^3 \psi}{\partial x \partial y^2} - \frac{1}{l^3} \frac{\partial \psi}{\partial x} \frac{\partial^3 \psi}{\partial y^3} \\ &- \frac{1}{l} \frac{\partial \psi}{\partial y} \frac{\partial^3 \psi}{\partial x^3} + \frac{1}{l} \frac{\partial \psi}{\partial x} \frac{\partial^3 \psi}{\partial y \partial x^2} + \frac{1}{l} T_r \frac{\partial w}{\partial \bar{y}} + \frac{M}{(1+m\alpha)^2 + m^2} \left(\frac{1}{l} m \frac{\partial w}{\partial y} - \frac{(1+m\alpha)}{l^2} \frac{\partial^2 \psi}{\partial y^2} \right) - G_r \frac{\partial T}{\partial x} \\ \therefore \frac{\partial}{\partial t} \left(\frac{\partial^2 \psi}{\partial x^2} + \frac{1}{l^2} \frac{\partial^2 \psi}{\partial y^2} \right) &= \frac{\partial^4 \psi}{\partial x^4} + \frac{2}{l^2} \frac{\partial^4 \psi}{\partial x^2 \partial y^2} + \frac{1}{l^4} \frac{\partial^4 \psi}{\partial y^4} - \frac{1}{l^3} \frac{\partial \psi}{\partial y} \frac{\partial^3 \psi}{\partial x \partial y^2} - \frac{1}{l^3} \frac{\partial \psi}{\partial x} \frac{\partial^3 \psi}{\partial y^3} - \frac{1}{l} \frac{\partial \psi}{\partial y} \frac{\partial^3 \psi}{\partial x^3} \\ &+ \frac{1}{l} \frac{\partial \psi}{\partial x} \frac{\partial^3 \psi}{\partial y \partial x^2} + \frac{T_r}{l} \frac{\partial w}{\partial \bar{y}} + \frac{M}{(1+m\alpha)^2 + m^2} \frac{1}{l} m \frac{\partial w}{\partial y} - \frac{M(1+m\alpha)}{(1+m\alpha)^2 + m^2} \frac{1}{l^2} \frac{\partial^2 \psi}{\partial y^2} - G_r \frac{\partial T}{\partial x} \end{aligned}$$

Energy equation

$$\frac{\partial T}{\partial t} + \frac{1}{l} \left(\frac{\partial \psi}{\partial y} \frac{\partial T}{\partial x} - \frac{\partial \psi}{\partial x} \frac{\partial T}{\partial y} \right) = \frac{1}{P_r} \left[\frac{\partial^2 T}{\partial x^2} + \frac{1}{l^2} \frac{\partial^2 T}{\partial \bar{y}^2} \right]$$

For steady flow, the fluid properties are independent of time, therefore these equations can be written as follows:

Finally the central line (axial) direction of Momentum equation

$$D_n + \frac{\partial^2 w}{\partial x^2} + \frac{1}{l^2} \frac{\partial^2 w}{\partial y^2} + \frac{1}{l} \left(\frac{\partial \psi}{\partial x} \frac{\partial w}{\partial y} - \frac{\partial \psi}{\partial y} \frac{\partial w}{\partial x} \right) - \frac{T_r}{l} \frac{\partial \psi}{\partial y} - \frac{M}{(1+m\alpha)^2 + m^2} \frac{1}{l} m \frac{\partial \psi}{\partial y} - \frac{M(1+m\alpha)}{(1+m\alpha)^2 + m^2} w = 0 \quad (6.13a)$$

Stream line for the secondary velocity of Momentum equation

$$\begin{aligned} \left(\frac{\partial^4 \psi}{\partial x^4} + \frac{2}{l^2} \frac{\partial^4 \psi}{\partial x^2 \partial y^2} + \frac{1}{l^4} \frac{\partial^4 \psi}{\partial y^4} \right) - \frac{1}{l} \left(\frac{\partial^3 \psi}{\partial x^3} + \frac{1}{l^2} \frac{\partial^3 \psi}{\partial x \partial y^2} \right) \frac{\partial \psi}{\partial y} + \frac{1}{l} \left(\frac{\partial^3 \psi}{\partial y \partial x^2} - \frac{1}{l^2} \frac{\partial^3 \psi}{\partial y^3} \right) \frac{\partial \psi}{\partial x} \\ + \frac{T_r}{l} \frac{\partial w}{\partial y} + \frac{M}{(1+m\alpha)^2 + m^2} \frac{1}{l} m \frac{\partial w}{\partial y} - \frac{M(1+m\alpha)}{(1+m\alpha)^2 + m^2} \frac{1}{l^2} \frac{\partial^2 \psi}{\partial y^2} - G_r \frac{\partial T}{\partial x} = 0 \end{aligned} \quad (6.13b)$$

And the Energy equation

$$\frac{1}{P_r} \left(\frac{\partial^2 T}{\partial x^2} + \frac{1}{l^2} \frac{\partial^2 T}{\partial \bar{y}^2} \right) - \frac{1}{l} \left(\frac{\partial \psi}{\partial y} \frac{\partial T}{\partial x} - \frac{\partial \psi}{\partial x} \frac{\partial T}{\partial y} \right) = 0 \quad (6.13c)$$

The boundary conditions are as follows :

$$w(\pm 1, \bar{y}) = w(x, \pm 1) = \psi(\pm 1, \bar{y}) = 0$$

$$\left(\frac{\partial \psi}{\partial x} \right) (\pm 1, \bar{y}) = \psi(x, \pm 1) = \left(\frac{\partial \psi}{\partial \bar{y}} \right) (x, \pm 1) = 0 \quad (6.13d)$$

6.3 Straight Square Duct for Non-Isothermal Fluid Flow:

Non-Isothermal Steady Flow through a Rotating Square Straight Duct with Hall and Ion-slip Currents

This study investigated the fully developed viscous, non-isothermal, steady, laminar, incompressible, fluid flow through the centreline of a straight square duct in the presence of the magnetic field; Hall and Ion-slip currents. To make the non-isothermal state of the flow, the right hand wall of the duct is considered as heated whereas left hand wall is cooled; the lower and upper walls are considered as adiabatic. A constant pressure gradient forces (namely Dean Forces) are applied through the centreline direction of the duct. Also, the external forces such as the gravitational force, Lorentz force, pressure gradient force, centrifugal force, and Coriolis force act on the flow. The Lorentz force is also modified by applying the Hall and Ion-slip currents. The Governing equations are obtained from Continuity equation, Navier-Stokes equation and energy equation. The spectral method are applied to find the numerical solutions as the main tool, whereas Chebyshev polynomial, Newton-Raphson, Collocation, and Arc-length methods are used as secondary tools. The effects of the parameters, namely Grashof number (G_r), Taylor number (T_r), Dean Number (D_n), Magnetic parameter (M), Hall parameter (m), and Ion-slip parameter (α) on the flow of the velocity and temperature distributions are investigated by the solution curve of the flux versus above mentioned parameters and their corresponding structures of the flow pattern are studied at several distinct point of the straight duct. As the new findings, the results are shown under the various distinct values of M , m and α at Dean Number $D_n=500, 5000, 10000$ with Taylor number is fixed at $T_r=20$.

6.3.1 Grid Spaces Accuracy

Prior to execute the FORTRAN program; it is necessary to discuss about grid space accuracy. To achieve reasonable accuracy, it is required to select the equal values for \bar{M} and \bar{N} , because of the duct's square cross-section. The flux Q has been calculated for several pairs of truncation numbers (\bar{M}, \bar{N}) such as (16, 16), (18, 18), (20, 20) and (22, 22). These are displayed in Table-7.

\bar{M}	\bar{N}	Q
16	16	221.0305027708467
18	18	221.0309667187638
20	20	221.0309062038524
22	22	221.0308693799025

Table-7: Fluxes Q at distinct pairs of truncation numbers \bar{M} and \bar{N} for fixed $G_r = 0, T_r = 20, D_n = 500, P_r = 7, M = 0, m = 0$ and $\alpha = 0$.

This table shows that the numerical results are sufficient accurate at $(\bar{M}, \bar{N})=(20, 20)$.

6.3.2 Results and Discussion

The study initially focused on understanding the impact of Grashof number (G_r), Taylor number (T_r), and Dean Number (D_n) on flow patterns under the following fixed conditions: magnetic parameter ($M = 0$), Hall parameter ($m = 0$), and Ion-slip parameter ($\alpha = 0$). This investigation allowed for a deeper understanding of the inherent flow characteristics.

Following this initial analysis, a subsequent investigation explored the influence of additional parameters: the magnetic parameter, Hall parameter, and the Ion-slip parameter, on fluid flow. These results were presented in a solution curve, along with corresponding flow structures. The simulations were conducted under fixed values of the Prandtl number $Pr = 7$ and Taylor number $Tr = 20$, with three different Dean Numbers $D_n = 500, 5000, \text{ and } 10000$. The program employed increments $\Delta w = 50$, $\Delta \psi = 0.5$ and $\Delta T = 0.1$ to execute these analyses.

A. Effects of Grashof Number (G_r) on the Fluid Velocity and Temperature

In Fig. 6.3a, the solution curve illustrates the relationship between the Grashof Number (G_r) and (i) velocity flux and (ii) mean Nusselt number, representing temperature variations with respect to the Grashof number, at the cooling and heating walls. These results are presented with fixed values of $D_n = 500$, $P_r = 7$, $M = 0$, $m = 0$ and $\alpha = 0$.

For the flux, a single branch of a symmetric solution curve is evident, bounded within the range $G_r \leq 2547$. This curve demonstrates that the flux increases for positive G_r values but decreases for negative G_r values. Regarding temperature, it's noteworthy that the Nusselt number values at the heating wall consistently exceed those at the cooling wall. Additionally, the temperature deviation gradually decreases, albeit at a slow rate, as the absolute value of $|G_r|$ increases.

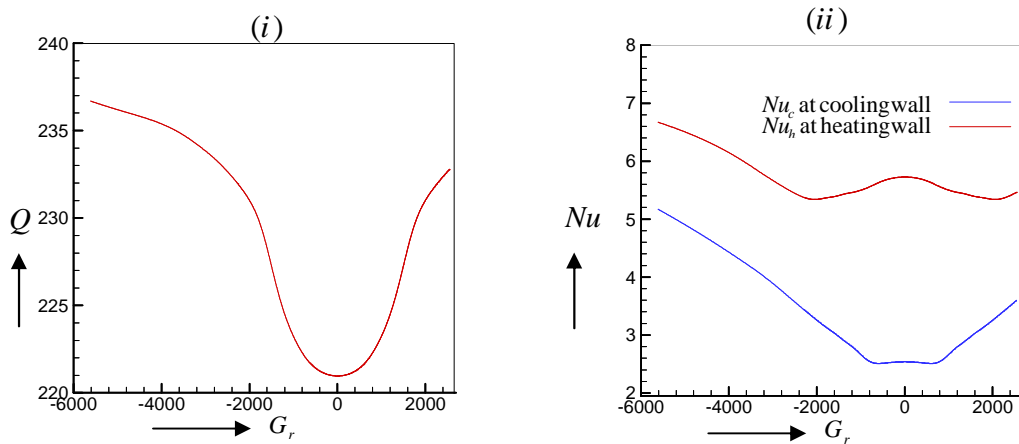


Figure 6.3a: Solution curve: Grashof Number G_r versus (i) flux Q (ii) Mean Nusselt number Nu at the heating and cooling wall for fixed $D_n = 500$, $T_r = 20$, $P_r = 7$, $M = 0$, $m = 0$ and $\alpha = 0$.

In Fig. 6.3b, corresponding flow and temperature structures at various points are depicted. Two vortex asymmetric flows have been identified in the secondary flow. Meanwhile, in

the axial flow, a simple contour is evident. The solution structure is notably influenced by the increase in the Grashof number. As the Grashof number increases, the asymmetric structures gradually become more prominent in both positive and negative directions. This asymmetry is primarily attributed to the influence of gravity. With the increase in rotation, the Coriolis force is counterbalanced by the Centrifugal force, pressure gradient force, and Lorentz force. This equilibrium results in the flow structure becoming approximately symmetric. However, the gravitational force acting on the fluid flow as an additional force introduces asymmetry into the flow pattern.

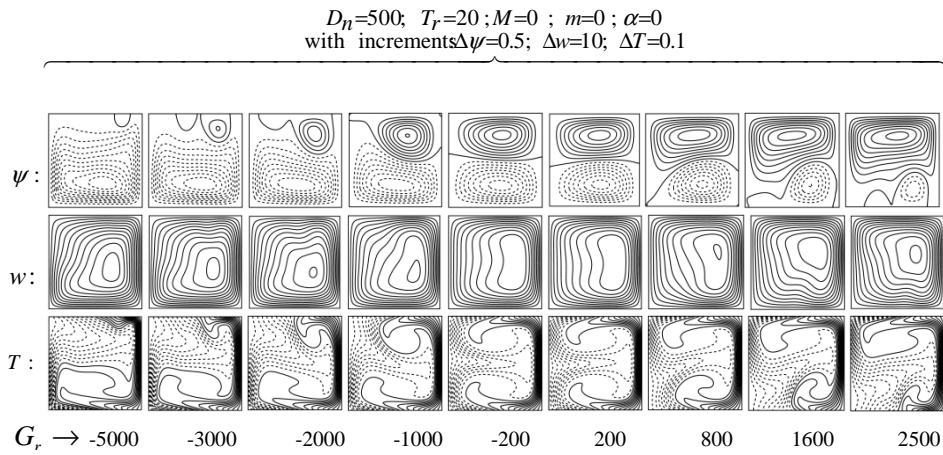


Figure 6.3b: Streamlines ψ (top), axial Contour flow w (middle) and Temperature profile T (bottom) in accordance with the solution curve in Fig.6.3a.

B. Effects of Taylor Number (T_r) on the Fluid Velocity and Temperature

Figure 6.4a presents the solution curve of Taylor Number (T_r) versus (i) velocity flux (Q) and (ii) mean Nusselt number (Nu), which represents temperature variations, at the cooling and heating walls. These results are obtained with fixed values of $D_n=1000$, $G_r=200$, $P_r=7$, $M=0$, $m=0$, and $\alpha=0$ Fig. 6.4b displays the corresponding flow structures at various points of T_r on these solution curves for velocity and temperature distribution. As $|T_r|$ increases, the strength of the secondary flow pattern becomes more pronounced, while the axial flow weakens. A critical zone is reached when the Taylor number reaches $|T_r|=672$. When $T_r > 0$, an increase in T_r results in the dominance of positive directed flow at the top of the duct, with it prevailing over the negative directed flow in terms of streamlines. However, the center of the axial flow contour gradually shifts closer to the cooling wall of the duct. In terms of temperature, the heating fluid dominates over the cooling fluid. Conversely, when $T_r < 0$, the opposite effect occurs as compared to $T_r > 0$.

The solution curve is bound within the range $-672 \leq T_r \leq 672$ and is symmetric about the vertical line at $T_r=0$. For the flux, it decreases for positive T_r but increases for negative T_r . In terms of temperature, for positive T_r , the Nusselt number values at the heating wall are greater than those at the cooling wall, while the opposite holds true for negative T_r . No

temperature deviation is observed at $T_r = 0$. Initially, the temperature deviation increases with the absolute value of T_r until a certain T_r value is reached, after which it gradually decreases with further increases in $|T_r|$.

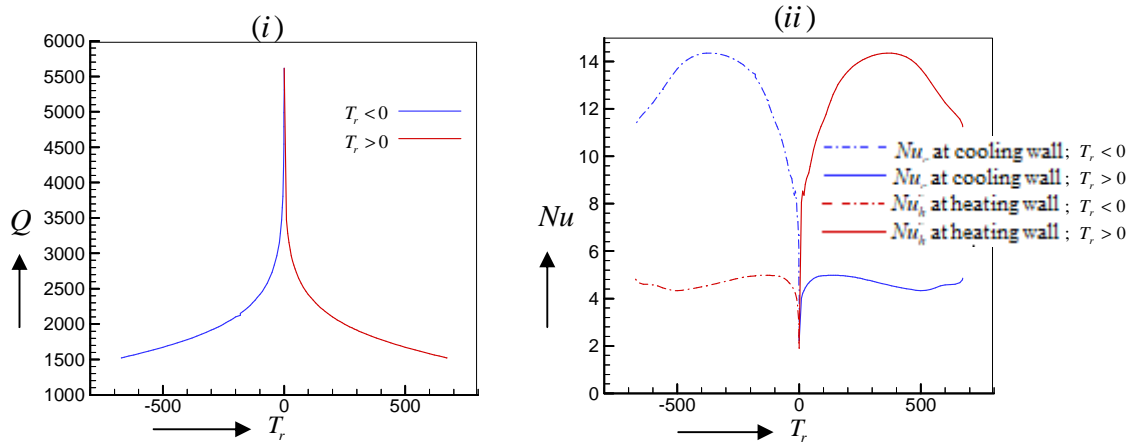


Figure 6.4a: Solution curve: Taylor Number T_r versus (i) flux Q (ii) Mean Nusselt number Nu at the heating and cooling wall for fixed $D_n = 10000$, $G_r = 200$, $P_r = 7$, $M = 0$, $m = 0$ and $\alpha = 0$.

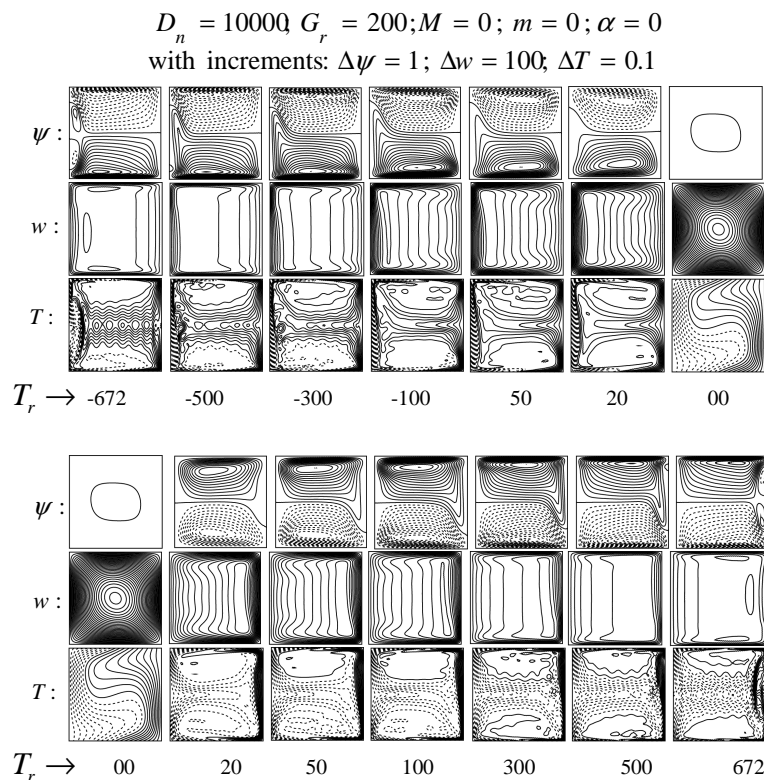


Figure 6.4b: Streamlines ψ (top), axial Contour flow w (middle) and Temperature profile T (bottom) in accordance with the solution curve in Fig.6.4a.

C. Effect of Dean Number (D_n) on the Fluid Velocity and Temperature

In Figure 6.5a, you can see the solution curve of Dean Number (D_n) versus (i) velocity flux and (ii) mean Nusselt number (Nu), which represents temperature variations, at the cooling and heating walls. These results are obtained with fixed values of $G_r=200$, $T_r=20$, $P_r=7$,

$M=0$, $m=0$, and $\alpha=0$. The solution curve is found for all positive values of the Dean Number. Three bifurcation solution curves are observed in a small range $25957.8 < D_n < 2722.7$ (approximately). In all the solution curves, the flux increases with the increase of Dean Number. However, for the temperature, the values of the Nusselt number at the heating wall are higher than at the cooling wall, except at $D_n = 0$. This difference gradually increases with the increase of D_n .

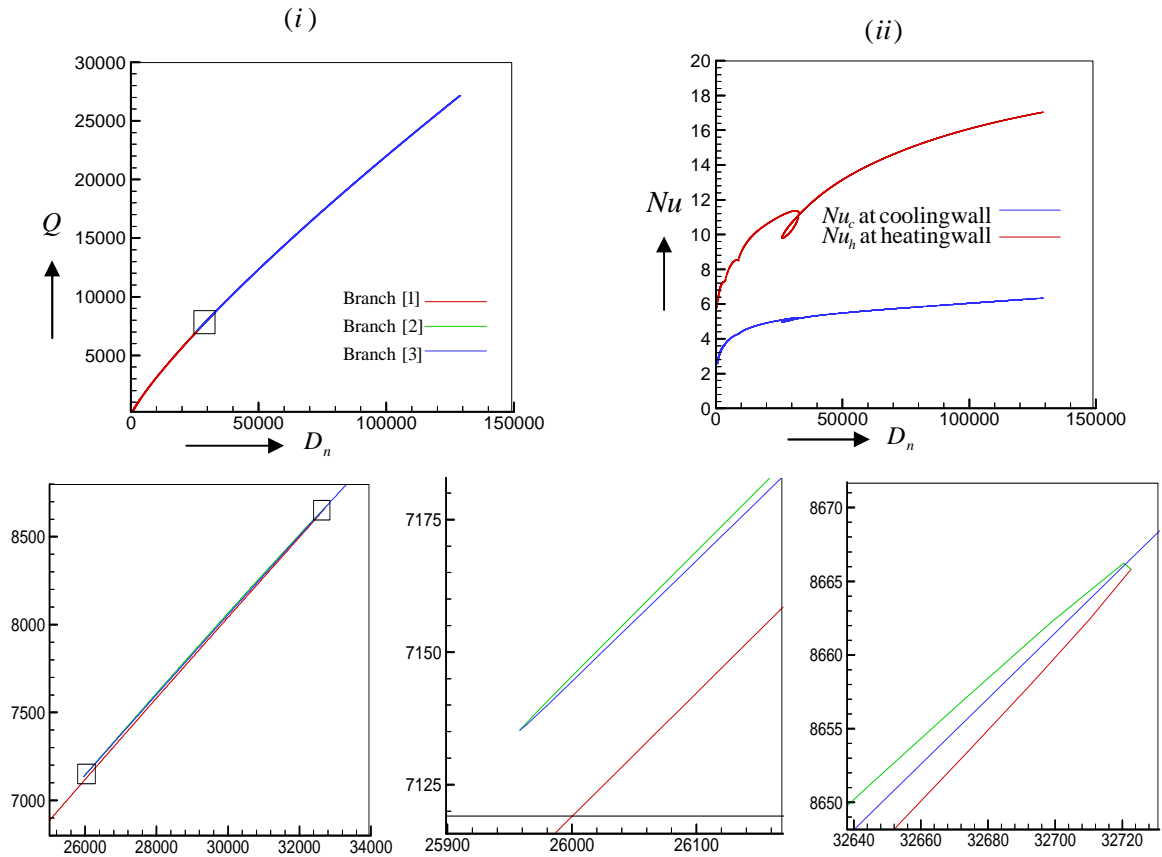


Figure 6.5a: Solution curve: Dean Number D_n versus (i) flux Q (ii) Mean Nusselt number Nu at the heating and cooling wall for fixed $T_r = 20$, $G_r = 200$, $P_r = 7$, $M = 0$, $m = 0$ and $\alpha = 0$.

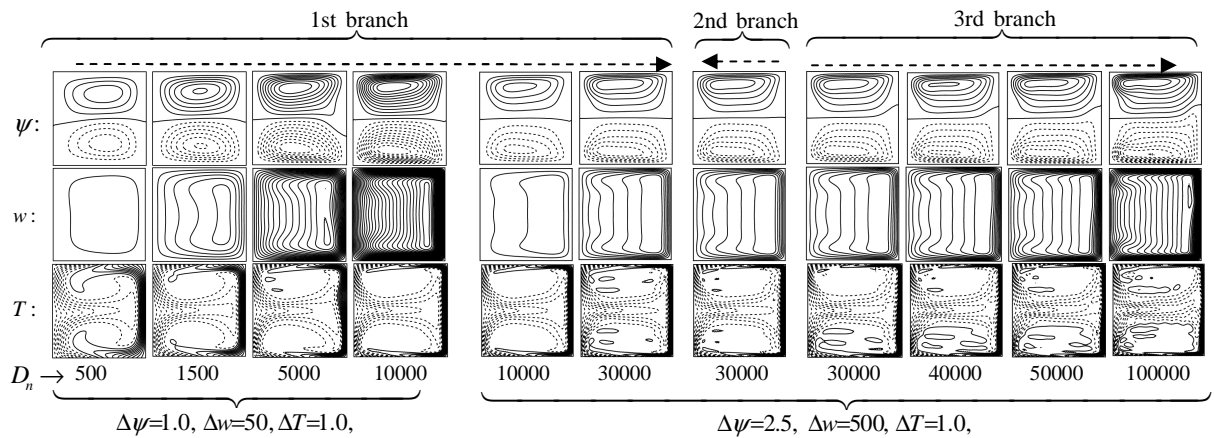


Figure 6.5b: Streamlines ψ (top), axial Contour flow w (middle) and Temperature profile T (bottom) in accordance with the solution curve in Fig.6.5a.

In Figure 6.5b, It is observed that the corresponding flow structures, including vortex structures of streamlines, contour distributions of axial flow, and temperature patterns. In all branches of the steady-state solution curve, a pair of counter-rotating vortices is observed for the secondary flow. The dominance between negative and positive rotational flow is reversed as D_n increases. The strength of the flow patterns gradually increases with the increase in D_n , both for velocity and temperature distribution. Asymmetrical flow structures are found in the 1st and 3rd branches of the steady-state solution curves. For the temperature distribution, the heated flow is dominated by the cooling flow.

D. Effects of Magnetic Parameter (M) on the Fluid Velocity and Temperature

Figure 6.6a shows the solution curve representing the relationship between the Magnetic parameter (M) with (i) the velocity flux (Q) and (ii) the mean Nusselt number (Nu) for the cooling and heating walls in the context of temperature distribution. These findings are presented with consistent parameters, including $G_r=200$, $T_r=20$, $P_r=7$, $m=0$, and $\alpha=0$. This investigation explores the influence of M across three different scenarios characterized by varying Dean Numbers such as $D_n=500$, 5000 and 10000.

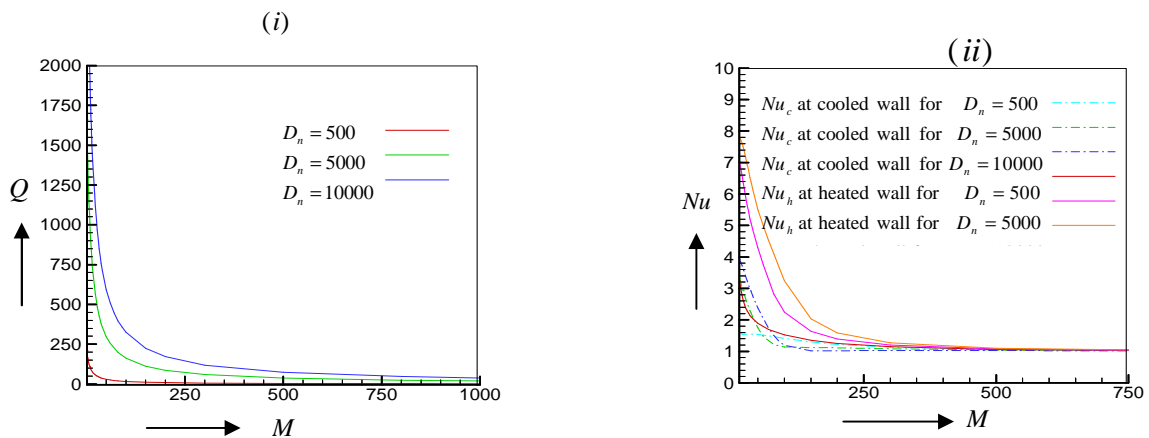


Figure 6.6a: Solution curve: Magnetic parameter M versus (i) flux Q (ii) Mean Nusselt number Nu at the heating and cooling wall for fixed $T_r = 20$, $G_r = 200$, $P_r = 7$, $m = 0$ and $\alpha=0$ where $D_n = 500, 5000, 10000$.

In all scenarios, the solution curves exhibit a decreasing trend, leading to a reduction in flux as M increases. For high values of M , fluxes tend to approach zero. It's worth noting that the fluxes increase with higher Dean Numbers. Regarding temperature, the Nusselt numbers at the heating wall consistently surpass those at the cooling wall. The temperature deviation slowly approaches zero after a certain threshold value of M .

In Figure 6.6b, it has been seen the vortex structures, contour distributions for velocity, and patterns of temperature flow. As M becomes larger, the strength of velocity distribution gradually weakens. Concerning temperature, the cooling wall's temperature dominates over the heating wall's temperature, and this dominance effect diminishes as M increases across all the Dean Number scenarios.

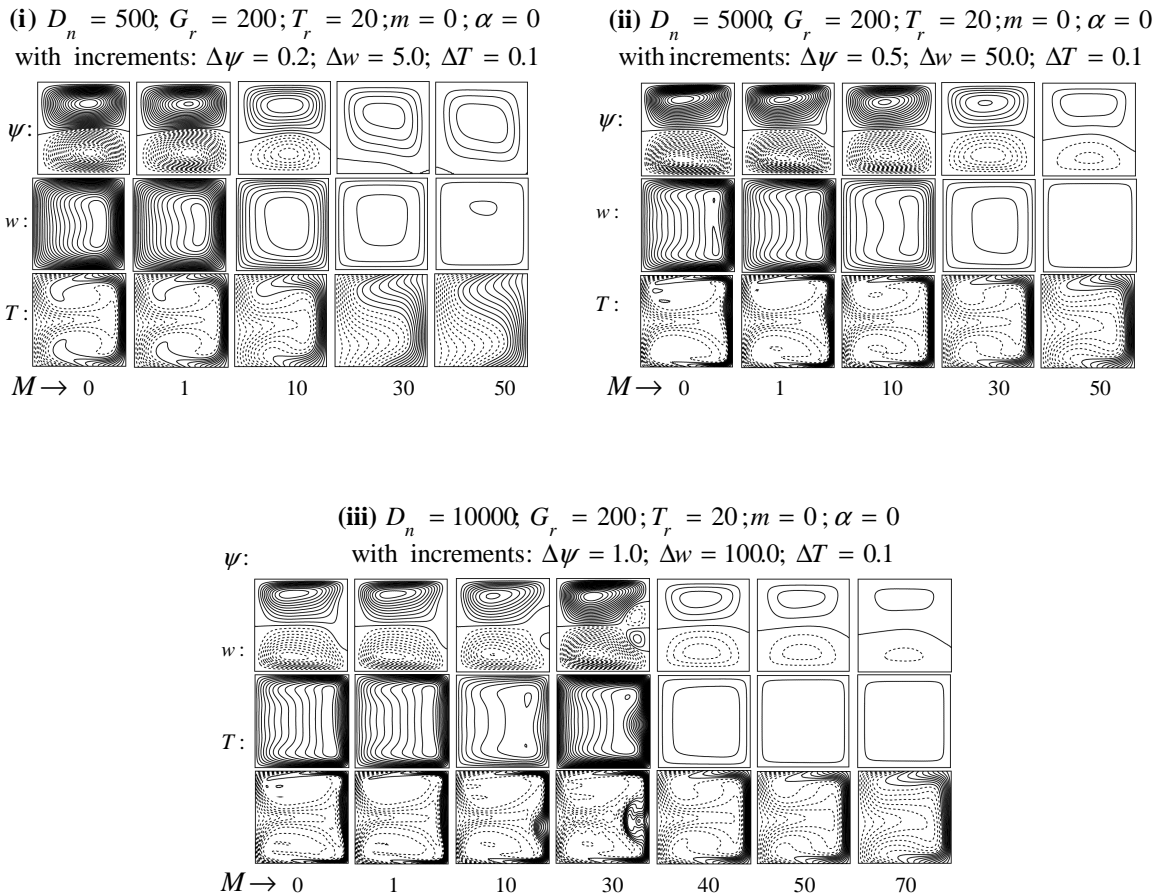


Figure 6.6b: Streamlines ψ (top), axial Contour flow w (middle) and Temperature profile T (bottom) in accordance with the solution curve in Fig.6.6a.

E. Effects of Hall Parameter (m) on the Fluid Velocity and Temperature

Figure 6.6a presents the solution curve for the Hall parameter (m) versus (i) the flux (Q) for velocity and (ii) the mean Nusselt number (Nu) at the cooling and heating walls for temperature. The fixed parameters are $G_r=200, T_r=20, P_r=7, M=13$, and $\alpha=0$ whereas three different Dean Numbers $D_n = 500, 5000$, and 10000 are considered.

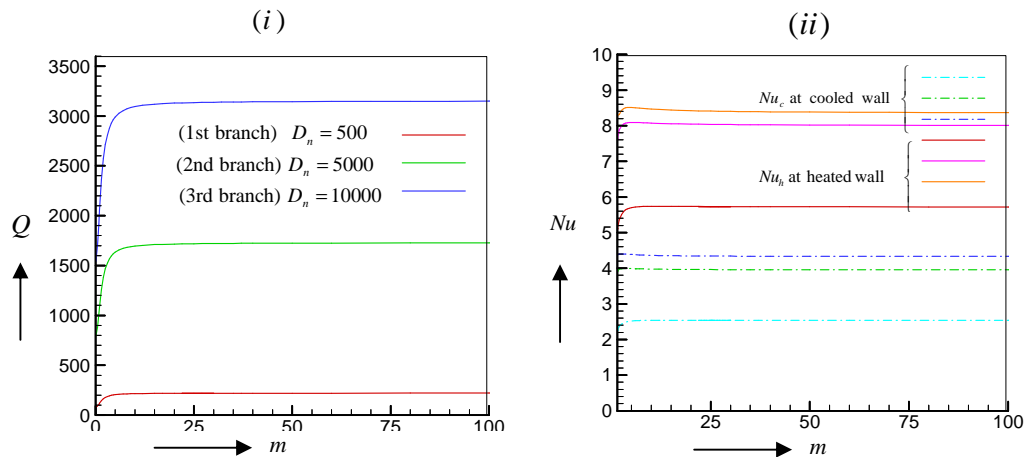


Figure 6.7a: Solution curve: Hall parameter m versus (i) flux Q (ii) Mean Nusselt number Nu at the heating and cooling wall for fixed $T_r = 20, G_r = 200, P_r = 7, M = 13$ and $\alpha = 0$ where $D_n = 500, 5000, 10000$.

In all Dean Number scenarios, the solution curves exhibit an increasing trend for the Hall parameter (m). The flux increases rapidly with a growing m within a specific range, approximately $0 \leq m \leq 5$. After this initial rapid increase, it exhibits a minor increase and eventually reaches a steady-state solution beyond a certain threshold value of m . The maximum flux is achieved at m values exceeding 200 (approximately). The numerical results show maximum flux values of 221, 1728.18, and 3150.84 for Dean Numbers 500, 5000, and 10000, respectively. It's worth noting that the flux increases with higher Dean Numbers. Regarding temperature, the Nusselt numbers at the heating wall consistently surpass those at the cooling wall across all m values. However, the temperature deviations remain unchanged as m increases.

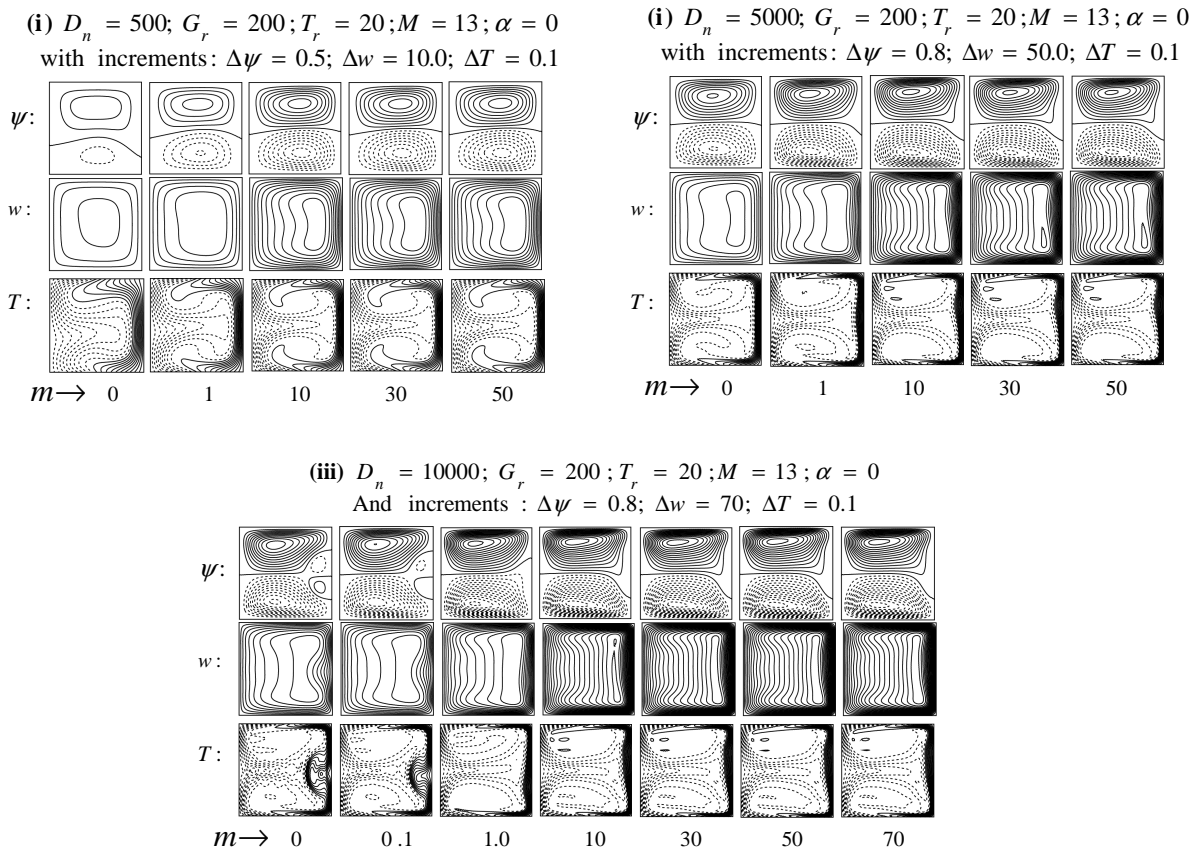


Figure 6.7b: Streamlines ψ (top), axial Contour flow w (middle) and Temperature profile T (bottom) in accordance with the solution curve in Fig.6.7a.

Figure 6.7b provides a visualization of the vortex structures, velocity distribution contours, and temperature flow patterns. These correspond to the solution curve depicted in Figure 6.7a at specific Hall parameter values. The strength of the velocity and temperature distribution exhibits an increase in pattern intensity within the range $0 \leq m \leq 10$. After this range, the structures remain consistent and do not change with further increases in m . Notably, for Dean Number $D_n=10000$, a pair of vortices is created in the secondary flow.

Regarding temperature, it's observed that the heating wall temperature consistently dominates over the cooling wall temperature across various m values. This effect remains unchanged with increasing m for all Dean Number scenarios.

F. Effects of Ion-slip Parameter (α) on the fluid flow and Temperature

Figure 6.6a presents the solution curve for the Ion-slip parameter (α) versus (i) the flux (Q) for velocity and (ii) the mean Nusselt number (Nu) at the cooling and heating walls for temperature. The fixed parameters are $G_r=200$, $T_r=20$, $P_r=7$, $M=13$, and $m=0.1$, whereas three different Dean Numbers $D_n = 500$, 5000 , and 10000 are considered.

For all cases of Dean Number, the solution curves exhibit an increasing trend as the Ion-slip parameter (α) varies. There is a rapid increase in flux within a certain range, typically between $0 \leq \alpha \leq 200$, followed by a gradual increase in flux, and eventually, a steady-state solution is reached after a specific value of α . The maximum flux is achieved when α is greater than or equal to 750 (approximately). The numerical results show maximum flux values of 217.7, 1710.4, and 3134.8 for Dean Numbers $D_n = 500$, 5000 , and 10000 respectively. It is also confirmed that the flux increases with an increase in Dean Number.

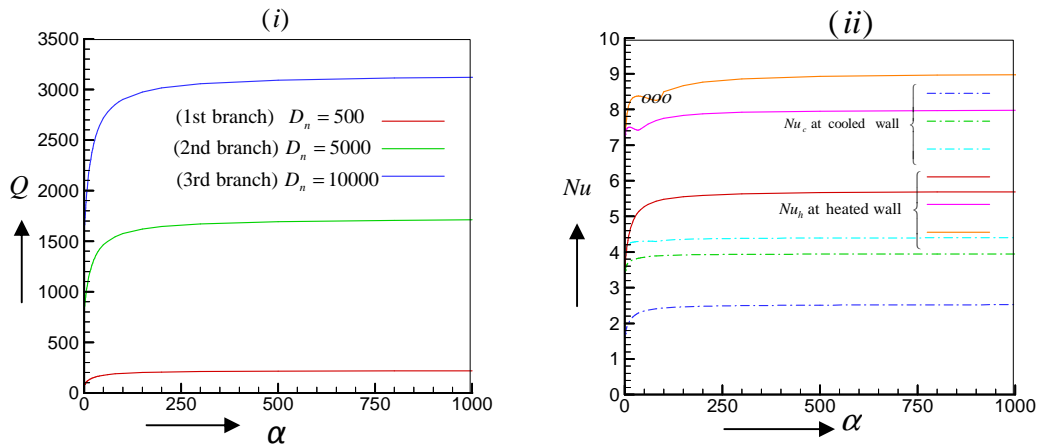
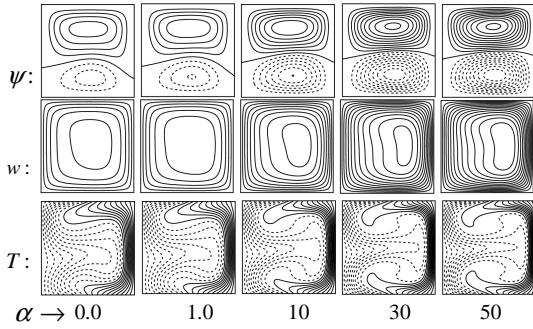


Figure 6.8a: Solution curve: Ion-slip parameter α versus (i) flux Q (ii) Mean Nusselt number Nu at the heating and cooling wall for fixed $T_r = 20$, $G_r = 200$, $P_r = 7$, $M = 13$ and $m = 0.1$ where $D_n = 500, 5000, 10000$.

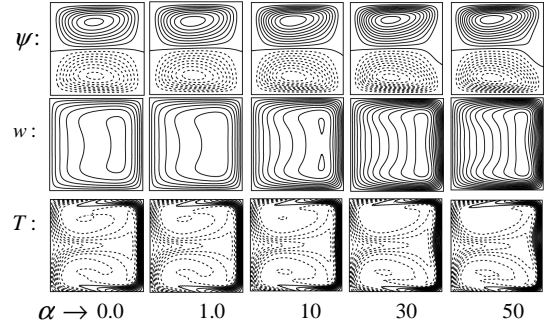
Concerning temperature, the Nusselt number values at the heating wall consistently exceed those at the cooling wall across various values of α . Importantly, the temperature deviation remains constant after reaching a certain value of α .

In Fig. 6.8b, the vortex structures, velocity distribution contours, and temperature flow patterns corresponding to the solution curve of Fig. 6.8a are presented at specific points along the Ion-slip parameter. Within the range of $0 \leq \alpha \leq 10$, both velocity and temperature distributions exhibit robust patterns. However, beyond this range, the structures remain relatively consistent and do not significantly change with further increases in α .

(i) $D_n = 500; G_r = 200; T_r = 20; M = 13; m = 0.1$
with increments : $\Delta\psi = 0.3; \Delta w = 6.0; \Delta T = 0.1$



(ii) $D_n = 5000; G_r = 200; T_r = 20; M = 13; m = 0.1$
with increments : $\Delta\psi = 0.8; \Delta w = 50.0; \Delta T = 0.1$



(iii) $D_n = 10000; G_r = 200; T_r = 20; M = 13; m = 0.1$
with increments : $\Delta\psi = 0.8; \Delta w = 100; \Delta T = 0.1$

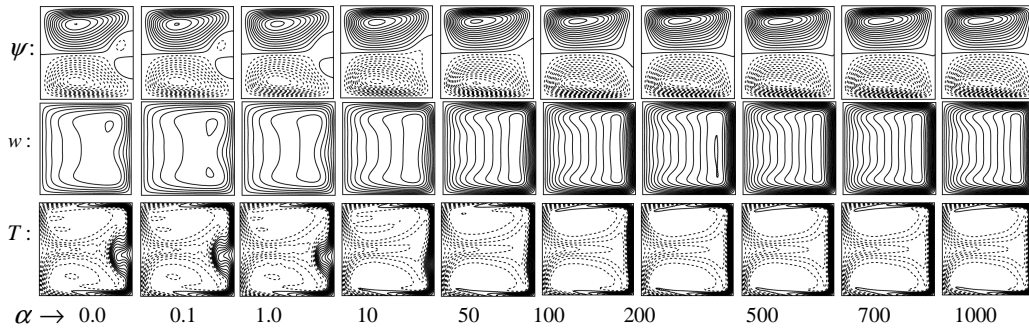


Figure 6.8b: Streamlines ψ (top), axial Contour flow w (middle) and Temperature profile T (bottom) in accordance with the solution curve in Fig.6.8a.

Notably, in the case of Dean Number $D_n = 10000$, a pair of vortices emerges in the secondary flow. Additionally, in terms of temperature, the heating wall temperature consistently dominates the cooling wall temperature throughout the evaluated range of Ion-slip parameter (α).

Chapter 7

General Discussion and Conclusions

7.1 General Discussion

This research has numerically simulated the fully developed two-dimensional flow of a viscous incompressible fluid through the straight and curved ducts with square and rectangular cross-sections for various curvatures of the duct. Flow characteristics are studied on various aspect ratios of the curved duct for both the isothermal ($G_r = 0$) and non-isothermal ($G_r > 0$) flows over a wide range of the Taylor Number (T_r), Dean Number (D_n) and curvature of the duct (δ). The steady solution have been obtained by using the spectral method as a primary tool and collocation, Chebyshev polynomial and arc length methods have been used as secondary tools. The outcomes of the isothermal and non-isothermal curved and straight duct flows have been thoroughly discussed in chapters 4, 5 and 6. A direct comparison of our results for isothermal flows could not be made because few experimental results are available for non-isothermal flows. In that case, the comparisons have been performed by the choice of the Grashof number $G_r = 0$ and in the absence of an energy equation. But for non-isothermal flows have been compared with the experimental results that are available [Yamamoto et al. (2006) and Chandratilleke et al. (2001)]. Since no experimental results for the flow through a rectangular curved duct with an aspect ratio of 3 are available, so a comparison of our results could not be made with the experimental data in that case. Overall, the demonstrated comparisons show good agreement with the experimental results both qualitatively and quantitatively. Considering the method of analysis and the trends of the data, it is recommended that the current study be expanded to incorporate additional research on curved duct flows. Comparing the experimental findings to those of the current study is also fascinating. The conclusions of our present studies are briefly summarized in section 7.2 below.

7.2 Conclusions

The present numerical results are accurately and sufficiently compared to the previously published experimental results. Therefore, it is conceivable that the study's findings are valid. The findings, which are based on the thorough examination of the relevant parameters discussed above, can be summarized as follows:

7.2.1 Curved Square Duct for Isothermal Fluid Flow

1. As the curvature (δ) increases, the peak value of flux (Q) gradually decreases.
2. Due to the duct's rotation, a larger proportion of the flow is directed toward the boundary, and this trend intensifies with an increase in the magnitude of the Taylor number $|T_r|$.
3. The strength of the fluid velocity gradually weakens with increasing $|T_r|$.
4. The vorticity of the secondary flow increases, and its tendencies become stronger as Dean Number increases.
5. A pair of counter-rotating vortex structures is present in the streamlines, and simply closed contours define the axial velocity for all considered parameter effects.
6. Symmetric two-cell vortex structures are created when D_n exceeds approximately 640.
7. Symmetric two-vortex solutions are observed for all values of the parameters M , m , or α when Dean Number is fixed at $D_n = 500$. However, at $D_n = 1000$, solutions include two and four-vortex patterns.
8. All the solution curves exhibit a decreasing function for positive values of the magnetic parameter (M). Consequently, the flux Q decreases with an increase in M , eventually approaching zero velocity after a specific value of the magnetic parameter.
9. With a small curvature and increasing M , a higher quantity of axial flow tends to pass closer to the outer wall before transitioning towards the centre of the duct. Conversely, in the case of significant curvature, flows are redirected toward the duct's interior side.
10. The flux increases rapidly within the limited range of $0 \leq m < 5$ and then rises slowly as m increases. After a certain value of m , a steady-state solution is achieved. The flow structures exhibit minor changes with increasing m .
11. The flux experiences a sharp reduction within the range $0 \leq \alpha < 0.8$, followed by a rapid increase within the range $0.8 \leq \alpha < 10$. Beyond this range, there is a slight increase in flux with further increases in α . A steady solution is found after a specific value of α , and the flow structures undergo negligible changes with increased α .
12. The flux undergoes reduction within the range $0 \leq \alpha < 0.8$, followed by a sharp increase within the range $0.8 \leq \alpha < 10$. Beyond this range, there is a slight increase in flux with increasing α . A steady solution is found after a specified value of α .

7.2.2 Curved Rectangular Duct for Isothermal Fluid Flow (Aspect Ratio 2)

1. Positive Taylor Number (T_r) is associated with co-rotation, whereas negative T_r is associated with counter-rotation.
2. As the Dean Number (D_n) increases, symmetric solutions with two, four, six, or even eight vortices are obtained for the secondary flow. In contrast, axial flow exhibits contour plots with one, two, three, or more shapes.
3. The maximum number of vortices gradually increases with rising Dean Number until reaching a specific value of D_n . Beyond this point, the number of vortices decreases, creating a strong and critical structure.
4. The flux Q steadily rises with increasing Dean Number.
5. The solution curve of Q versus T_r exhibits a simpler structure for larger values of the curvature (δ) compared to smaller values.
6. The maximum flux decreases as the curvature increases.
7. An increase in the magnetic parameter (M) leads to a rapid decrease in Q .
8. As M increases, both axial and secondary flow structures deteriorate progressively.
9. With an increase in the Hall parameter (m), the flux Q increases rapidly. A steady solution is reached after a certain value of m .
10. Secondary flow patterns and axial flow shapes undergo negligible changes as m increases.
11. The flux Q initially drops within a narrow range before rapidly increasing with rising α . A steady-state solution emerges after a specific value of α .
12. An increase in α leads to minimal alterations in the secondary flow structures and axial flow contours.

7.2.3 Curved Rectangular Duct for Isothermal Fluid Flow (Aspect Ratio 3)

1. Positive and negative values of the Taylor Number (T_r) correspond to co-rotation and counter-rotation of the flow, respectively.
2. Flow patterns for positive T_r are simpler compared to those for negative T_r .
3. Increasing the rotation parameter T_r leads to a gradual decrease in the flow's strength.
4. An admissible flow pattern is observed over a wide range of Dean Numbers $0 \leq D_n < 800$.
5. The flux Q gradually increases with the rising value of Dean Number (D_n).
6. The flux Q consistently increases with the increase of Dean Number D_n .

7. Small curvature, as opposed to larger curvature, results in more complex flow patterns. Small curvature combined with a high value of Dean Number leads to asymmetric solutions for the secondary flow and uncountable contour plots for the axial flow.
8. All cases demonstrate a similar unrestricted application with a curvature of $\delta = 0.1$.
9. Increasing the magnetic parameter M results in a gradual deterioration in the strength of the flow. Unlike axial flow, which exhibits multiple contours, the solution structure for the secondary flow consists of symmetric four- and six-vortex streamlines.
10. An increase in the Hall parameter (m) has negligible effects on the secondary flow vortices and axial flow contours. The flux rapidly decreases within the range of $0 \leq m \leq 0.7$, then quickly rises within the range of $0.7 \leq m \leq 4$, before gradually increasing. A steady-state value is achieved after a specific value of m .
11. As the Ion-slip parameter α increases, there are minimal effects on the secondary flow vortices and axial flow contours. The strength of both flows remains consistent for all values of the Ion-slip parameter.

7.2.4 Curved Square Duct for Non-Isothermal Fluid Flow

Velocity Profile:

1. The symmetrical flow gradually becomes asymmetrical due to the influence of gravity.
2. The degree of asymmetry increases with higher values of G_r and D_n .
 1. Asymmetrical condition decreases with the increase of T_r
3. At $T_r = -261.2$, the flux exhibits a peak with six secondary flow vortices.
4. In the case of a large D_n , most of the flow is pushed towards the duct's boundary wall.
5. The flux increases with higher values of G_r , D_n , and m but decreases with higher values of T_r , M , and δ .
6. Steady-state flux is achieved after specific large values of M , m , and α .
7. The fluid velocity's intensity increases with a higher D_n but weakens with higher values of M , T_r , and δ .
8. The strength of fluid velocity remains relatively unchanged with variations in G_r , m , and α .

Temperature Profile:

1. The temperature distribution becomes chaotic with large values of D_n .
2. Temperature deviation gradually increases with higher values of D_n .
3. Temperature deviation gradually decreases with higher values of G_r and M .
4. The temperature deviation remains consistent with changes in m and α .
5. Temperature deviation initially decreases with higher T_r within the range $-274.66 < T_r < -261.20$, but then reverses this effect.

7.2.5 Curved Rectangular Duct for Non-Isothermal Fluid Flow (Aspect Ratio 2)

Velocity Profile:

1. The influence of gravity on fluid flow leads to a transition from a symmetrical pattern to an asymmetrical one. The solution curves for the flow are confined within the range $-1188.76 \leq G_r \leq 1190.17$, and they exhibit symmetry about the vertical line at $G_r = 0$.
2. For all positive values of D_n , the solution curves are increasing functions, resulting in an increase in flux as this parameter rises.
3. Conversely, the solution curves are decreasing functions for positive values of G_r , T_r , and M . Therefore, an increase in these parameters leads to a decrease in flux.
4. In the positive direction, the flux gradually decreases as T_r increases, while in the negative direction, a critical zone is reached at $T_r = -237.44$, and further progression in this direction ceases.
5. Both the strength of vortices and contours progressively diminish with increasing T_r and M . However, there are minor changes in these aspects with variations in Hall and Ion-slip parameters.
6. The flux experiences a rapid drop in one branch when magnetic parameters are increased. In another branch, radial flow initially consists of two vortices, with two additional vortices forming near the duct's outer wall.
7. An increase in the Hall and Ion-slip parameters results in a swift increase in flux. After reaching specific values of Hall and Ion-slip parameters, a steady-state solution is attained.

Temperature Profile:

1. With a large value of D_n , the temperature distribution exhibits chaotic behaviour.
2. The temperature deviation gradually decreases as T_r increases.
3. Both the Hall parameters and Ion-slip parameters have minimal effects on the temperature profiles. In both cases, the cooling temperature dominates the heating temperature.

7.2.6 Curved Rectangular Duct for Non-Isothermal Fluid Flow (Aspect Ratio 3)

Velocity Profile:

1. Due to gravity, the initially symmetrical situation gradually becomes asymmetrical.
2. With an increase in G_r in the positive direction, positive rotational radial flow dominates over negative flow, while the opposite occurs in the negative direction.
3. Increasing D_n results in a maximum of two vortex structures in the radial flow and simple contour shapes in the axial flow. For larger D_n values, the majority of the flow is pushed toward the duct's outer wall.
4. The solution curves increase when influenced by parameters like D_n , m , and α , while they decrease when affected by parameters like G_r , T_r , and M . This leads to an increase in flux with increasing D_n , m , and α , while it decreases with increasing G_r , T_r , and M .
5. After reaching particular values of M , m , and α , steady solutions are discovered.
6. The fluid velocity strengthens with increasing D_n but weakens with increasing M and T_r .
7. The fluid velocity undergoes slight changes as G_r , m , and α increase. After a specific value of D_n , the temperature distribution becomes chaotic.

Temperature Profile:

1. The Nusselt number values at the heating wall are consistently higher than at the cooling wall for positive values of all parameters such as G_r , T_r , D_n , m , and α , except for M .
2. The heating flow is consistently dominated by the cooling flow across variations in parameters like G_r , T_r , D_n , M , m , and α .
3. The temperature deviation remains constant after reaching specific values of parameters m and α .

7.2.7 Straight Square Duct for Non-Isothermal Fluid Flow

Velocity Profile:

1. The solution curves exhibit an increasing trend for parameters like G_r ($G_r > 0$), T_r ($T_r < 0$), D_n ($D_n > 0$), m ($m > 0$), and α ($\alpha > 0$). Consequently, the flux increases within these parameter ranges.
2. Conversely, the solution curves demonstrate a decreasing trend for parameters like G_r ($G_r < 0$), T_r ($T_r > 0$), and M ($M > 0$). Consequently, the flux decreases within these parameter ranges.
3. The fluid velocity structure is initially symmetric at $G_r = 0$, but this symmetry gradually becomes asymmetric as $|G_r|$ increases.

4. The solution curve remains symmetric about the vertical line at $T_r = 0$.
5. Steady-state solution branches exhibit a pair of counter-rotating vortices for the secondary flow in all cases.
6. The fluid velocity's strength increases with higher values of D_n and T_r , while it weakens with higher values of M .
7. The strength of both velocity and temperature distributions becomes strong within a certain parameter range, and beyond this range, their structures remain unchanged with increasing values of m and α .

Temperature Profile:

1. At various parameter variations, including G_r , T_r , D_n , M , m , and α , the Nusselt number values at the heating wall are consistently higher than those at the cooling wall.
2. The heating flow consistently dominates over the cooling flow across different parameter variations, including G_r , T_r , D_n , M , m , and α .
3. No temperature deviation is observed at $T_r = 0$. The temperature deviation gradually increases with the absolute value of T_r until a certain T_r value, after which it decreases slowly as the absolute value of T_r continues to rise.
4. The temperature deviation gradually increases with the increase in D_n .
5. The temperature deviation decreases as M increases.
6. The temperature deviation remains constant beyond certain values of m and α .

Incorporating Hall and Ion-slip currents in the study of curved duct flow has considerable significance not only in improving the efficiency of mechanical devices but also in advancing our understanding of fluid dynamics in various engineering applications. Given that the universe consists of highly charged particles and is influenced by magnetic fields, these considerations provide a more accurate framework for analyzing the behaviour of fluid flow in curved ducts. Based on the insights discussed above, the utilization of Hall current and Ion-slip in the context of curved duct flow represents a promising and valuable avenue for research in the field of magneto-hydrodynamics (MHD) and engineering applications.

References

- Adler, M. (1934). Strömung in gekrümmten Rohren, *Zeitschrift für Angewandte Mathematik und Mechanics (ZAMM)*, 14, 257-275.
- Agarwall, Y. Talbot, L and Gong, K. (1978). Laser anemometer study of flow development in curved circular pipes, *Journal of Fluid Mechanics*, 85, 497-518.
- Akiyama, M and Cheng, K. C. (1974). Graetz problem in curved pipes with uniform wall Heat flux, *Applied Science and Research*, 29, 401-418.
- Anderson, R. and Lauriat, G. (1986). The horizontal natural convection boundary layer regime in a closed cavity, *Proc. of the 8th Int. Heat Transfer Conf.*, 4, San Francisco, CA, 1453-1458.
- Arnal, M. P., Goering, D. J. and Humphrey, J. A. C. (1992). Unsteady laminar flow developing in a curved duct, *Int. J. of Heat and Fluid Flow*, 13(4), 347-357.
- Austin, L. R. and Seader, J. D. (1973). Fully developed viscous flow in coiled circular pipes, *AIChE Journal*, 19(1), 85-94.
- Aydin, O., Unal, A. and Ayhan, T. (1999). Natural convection in rectangular enclosures heated from one side and cooled from the ceiling, *Int. J. Heat Mass Transfer*, 42, 2345-2355.
- Bara, B., Nandakumar, K. and Masliyah, J. H. (1992). An experimental and numerical study of the Dean problem: flow development towards two-dimensional multiple solutions, *Journal of Fluid Mechanics*, 244, 339-376.
- Barua, S. N. (1955), Secondary flow in rotating straight pipe, *Proceeding of Royal Society of London A*, 227, 133-139.
- Barua, S. N. (1963), On secondary flow in stationary curved pipes, *Quarterly Journal of Mechanics and Applied Mathematics*, 16, 61-67.
- Baylis, J. A. (1971). Experiments on Laminar flow in curved channes of square cross-section, *Journal of Fluid Mechanics*, 48(3), 417-422.
- Bejan, A. (1995). *Convective Heat Transfer*, Wiley, New York, 219.
- Benjamin, T. B. (1978a). Bifurcation phenomena in steady flows of a viscous fluid I. Theory, *Proceeding of Royal Society of London A*, 359, 1-26.
- Benjamin, T. B. (1978b). Bifurcation phenomena in steady flows of a viscous fluid II. Experiment, *Proceeding of Royal Society of London A*, 359, 27-43.
- Benton, G. S. and Baltimore, M. D. (1956). The effect of the earth's rotation on laminar flow in pipes, *Journal of the Applied Mechanics*, March Issue, 123-127.
- Berg, R.R. and Bonilla, C.F. (1950). Heating of Fluids in Coils, *Trans. NY Academic Science*, 13, 12-18.

- Berger, S. A., Talbot, L. and Yao, L. S. (1983). Flow in curved pipes, *Annual Reviews of Fluid Mechanics*, 15, 461-512.
- Bottaro, A., Matsson, O. J. E. and Alfredsson, P. H. (1991). Numerical and experimental results for developing curved channel flow, *Physics of Fluids A*, 3(6), 1473-1476.
- Bottaro, A. (1993). On longitudinal vortices in curved channel flow, *Journal of Fluid Mechanics*, 251, 627-660.
- Brewster, D. B. Grosberg, P. And Nissan, A. H. (1959). The Stability of viscous flow between horizontal concentric cylinders, *Proceedings of Royal Society of London A*, 251, 76-91.
- Calcagni, B. Marsili, F. and Paroncini, M. (2005). Natural convective heat transfer in square enclosures heated from below, *Appl. Thermal Engineering.*, 25(16), 2225-2231.
- Chandratilleke, T.T.(2001). Secondary flow characteristics and convective heat transfer in a curved rectangular duct with external heating, *Proceedings of 5th World Conference on Experimental Heat Transfer, Fluid Mechanics and Thermodynamics Step.* 24-28, Thessaloniki, Greece.
- Chandratilleke T.T. and Nursubyakto (2003). Numerical prediction of secondary flow and convective heat transfer in externally heated curved rectangular ducts, *International Journal of Thermal Science*, 42, 187-198.
- Chandratilleke, T. T. Nadim, N. and Narayanaswamy, R. (2012). Vortex structurebased analysis of laminar flow behavior and thermal characteristics in curved ducts, *Int. J. Therm. Sci.* 59, 75–86.
- Chandratilleke, T. T. Nadim, N. and Narayanaswamy, R. (2013). Analysis of secondary flow instability and forced convection in fluid flow through rectangular and elliptical curved ducts, *Heat Transfer Eng.* 34, 1237–1248.
- Cheng, K.C. and Akiyama, M. (1970). Laminar forced convection heat transfer in curved rectangular channels, *Int. J. Heat Mass Transfer*, 13, 471-490.
- Cheng, K. C., Lin, R. C. and Ou, J. W. (1975). Graetz problem in curved square channels, *Trans. ASME, J. of Heat Transfer* , 97, 244-248.
- Cheng, K. C., Lin, R. and Ou, J. W. (1976). Fully Developed Laminar Flow in Curved racrangular channels, *ASME, Journal of Fluids Engineering*, 98, 41-48.
- Chilukuri, R. and Humphrey, J. A. C. (1981). Numerical computation of buoyancy induced recirculation in curved square duct laminar flow, *Int. J. Heat Mass Transfer*, 24, 305-314.
- Chung, J. H. and Hyun, J. M. (1992). Convective heat transfer in the developing flow region of a square duct with strong curvature, *Int. J. Heat Mass Transfer*, 35, 2537-2550.
- Collins, W. M. and Dennis, S. C. R. (1975). The steady motion of a viscous fluid in a curved tube, *Quarterly J. of Mech. and Appl. mathematics*, 28, 133-156.

- Collins, W. M. and Dennis, S. C. R. (1976a). Steady flow in a curved tube of triangular cross-section, *Proceeding of Royal Society of London A*, 352, 189-211.
- Collins, W. M. and Dennis, S. C. R. (1976b). Viscous eddies near a 90^0 and a 45^0 degree corner in flow through a curved tube of triangular cross-section. *Journal of Fluid Mechanics*, 76(3), 417-432.
- Cuming, H. G. (1952). The secondary flow in curved pipes, *Aeronautic Research Council Report*, Memo No. 2880.
- Cunff, C. L. and Bottaro, A. (1993). Linear stability of shear profiles and relation to secondary instabilities of the Dean flow, *Physics of Fluids A*, 5(9), 2161-2171.
- Das, S. P. Chakraborty, S and Dutta, P. (2002). Natural convection in a two dimensional enclosure heated symmetrically from both sides, *Int. Comm. Heat Mass Transfer*, 29, 345-354.
- Daskopoulos, P and Lenhoff, A. M. (1989). Flow in curved ducts: bifurcation structure for stationary ducts, *Journal of Fluid Mechanics*, vol.203, 125-148.
- Daskopoulos, P and Lenhoff, A. M. (1990). Flow in curved ducts: Part 2. Rotating ducts, *Journal of Fluid Mechanics*, 217, 575-593.
- Dean, W. R. (1927). Note on the motion of fluid in a curved pipe, *Philosophical Magazine and Journal of Science* 4(20), 208-223.
- Dean, W. R. (1928). The stream-line motion of fluid in a curved pipe, *Philosophical Magazine and Journal of Science* 5(30), 673-695.
- Dennis, S. C. R (1980). Calculation of the steady flow through a curved tube using a finite difference method, *Journal of Fluid Mechanics*, 99, 449-467.
- Dennis, S. C. R. and Ng, M. (1982). Dual solutions for steady laminar flow through a curved tube, *Quarterly J. of Mech. and Appl. Math.*, 35(3), 305-324.
- Dennis, S. C. R. and Riley, N. (1991). On Fully developed Flow in a Curved Pipe at Large Dean Number, *Proceedings of Royal Society of London A*, 434, 473-478.
- De Vriend, H. J. (1981). Velocity redistribution in curved rectangular channels, *Journal of Fluid Mechanics*, 107, 423-439.
- Dravid, A.N., Smith, K.A., Merrill, E. W. And Brain, P.L.T. (1971). Effect on Secondary fluid motion of laminar flow heat transfer in helically coiled tube, *AIChE Journal*, 17, 1114-1122.
- Duck, P. W. (1983). Flow through rotating straight pipes of a circular cross-section. *Physics of Fluids A*, 26(3), 614-618.
- Eustice, J. (1910). Flow of water in curved pipes, *Proceedings of Royal Society of London A*, 84, 107-118.

- Eustice, J. (1911). Experiments on stream-line motion in curved pipes, *Proceeding of Royal Society of London A*, 85, 119-131.
- Eustice, J. (1925). Flow of fluids in curved passages, *Engineering*, Vol. 13, pp 604-605.
- Fargie, D and Martin, B. W. (1971). Developing laminar flow in a pipe of circular cross-section, *Proceeding of Royal Society of London A*, 321, 461-467.
- Fellouah, H., Castelain, C., Ould-ElMoctar, A. and Peerhossaini, H. (2010). The Dean Instability in Power-law and Bingham Fluids in a Curved Rectangular Duct, *Journal of Non Newtonian Fluid Mech.*, 165, 163–173.
- Finlay, W. H., Keller, J. B. and Ferziger, J. H. (1988). Instability and transition in curved channel flow, *Proceeding of Royal Society of London A*, 321, 461-476.
- Finlay, W. H. (1989). Perturbation expansion and weakly non-linear analysis for two-dimensional vortices in curved or rotating channels, *Physics of Fluids A*, 1(15), 854-860.
- Finlay, W. H. and Nandakumar, K. (1990). Onset of two-dimensional cellular flow in finite curved channels of large aspect ratio, *Physics of Fluids A*, 2(7), 1163-1174.
- Finlay, W. H. Guo, Y. and Olsen, D. (1993). Inferring secondary flows from smoke or dye flow visualization: Two case studies, *Physics of Fluids A*, 5(11), 2689-2701.
- Fusegi, T., Hyun, J. M. Kuwahara, K. and Farouk, B. (1991). A numerical study of three-dimensional natural convection in a differentially heated cubical enclosure, *Int. J. Heat Mass Transfer*, 34, 1543-1557.
- Ganzarolli, M. M. and Milanez, L. F. (1995). Natural convection in rectangular enclosures heated from below and symmetrically cooled from the sides, *Int. J. Heat Mass Transfer*, 38, 1063-1073.
- Ghia, K. N. and Sokhey, J. S. (1977). Laminar incompressible viscous flow in curved ducts of rectangular cross section, *Trans. ASME, J. of Fluids Engineering*, 99, 640-648.
- Gottlieb, D. and Orszag, S. A. (1977). Numerical analysis of Spectral Methods, *Society for Industrial and Applied Mathematics, Philadelphia*.
- Guo, Y and Finlay, W. H. (1991). Splitting, margining and wavelength selection of vortices in curved and or rotating channel flow due to Eckhaus instability, *Journal of Fluid Mechanics*, 228, 661-691.
- Guo, Y and Finlay, W. H. (1994). Wave number selection and irregularity of spatially developing non-linear Dean Gortler vortices, *Journal of Fluid Mechanics*, Vol. 264, 1-40.
- Hall, P. (1974). Unsteady viscous flow in a pipe of slowly varying cross section, *Journal of Fluid Mechanics*, 64(2), 209-226.
- Hausen, H. (1943). Darstellung des war-menberganges potenzbeziehungen, *Z. VerDisch. Ing. Beih. Verfahrenstech.*, 4, 91-98.

- Hille, P., Vehrenkamp, R. and Schulz-Dubois, E. O. (1985). The development and structure of primary and secondary flow in a curved square duct, *Journal of Fluid Mechanics*, 151, 219-241.
- Hocking, L.M. (1967). Boundary and shear layers in a curved rotating pipe, *Journal of Mathematical and Physical Sciences*, 1, 123-136.
- Hoover, M. D., Stober, W. and Morawietz, G. (1984). Experiment on Laminar flow in a rotating, curved rectangular cross-section, *Trans. ASME Journal of Fluid Engineering*, 106, 38-44.
- Humphrey, J. A. C. (1978). Numerical calculations of developing laminar flow in pipes of arbitrary curvature radius, *Canadian J. Chem. Engineering*, 56, 151-164.
- Humphrey, J. A. C., Iacovides, H. and Launder, B. E. (1985). Some numerical experiments on developing laminar flow in circular sectioned bends, *Journal of Fluid Mechanics*, 154, 357-375.
- Humphrey, J. A. C., Taylor, A. M. K. and Whitelaw, J. H. (1977). Laminar flow in a square duct of strong curvature, *Journal of Fluid Mechanics*, 83(3), 509-527.
- Ito, H. (1951). Theory on laminar flows through curved pipes of elliptic and rectangular cross section, *The reports of the Institute of high speed Mechanics, Tohoku University, Sendai, Japan*, 1, 1-16.
- Ito, H. (1969). Laminar flow in curved pipes, *Zeitschrift for Angewandte Mathematics and Mechanics (ZAMM)*, 49, 653-663.
- Ito, H. (1970). Laminar flow in curved pipes, *The Reports of the Institute of high speed Mechanics, Tokiyo University, Sendai, Japan*, 22 (224), 161-180.
- Ito, H. and Nanbu, K. (1971). Flow in straight pipes of circular cross-section, *ASME Journal of Basic Engineering*, September Issue, 383-394.
- Ishigaki H. (1994). Analogy between laminar flows in curved pipes and orthogonally rotating pipes, *Journal of Fluid Mechanics*, 268, 133-145. <https://doi.org/10.1017/S0022112094001291>
- Ishigaki H. (1996). Laminar flow in rotating curved pipes, *Journal of Fluid Mechanics*, 329, 373-388.
- Janssen, L.A.M. and Hoogendoorn, C.J. (1978). Laminar convective heat transfer in helically coiled tubes, *International Journal of Heat and Mass Transfer*, 21, 1179-1206.
- Jayanti, S. and Hewitt, G. F. (1992). A numerical study of bifurcation in laminar flow in curved ducts, *Int. J. for Numerical Methods in Fluids*, 14, 253-266.
- Joseph, B., Smith, E. P. and Adler, R. J. (1975). Numerical treatment of laminar flow in helically coiled tubes of square cross section, *AIChE Journal*, 21, 965-974.
- Kajishima, T., Miyake, Y. and Inaba, T. (1989). Numerical simulation of laminar flow in curved ducts of rectangular cross-section, *JSME, International Journal, Series II*, 32(4), 516-522.

- Kalb, C.E. and Seader, J.D. (1972). Heat and Mass transfer phenomena for viscous flow in curved circular tube, *International Heat and Mass Transfer*, 15, 801-817.
- Kalb, C.E. and Seader, J.D. (1974). Fully developed viscous flow heat transfer in curved circular tube with uniform wall temperature, *AIChE Journal*, 20, 340-346.
- Kao, H. C. (1992). Some aspects of bifurcation structure of laminar flow in curved ducts, *Journal of Fluid Mechanics*, 243, 519-539.
- Kelleher, M. D., Flentle, D. L. and McKee, R. J. (1980). An experimental study of the secondary flow in a curved rectangular channel, *Trans. ASME, Journal of Fluids Engineering*, 102, 92-96.
- Keller, H. B. (1987). Lectures on Numerical Methods in Bifurcation Problems, *Tata Institute of Fundamental Research, Springer -Verlag*, Berlin Heidelberg New York Tokyo.
- Kheshgi, H.S. and Scriven, L. E. (1985). Viscous flow through a rotating square channel, *Physics of Fluids A*, 28(10), 2968-2979.
- Komiyama, Y., Mikami, F. and Okuni, K. (1984). Laminar forced convection heat transfer in curved channels of rectangular cross-section, *Trans. JSME, Int. Journal, Series B*, 50, 424-434.
- Kotorynski, W. P. (1986). Steady laminar flow through a twisted pipe of electrical cross-section, *Computers and Fluids*, 14(4), 433-444.
- Kubair, V. and Kuloor, N. R. (1966). Heat transfer to Newtonian fluids in coiled pipes in laminar flow, *International Heat and Mass Transfer*, 9, 63-75.
- Kun, M. A, Yuan S., Chang, H. and Lai, H. (2014). Experimental Study of Pseudoplastic Fluid Flows in a Square Duct of Strong Curvature, *J. Thermal Science*, 23(4), 359–367.
- Lei, U. and Hsu, C. H. (1990). Flow through a straight pipes, *Physics of Fluids A*, 2(1), 63-75.
- Li, Y., Wang, X., Yuan, S. and Tan, S.K. (2016). Flow development in curved rectangular ducts with continuously varying curvature. *Experimental Thermal and Fluid Science*, 75, 1-15.
- Li, Y., Wang, X., Zhou, B., Yuan, S. and Tan, S.K. (2017). Dean instability and secondary flow structure in curved rectangular ducts. *Int. J. Heat and Fluid Flow*, 68, 189-202.
- Ligrani, P. M., Choi, S., Scallert, A. R. and Skogerboe, P. (1996). Effects of Dean vortex pairs on surface heat transfer in curved channel flow, *Int. J. Heat Mass Transfer*, 39, 27-37.
- Lima, K. F. and Alam, M. (2019). Fluid flow through a straight pipe in a rotating system with magnetic field acting along centre line having hall current. *Modell. Meas. Control B*, 88(2–4), 79–86. https://doi.org/10.18280/mmc_b.882-406
- Liu, F. and Wang, L. (2009). Analysis on multiplicity and stability of convective heat transfer in tightly curved rectangular ducts. *Int. J. Heat and Mass Transfer*, 52, 5849-5866.

- Lyne, W. H. (1970). Unsteady viscous flow in a curved pipe, *Journal of Fluid Mechanics*, 45(1), 13-31.
- Mansour, K. (1985). Laminar flow through a slowly rotating straight pipe, *Journal of the Fluid Mechanics*, 150,1-21.
- Manton, M. J. (1971). Low Reynolds number flow in slowly varying axisymmetric tube, *Journal of Fluid Mechanics*, 49(3), 451-459.
- Masliyah, J. H. (1980). On laminar flow un curved semi-circular ducts, *Journal of Fluid Mechanics*, 99, 469-479.
- Matsson, O. J. E. and Alfredsson, P. H. (1992). Experiments on instabilities in curved channel flow, *Physics of Fluids A*, 4(8), 1666-1676.
- McConalogue, D. J. and Srivastava, R. S. (1968). Motion of a fluid in curved tube, *Proceeding of Royal Society of London A*, 307, 37-53.
- McCormack, P. D., Welker, H. and Kelleher, M. (1969). Taylor-Goertler vortices and their effect on heat transfer, *ASME-AIChE Heat Transfer Conference*, Paper no. 69-HT-3.
- Miyazaki, H. (1971). Combined free- and forced-convective heat transfer and fluid flow in rotating curved circular tube, *International Journal of Heat Mass Transfer*, 14, 1295-1309.
- Miyazaki H. (1973). Combined free- and forced-convective heat transfer and fluid flow in rotating curved rectangular tube, *ASME Journal of Heat Transfer*, February Issue, 64-71.
- Miykae, H., Kajishima, T, and Inaba, T. (1988). Numerical experiments of laminar flow laminar flow in curved duct of rectangular cross-section, *Proceeding of Experimental heat transfer, fluid mechanics and thermodynamics conference*, 1192-1199.
- Mondal, R.N., Kaga, Y., Hyakutake, T. and Yanase, S. (2006). Effects of curvature and convective Heat Transfer in Curved Square Duct Flows, *Transactions of the ASME Journal of Fluids Engineering* , 128, 1013-1022.
- Mondal, R.N.,and Yanase, S. (2006). Isothermal and Non-isothermal Flows through Curved Ducts with Square and Rectangular Cross Sections, *PhD Thesis, March 2006*, The Graduate School of Natural Science and Technology, Okayama University, Japan.
- Mori, Y. and Nakayama, W. (1965). Study on forced convective heat transfer in curved pipes (1st report), *International Journal of Heat Mass Transfer*, 8, 67-82.
- Mori, Y. and Nakayama, W. (1967). Study on forced convective heat transfer in curved pipes, (3rd report), *International Journal of Heat Mass Transfer*, 10, 681-695.
- Mori, Y. and Uchida, Y. And Ukon, T. (1971). Forced convective heat transfer in a curved channel with square cross-section, *International Journal of Heat Mass Transfer*, 14, 1787-1805.
- Murata , S., Miyake, Y., and Inaba, T. (1976). Laminar flow in a curved pipe with varing curvature, *Journal of Fluid Mechanics*, 73(4), 735-752.

- Nandakumar, K. and Masliyah, J. H. (1982). Bifurcation in steady laminar flow through curved tubes, *Journal of Fluid Mechanics*, 119, 475-490.
- Nandakumar, K. and Masliyah, J. H. (1986). Swirling flow and heat transfer in coiled and twisted pipes, *Adv. Transp. Processes* 4, 49-112.
- Nandakumar, K., Raszillier, H. And Durst, F. (1991). Flow through rotating rectangular duct, *Physics of Fluid A*, 3(5), 770-781.
- Nandakumar, K., Mees, P. A. J. and Masliyah, J. H. (1993). Multiple two dimensional solutions to the Dean problem in triangular ducts, *Physics of Fluid A*, 5(5), 1182-1187.
- Norouzi, M., Kayhani, M. H., Nobari, M. R. H. and Demneh, M. K. (2009). Convective heat transfer of viscoelastic flow in a curved duct. *World Acad. Sci. Eng. Tech.*, 32, 327-33.
- November, M. and Nansteel, M. W. (1987). Natural convection in enclosures heated from below and symmetrically cooled along one side, *Int. J. Heat Mass Transfer*, 30, 2433-2440.
- Nunge, R. J. and Lin, T. S. (1973). Laminar flow in strongly curved tubes, *AIChE Journal*, 13(1), 17-36.
- Ohba, K., Tsuda, N. and takagi, K. (1986). A velocity fluctuation in developing laminar flow through a moderately curved U-bend of square cross-section, *Technical Report, Kansai University, Japan*, 27, 33-42.
- Oliver, D. R. and Asghar, S.M. (1976). Heat transfer to Newtonian and viscoelastic liquids during laminar flow in helical coils, *Transactions Institute of Chemical Engineering*, 54, 218-224.
- Owhadi, A., Bell, K. J and Crain B. Jr. (1968). Forced convection boiling inside helically coiled tubes, *International Journal of Heat Mass Transfer*, 11, 779-793.
- Patankar, S. V., Pratap, V. S. and Spalding, D. B. (1974). Prediction of laminar flow and heat transfer in helically coiled pipes, *J. Fluid Mech.*, 62, 539-551.
- Patankar, S. V. (1980). Numerical heat transfer and fluid flow, Washington, DC: Hemisphere. <https://doi.org/10.1201/9781482234213>
- Pedley, T. J. (1980). The Mechanics of Large Blood Vessel, P. 235. *Cambridge University Press*.
- Philip, A. J. Mess, Nandakumar, K. and Masliyah, J. H. (1996a). Instability and transition of flow in a curved square: the development of two pairs of Dean vortices, *Journal of Fluid Mechanics*, 314, 227-246.
- Philip, A. J. Mess, Nandakumar, K. and Masliyah, J. H. (1996b). Secondary instability of flow in a curved duct square cross-section, *Journal of Fluid Mechanics*, 323, 387-409.
- Philip, A. J. Mess, Nandakumar, K. and Masliyah, J. H. (1996c). Steady spatial oscillation in a curved duct of square cross-section, *Physics of Fluids A*, 8(12), 3264-3270.

- Piesche, M. and Felsch, K. O. (1980). Experimental investigation of pressure loss in rotating curved rectangular channels, *Arch, Mech.*, Vol.32(5), 747-756.
- Pratap, V. S. and Spalding, D. V. (1975). Numerical computations of the flow in curved ducts, *Aeronautical Quarterly, August Issue*, 219-228.
- Prusa, J. and Yao, L. S. (1982). Numerical solution of fully developed flow in heated curved tubes, *Journal of Fluid Mechanics*, 123, 503-522.
- Razavi, S.E., Soltanipour, H. and Choupani, P. (2015). Second law analysis of laminar forced convection in a rotating curved duct. *Thermal Sciences*, 19(1): 95-107.
- Reid, W. H. (1958). On stability of viscous flow in curved channel, *Proceeding of Royal Society of London A*, 244, 186-198.
- Sankar, S. R., Nandakumar, K. and Masliyah, J. H. (1988). Oscillatory flows in coiled square ducts, *Physics of Fluids A*, 31(6), 1348-1359.
- Schimdt, E. F. (1967). Wärmeübergang and Drukverlust in Rohrschlangen, *Chemical Ing. Tech.*, 13, 781-789.
- Schladow, S. G. (1990). Oscillatory motion in a side-heated cavity. *J. Fluid Mech.*, 213, 589-610.
- Selmi, M. and Nandakumar, K. and Finlay, W.H. (1994). A Bifurcation Study of Viscous Flow Through a Rotating Curved Duct. *J. Fluid Mechanics*, 262, 353-375.
- Selmi, M. Nandakumar, K. and Finlay, W.H. (1999). Bifurcation study of flow through rotating curved ducts, *Physics of Fluids*, 11, 2030-2043.
- Shanthini, W. and Nandakumar, K. (1986). Bifurcation phenomena of generalized Newtonian fluids in curved rectangular ducts, *Journal of Non-Newtonian Fluid Mechanics*, 22, 35-60.
- Sharma, R. K. and Nandakumar, K. (1995). Multiple, two-dimensional solutions in a rotating straight pipe, *Physics of Fluids A*, 7(7), 156668-1575.
- Singh, M. P. (1974). Entry flow in a curved pipe, *J. Fluid Mech.*, 65, 517-539.
- Singh, S.P. and Bell, K.J. (1974). Laminar flow heat transfer in a Helically coiled tube, *International Heat Transfer Conference, Tokyo*, 2, 193-197.
- Simon, H. A., Chang, M. H and Chow, J. C. F. (1977). Heat transfer in curved tubes with pulsatile, fully developed laminar flows, *Int. J. Heat Transfer*, 99, 590-595.
- Smith, F. T. (1976a). Steady motion within a curved pipe, *Proceeding of Royal Society of London A*, 347, 345-370.
- Smith, F. T. (1976b). Fluid flow in a curved pipe, *Proceeding of Royal Society of London A*, Vol.351, 71-87.

- Snyder, B. and Lovely, C. (1990). A Computational study of developing 2-D laminar flow in curved channels, *Physics of Fluids A*, 2(10), 1808-1816.
- Soh, W. Y. (1988). Developing fluid flow in a curved duct of square cross-section and its fully developed dual solutions, *Journal of Fluid Mechanics*, 188, 337-361.
- Soh, W. Y. and Berger, S. A. (1984). Laminar entrance flow in a curved pipe, *Journal of Fluid Mechanics*, 148, 109-135.
- Speziale, C. G. (1982). Numerical study of viscous flow in rotating rectangular ducts, *Journal of Fluid Mechanics*, 122, 251-271.
- Speziale, C. G. and Thangam, S. (1983). Numerical study of secondary flows and roll-cell instabilities in rotating channel flows, *Journal of Fluid Mechanics*, 130, 377-395.
- Stewartson, K., Cebece, T. and Chang, K. C. (1980). A boundary layer collision in a curved duct, *Quarterly Journal of mechanics and applied mathematics*, 33, 59-75.
- Stewartson, K., and Simpson, C. J. (1982). A On asingularity initiating a boundary layer collision, *Quarterly Journal of mechanics and applied mathematics*, 35, 1-16.
- Sturgis, J. C. and Mudawar, I. (1999). Single-phase heat transfer enhancement in a curved, rectangular channel subjected to concave heating, *Int. J. Heat Mass Transfer*, 42, 1255-1272.
- Sugiyama, S., Hayashi, T and Yamazaki, K. (1983). Flow characteristics in the curved rectangular channels, *Bull. of the JSME*, 26, 964-969.
- Sugiyama, S., Aoi, T., Yamamoto, M., Narisawa, N. And Miyake, Y. (1988). Measurements on developing laminar flow in a curved rectangular duct by means of LDP, *Proceeding of Experimental Heat transfer, fluid mechanics and thermodynamics conference*, 1185-1191, September 4-9, Dubrovnik, Yugoslavia.
- Tarbell, J.M. and Samuels, M.R. (1973). Momentum and heat transfer and in helical coil, *Chemical Engineering Journal*, 5, 117-127.
- Takami, T. and Sudou, K. (1984). Flow in a curved pipes with elliptic cross-section, *Buletin of the JSME*, 27(228-16), 1176-1181.
- Taylor, A. M. K. P., Whitelaw, J. H. and Yianneskis, M. (1982). Curved ducts with strong secondary motion: velocity measurements of developing laminar and turbulent flow, *Trans. ASME, Journal of Fluids Engineering*, 104, 350-358.
- Thangam, S. and Hur, N. (1990). Laminar secondary flows in curved rectangular ducts, *Journal of Fluid Mechanics*, 217, 421-440.
- Todd, L. (1977). Some comments on steady laminar flow through twisted pipes, *Journal of Engineering Mathematics*, 11, 29-48.

- Todd, L. (1987). Steady laminar flow through thin curved pipes, *Fluid Dynamic Research*, 1 , 237-255. [https://doi.org/10.1016/0169-5983\(87\)90008-6](https://doi.org/10.1016/0169-5983(87)90008-6)
- Topakoglu, H. C. (1967). Steady laminar flows of an incompressible viscous fluid in curved pipe, *Journal of Mathematics and Mechanics*, 16(12) 1321-1337.
- Topakoglu, H. C. and Ebadain, M. A. (1985). On the steady laminar flow of an incompressible viscous fluid in a curved pipe of electrical cross-section, *Journal of Fluid Mechanics*, 158, 329-340.
- Topakoglu, H. C. and Ebadain, M. A. (1987). Viscous laminar flow in a curved pipe of electrical cross-section, *Journal of Fluid Mechanics*, 184, 571-580.
- Tsuda, N. and Ohba, K. (1984). Laser Doppler measurement of developing laminar flow in a moderately curved U-bend of square cross-section, *Proc. of 2nd Osaka Symp. on flow measuring Tech., July 13, Osaka, Japan*, pages 1-15.
- Van Dyke, M. (1978). Extended Stokes series: Laminar flow through a loosely coiled pipe, *Journal of Fluid Mechanics*, 107, 423-430.
- Wang, L. and Cheng, K. C. (1995). Flow in curved channels with a low negative rotation speed, *Physical Review E*, 51(2), 1155-1161.
- Wang, L.Q. and Liu, F. (2007). Forced Convection in Slightly Curved Microchannels, *Int. J. Heat Mass Transfer*, 50, 881-896.
- Wang, L., Yang, T. (2003). Bifurcation and stability of forced convection in rotating curved ducts of square cross section. *Int. J. Heat Mass Transf.* 46, 613–629.
- Wang, L.Q., Yang, T.L. (2004). Multiplicity and stability of convection in curved ducts: review and progress. *Adv. Heat Transf.* 38, 203–256
- Wang, L. and Yang, T. (2004). Bifurcation and stability of forced convection in curved ducts of square cross section, *Int. J. Heat Mass Transfer*, 47(14-16), 2971-2987.
- Wang, L and Yang, T. (2005). Periodic oscillation in curved duct flows, *Physica D.*, 200, 296-302.
- Wang, L., Pang, O. and Cheng, L. (2005). Bifurcation and stability of forced convection in tightly coil ducts: multiplicity, *Chaos, Solitons and Fractals*, 26, 337-352.
- Wang, L., Pang, O. and Cheng, L. (2006). Bifurcation and stability of forced convection in tightly coil ducts: stability, *Chaos, Solitons and Fractals*, 27(4), 991-1005.
- Wanger, R.E. and Velkoff, H. R. (1972). Measurements of secondary flows in a rotating duct, *ASME Journal of Engineering for Power*, 94, 261-270.
- Williams, G. S., Hubbell, C. W. and Finkell, G. H. (1902). Experiments at Detroit, Michigan on the effects of curvature on the flow of water in pipes, *Trans. ASCH*, 47, 1-196.

- Winters, K. H. (1987). A bifurcation study of laminar flow in a curved tube of rectangular cross section, *Journal of Fluid Mechanics*, 180, 343-369.
- Wu, X.Y., Lai, S.D., Yamamoto, K. and Yanase, S. (2013). Numerical analysis of the flow in a curved duct. *Advanced Materials Research*, 706-708: 1450-1453.
- Yamamoto, K., Yanase, S., Alam, M.M. (1999). Flow through a rotating curved duct with square cross-section. *J. Phys. Soc. Jpn.* 68, 1173–1184.
- Yamamoto, K., Alam, M.M., Yasuhara, J., Aribowo, A. (2000). Flow through a rotating helical pipe with circular cross section. *Int. J. Heat Fluid Flow* 21, 213–220.
- Yamamoto, K., Xiaoyum, W., Kazou, N., Yasutuka, H. (2006). Visualization of Taylor-Dean flow in a curved duct of square cross section. *Fluid Dyn. Res.* 38, 1–18
- Yanase, S. (1991). Time dependent analysis of bifurcating flows through a curved tube, *Eur. J. Mech., B/Fluids*, 10, 321.
- Yanase, S., Goto, N. and Yamamoto, K. (1988). Stability of Dual solutions of the flow in a curved circular tube, *Journal of the Physical Society of Japan*, 57(8), 2602-2604.
- Yanase, S., Goto, N. and Yamamoto, K. (1989). Dual solutions of the flow through a curved tube, *Fluid Dynamics Research*, 5, 191-201.
- Yanase, S., Kaga, Y. and Daikai, R. (2002). Laminar flow through a curved rectangular duct over a wide range of the aspect ratio, *Fluid Dynamics Research*, 31, 151-183.
- Yanase, S., Mondal, R.N., Kaga, Y., and Yamamoto, K. (2005a). Transition from Steady to Chaotic State of Isothermal and Non-Isothermal Flows Through a Curved Rectangular Duct, *Journal of Physical Society Japan*, 74(1), 345-358.
- Yanase, S., Mondal, R.N. and Kaga, Y. (2005b). Numerical Study of Non-Isothermal Flow with Convective Heat Transfer in a Curved Rectangular Duct, *International Journal of Thermal Science*, 44(1), 1047-1060.
- Yanase, S. and Nishiyama, K. (1988). On the bifurcation of laminar flows through a curved rectangular tube, *J. Phys. Soc. Japan*, 57(11), 3790-3795.
- Yanase, S., Watanabe, T. and Hyakutake, T. (2008). Traveling-wave solutions of the flow in a curved-square duct. *Physics of Fluids*, 20(124101), 1-8.
- Yang, R. and Chang, S. F. (1994). Combined free and forced convection in curved pipes with finite curvature ratio, *Int. J. Heat Fluid Flow*, 15, 470-476.
- Yang, Z. and Keller, H. B. (1986). Multiple laminar flows through curved pipes, *Applied Numerical Mathematics*, 2, 257-271.
- Yao, L. S. and Berger, S. A. (1975). Entry flow in a curved pipe. *Journal of Fluid Mechanics*, 67, 177-196.

- Yao, L. S. and Berger, S. A. (1978). Flow in heated curved pipes. *Journal of Fluid Mechanics*, 88, 339-354.
- Yao, L. S. and Berger, S. A. (1988). The three dimensional boundary layer in the entry region of curved pipes with finite curvature ratio, *Physics of Fluid A*, 31(3) , 486-495.
- Yee, G., Chilukuri, R. and Humphrey, J. A. C. (1980), Developing flow and Heat transfer in strongly curved ducts of rectangular cross section, *Trans. ASME, Journal of Heat Transfer*, 102, 285-291.
- Yeung, W. S. (1980). Laminar boundary-layer flow near the entry of a curved circular pipe, *ASME, Journal of Applied Mechanics*, 47, 697-702.
- Zapryanov, Z., Christov, C. and Toshev, E. (1980). Fully developed laminar flow and heat transfer in curved tubes, *International Journal of Heat Mass Transfer*, 23, 873-880.
- Zhang, J.S., Zhang, B. Z. and Jii, J., (2001). Fluid Flow in a Rotating Curved Rectangular Duct". *Int. J. Heat and Fluid Flow*, 22, 583-592.